Lucy Randel

I am commenting as a citizen with a technical background in chemical engineering who has previously participated in TCEQ flare task force stakeholder groups. I urge TCEQ to implement the most stringent possible plan to bring the Houston-Galveston-Brazoria (HGB) area back into attainment for ozone pollution in accordance with the 2008 National Ambient Air Quality Standards as required by the Clean Air Act.

In the HGB area, a group of large industrial plants, oil refineries, and chemical and petrochemical plants are the largest ozone-precursor sources and need to reduce both VOCs and NOx emissions in order to improve Houston's are quality. NRG's Parish coal plant in Fort Bend County is by far the #1 source of NOx pollution locally. ExxonMobil's Baytown complex is the largest sources of VOC pollution.

Chapter 3 of APPENDIX B Conceptual Model for the Houston-Galveston -Brazoria Nonattainment Area for the 2008 Eight-Hour Ozone National Ambient Air Quality Standard discusses ozone precursor concentrations and trends. HRVOCs are a driving force in ozone formation and are mainly emitted by large industrial point source facilities. Ozone nonattainment days are often correlated with emission events that emit large quantities of HRVOCs. Examples include emergency flaring and plant shutdowns for maintenance, which also often involve flaring. Turnaround operations planning to minimize flaring can be used to reduce HRVOC and other VOC emissions. Further, flare operations should be monitored to prevent over-steaming which reduces combustion efficiency. Flare minimization plans should be required of facilities within the nonattainment area. Scheduling of major maintenance during cooler seasons should also be encouraged as an additional tool to reduce ozone formation.

The TCEQ 2010 Flare Study Final Report discusses steam assist issues with flares. The 2007 study The effect of variability in industrial emissions on ozone formation in Houston, Texas discusses the nature of HRVOC emissions from industrial sources in the HGB area. Both are attached.

I appreciate your consideration of additional methods to reduce ozone formation.

Texas Commission on Environmental Quality
PGA No. 582-8-862-45-FY09-04
Tracking No. 2008-81
with
Supplemental Support from the
Air Quality Research Program
TCEQ Grant No. 582-10-94300

TCEQ 2010 Flare Study
Final Report

Prepared by

David T. Allen, Ph.D.
Principal Investigator

Vincent M. Torres
Project Manager

The University of Texas at Austin
The Center for Energy and Environmental Resources

August 1, 2011

Executive Summary

In May 2009, the TCEQ contracted with The University of Texas at Austin (UT Austin) to conduct the Comprehensive Flare Study project (PGA No. 582-8-86245-fy09-04, Tracking Number 2008-81) (TCEQ, 2009). In August 2010, the project was provided supplemental funding by the Air Quality Research Program (TCEQ Grant No. 582-10-94300). The purpose of this project was to conduct field tests to measure flare emissions and collect process and operational data in a semi-controlled environment to determine the relationship between flare design, operation, vent gas lower heating value (LHV) and flow rate, destruction and removal efficiency (DRE), and combustion efficiency (CE). The TCEQ's primary objectives for this study in order of decreasing priority were:

- Assess the potential impact of vent gas flow rate turndown on flare CE and VOC DRE;
- Assess the potential impact of steam/air assist on flare CE and Volatile Organic Compound (VOC) DRE at various operating conditions, including low vent gas flow rates;
- Determine whether flares operating over the range of requirements stated in 40 Code of Federal Regulations (CFR) § 60.18 achieve the assumed hydrocarbon DRE of 98 percent at varying vent gas flow rate turndown, assist ratios and vent gas heat content; and
- Identify and quantify the hydrocarbon species in flare plumes visualized with passive infrared cameras.

In this report, the term vent gas will be used to represent the waste gas stream that would be sent to the flare for destruction in an industrial facility. The terms flare plume and plume will always refer to the total stream of gases that leave the flare and change composition due to some level of combustion.

This final report is submitted to fulfill the requirements of PGA No. 582-8-86245-fy09-04, Tracking Number 2008-81, Task 10 and Task Order No. UTA10-000924-LOAT-RP9, Task 1 and presents the results for this project and the data collected to address the Study Objectives.

Project Scope and Design

Extensive research has been conducted in controlled environments on devices that are not full-scale flares, i.e., with diameters less than three inches as opposed to industrial scale flares, which are typically on the order of multiple feet in diameter and can be as large as ten feet in diameter. To make the results of this study most directly applicable to industrial scale operations, the field tests performed for this study were conducted on full-scale industrial design flares. Specifically, the flare designs selected were the John Zink Models EE-QSC-36" Flare Tip (36-inch diameter) with (3) EEP-503 pilots (steam assist) and the LHTS-24/60 Flare Tip (24-inch diameter) with (3) Pilots (air assist), with maximum capacities of 937,000 lb/hr and 144,000 lb/hr, respectively. These sizes and design configurations were selected as they represent a large number of flare models currently in the field and the results will be applicable to these and similar flare designs when operated under similar conditions to those used in this study.

Controlled Environment Laboratory

To measure flare emissions on full-scale flares in a semi-controlled environment (i.e., controlled flare operations but uncontrolled ambient conditions), the study was conducted at the outdoor flare test facility of the John Zink Company, LLC (Zink), in Tulsa, Oklahoma. Zink is a flare tip manufacturer whose flare test facility is capable of accommodating a wide range of flare tips, test configurations and operating conditions.

Figure ES-1. Flare Plume Sampling System. Flare Plume Sampling System making measurements of flare plume from the steam assist flare while the sampling system is held in position by crane and ground crew [4-7]*

* Numbers in brackets at the end of Tables and Figures are the table or figure number for the same Table or Figure in the main body of the report.

Measurement of Flare Emissions

A core element of UT Austin's study approach was to directly measure flare emissions at the end of the flare plume, and calculate DRE and CE based on those measurements. To measure these emissions, UT Austin selected Aerodyne Research, Inc., (ARI) due to their extensive experience in ambient air quality studies and their unique capability to make continuous (1 Hz frequency, i.e., 1 measurement per second) measurements of the chemical species expected to be present in

the flare plume. These direct measurements of the flare emissions serve as the primary data used to address the study objectives.

The measurement of the actual flare emissions was important to the TCEQ as the estimation method for calculating emission rates from flares prescribed by the TCEQ (Air Permit Division's *Technical Guidance for Flares and Vapor Oxidizers*, RG-109 Dated October 2000 and *2010 Emissions Inventory Guidelines, Technical Supplement 4: Flares*, Revised January 2008), assumes a constant DRE for propylene of 99% for a flare operated in compliance with the flow and thermal requirements of 40 CFR § 60.18.

Compare Remote Sensing Technologies
Remote sensing technologies were also included in the study and a comparison of their performance is included in the study results. The following remote sensing measurement methods were included:

1. Infrared Hyper-Spectral Imaging Technology (Contractor: Telops Inc.)
   Identify flare hydrocarbon plume species and determine plume species concentrations.
2. Passive and Active Fourier Transform Infrared (PFTIR, AFTIR) Spectroscopy (Contractor: Industrial Monitor and Control Corporation)
   Collect the required data to determine flare combustion efficiency.
3. FLIR GasFindIR Passive Infrared (IR) Cameras (Contractor: Leak Surveys Inc.)
   Provide a visual comparison of IR images to the infrared hyper-spectral imaging technology results, and assist other remote sensing tools to take measurements.

A single blind approach was used to compare the remote sensing technology measurements, i.e., the only information provided to the contractors performing remote sensing measurements was that which would be provided to them if they were engaged to measure combustion efficiencies at an industrial facility. The results of the CE and DRE measurements made by ARI were not made available to the remote sensing teams until this report was released to the public.

Performance and Comparison Metrics
VOC DRE was selected as the primary metric for assessing flare performance because of the critical role VOCs play in contributing to the formation of ozone. CE was selected as a secondary metric because the remote sensing technologies included in the study can only measure CE. DRE (hydrocarbon species X) is the mass percentage of species X that is destroyed relative to the quantity of species X entering the flare. Numerically, this is represented as

$$DRE\ (\%) = \left(1 - \frac{X_{plume}}{X_{in}}\right) \times 100 \qquad \text{Eq. ES.1}$$

where

DRE (%) =	destruction and removal efficiency (%)
X_{plume} =	mass flow rate of species X found in the flare plume after combustion has ceased
X_{in} =	mass flow rate of species X in the vent gas entering the flare

CE is the percentage of the total hydrocarbon stream entering the flare that burns completely to form only carbon dioxide and water. Numerically, this is represented as

$$CE\ (\%) = \left(\frac{CO_2\ (plume)}{CO_2\ (plume) + CO\ (plume) + \sum hydrocarbons\ (plume)}\right) \times 100 \quad \text{Eq. ES.2}$$

where

CE (%) = combustion efficiency (%)
CO_2 (plume) = volume concentration of carbon dioxide in the plume (ppmv) after combustion has ceased
CO (plume) = volume concentration of carbon monoxide in the plume (ppmv) after combustion has ceased
Σ hydrocarbons (plume) = volume concentration of all the unburned hydrocarbons in the plume after combustion has ceased multiplied by the number of carbons in the hydrocarbon (ppmCv)

Vent Gas Composition and Flow Rates
For this study, the vent gas composition was a mixture of natural gas, propylene and nitrogen. The ratio of natural gas to propylene was 1:4 by volume. Nitrogen was used as the diluent to achieve the desired lower heating value (LHV) for the vent gas. This study focused on vent gases with low LHV (350 Btu/scf and 600 Btu/scf) and low flow rates because this range of LHV is close to the minimum (300 Btu/scf) LHV allowed for a vent gas in an assisted flare that complies with 40 CFR § 60.18. The range of vent gas flow rates was 0.1% to 0.65% of the flare's design capacity. These vent gas flow rates were selected as they are in the range of operation for typical flow rates (less than 0.5%) used in industry. In the case of a steam-assisted flare, these flow rates introduce the greatest probability for over-assisted steam operation because of minimum levels of steam assist recommended to industry by flare manufacturers (email message from R. Nettles, TCEQ, to V. Torres, UT Austin, on September 8, 2010), 500 lb/hr center, 750 lb/hr upper, for the 36-inch diameter steam assisted flare used in this study to prevent thermal shock and condensation in the piping.

Quality Assurance
UT Austin prepared a Category 2 Quality Assurance Project Plan (The University of Texas at Austin, 2010) for this project that complied with the requirements of the Environmental Protection Agency's (EPA) *Requirements for Quality Assurance Project Plans*, EPA QA/R-5, and Guidance for Quality Assurance Project Plans, EPA QA/G-5. This QAPP was posted for public comment by the TCEQ and was reviewed by the EPA.

Test Plan

A summary of the test series is shown in Table 1, where steam flare tests begin with the letter "S" in the designation of the test series and air flare tests begin with the letter "A". The test plan consisted of multiple flare test series conducted on the air-assisted flare tip and multiple test series conducted on the steam-assisted flare tip. The designation used to identify each test point and run was: S[number 1].[number 2]R[number 3], where the number 1 is the test series number and number 2 designates the level of assist (air or steam) used in the test series. Number 3 is the run or repetition number for the test point. So, for example, S3.2R2 is steam flare test series number 3, the second set of assist conditions, repetition number 2. The Test Plan was designed to systematically vary only one flare operational parameter at a time while holding all other parameters constant during a test.

To focus on low LHV vent gas streams and still comply with 40 CFR § 60.18, a LHV of 350 Btu/scf ± 50 Btu/scf was selected as the lowest target LHV for the vent gases used in the Test Plan. To obtain additional data on the effect of LHV on DRE and CE, a second LHV of 600 Btu/scf ± 80 Btu/scf was also included in the Test Plan.

The steam flare burner used for this study had a design capacity of 937,000 lb/hr for use with propylene. Therefore the 0.1% and 0.25% of design capacity vent gas flow rates for this flare are 937 lb/hr and 2,342 lb/hr, respectively. The air flare burner used for this study had a design capacity of 144,000 lb/hr for use with propylene. The 0.1% of design capacity vent gas flow rate for this flare was thought to be too low for this air flare model, so values of 0.25% and 0.65% of design capacity were selected for the air flare, which were still in the range of interest of the TCEQ. Therefore vent gas flow rates used for the air flare were 359 lb/hr and 937 lb/hr, respectively.

Because of favorable weather conditions and more rapid than anticipated completion of test conditions, a larger number of test points than originally planned were completed. The actual number of test points and replicates that were performed were almost twice the number of steam test points and 27% more air test points than originally planned.

Table ES-1. Summary of Flare Test Plan [3-1]

Steam Flare Tests

Test Series	Vent Gas (Nominal)			Target (Nominal) Steam Assist (lb/hr)	
	Flow Rate lb/hr	LHV Btu/scf	Composition %	Center	Upper
S1	2342	2149	100% Propylene	500	ISP to <Snuff
S2	937	2149	100% Propylene	500	ISP to <Snuff
S3	937	350	1:4 TNG to Propylene Ratio Diluted to Target LHV	500	ISP to <Snuff
S3	937	350	1:4 TNG to Propylene Ratio Diluted to Target LHV	100	230
S3	937	350	1:4 TNG to Propylene Ratio Diluted to Target LHV	0	230
S3	937	350	1:4 TNG to Propylene Ratio Diluted to Target LHV	0	0
S4	2342	350	1:4 TNG to Propylene Ratio Diluted to Target LHV	500	ISP to <Snuff
S4	2342	350	1:4 TNG to Propylene Ratio Diluted to Target LHV	330	110
S4	2342	350	1:4 TNG to Propylene Ratio Diluted to Target LHV	0	330
S5	937	600	1:4 TNG to Propylene Ratio Diluted to Target LHV	500	ISP to <Snuff
S6	2342	600	1:4 TNG to Propylene Ratio Diluted to Target LHV	500	ISP to <Snuff
S7	2342 - 937	350	1:4 TNG to Propylene Ratio Diluted to Target LHV	500	525
S8	2342 - 937	350	1:4 TNG to Propylene Ratio Diluted to Target LHV	0	500
S9	2342 - 937	350	1:4 TNG to Propylene Ratio Diluted to Target LHV	0	1025
S10	2342 - 937	350	1:4 TNG to Propylene Ratio Diluted to Target LHV	0	825
S11	2342 - 937	350	1:4 TNG to Propylene Ratio Diluted to Target LHV	300	525
S12	2342 - 937	350	1:4 TNG to Propane Ratio Diluted to Target LHV	500	525
S13	2342 - 937	350	1:4 TNG to Propane Ratio Diluted to Target LHV	325	525
S14	2342 - 937	350	1:4 TNG to Propane Ratio Diluted to Target LHV	0	525

TNG = Tulsa Natural Gas
Snuff = Visible flame extinguished
ISP = Incipient Smoke Point
LHV = Lower Heating Value

Air Flare Test Tests

Test Series	Vent Gas (Targets)			Target (Nominal) Air Assist (lb/hr)
	Flow Rate lb/hr	LHV Btu/scf	Composition %	
A1	937	2149	100 % Propylene	ISP to <Snuff
A2	359	2149	100 % Propylene	ISP to <Snuff
A3	937	350	1:4 TNG to Propylene Ratio Diluted to Target LHV	ISP to <Snuff
A4	937	600	1:4 TNG to Propylene Ratio Diluted to Target LHV	ISP to <Snuff
A5	359	350	1:4 TNG to Propylene Ratio Diluted to Target LHV	ISP to <Snuff
A6	359	600	1:4 TNG to Propylene Ratio Diluted to Target LHV	ISP to <Snuff
A7	359	350	1:4 TNG to Propane Ratio Diluted to Target LHV	ISP to <Snuff

TNG = Tulsa Natural Gas
Snuff = Visible flame extinguished
ISP = Incipient Smoke Point
LHV = Lower Heating Value

Summary of Flare Tests Results

Figures ES-2a and ES-2b show DRE (propylene) versus steam assist rate and CE versus steam assist rate, respectively, for the two nominal steam flare vent gas flow rates, 937 lb/hr and 2,342 lb/hr at a nominal LHV of 350 Btu/scf. At this LHV, the 937 lb/hr vent gas flow rate (Test Series S3) was only able to achieve a DRE (propylene) > 99% at a steam-to-vent gas (S/VG) ratio of 0.25 or less, 230 lb/hr total steam assist rate (center steam = 0 lb/hr). The 2,342 lb/hr vent gas flow rate (Test Series S4) was able to sustain a 99% DRE (propylene) up to a S/VG = 0.29, 670 lb/hr total steam assist (center steam = 560 lb/hr) before the DRE and CE fell below 99% DRE. These levels of steam assist are lower than the minimum levels of steam assist (500 lb/hr center, 750 lb/hr upper) recommended to industry by flare manufacturers as reported to the TCEQ by industry representatives for the 36-inch diameter steam flare model used in this study with center and upper steam assist. Zink recommends a minimum continuous steam flow rate of 300 lb/hr center steam and 525 lb/hr upper steam for this steam flare tip.

Figures ES-3a and ES-3b show DRE (propylene) versus S/VG ratio and CE versus S/VG ratio, respectively, for all of tests series S3 and S4 on one graph. Figures ES-4a and ES-4b are the same graphs focusing on the range DRE (propylene) ≥ 84%. It can be seen from Figures ES-4a and ES-4b that in this range of S/VG ratios there can be multiple DREs for a singe S/VG. This is due in part to the fact that, in this range of S/VG ratios, steam added at the center has a different effect on DRE than steam added at the upper nozzles. Center steam adds momentum to the vent gas flow but acts as a diluent, reducing the LHV of the vent gas flow. Adding momentum to the vent gas helps prevent combustion from occurring in the tip. Upper steam entrains air and provides turbulence and oxygen for combustion.

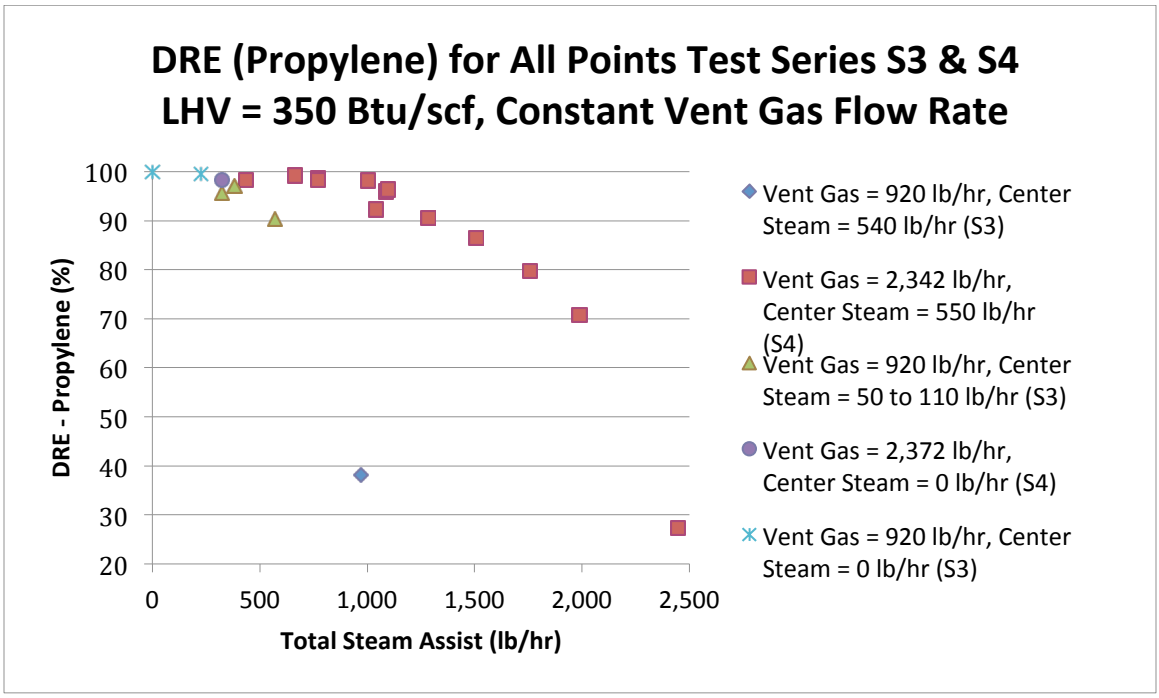

Figure ES-2a. DRE vs Steam Assist for All Test Series S3 and S4 [5-12a]

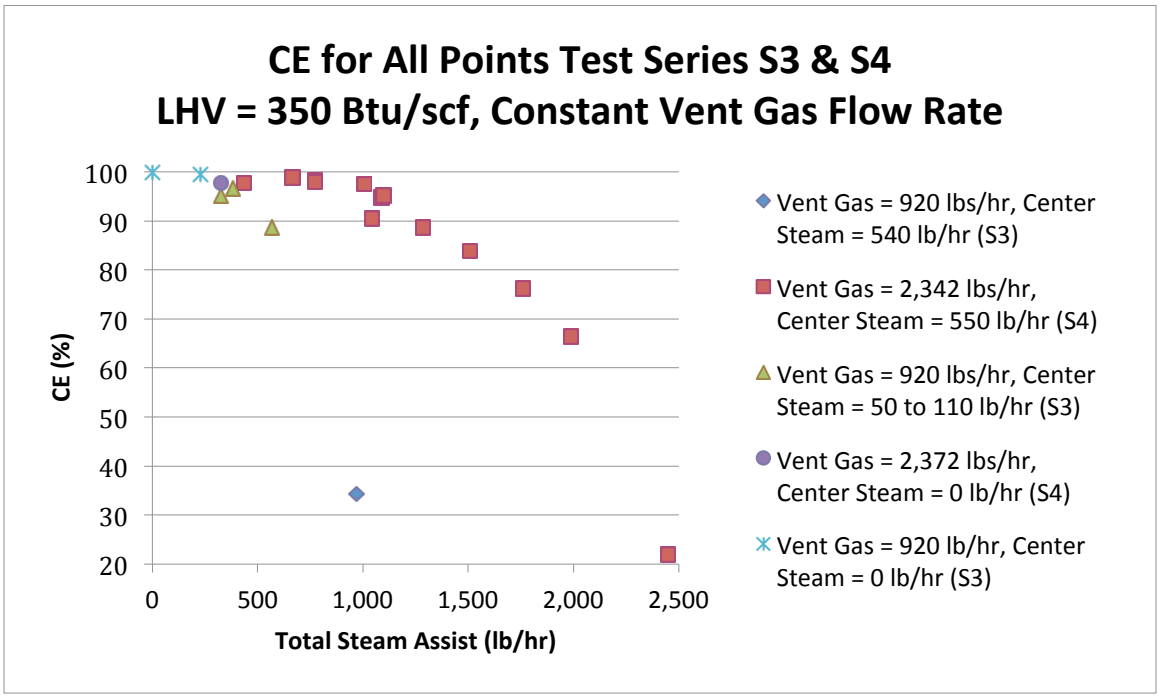

Figure ES-2b. CE vs Steam Assist for All Test Series S3 and S4 [5-12b]

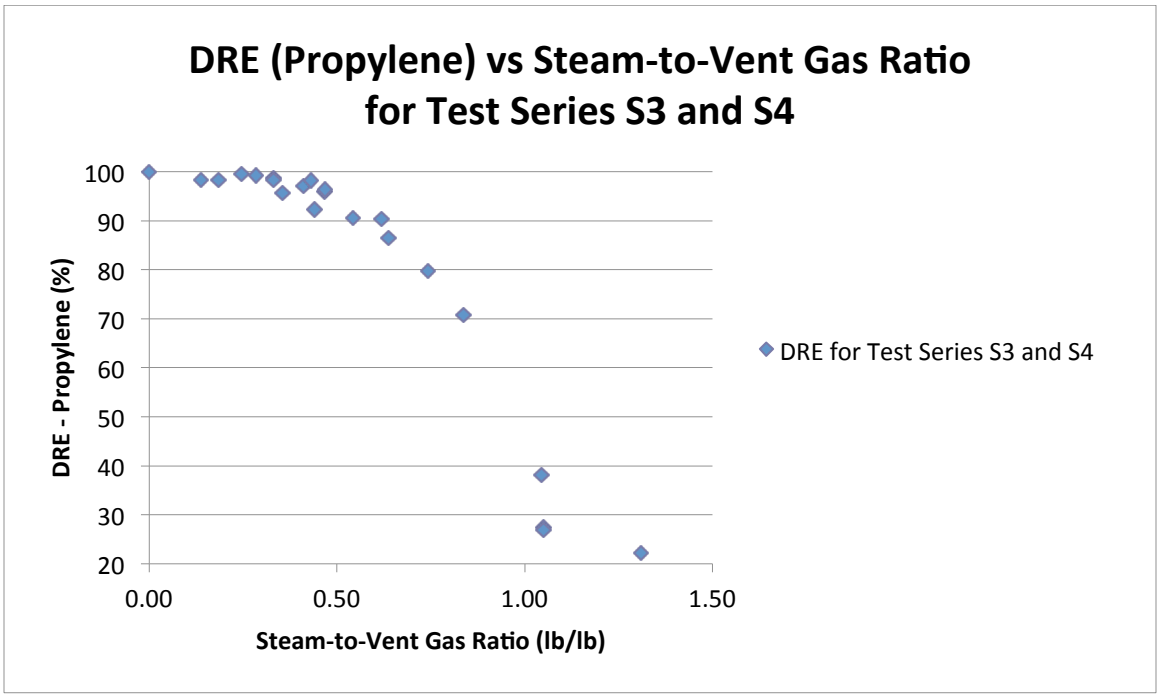

Figure ES-3a. DRE vs Steam-to-Vent Gas Ratio for All Test Series S3 and S4 [5-14a]

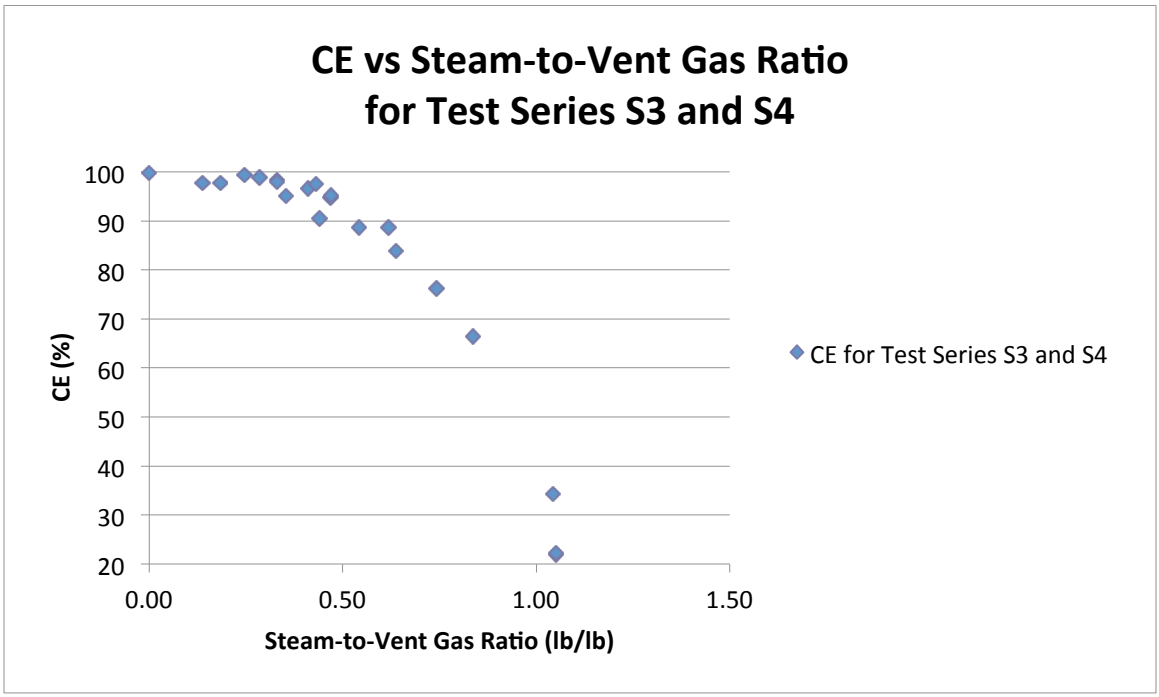

Figure ES-3b. CE vs Steam-to-Vent Gas Ratio for All Test Series S3 and S4 [5-14b]

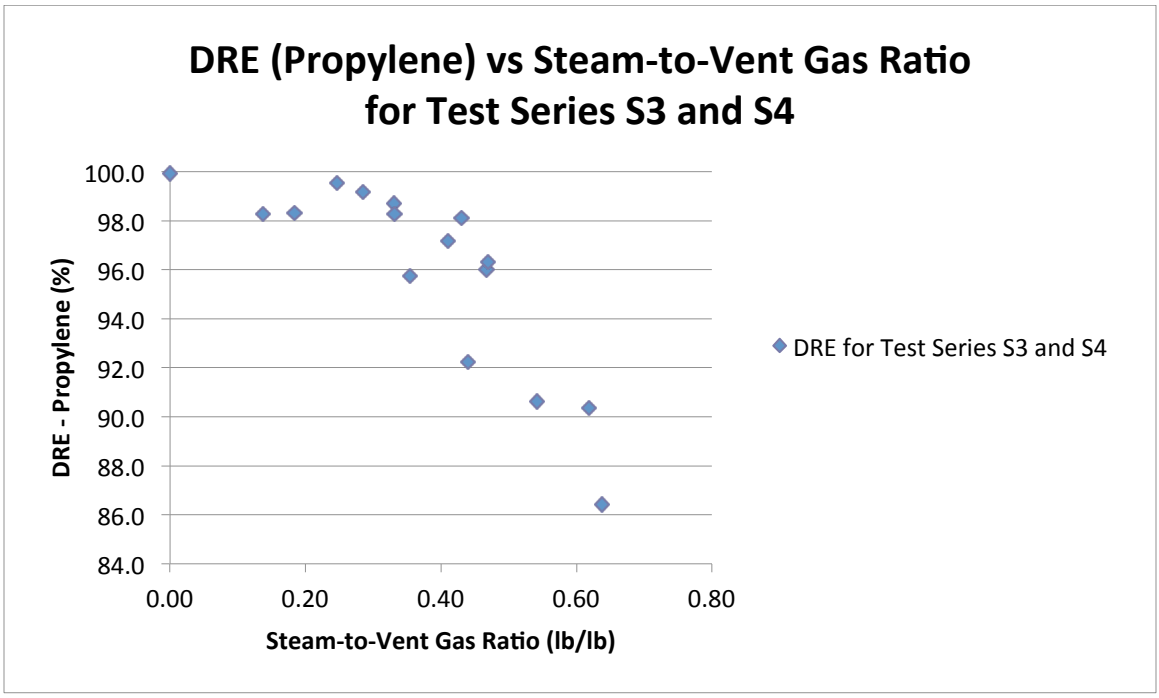

Figure ES-4a. DRE vs Steam-to-Vent Gas Ratio for All Test Series S3 and S4 [5-15a]
(Note DRE (Propylene) range = 84 to 100%)

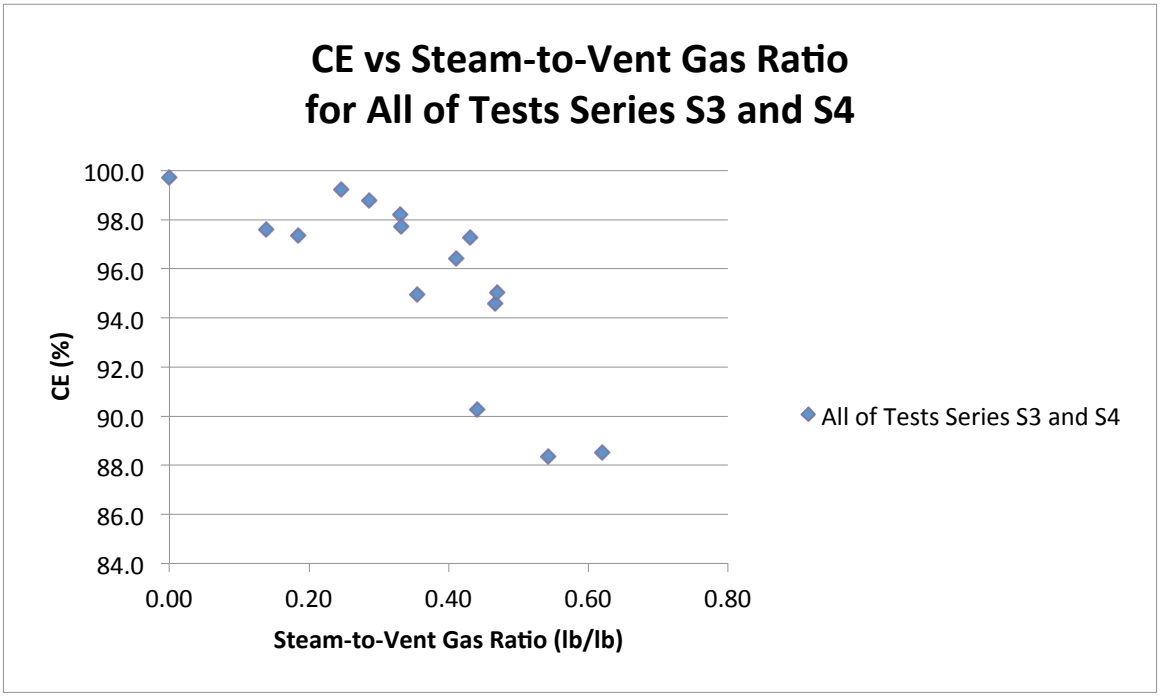

Figure ES-4b. CE vs Steam-to-Vent Gas Ratio for All Test Series S3 and S4 [5-15b]
(Note CE range = 84 to 100%)

Figures ES-5a and ES-5b show DRE (propylene) versus steam assist rate and CE versus steam assist rate, respectively, for the two nominal steam flare vent gas flow rates, 937 lb/hr and 2,342 lb/hr at a nominal LHV of 600 Btu/scf. For a nominal 937 lb/hr vent gas flow rate (Test Series S5), a DRE (propylene) ≥ 98% was achieved at a S/VG = 0.82, 770 lb/hr total steam assist (center steam = 490 lb/hr). A lower S/VG would have been required to achieve a DRE (propylene) ≥ 99%. The 2,342 lb/hr vent gas flow rate (Test Series S6) was able to sustain a 99% DRE (propylene) up to a S/VG = 0.84, 2,000 lb/hr total steam assist (center steam = 520 lb/hr) before the DRE and CE fell below 99% DRE. This LHV and vent gas flow rate did achieve a DRE (propylene) ≥ 99% with a level of steam assist greater than the minimum levels of steam assist (500 lb/hr center, 750 lb/hr upper) recommended to industry by flare manufacturers as reported to the TCEQ by industry representatives for the 36-inch diameter stream flare model used in this study.

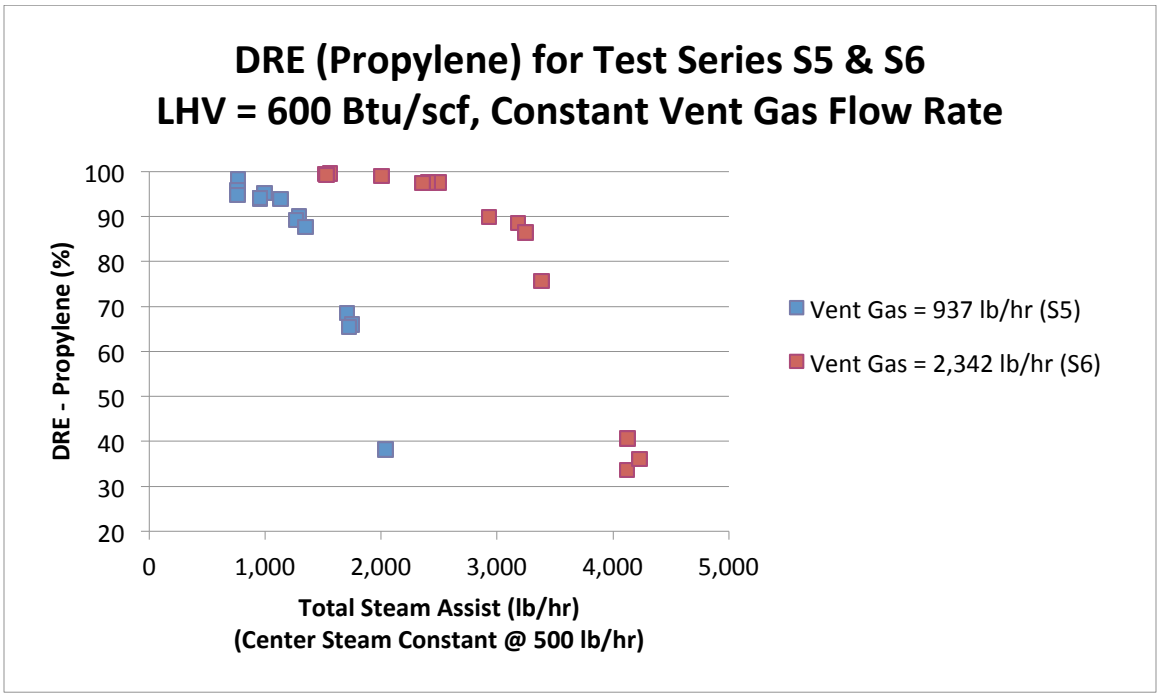

Figure ES-5a. DRE vs Steam Assist for Test Series S5 and S6 [5-13a]

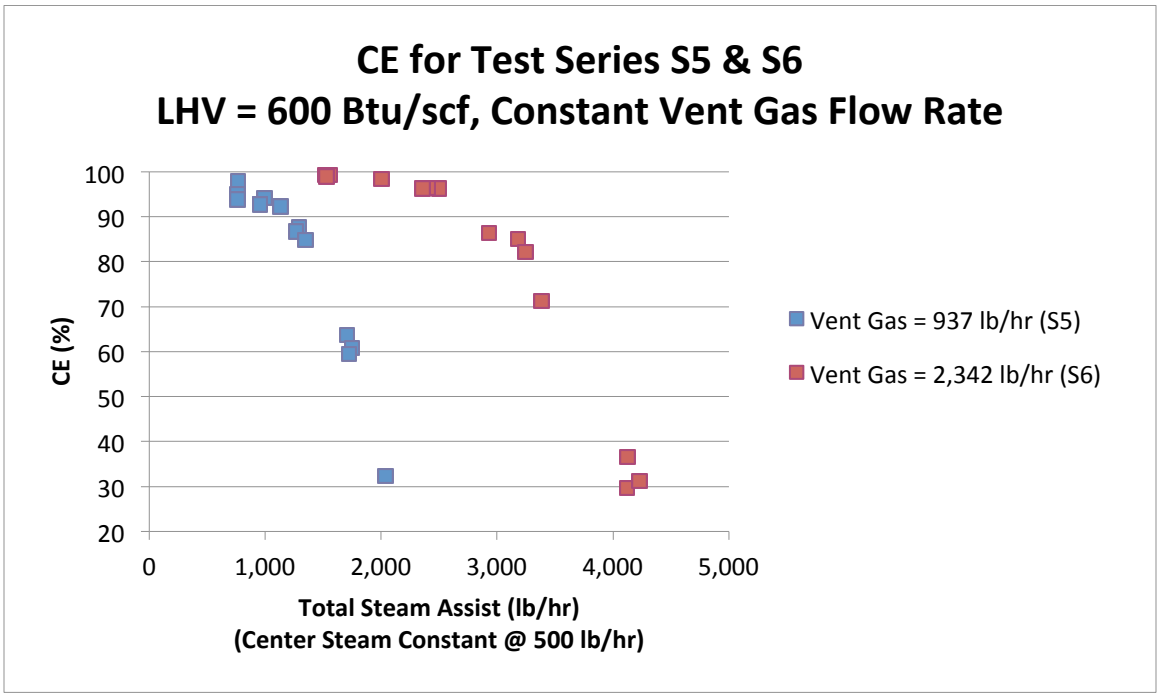

Figure ES-5b. DRE vs Steam Assist for Test Series S5 and S6 [5-13b]

Figures ES-6a and ES-6b show DRE (propylene) versus S/VG ratio and CE versus S/VG ratio, respectively, for all of tests series S5 and S6 on one graph. Figures ES-7a and ES-7b are the same graphs focusing on the range DRE (propylene) ≥ 84%. It can be seen from Figures ES-7a and ES-7b that in this range of S/VG ratios there can be multiple DREs.

The previous graphs have illustrated the effect of varying steam assist on a vent gas of constant flow rate and constant LHV. Figures ES-8a and ES-8b show how DRE and CE vary as the vent gas flow rate is varied for five different steam assist combinations that were held constant as the vent gas flow rate was varied. The nominal LHV was held constant at 350 Btu/scf for all tests shown in these two figures. Note that the horizontal axis (vent gas flow rate) is reversed and decreases from left to right. These graphs show the significant effect center and total steam have on DRE at low vent gas flow rates. The flare performance curves with small negative slopes are those with the lowest level of center steam (0 lb/hr) followed by low levels (500 lb/hr and 835 lb/hr) of upper steam assist flow rates (Test Series S8 and S10). The graph with the larger negative slopes (Test Series S7) has the highest center steam flow rate (500 lb/hr). For all graphs, if steam assist is held constant, as vent gas flow rate increases, DRE increases.

Figures ES-9a and ES-9b show the relationship between DRE (propylene) and combustion zone gas net heat value (CZG NHV) for Test Series S3 to S6. Figures ES-10a and ES-10b provide the same information for Test Series S7 to S11. Note that the horizontal axis (CZG NHV) in Figures ES-9b and ES-10b has been reversed and decreases from left to right. Figures ES-9b and ES-10b focus on the range of DRE (Propylene) ≥ 84 % to better examine the relationship between these two parameters. There can be multiple DREs for CZG NHVs up to at least 250 Btu/scf and perhaps as high as 300 Btu/scf. Once again, this is due in part to the fact that, in this range of S/VG ratios, steam added at the center has a different effect on DRE than steam added at the upper nozzles.

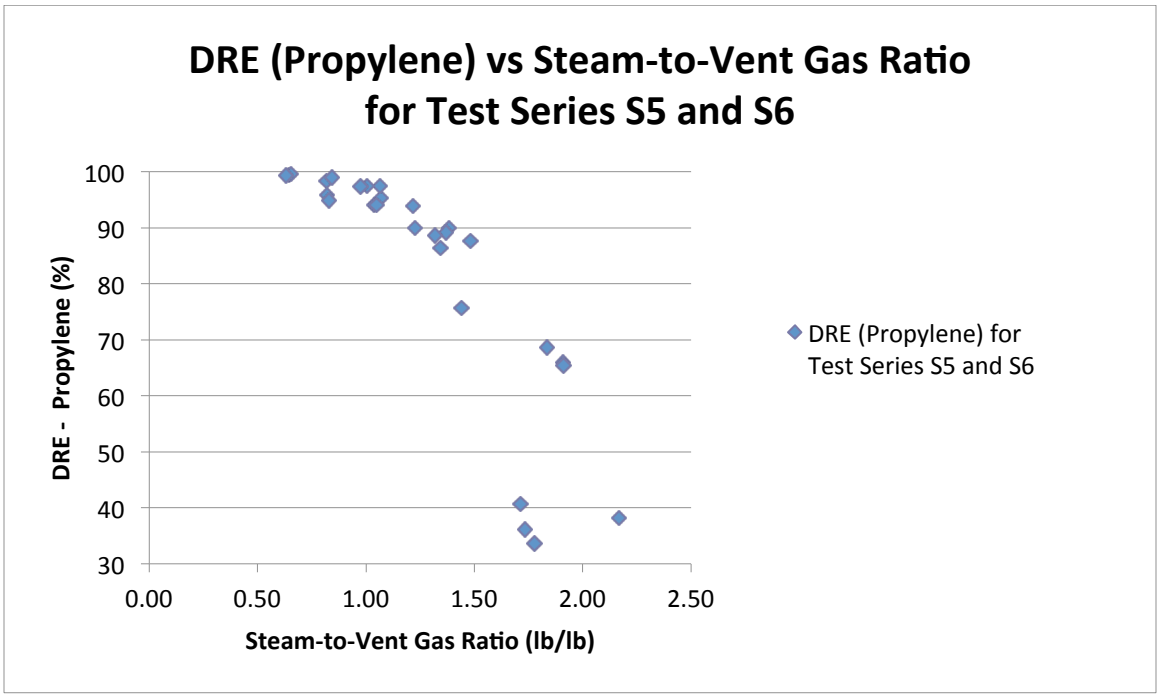

Figure ES-6a. DRE vs Steam-to-Vent Gas Ratio for All Test Series S5 and S6 [5-16a]

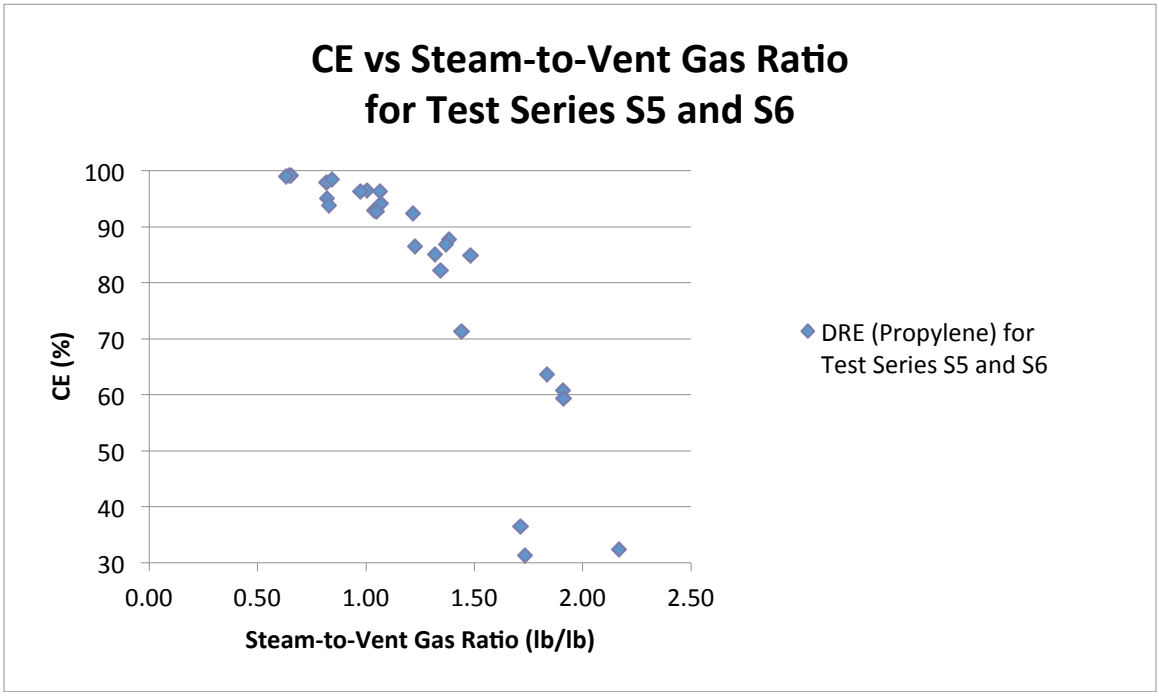

Figure ES-6b. CE vs Steam-to-Vent Gas Ratio for All Test Series S5 and S6 [5-16b]

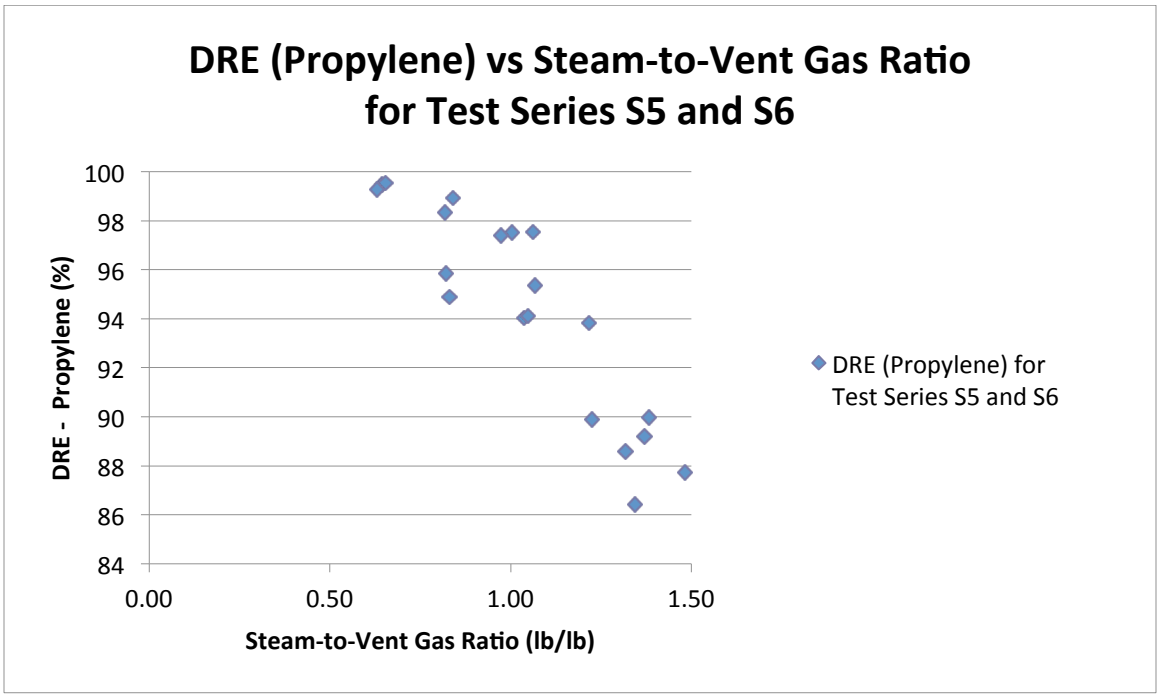

Figure ES-7a. DRE vs Steam-to-Vent Gas Ratio for All Test Series S5 and S6 [5-17a]
(Note DRE (Propylene) range = 84 to 100%)

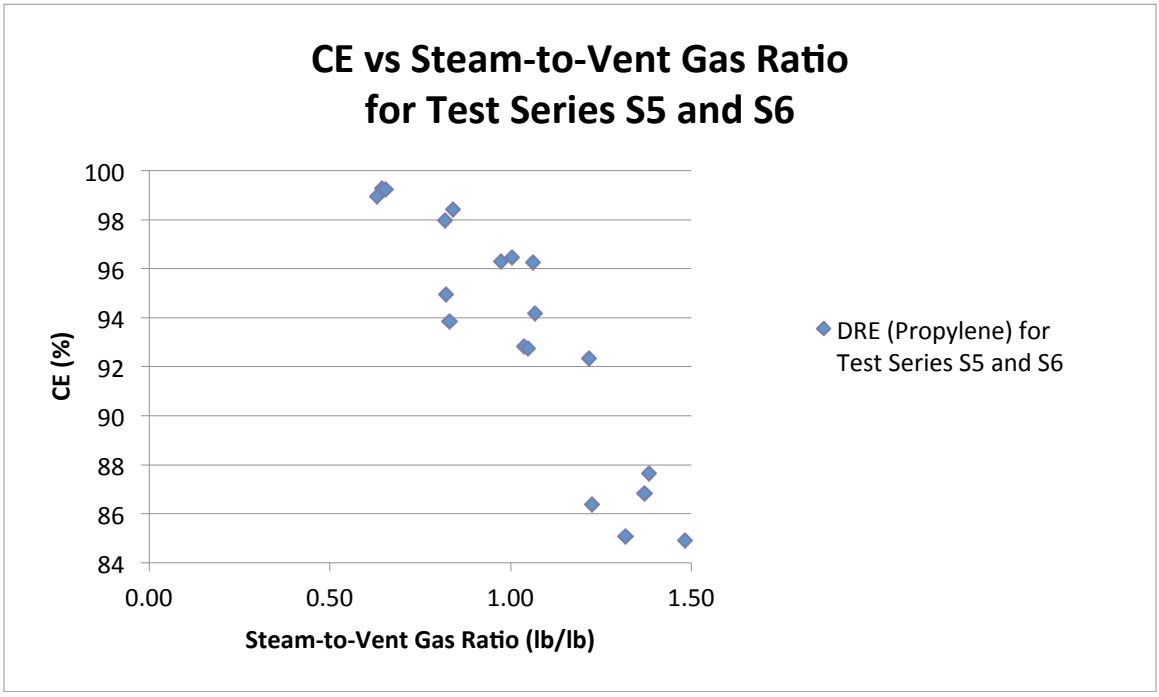

Figure ES-7b. CE vs Steam-to-Vent Gas Ratio for All Test Series S5 and S6 [5-17b]
(Note CE range = 84 to 100%)

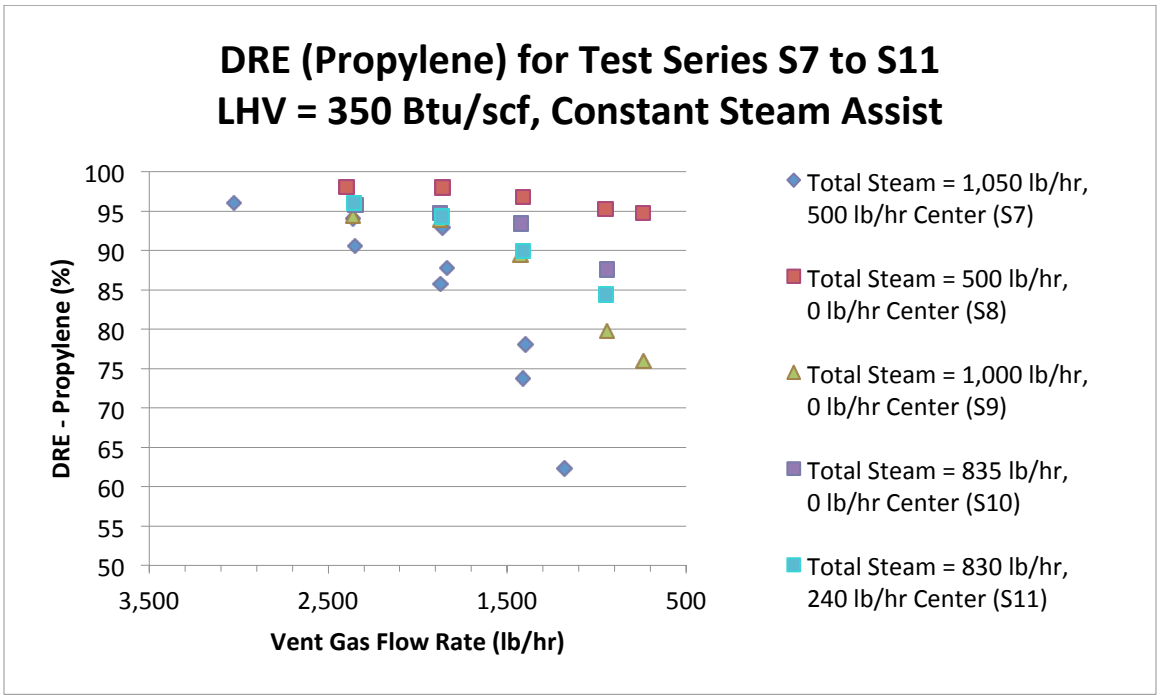

Figure ES-8a. DRE vs Vent Gas Flow Rate for Test Series S7, S8, S9, S10 and S11 [5-19a]
(Note values on horizontal axis decrease from left to right)

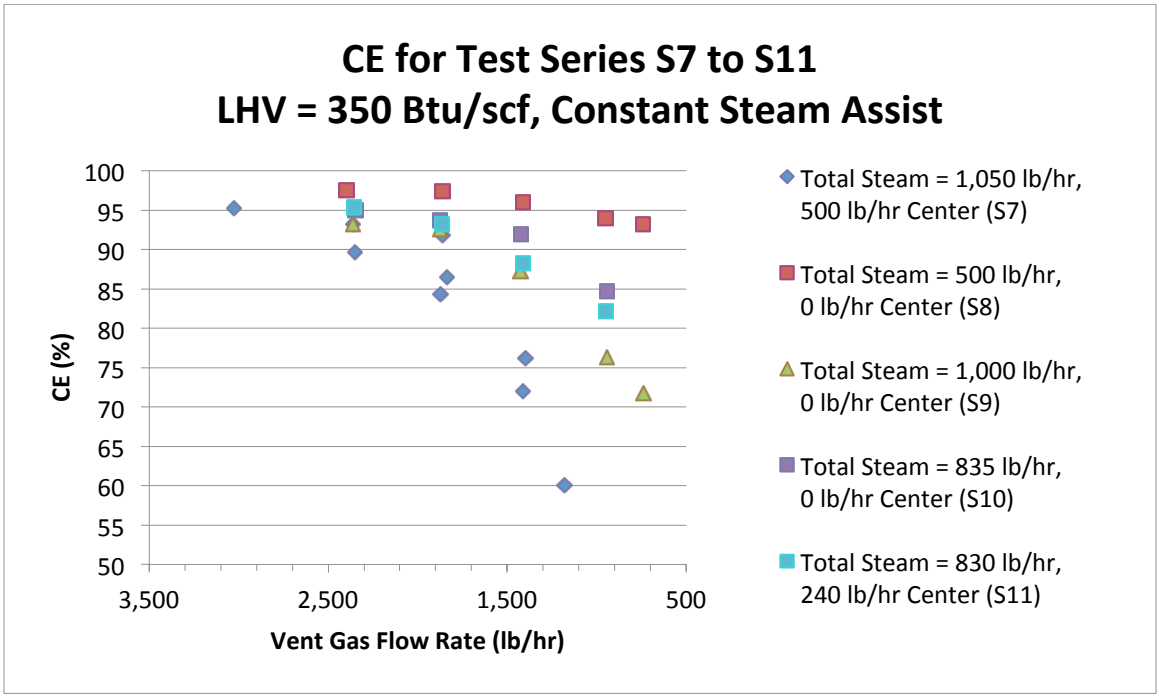

Figure ES-8b. CE vs Vent Gas Flow Rate for Test Series S7, S8, S9, S10 and S11 [5-19b]
(Note values on horizontal axis decrease from left to right)

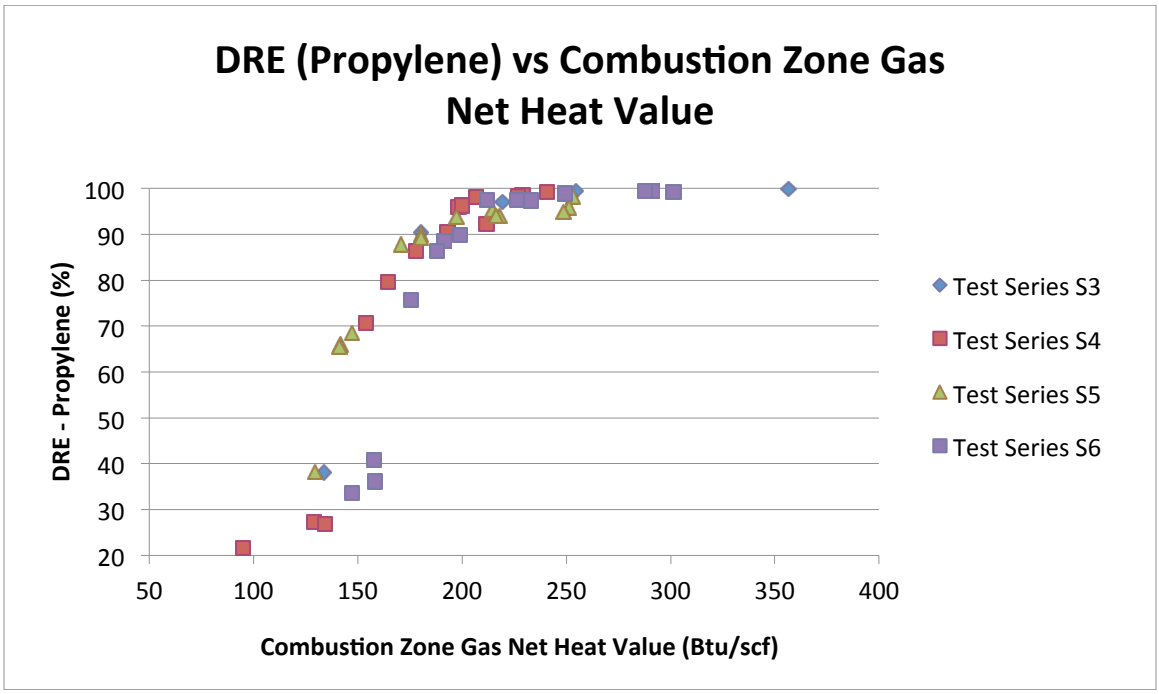

Figure ES-9a. DRE vs CZG NHV for Test Series S3, S4, S5 and S6 [5-20a]

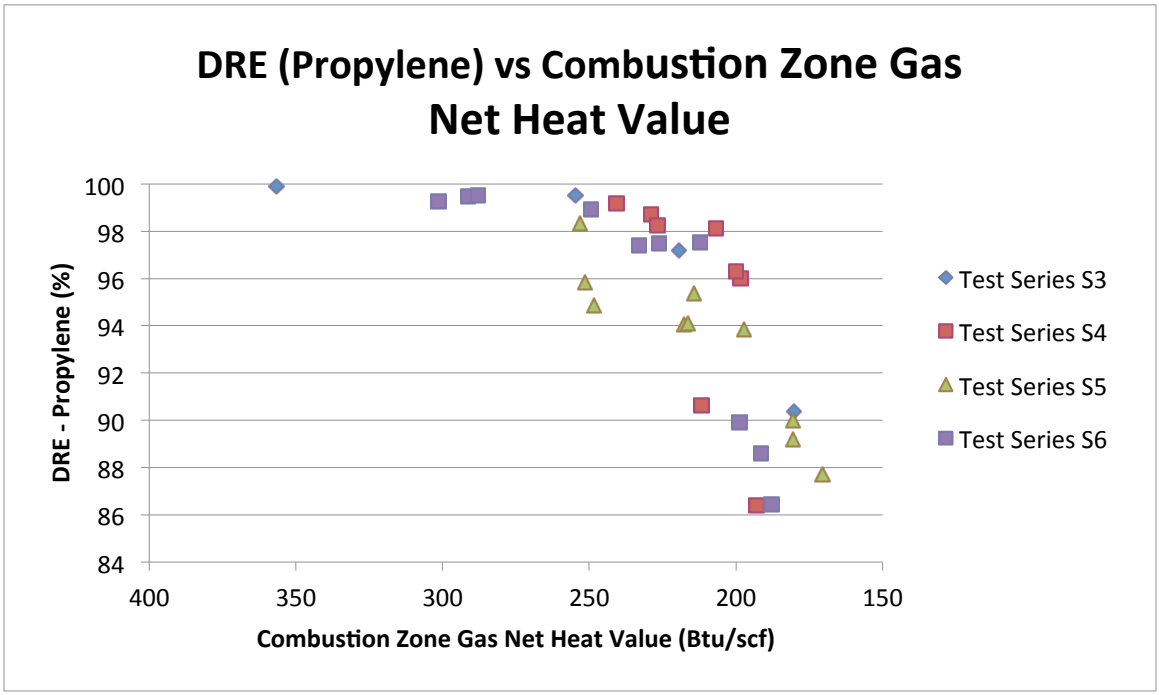

Figure ES-9b. DRE vs CZG NHV for Test Series S3, S4, S5 and S6 [5-20b]
(Note vertical axis DRE (Propylene) range = 84 to 100% and
values on horizontal axis decrease from left to right)

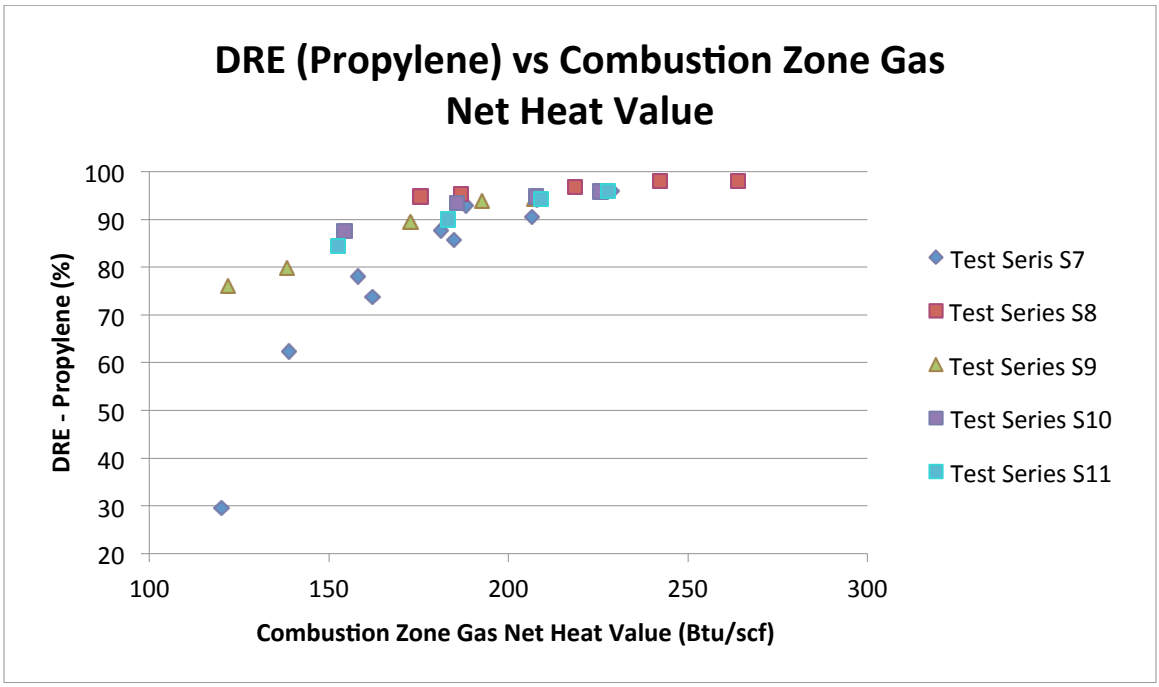

Figure ES-10a. DRE vs CZG NHV for Test Series S7, S8, S9, S10 and S11 [5-21a]

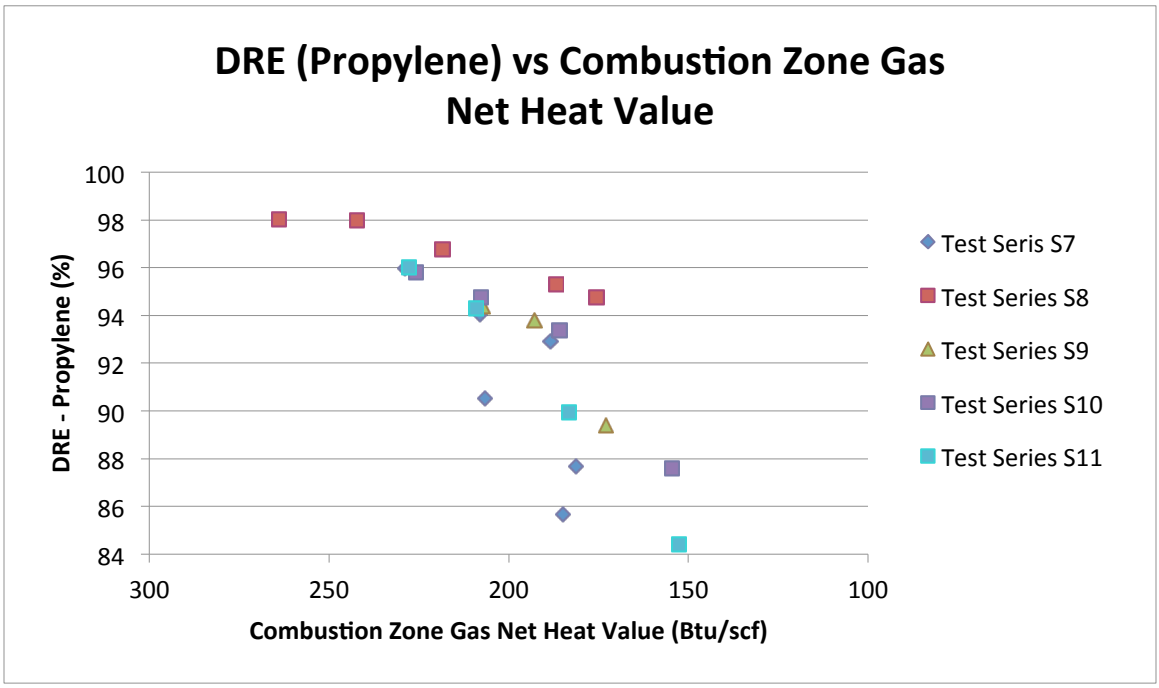

Figure ES-10b. DRE vs CZG NHV for Test Series S7, S8, S9, S10 and S11 [5-21b]
(Note vertical axis DRE (Propylene) range = 84 to 100% and
values on horizontal axis decrease from left to right)

Figures ES-11a and ES-11b show DRE (propylene) versus air assist and CE versus air assist for the nominal LHV = 350 Btu/scf and the two nominal vent gas flow rates, 359 lb/hr and 937 lb/hr. Figures ES-12a and ES-12b show DRE (propylene) versus air assist and CE versus air assist for the nominal LHV = 600 Btu/scf and the two nominal vent gas flow rates, 359 lb/hr and 937 lb/hr. These show an almost linear decline in DRE and CE as air assist increases. The A4 and A6 test series with the vent gas flow rate having an LHV = 600 Btu/scf has a slope that is not as steep but falling below DRE = 99 % at air assist levels that equal approximately 6 times the quantity of air required for stoichiometric combustion. As air assist is increased beyond this quantity, the DRE decreases almost linearly for both of the nominal LHVs used in this study.

Figures ES-13a and ES-13b show DRE (propane) versus vent gas flow rate and CE versus vent gas flow rate for three different steam assist combinations that were held constant as the vent gas flow rate was varied. The LHV was held constant at the nominal 350 Btu/scf for all tests shown in these two figures. As with propylene, the highest DREs (> 99.0%) are achieved in test series (S14) with the lowest center steam (0 lb/hr) and 540 lb/hr upper steam flow rates, while test series S12 with the highest center steam (490 lb/hr) and upper (560 lb/hr) steam assist flow rates only achieved a DRE = 97.7% (CE = 97.4%).

Figures ES-14a and ES-14b show DRE (propane) versus air assist and CE versus air assist. The LHV was held constant at the nominal 350 Btu/scf for all tests shown in these two figures. As with propylene, at air assist levels that equal approximately 6 times the quantity of air required theoretically for stoichiometric combustion or less, SR $\leq$ 6, DRE (propane) was $\geq$ 99%.

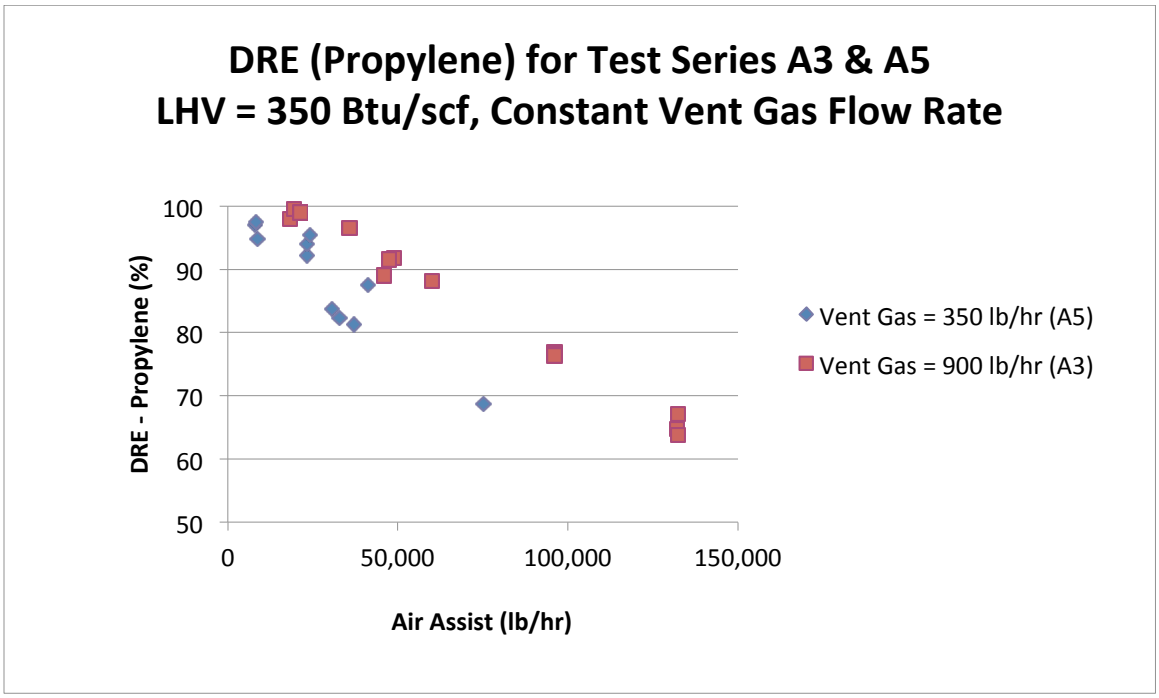

Figure ES-11a. DRE vs Air Assist for Test Series A3 and A5 [5-22a]

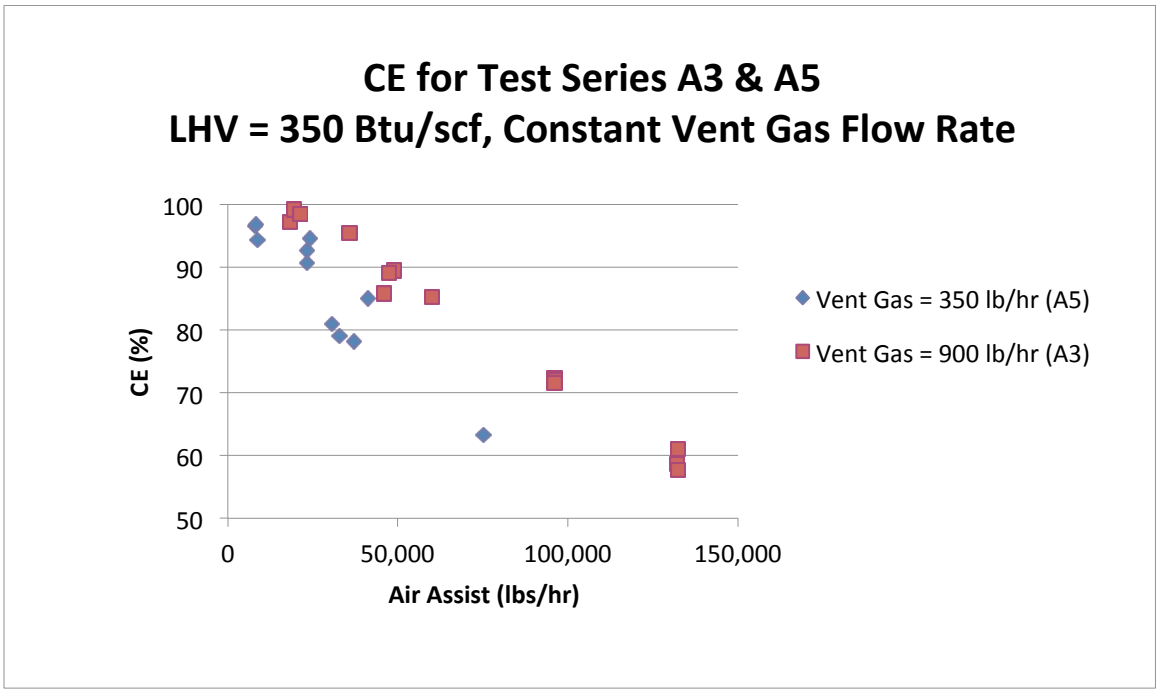

Figure ES-11b. CE vs Air Assist for Test Series A3 and A5 [5-22b]

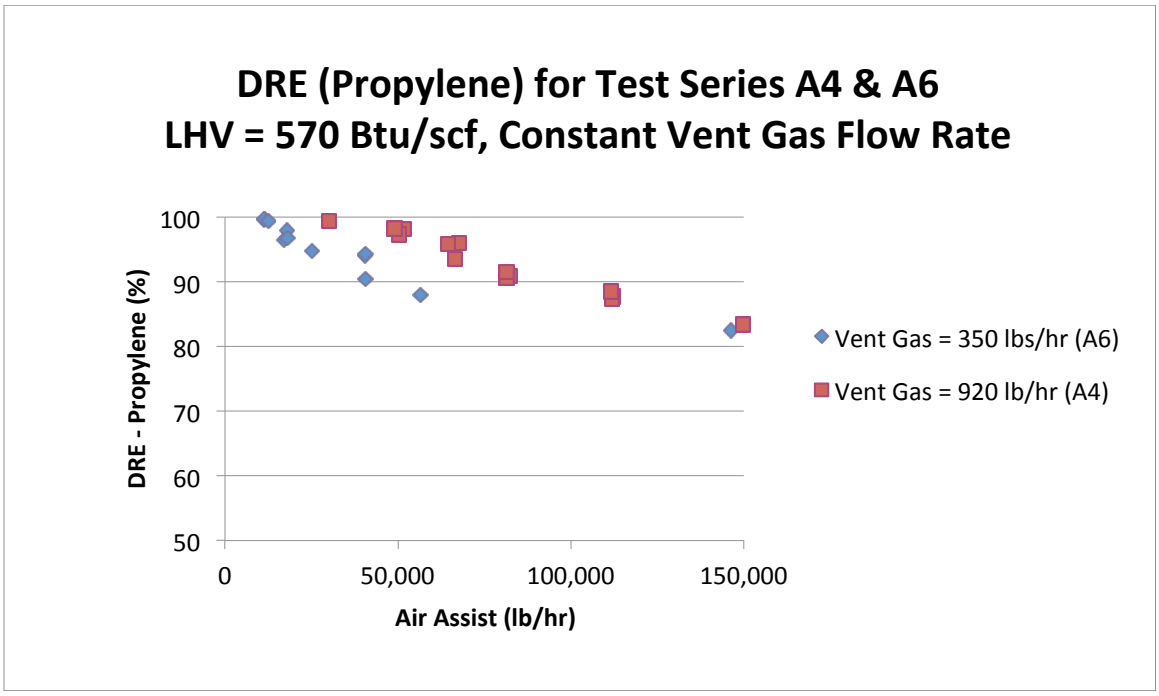

Figure ES-12a. DRE vs Air Assist for Test Series A4 and A6 [5-23a]

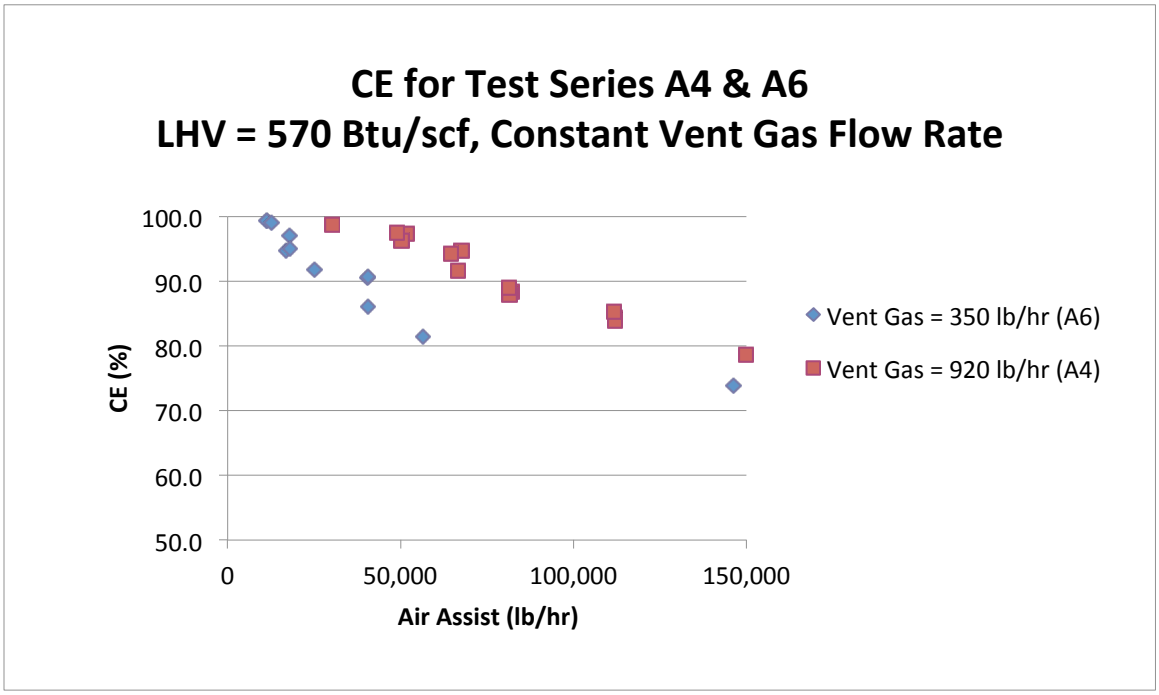

Figure ES-12b. CE vs Air Assist for Test Series A4 and A6 [5-23b]

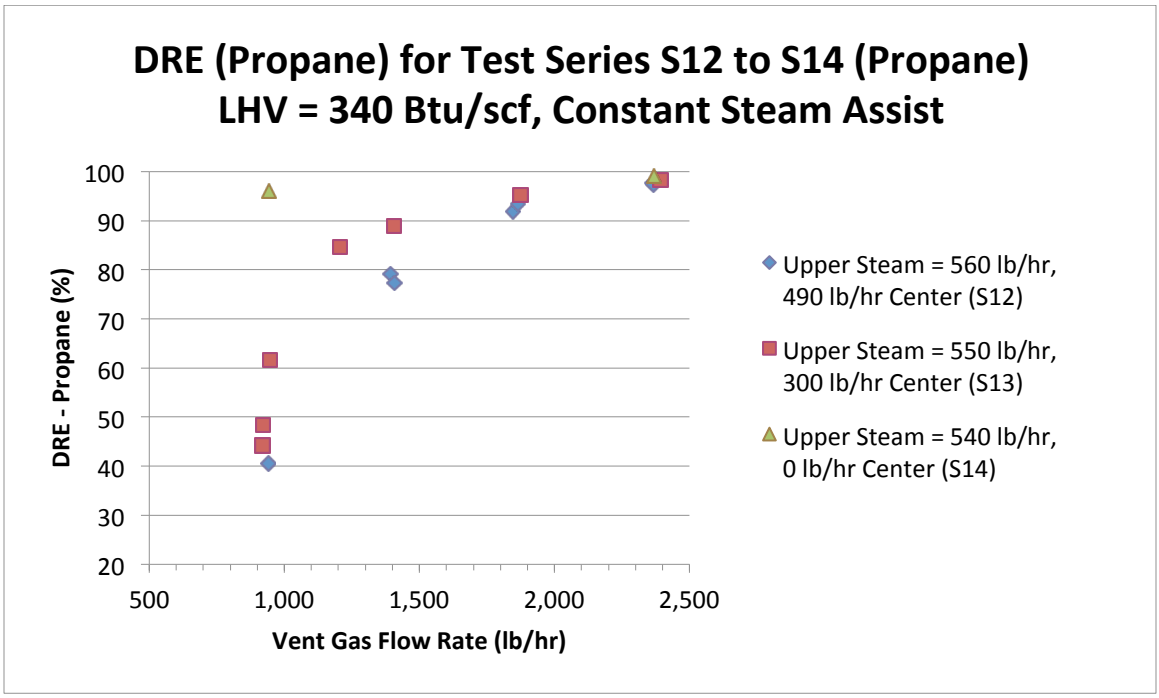

Figure ES-13a. DRE vs Vent Gas Flow Rate for Test Series S12, S13 and S14 [5-24a]

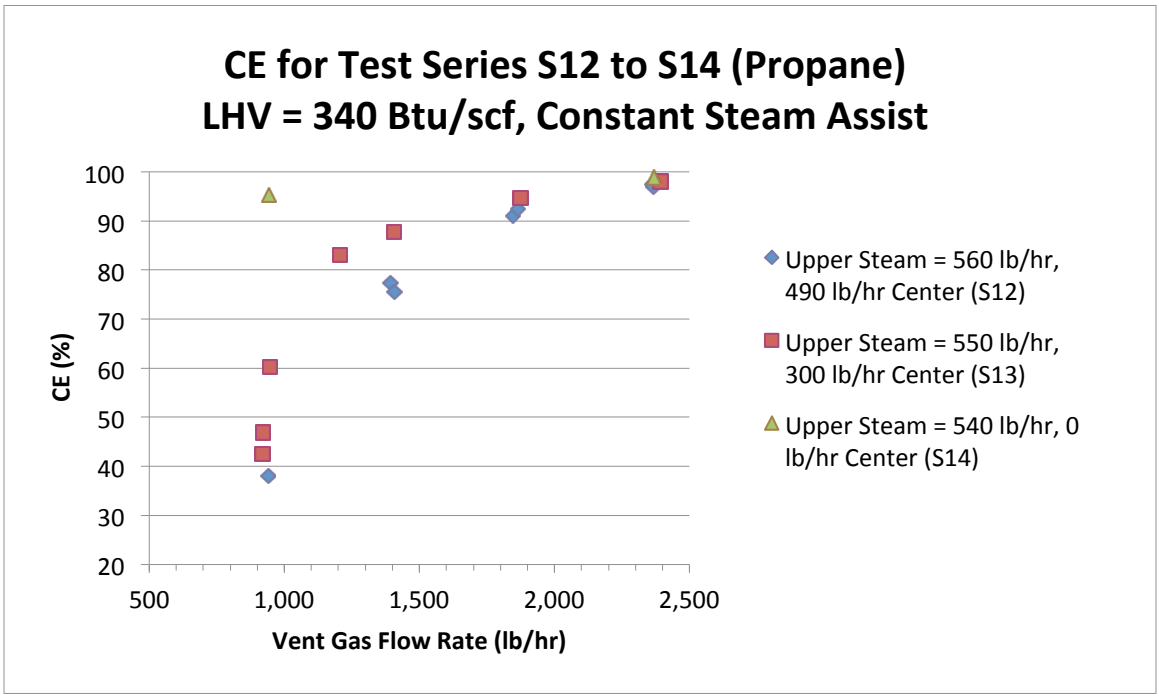

Figure ES-13b. CE vs Vent Gas Flow Rate for Test Series S12, S13 and S14 [5-24b]

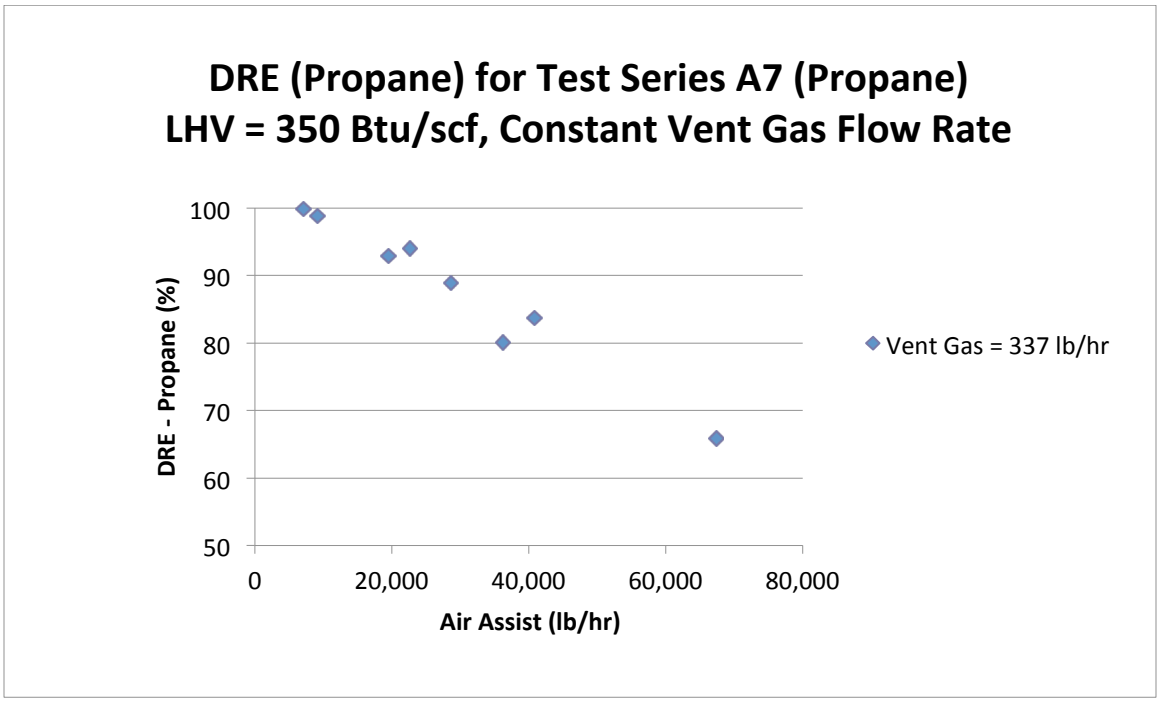

Figure ES-14a. DRE vs Air Assist for Test Series A7 [5-25a]

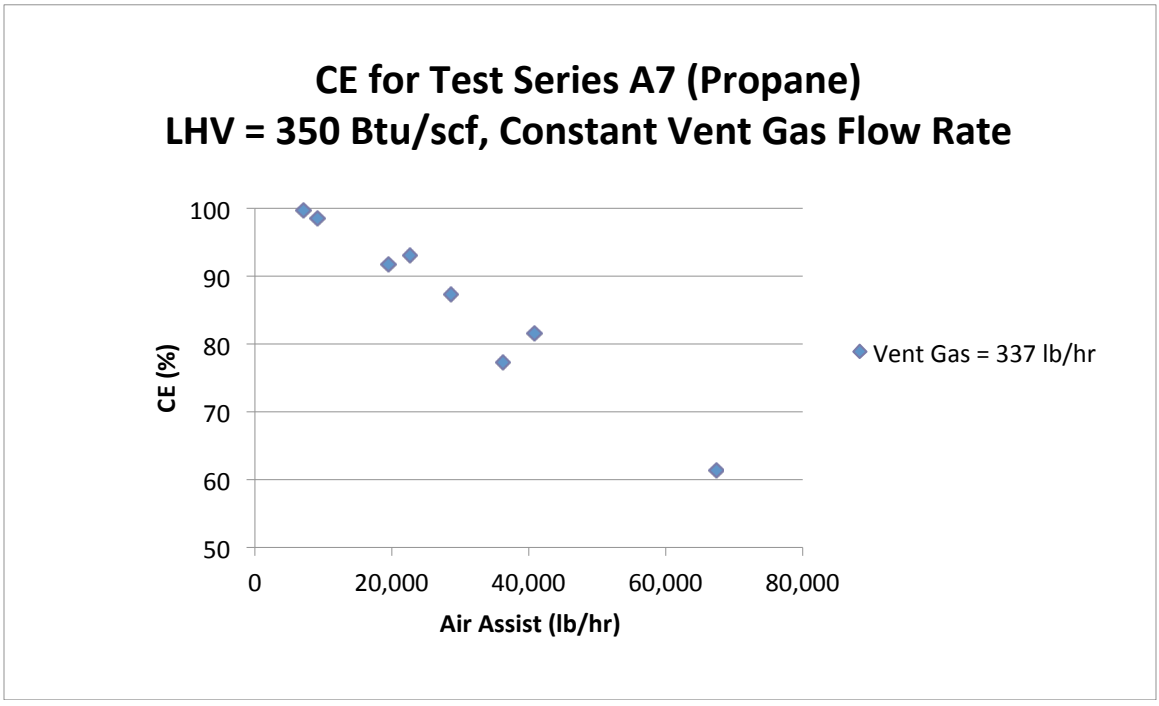

Figure ES-14b. CE vs Air Assist for Test Series A7 [25b]

Comparison with Remote Sensing Technology Measurements with Test Results

There were three remote sensing technologies participating in the study: IMACC PFTIR and AFTIR spectrometers, Telops Hyper-cam passive imaging radiometric spectrometer, and LSI FLIR GasFindIR and thermal IR cameras. The LSI cameras provide visual images of hydrocarbons in the gas phase and are useful in detection of these gases but were not used for quantitative assessment of flare combustion. The discussion in this section will focus on the IMACC and Telops instruments, which can measure the combustion efficiency of the flare. Telops can also make mass flow rate measurements of hydrocarbons in the plume. However, these results were provided so late in the preparation of this report that the comparison of the Telops mass flow rate results will be provided as an addendum to this report at a later date.

As summarized in Section 3, the measurement of emissions in samples extracted from the plume and analyzed by ARI provided the baseline or reference DRE and CE values against which the remote sensing technologies would be compared. The results of the analyses of the extractive samples and determination of DRE and CE by ARI were not provided to IMACC or Telops. Subsequent to the field tests, IMACC and Telops submitted their CE measurements for each test run, including their standard deviation (σ) for their measurements.

Three statistical criteria were selected to compare the measurements of IMACC and Telops with the ARI values. The first two are the mean difference and the standard deviation of the difference. These terms are defined numerically as follows.

$$mean\ difference = \frac{\sum_{i=1}^{N} ABS\ (CE_{RS} - CE_{ARI})_i}{N} \qquad \text{Eq. ES.3}$$

$$standard\ deviation = \sqrt{\frac{\sum_{i=1}^{N} [(CE_{RS} - CE_{ARI})_i]^2}{N-1}} \qquad \text{Eq. ES.4}$$

where

mean difference =	average of the absolute values of the difference between the CE determined by the remote sensing contractor and the CE determined by ARI for test point i
standard deviation =	standard deviation of the differences between the CE determined by the remote sensing contractor and the CE determined by ARI for the test point *i*
CE_{RS} =	combustion efficiency determined by the remote sensing contractor for the test point *i*
CE_{ARI} =	combustion efficiency determined by ARI for the test point *i*
N =	total number of test points in the subset

The third criterion is data return. Data return is the percentage of the total number of possible test points for which data were reported. It is defined numerically as follows.

$$data\ return = \frac{Number\ of\ test\ points\ for\ which\ data\ were\ reported}{Total\ number\ of\ test\ points} \times 100 \quad \text{Eq. ES.5}$$

To more easily compare IMACC's and Telops' data with ARI's, the CE data sorted by ARI CE (CE_{ARI}) value in descending order for the range 100% ≥ CE ≤ 80%. On the assumption that the accuracy of the CE values may not be constant across this entire range, the data have been divided as follows: CE_{ARI}≥ 95%; 90 ≥ CE_{ARI} < 95%; 85% ≥ CE_{ARI} < 90%; and 80% ≥ CE_{ARI}< 85%. The difference between the IMACC's and Telops's CE values and the CE_{ARI} values are shown in each table. The CE mean differences and the standard deviation of the CE differences are calculated using Eqs. ES-3 and ES-4. These two criteria are summarized in Table ES-2, with data return.

Steam Flare Tests
As shown in Table ES-2, the mean difference and the standard deviation of the CE differences for the IMACC AFTIR and PFTIR increase as the CE_{ARI} decreases. The mean difference and the standard deviation of the CE differences for the Telops CE values do not have a clear trend. In examining the differences in CE values in Table D-2, the inaccuracies in the IMACC AFTIR and PFTIR do not appear to have a bias relative to CE_{ARI}, while the Telops values tend to be biased lower than the CE_{ARI} values.

In examining the data return in Table ES-2, the IMACC AFTIR was 100% in all four ranges, while the PFTIR was 100% in all ranges except 90% ≤ CE_{ARI} < 95%, where it was 95%. Data return for the Telops CE values was less than 45% for all ranges except 80% ≤ CE_{ARI} < 85%, where it was 88%.

Air Flare Tests
As shown in Table ES-2, the mean difference and the standard deviation of the CE differences for the IMACC PFTIR increase as the CE_{ARI} decreases. The IMACC AFTIR was not deployed for any of the air flare tests. In examining the CE differences in Table ES-2, the inaccuracies in these data tend to be biased low relative to the CE_{ARI} values.

The number of Telops data points, five, for all four ranges of the air flare tests are too few to statistically develop trend data. Additionally, the data return for these four CE_{ARI} ranges did not exceed 15%. Therefore, no additional analyses will be performed on the Telops air flare data.

Table ES-2. Summary of Comparison Criteria for Remote Sensing CE Values for CE_{ARI} > 80% [10-1]

Steam					
Range	Criterion	Telops	AFTIR	PFTIR	ARI
$CE_{ARI} \geq 95\%$	Mean Difference (% pts)	20.2	1.7	1.1	
	Standard Deviation (% pts)	32.2	2.5	2.1	
	Data Return (%)	39	100	100	
	Number of Test points	14	22*	36	36
$90\% \leq CE_{ARI} < 95\%$	Mean Difference (% pts)	9.6	3.2	2.2	
	Standard Deviation (% pts)	11.3	3.7	2.9	
	Data Return (%)	40	100*	95	
	Number of Test points	8	8	19	20
$85\% \leq CE_{ARI} < 90\%$	Mean Difference (% pts)	3.8	12.2	2.8	
	Standard Deviation (% pts)	6.1	14.8	3.4	
	Data Return (%)	27	100*	100	
	Number of Test points	3	6	11	11
$80\% \leq CE_{ARI} < 85\%$	Mean Difference (% pts)	18.8	12.2	4.6	
	Standard Deviation (% pts)	26.1	16.7	5.9	
	Data Return (%)	75	100*	100	
	Number of Test points	6	4	8	8
Air					
Range	Criterion	Telops	AFTIR	PFTIR	ARI
$CE_{ARI} \geq 95\%$	Mean Difference (% pts)	1.2		1.9	
	Standard Deviation (% pts)	2.0		2.5	
	Data Return (%)	10		100	
	Number of Test points	2		21	21
$90\% \leq CE_{ARI} < 95\%$	Mean Difference (% pts)	4.4		3.5	
	Standard Deviation (% pts)	6.3		4.1	
	Data Return (%)	11		100	
	Number of Test points	2		18	18
$85\% \leq CE_{ARI} < 90\%$	Mean Difference (% pts)	NMR		5.5	
	Standard Deviation (% pts)	NMR		6.5	
	Data Return (%)	0		100	
	Number of Test points	0		10	10
$80\% \leq CE_{ARI} < 85\%$	Mean Difference (% pts)	10.2		8.5	
	Standard Deviation (% pts)	10.2		9.9	
	Data Return (%)	13		100	
	Number of Test points	1		8	8

NMR = No CE vales were reported for these tests.

*Instrument not on site to obtain measurements during some of these test points.

In summary, the IMACC PFTIR mean differences for the range $CE_{ARI} \geq 90\%$ for both the air and steam flare tests averaged 2.2 percentage points, with an average standard deviation of the CE differences of 2.9 percentage points and average data return of 99%.

The IMACC AFTIR mean difference for the range $CE_{ARI} \geq 90\%$ for the steam flare tests averaged 2.5 percentage points, with an average standard deviation of the CE differences of 3.1 percentage points and an average data return of 100%.

The Telops Hyper-Cam mean difference for the range $CE_{ARI} \geq 90\%$ for the steam flare tests averaged 14.9 percentage points, with an average standard deviation of the CE differences of 22.8 percentage points and an average data return of 39%.

It is important to note that the difference in some of the values between the IMACC and Telops instruments and the ARI measurements may due to less than ideal aiming due to interference of the plume sampling system. In a few instances, the remote sensing operators indicated that the position of the plume sampling system had restricted their ability to aim their instruments.

All participants were required to submit their preliminary data within six weeks of completion of the field campaign. Telops was unable to do so. Their report explains some of the challenges they had in making measurements and processing the large volume of data generated by their sensor and the number of test points conducted in this study.

Major findings of the study were:

1. At a vent gas LHV = 350 Btu/scf and flow rates of 0.1% and 0.25% of rated design capacity (propylene) for the John Zink Model EE-QSC-36" steam flare this flare design was able to achieve DREs (propylene) of > 99% and CE > 99%. At a nominal vent gas flow rate 937 lb/hr (0.1%), an S/VG = 0.25 or less was required to achieve a DRE (propylene) > 99%. This S/VG would equate to a total steam assist of approximately 234 lb/hr, which would be less than the minimum recommended (as reported by industry) steam-assist rates of center = 500 lb/hr and upper = 750 lb/hr for this flare. The John Zink Company LLC recommends continuous minimum center steam of 300 lb/hr and 525 lb/hr upper steam for this flare design. This study does not recommend that steam assist rates less than that recommended by the flare manufacturer be used.

2. At a vent gas LHV = 350 Btu/scf and flow rates of 0.25% and 0.65% of rated design capacity (propylene) for the John Zink Model LHTS-24/60 air flare, this flare model was able to achieve DREs (propylene) of > 99% and CE > 99%.

3. The most efficient flare operation, as measured by the DRE and CE, for the flare operating conditions tested, was achieved at or near the incipient smoke point (ISP). Higher efficiencies could have been achieved with steam or air assist slightly less than the ISP assist value but this condition, i.e., a smoking flare, would not have been in compliance with 40 CFR § 60.18. Therefore, the minimum levels of steam or air assist that comply with the flare manufacturer's recommendations should be used when possible.

4. At these low vent gas flow rates (nominally 937 lb/hr and 2,342 lb/hr) and low LHVs (nominally 350 Btu/scf and 600 Btu/scf), the flare performance curve of DRE vs steam assist has a very short to non-existent "shelf" before the DRE falls off to less than 98%. Beyond this point, the DRE and CE decrease almost linearly as steam assist increases.

5. For nominal LHVs of 350 Btu/scf and 600 Btu/scf and vent gas flow rates of 359 lb/hr and 937 lb/hr, air flare test data showed that an air assist quantity of 6 times the stoichiometric air-to-fuel ratio (lb/lb) produced a DRE > 99%. Higher levels of air assist produced lower DREs in an almost linearly decreasing manner.

6. The IMACC PFTIR and AFTIR mean differences between their values of CE and the ARI values of CE averaged 2.2 and 2.5 percentage points, respectively, and had average standard deviations of the CE differences of 2.9 and 3.1 percentage points in the range $CE_{ARI} \geq 90\%$ for the air and steam flare tests. The PFTIR and AFTIR had average data returns of 99% and 100% in this range.

7. The Telops Hyper-Cam mean differences between their values of CE and the ARI values of CE averaged 14.9 percentage points, with an average standard deviation of the CE differences of 22.8 percentage points in the range $CE_{ARI} \geq 90\%$. The Telops Hyper-Cam had average data return of 39% in this range.

Table of Contents

Appendix D – Summary of Steam-Assisted Flare Test Data

Appendix E – Summary of Air-Assisted Flare Test Data

Appendix F – Emissions Measured During Propylene Flare Tests for DRE (Propylene) > 60%

Appendix G – Method for Determining Vent Gas Composition and Flow Rate

Appendix H – Tulsa Natural Gas Analyses

Appendix I – Method of Determining Destruction Removal Efficiency and Combustion Efficiency Using the Flare Plume Extractive Sampling System and Quality Assurance Procedures Employed During Field Tests

Appendix J – Wind Speed and Direction Variation for Test Series S3, S4, S5, S6, A3, A4, A5, and A6

Appendix K – Quality Assurance Documentation for Test Systems and Instrumentation Used During Field Tests (This Appendix is included on the digital media section of the report. It is available only upon request.)

Appendix L – Video Image and Raw Data Files (This Appendix is included on the digital media section of the report. Due to the size of the electronic files, it is available only upon request.)

List of Figures

List of Figures
(continued)

List of Figures
(continued)

List of Tables

List Acronyms, Abbreviations and Symbols

A

A/F	Theoretical stoichiometric air-to-fuel ratio, mass basis (lb/lb)
ARI	Aerodyne Research, Inc.
AFTIR	Active Fourier Transform Infrared

B

Btu	British thermal unit

C

CE	Combustion efficiency
CEER	Center for Energy and Environmental Resources
CFD	Computational Fluid Dynamics
CFR	Code of Federal Regulations
CH_3CHO	Acetaldehyde
CH_4	Methane
C_2H_4	Ethylene, ethene
C_3H_6	Propylene, propene
CO	Carbon monoxide
CO_2	Carbon dioxide

D

°	Degree of temperature
°F	Degree Fahrenheit
DQO	Data Quality Objective
DRE	Destruction and removal efficiency

E

EPA	U.S. Environmental Protection Agency

F

FLIR	Forward Looking Infrared
fps	Feet per second
ft^2	Feet squared

G

GC	Gas Chromatograph
GPS	Global Positioning System

H

HCHO	Formaldehyde

List Acronyms, Abbreviations and Symbols (continued)

HCOOH	Formic acid

I

IMACC	Industrial Monitor and Control Corporation
in	Inch
IR	Infrared
ISP	Incipient smoke point

J

JZ	John Zink Company, LLC

L

lb/hr	Pounds per hour
LHV	Lower Heating Value
LL	Lower Limits
LSI	Leak Surveys, Inc.

M

MPH	Miles per hour
mm/Hg	Millimeters of mercury
min	Minutes
MFR	Momentum flux ratio

N

NA	Not Applicable
NO	Nitric oxide
NO_2	Nitrogen dioxide
No.	Number

O

O_3	Ozone

P

%	Percent
PFTIR	Passive Fourier Transforms Infrared
PGA	Proposal for Grant Activities
ppbC	Parts per billion carbon
ppbv	Parts per billion volume
ppm	Parts per million
ppmC	Parts per million carbon

List Acronyms, Abbreviations and Symbols (continued)

ppmv	Parts per million volume
pptv	Parts per trillion volume
psia	Pounds per square inch absolute
±	Plus or minus

Q

QA	Quality Assurance
QAPP	Quality Assurance Project Plan
QC	Quality Control

S

sec	Seconds
scf	Standard cubic feet
scfm	Standard cubic feet per minute
SO_2	Sulfur dioxide
ó	Standard deviation
SA	Stoichiometric air
SR	Stoichiometric ratio

T

TCEQ	Texas Commission on Environmental Quality
THC	Total hydrocarbons
TRC	TRC Company
TNG	Tulsa Natural Gas

U

UT Austin	The University of Texas at Austin

V

VOC	Volatile organic compound
vs	Versus

W

WD	Wind direction
WS	Wind speed

Z

ZINK	John Zink Company, LLC

Acknowledgements

The 2010 TCEQ Flare Study Project Team express their appreciation to the project sponsors: the Texas Commission on Environmental Quality and the State of Texas Air Quality Research Program for their financial and technical support. In particular, we express our appreciation to Ms. Danielle Nesvacil and Mr. Russ Nettles, TCEQ Project Managers, whose input, support and guidance have been greatly appreciated.

We also express our appreciation to the TCEQ's Technical Review Panel:

Peter E. G. Gogolek, Ph.D., CanmetENERGY, Canada
John Pohl, SC.D., Virginia Polytechnic Institute and State University
Eben Thoma, Ph.D., U.S. Environmental Protection Agency,

for their technical input and review of the QAPP and preliminary and final project reports.

We want to thank those who visited and observed the tests at the John Zink Test Facility and the organizations they represented: Lucy Randel, Industry Professionals for Clean Air; Bruce Davis, Texas Chemical Council; Scot Evans and Steve Smith, Texas Oil and Gas Association; and Brian Dickens, Eben Thoma, and Edgar Thompson, US EPA.

Finally, we express our thanks to the John Zink, LLC flare test facility team:

Scott Fox	Vice President, Flare Systems Division
Robert Schwartz	Project Representative / Project Director
Wes Bussman	Project Quality Assurance Officer
Zachary Kodesh	Project Operations Officer
Richard Lawhead	Test Center Technician, steam / fuel control
Clifford Pugh	Test Center Technician, steam / fuel control
Garrett Spaulding	Test Center Technician, steam / fuel control
Charlie Crown	Test Center Technician, chain gang lead, Instrumentation
Michael Bryant	Test Center Technician, chain gang
Chris Patrick	Test Center Technician, chain gang
Craig Skaggs	Test Center Technician, instrumentation
Leon Longacre	Test Center Supervisor, fuel supply coordinator
Dan Doss	Test Center Safety Manager
Jerry Buhler	Test Center Manager
Crane Operator	
Joe Potter	Belger Cartage Service, Inc.

whose hard work, cooperation and support helped make the flare testing a success.

1.0 Introduction and Background

The results of previous research funded by and work performed for the Texas Commission on Environmental Quality (TCEQ) indicated a need to conduct a study to determine the relationship between flare design, operation and destruction and removal efficiency (DRE) (NPL 2008, URS 2004). In May 2009, the TCEQ contracted with The University of Texas at Austin (UT Austin) to conduct the 2010 TCEQ Flare Study project (PGA No. 582-8-86245-fy09-04, Tracking Number 2008-81) (TCEQ, 2009). The purpose of the 2010 TCEQ Flare Study project was to conduct field tests to measure flare emissions and collect process and operational data in a semi-controlled environment to determine the relationship between flare design, operation, vent gas lower heating value (LHV) and flow rate, DRE, and combustion efficiency (CE). Because the study was conducted outdoors, in a full-scale test facility, there was no attempt to control ambient conditions, i.e., temperature, humidity and wind speed and direction. It was anticipated that the results of these field tests would provide insight into operational conditions that may impact flare volatile organic compound (VOC) DRE and flare CE, such as assist rates or vent gas volumetric flow rates. In August 2010, the Air Quality Research Program funded a project (Task Order No. UTA10-000924-LOAT-RP9) that supplemented funding for this study.

This final report is submitted to fulfill the requirements of PGA No. 582-8-86245-fy09-04, Tracking Number 2008-81, Task 10 and Task Order No. UTA10-000924-LOAT-RP9, Task 1 and presents the results for this project and the data collected to address the Study Objectives (see Section 2.0), as defined by the TCEQ.

During this study and, in particular the field tests, data were collected that provided the information needed to address the Study Objectives. Due to excellent weather conditions, no major equipment problems that affected data quality, and efficient planning of the test series, the study team was able to collect data on almost 96% more test runs on the steam-assisted test flare and 27% more test runs on the air-assisted test flare than originally planned. The data collected are a valuable resource for addressing many questions related to flare operation and performance; however, work to date has focused on addressing the Study Objectives. The Study team recognizes that follow-on work with the data collected in this project would be valuable and looks forward to the opportunity to participate in those analyses.

2.0 Project Scope and Design

UT Austin was contracted to measure flare emissions in a semi-controlled environment and collect and analyze process and operational data to fulfill TCEQ's study objectives for the project. The TCEQ's primary study objectives, in order of decreasing priority, were:

- Assess the potential impact of high vent gas flow rate turndown on flare CE and VOC DRE;
- Assess the potential impact of steam and air assist on flare CE and VOC DRE at various operating conditions, including low vent gas flow rates, i.e., high vent gas flow rate turndown;
- Determine whether flares operating over the range of requirements stated in 40 Code of Federal Regulations (CFR) § 60.18 achieve the assumed hydrocarbon DRE of 98% at varying vent gas flow rate turndown, assist ratios, and waste stream heat content; and
- Identify and quantify the hydrocarbon species in flare plumes visualized with passive infrared cameras.

In this study, the term vent gas will be used to represent the waste gas stream that would be sent to the flare for destruction in an industrial facility. The terms flare plume and plume will always refer to the total stream of gas that leaves the flare tip and changes composition due to some level of combustion.

Industrial Scale Flares

Extensive research has been conducted in controlled environments on devices that are not full-scale flares, i.e., with diameters less than three inches as opposed to industrial scale flares, which are typically on the order of multiple feet in diameter and can be as large as ten feet in diameter. To make the results of this study most directly applicable to industrial scale operations, the TCEQ required that the field tests performed for this study be conducted on full-scale industrial design flares. Specifically, the TCEQ required that both air-and steam-assisted flares be included in the study and that the minimum design capacity and diameter of the flare burners be one million lb/hr and 36 inches, respectively. While these minimum specifications were appropriate for steam-assisted flares, a comparable design capacity for an air-assisted flare would mean the nominal diameter of the air flare would need to be about 4 feet to comply with the maximum exit velocity limitation of 40 CFR § 60.18, which was also a requirement of the study. This diameter for an air-assisted flare would not typically represent the size of flares currently found in the field as reported by John Zink Company, LLC (Zink) representatives (email message from Z. Kodesh to V. Torres, UT Austin, February 15, 2010). So, this specification was modified to include an air-assisted flare burner representative of a design and size typically found in the field.

There are multiple flare manufacturers who have a wide range of proprietary flare burner designs. It was not within the scope of this project to attempt to test representative samples of every different flare design each with its own set of design options. Instead, the decision was made to select one design of an air flare and one design of a steam flare that would represent a large number of flare burners currently in the field. Zink was asked to identify models of flares, based on their market data, which satisfied this criterion. Additionally, the TCEQ required that the steam flare design selected have both center and upper steam assist.

The TCEQ established these flare design criteria on the following data from their 2009 Point Source Emissions Inventory (email message from D. Nesvacil, TCEQ, to V. Torres, UT Austin, July 22, 2001) so that the flare configurations tested represent flares commonly used in both routine process and emergency service (dual service).

- Of 1,519 total flares in the TCEQ 2009 Emissions Inventory:
  - 684 (45.0%) are designated as being in both routine and emergency/maintenance service
  - 322 (21.2%) are designated as being in routine service
  - 275 (18.1%) are designated as being in emergency/maintenance service
  - 238 (15.7%) are not designated as being in any service (blank)
- Out of 684 flares in both routine and emergency/maintenance service:
  - 143 (21%) are air-assisted
  - 305 (45%) are steam-assisted
  - 218 (32%) are unassisted
  - 18 (3%) have no designated assist type
- For these dual-service flares, 2009 TCEQ Emissions Inventory data indicates:
  - 21% of dual-service flares are air-assisted. Of these air-assisted, dual-service flares:
    - 77% are 12 to 36 inches in diameter and represent 95% of total 2009 emissions for dual-service, air-assisted flares.
  - 45% of dual-service flares are steam-assisted. Of these steam-assisted, dual-service flares:
    - 41% are 24 to 48 inches in diameter and represent 57% of total 2009 emissions for dual-service, steam-assisted flares.

Based on these requirements for the flare burners, the John Zink Models EE-QSC-36" Flare Tip (36-inch diameter) with (3) EEP-503 pilots and the LHTS-24/60 (24-inch diameter) with (3) Pilots (Figure 2-1) were selected for the steam flare and air flares, respectively. Data sheets and drawings of these two flare tips are included in Appendix B.

Figure 2-1. Flare Burners Used in Study. Air Flare John Zink Model LHTS-24/60 (left) and Steam Flare John Zink Model EE-QSC-36" Flare Tip (right) used in the study

Controlled Environment Laboratory

To measure flare emissions on full-scale flares in a semi-controlled environment (i.e., controlled flare operations but uncontrolled ambient conditions), UT Austin decided to conduct the study at the outdoor flare test facility of Zink in Tulsa, Oklahoma. Zink is a flare tip manufacturer whose flare test facility is capable of accommodating a wide range of flare tips, test configurations and operating conditions. Once the flare test configurations were made at their facility and approved by UT Austin, Zink dedicated their flare test facility exclusively to this project with uninterrupted operation for the duration of the study, which lasted almost three weeks.

Measurement of Flare Emissions
A core element of UT Austin's study approach was to directly measure flare emissions at the end of the flare plume where combustion had ceased, and calculate DRE and CE based on those measurements. To measure these emissions, UT Austin selected Aerodyne Research, Inc., (ARI) due to their extensive experience in ambient air quality studies and their unique capability to make continuous (1 Hz frequency) measurements of the chemical species expected to be present in the flare plume. These direct measurements of the flare emissions serve as the primary data used to address the study objectives.

Compare Remote Sensing Technologies
The TCEQ also required that remote sensing technologies be included in the study and a comparison of their performance be included in the study results. The following remote sensing measurement methods were specified by the TCEQ for inclusion in this study (TCEQ, 2009):

1. Infrared Hyper-Spectral Imaging Technology (Contractor: Telops Inc.)
   Identify flare hydrocarbon plume species and determine plume species concentrations.
2. Passive Fourier Transform Infrared (PFTIR) Spectroscopy (Contractor: Industrial Monitor and Control Corporation)
   Collect the required data to determine flare combustion efficiency.
3. FLIR GasFindIR Passive Infrared (IR) Cameras (Contractor: Leak Surveys Inc.)
   Provide a visual comparison of IR images to the infrared hyper-spectral imaging technology results, and assist other remote sensing tools to take measurements.

During the course of the study planning, UT Austin recommended that Active Fourier Transform Infrared (AFTIR) spectroscopy also be considered for comparison with these remote sensing technologies as this instrument is reported to be able to detect all organics and have better performance (Hashmonay 2010) in minimum detection levels and data quality than the PFTIR, thereby having greater precision in the determination of CE than the PFTIR systems (email from R. Spellicy, IMACC to E. Michel, UT Austin May 19, 2010).

It was also decided by the UT Team that a single blind approach should be used to compare the remote sensing technology measurements, i.e., the only information provided to the contractors performing remote sensing measurements was that which would be provided to them if they were engaged to measure combustion efficiencies at an industrial facility. The results of the CE and DRE measurements made by ARI were not made available to the remote sensing teams until this report was released to the public.

Performance and Comparison Metrics
VOC DRE was selected by the TCEQ to be the primary metric for assessing flare performance. TCEQ selected this metric because of the critical role VOCs play in contributing to the formation of ozone. CE was selected as a secondary metric because the remote sensing technologies included in the study can only measure CE. DRE (hydrocarbon species X) is the percentage of species X that is destroyed relative to the quantity of species X entering the flare. Numerically, this is represented as

$$DRE\ (\%) = \left(1 - \frac{X_{plume}}{X_{in}}\right) \times 100 \qquad \text{Eq. 1.1}$$

where

DRE (%) = destruction and removal efficiency (%)
X_{plume} = mass flow rate of hydrocarbon species X found in the flare plume after combustion has ceased
X_{in} = mass flow rate of hydrocarbon species X entering the flare

CE is the percentage of the total hydrocarbon stream entering the flare that burns completely to form only carbon dioxide and water. Numerically, this is represented as

$$CE\ (\%) = \left(\frac{CO_2\ (plume)}{CO_2\ (plume) + CO\ (plume) + \sum hydrocarbons\ (plume)}\right) \times 100 \qquad \text{Eq. 1.2}$$

where

CE (%) = combustion efficiency (%)
CO_2 (plume) = volume concentration of carbon dioxide in the plume (ppmv) after combustion has ceased
CO (plume) = volume concentration of carbon monoxide in the plume (ppmv) after combustion has ceased
Σ hydrocarbons (plume) = volume concentration of all the unburned hydrocarbons in the plume after combustion has ceased multiplied by the number of carbons for each hydrocarbon (ppmC)

Vent Gas Composition and Flow Rates

For this study, the TCEQ specified that the vent gas composition should be a mixture of natural gas, propylene and nitrogen. The ratio of the natural gas to propylene was to be 1:4 by volume. Nitrogen would be used as the diluent to achieve the desired LHV for the vent gas. This study focused on vent gases with low LHV and low flow rates. Flare performance data representative of vent gas streams with LHVs close to 300 Btu/scf was desired by the TCEQ. This range of LHVs was selected because it is at the lowest end of the LHVs allowed by 40 CFR § 60.18 for hydrocarbon streams (300 Btu/scf) in assisted flares.

The desired range of vent gas flow rates to be used was 0.1% to 0.25% of the flare's design capacity. Vent gas flow rates of 0.1% and 0.25% of nominal design capacity were selected as they are in the range of operation for typical flow rates (less than 0.5%) used in industry. These flow rates account for approximately 25% of flare operation time (ENVIRON International Corporation, 2009) and introduce the greatest probability for over-assisted operation of steam flares because of some minimum levels of steam assist recommended to industry by flare

manufacturers, 500 lb/hr center, 750 lb/hr upper, for the size and model of steam flare used in this study (email message from R. Nettles, TCEQ, to V. Torres, UT Austin, on September 8, 2010), potentially producing less than a 98% DRE (Marathon June 2010, Marathon November 2010). It was desired to increase the range to 0.5% of maximum design capacity for both the steam and air flares but the Zink test facility would not have been able to provide the nitrogen gas flow rates needed to achieve the LHVs specified by the TCEQ for the steam flare. Therefore, the vent gas flow rates used for the air flare were increased to 0.25% and 0.65% of the maximum design capacity of the air flare.

Quality Assurance

UT Austin prepared a Category 2 Quality Assurance Project Plan (The University of Texas at Austin, 2010) for this project that complied with the requirements of the Environmental Protection Agency's (EPA) *Requirements for Quality Assurance Project Plans*, EPA QA/R-5, and Guidance for Quality Assurance Project Plans, EPA QA/G-5. This QAPP was posted for public comment by the TCEQ and was reviewed by the EPA.

Reference Values and Standard Conditions

The reference values for properties of gases used during the test and for subsequent calculations and analyses are taken from *Perry's Chemical Engineer's Handbook, 8th Edition,* 2008, unless otherwise stated. Standard conditions used in this study are atmospheric pressure = 14.696 psia and 68°F.

3.0 Test Plan

UT Austin worked with Zink, ARI and the TCEQ to develop a test plan that would provide data that would form the basis for addressing as many of the study objectives as possible within the project schedule and available budget ($2,191,332). The test plan developed for the study is included in Appendix A. A summary of the test series actually conducted is shown in Table 3-1, where steam flare tests begin with the letter "S" in the designation of the test series and air flare tests begin with the letter "A". The test plan consisted of multiple flare test series conducted on the air-assisted flare tip and multiple test series conducted on the steam-assisted flare tip. The designation used to identify each test point and run was: S[number X].[number Y]R[number Z], where the number X is the test series number, number Y designates the level of assist (air or steam) used in the test series and number Z is the run or repetition number for the test point. So, for example, S3.2R2, is steam flare test series number 3, the second assist condition tested, repetition number 2.

As stated in the previous section, the TCEQ specified that the vent gas be a mixture of natural gas (Tulsa Natural Gas was available at the Zink test facility) and propylene (1:4 ratio by volume) diluted with nitrogen to achieve the desired LHV. To focus on low LHV vent gas streams and still comply with 40 CFR § 60.18, a LHV of 350 Btu/scf ± 50 Btu/scf was selected as the lowest target LHV for the vent gases used in the Test Plan. To obtain additional data on the effect of LHV on DRE and CE, a second LHV of 600 Btu/scf ± 80 Btu/scf was also included in the Test Plan.

The steam flare burner used for this study had a design capacity of 937,000 lb/hr for use with propylene. Therefore the 0.1% and 0.25% of design capacity vent gas flow rates for this flare are 937 lb/hr and 2,342 lb/hr, respectively. These two flow rates were the target vent gas flow rates used for the steam flare tests. The air flare burner used for this study had a design capacity of 144,000 lb/hr for use with propylene. The 0.25% and 0.65% of design capacity vent gas flow rates for this flare are 359 lb/hr and 937 lb/hr, respectively. These two flow rates were the target vent gas flow rates used for the air flare tests.

Table 3-1. Summary of Flare Test Plan

Steam Flare Tests

Test Series	Vent Gas (Nominal)			Target (Nominal) Steam Assist (lb/hr)	
	Flow Rate lb/hr	LHV Btu/scf	Composition %	Center	Upper
S1	2342	2149	100% Propylene	500	ISP to <Snuff
S2	937	2149	100% Propylene	500	ISP to <Snuff
S3	937	350	1:4 TNG to Propylene Ratio Diluted to Target LHV	500	ISP to <Snuff
S3	937	350	1:4 TNG to Propylene Ratio Diluted to Target LHV	100	230
S3	937	350	1:4 TNG to Propylene Ratio Diluted to Target LHV	0	230
S3	937	350	1:4 TNG to Propylene Ratio Diluted to Target LHV	0	0
S4	2342	350	1:4 TNG to Propylene Ratio Diluted to Target LHV	500	ISP to <Snuff
S4	2342	350	1:4 TNG to Propylene Ratio Diluted to Target LHV	330	110
S4	2342	350	1:4 TNG to Propylene Ratio Diluted to Target LHV	0	330
S5	937	600	1:4 TNG to Propylene Ratio Diluted to Target LHV	500	ISP to <Snuff
S6	2342	600	1:4 TNG to Propylene Ratio Diluted to Target LHV	500	ISP to <Snuff
S7	2342 - 937	350	1:4 TNG to Propylene Ratio Diluted to Target LHV	500	525
S8	2342 - 937	350	1:4 TNG to Propylene Ratio Diluted to Target LHV	0	500
S9	2342 - 937	350	1:4 TNG to Propylene Ratio Diluted to Target LHV	0	1025
S10	2342 - 937	350	1:4 TNG to Propylene Ratio Diluted to Target LHV	0	825
S11	2342 - 937	350	1:4 TNG to Propylene Ratio Diluted to Target LHV	300	525
S12	2342 - 937	350	1:4 TNG to Propane Ratio Diluted to Target LHV	500	525
S13	2342 - 937	350	1:4 TNG to Propane Ratio Diluted to Target LHV	325	525
S14	2342 - 937	350	1:4 TNG to Propane Ratio Diluted to Target LHV	0	525

TNG = Tulsa Natural Gas
Snuff = Visible flame extinguished
ISP = Incipient Smoke Point
LHV = Lower Heating Value

Air Flare Test Tests

Test Series	Vent Gas (Targets)			Target (Nominal) Air Assist (lb/hr)
	Flow Rate lb/hr	LHV Btu/scf	Composition %	
A1	937	2149	100 % Propylene	ISP to <Snuff
A2	359	2149	100 % Propylene	ISP to <Snuff
A3	937	350	1:4 TNG to Propylene Ratio Diluted to Target LHV	ISP to <Snuff
A4	937	600	1:4 TNG to Propylene Ratio Diluted to Target LHV	ISP to <Snuff
A5	359	350	1:4 TNG to Propylene Ratio Diluted to Target LHV	ISP to <Snuff
A6	359	600	1:4 TNG to Propylene Ratio Diluted to Target LHV	ISP to <Snuff
A7	359	350	1:4 TNG to Propane Ratio Diluted to Target LHV	ISP to <Snuff

TNG = Tulsa Natural Gas
Snuff = Visible flame extinguished
ISP = Incipient Smoke Point
LHV = Lower Heating Value

The range of steam or air assist values to be used in this study was bracketed on the lower end by the incipient smoke point and on the upper end by the snuff point. The definition of incipient smoke point (ISP) used for this project is the point of operation of the flare with the minimum amount of air or steam required, as appropriate for the flare type, so that no visible smoke emissions are observed two flame lengths away from the flare tip. For this study, as defined in the QAPP, a panel of three people, R. Schwartz (Zink), R. Nettles (TCEQ), and V. Torres (UT Austin), determined when this criterion was achieved. The snuff point is the point when the visible flame has been extinguished, i.e., no visible combustion is occurring at the flare. Visible smoke emissions are defined in this study as the appearance of a group of black particles produced by the flare combustion process. A requirement of this study was that all data be obtained at flare operating points that comply with 40 CFR § 60.18. A requirement of 40 CFR § 60.18 is that flares be operated with no visible smoke emissions, except for periods not to exceed 5 minutes during any two consecutive hours. If the vent gas in a flare does produce smoke during combustion, then the ISP air or steam assist value represents the flare operating point of minimum assist that achieves compliance with 40 CFR § 60.18. So the incipient smoke point was selected as the lower end of the range of steam or air assist values used for the study.

The snuff point was selected as the upper bound of the range of steam or air assist and the value beyond which there is no further visible flare combustion occurring and therefore no further change in DRE or CE. In practice, the snuff point was never attained during this study before the maximum design rates for this project were reached. So the snuff point was a target not an actually achievable operating point at the maximum level of assist used in any test series.

The target flow rate used for center steam was 500 lb/hr. This value was selected for use as it represented the level reported to the TCEQ by industry (email message from R. Nettles, TCEQ, to V. Torres, UT Austin, on September 8, 2010) as the value recommended most frequently for use by flare burner manufacturers to prevent thermal shock and condensation in the piping. Zink also agreed (meeting with J. Franklin and Z. Kodesh, Zink with E. Michel and V. Torres, UT Austin, and D. Nesvacil and R. Nettles, TCEQ, on February 11, 2010) that this would be a reasonable level to use with the Zink model steam-assisted flare burner that was to be used on this project.

The Test Plan was designed to systematically vary only one flare operational parameter at a time while holding all other parameters constant. The approach used in implementation of the test plan and reflected in the Test Plan in Appendix A was to start a test series using one of the two study vent gas flow rates (0.1% or 0.25% of flare design capacity) and one of the two study LHVs (350 Btu/scf or 600 Btu/scf) and begin the first test point of the test series with the ISP level of steam or air assist. After data were collected for that test point and while maintaining this vent gas flow rate and LHV, the assist would be increased to the snuff point as the second test point in the series. Then, two more steam or air assist levels between the ISP level and the snuff would be run to complete the test series for a total of four test points, minimum, per test series. For the core test series, these same test points would be repeated two more times. For the next test series, this process would be repeated with the other LHV. If the 0.1% vent gas flow rate were used first, then the next test series would use the 0.25% vent gas flow rate and this whole process repeated with this vent gas flow rate.

Test series S1, S2, A1, and A2 do not contain mixtures of natural gas and propylene. These tests were included as preparatory tests to allow all participants to practice with their equipment and optimize their measurement process on the specific flare about to be tested. The data from these tests are not included the data analysis of this study.

Test series S3, S4, S5, S6, A3, A4, A5, and A6 are the core test series that were identified in the Study Plan. Because of very favorable weather conditions and no major equipment problems affecting data quality, the core test series were completed in less time than anticipated and tests in addition to the core test series could be conducted. In compliance with Appendix E, Flare Test Plan Modification Procedure, of the QAPP, a strategy was proposed for conducting additional tests that were not part of the original test plan. The strategy for conducting the additional tests was to run more operating points, which would help to better define the efficiency curve, and fewer, if any, repetitions. Preliminary data indicated that reproducibility of estimated DRE during the repetitions of the core test series was high with a percent standard deviation of less than 5%. (The percent standard deviation being equal to the standard deviation of the DREs for the three repetitions divided by the average DRE for the repetitions.) Another strategy incorporated in the proposal for more tests was to hold steam assist constant and vary vent gas flow rate rather than holding vent gas flow rate constant and varying steam assist. This strategy was proposed because during the core test series it was found that the Zink test facilities had greater difficulty making small incremental increases/decreases in steam flow rates and then returning to reproduce the same steam flow rate. Zink could more easily hold steam rate constant and quickly vary and stabilize the vent gas flow rate. So Test Series S7, S8, S9, S10, S11, S12, S13, S14 and A7 have few, if any repetitions. These test series are conducted at constant nominal steam assist levels (for the S test series) with the vent gas flow rates as the variable during the test series.

One additional test plan modification was the inclusion of propane instead of propylene. Test Series S12, S13, S14, and A7 are test runs substituting propane for propylene. All other parameters remained the same as in the propylene runs for these four test series.

The ARI team collected data in all of the test series, and the IMACC PFTIR and Telops Hyper-Cam collected data during the entire field test campaign. The IMACC AFTIR participated in the core steam tests but did not participate in the air flare tests as the air flare test configuration and height limitations of the scissor lifts supporting the reflectors would have prevented proper alignment of the camera, reflectors, and air flare plume. The data return (percent of test points reporting data relative to the total number of test points conducted) for all quality assured data reported in time to include in this report is reflected in the summary of test data in Appendices D and E.

4.0 Overview of Flare Test Facility and Instrumentation

Once the test plan was developed, UT Austin worked with ARI and Zink to design the test facility and instrumentation needed to make measurements of all the flare operational parameters and flare emissions in the plume. A brief description of the test facility and instrumentation follow. A detailed description the major test facility equipment and instrumentation is included in Appendix B.

The flare test facility was composed of two major systems: the flare test system (Figure 4-1) and the flare plume sampling system (Figure 4-2). The flare test system consisted of the flare burners (air- and steam-assisted), the vent gas supply system, the air- or steam-assist system and the flare control room. The flare plume sampling system consisted of the sample collector, the eductor, global positioning system, crane, meteorology system, and the sampling probes and lines.

Figure 4-1. Overall View of Flare Test Facility

Figure 4-2. Flare Plume Sampling System During Morning Steam Only Start-up Routine

The operation of the flare burners (Figure 4-3) were controlled by Zink personnel and monitored using their standard process and control instrumentation with additional instrumentation and sampling ports added for this study where necessary. Vent gas supply (Figure 4-4) was controlled, flow rates measured and blended at the vent gas supply station before being sent to the flare. All operating data were recorded in a data acquisition system in the flare control room (Figures 4-5 and 4-6).

To verify and determine the actual composition of the vent gas being used during each test run, a stack testing company, TRC, was employed to provide measurements of the vent gas composition entering the flare from a sample obtained at the beginning of the test run and one five minutes later. From these same samples, TRC made measurements of propylene/propane, methane and ethane in the flare plume as a back-up to ARI's primary determination of DRE and CE. Appendix G describes the method used to calculate the vent gas composition and flow rate from the TRC and Zink measurements.

The exits of the steam- and air-assisted flare burners were 13 and 33 feet above ground level, respectively.

Figure 4-3. Flare Burners. Air-assisted on left and steam-assisted on right

Figure 4-4. Vent Gas Supply. Piping for flow control, mixing and measurement of the vent gas supply

Figure 4-5. Control Room for the Flare Test System

Figure 4-6. Control Room Display. Monitor displayed Zink measurement of flare operating parameters (top left), LSI's FLIR and IR video (right half) and ARI's flare emissions measurements (bottom left)

Flare Plume Sampling System

The primary component of the Flare Plume Sampling System (Figure 4-7) was the sample collector. The goal of this sample collector (Figure 4-8) was to determine the "plume average" DRE and CE for a given set of flare operating conditions. It was not to determine the instantaneous combustion efficiency at a given point in the active combustion zone of the plume. Therefore, the sampler collector was designed to continuously draw as large a sample of the plume as possible, homogenize the sample and then obtain a sample of this well mixed portion of the plume for analysis.

Figure 4-7. Flare Plume Sampling System. Plume sampling system making measurements of flare plume while held in position by crane and ground crew

The sample collector was moved into position so that during a test it was located approximately in the center of the flare plume at a distance far enough downwind from the flare tip to ensure that combustion reactions had ceased and with the face of the inlet oriented perpendicular to the travel of the plume. The method used as the gauge to know that the collector inlet was past the

combustion zone was to position the inlet to the sample collector so that the plume temperature at the inlet was 250°F or less, as measured by three thermocouples in the inlet to the sample collector. The position of the sample collector at the midpoint of the plume was facilitated using the visual, two FLIR and one IR video camera images (Figure 4-6) filmed by Leak Surveys, Inc. (LSI) and the temperature of the flare plume as it entered the sample collector. The two FLIR cameras were positioned to view the flame approximately perpendicular to the plume and coincident with the wind direction.

The eductor (Figure 4-8) of the sample collector would continuously draw approximately 1950 cfm of flare plume through the collector. The inlet of the sample collector was 20 inches in diameter with an effective draw of more than 24 inches in diameter. A mixing and flow conditioning section at the entrance to the sample collector would mix and then straighten the flow prior to reaching ARI's and TRC's sampling probes. Samples (approximately 1 liter per minute for the vent gas sample line and 8 liters per minute for plume sample line) would be continuously drawn through the sample lines to the analyzers and instruments in each company's mobile laboratory trailers (Figure 4-8). Draw of the samples began at the start of testing in the morning and continue until the lunch break. This draw would start again before testing began in the afternoon and continue until the end of test day.

Figure 4-8. Sample Collector at Near Ground Level. Collector inlet is at foreground and eductor is at far end. In photo, Zink personnel make adjustments to heated transfer line supports. Shackles and cable at center allow crane to lift and position Sample Collector.

The height of the sample collector inlet was tracked using a graduated chain attached to the sample collector. Zink personnel on the ground would also report the radial distance from the inlet of the sample collector to the center of the flare burner to the control room, where it would be logged. ARI also tracked the position of the inlet to the sample collector using a global positioning system (GPS) attached to the sample collector.

TRC used gas chromatography to analyze both flare stack and plume gases (methane, ethane and propylene). Two grab samples were collected per test run, 5 minutes apart. Flare plume constituents (CO, CO_2, O_2, speciated VOCs, HCHO, NOx, particulate matter and THC) were measured continuously (1 Hz) by ARI using their mobile laboratory, which has two dual quantum cascade laser instruments and several LiCOR non-dispersive infrared sensor instruments. Destruction removal and combustion efficiencies were calculated based on the measurements of TRC (vent gas) and the ARI (flare plume) measurements using the carbon content of the constituents in the vent gas and flare plume. A detailed description of the method used to calculate the DRE and CE by ARI is included in Appendix I. A discussion of the accuracy and precision of these values is presented in Section 6.0.

Meteorology measurements, i.e., wind speed, direction, temperature, and barometric pressure, were made to characterize the speed and direction of the cross wind at the exit of the flare burners. These measurements were made by ARI (Figure 4-9).

Figure 4-9. Meteorology System

Method for Measurement of Flare Emissions and Calculation of DRE and CE

This section describes the methodology used to compute DRE and CE from the time series of measurements on the sample line. A more detailed description of this derivation can be found in Appendix I. The discussion of the sources of error in this approach is outlined in Section 7. The purpose of the description here is to go through an event analysis and describe the computational steps.

The two fundamental characteristics of interest in this test are DRE and CE. The equations that define these quantities have been discussed previously, Equation 1.1 and 1.2. Appendix I derives an alternative form of Equation 1.1, labeled here as Equation 4.1

$$DRE/100 = 1 - \frac{\left[\frac{propylene_{out}\ (molesC)}{C_{out}\ (molesC)}\right]}{\left[\frac{propylene_{in}\ (molesC)}{C_{in}\ (molesC)}\right]} = 1 - \frac{CF^{propylene}\ (out)}{CF^{propylene}\ (in)} \qquad \text{Eq. 4.1}$$

where $CF^{propylene}$ (in) is based on the fraction of carbon found as propylene in the vent gas mixture, i.e., the carbon fraction of propylene. The carbon fraction of any species in a mixture is the ratio of the amount of carbon present in the species to the total amount of carbon present in the mixture. Nominally, in the 80% propylene, 20% TNG mixture this can be approximated as

$$CF^{propylene}\ (in) = \frac{propylene\ (ppmC)}{propylene\ (ppmC) + methane\ (ppmC) + \sum other\ carbon\ (ppmC)}$$

Eq. 4.2

or

$$CF^{propylene}\ (in) = \frac{3\ *\ 0.8}{3 * 0.8\ +\ 1 * 0.2\ +\ \sum other\ carbon\ (ppmC)} \approx 0.923 \qquad \text{Eq. 4.3}$$

where the contribution of other carbon constituents in the Tulsa Natural Gas are considered to be negligible. Note that for the actual computation of DRE, the measurement of the vent gas composition has been used, the example above is used for illustration.

The other term required for DRE evaluation using Equation 4.1 is the $CF^{propylene}$ (out) term. In this case, the combustion has occurred and species such as CO_2 and CO are significant in the carbon fraction term.

$$CF^{propylene}\ = \frac{propylene\ (ppmC)}{propylene\ (ppmC) + CO_2 + CO + \sum other\ carbon\ (ppmC)} \qquad \text{Eq. 4.4}$$

It will be illustrative to demonstrate how $CF^{propylene}$ (out) is calculated for one of the test conditions. As a prelude to the calculation, however, it is important to examine the event from some simple metrics to be sure that the sample collector is sampling the flare plume.

The first detail to be examined is the relationship between the temperature of the incoming sample and the relationship with the 1 Hz CO_2 measurement, presuming this is the dominant product of the flare's combustion. During every test series, ARI would continuously extract a sample from the portion of the flare plume drawn through the sample collector using a probe that would dilute the sample with pure dry nitrogen immediately as it entered the probe tip. Sample collection would begin well before a test series was conducted. Figure 4-10, shows a time series of the sample collector inlet temperature and CO_2 concentration of the sample obtained by the dilution probe.

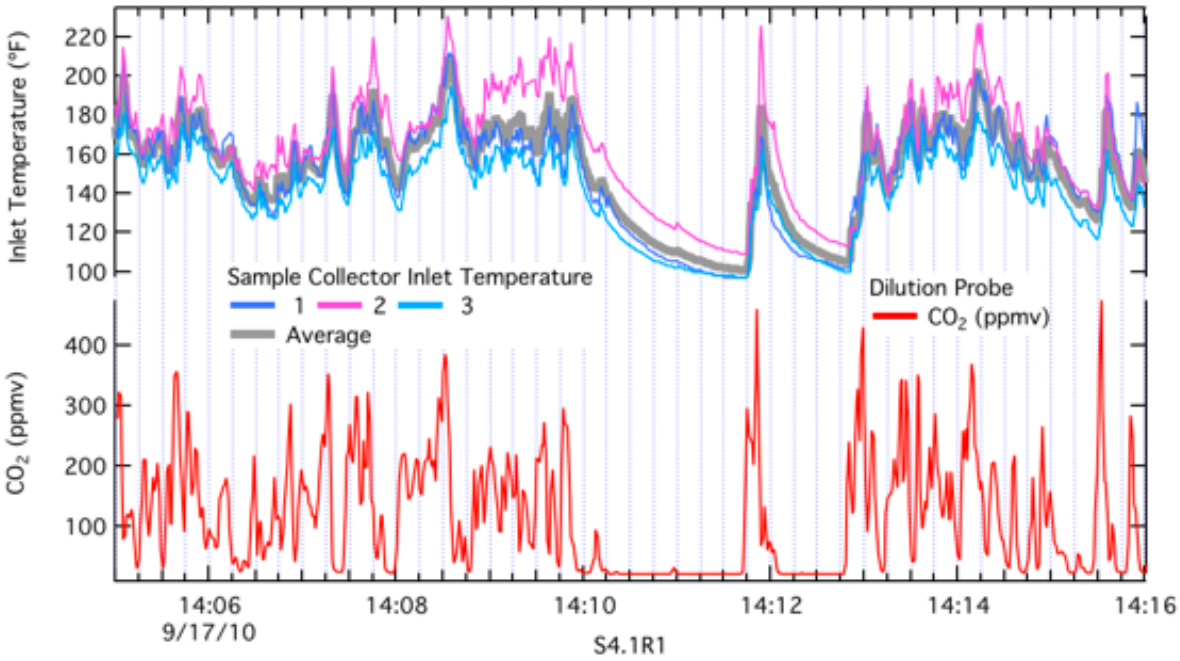

Figure 4-10. Time Series of Sample Collector Inlet Thermocouples and CO_2 Concentration for Test Point S4.1R1. In the upper panel, the temperatures of the three thermocouples at the sample collector inlet (shown in Figure 4-8) are shown in the noted pastel colors. An average of these three is also shown in the grey trace. The CO_2 time series of the sample obtained by the dilution probe is depicted in the lower panel in red.

The test point, S4.1R1, sample collector data is characterized by three periods. In the first section, from ~ 14:05 to 14:10, the sample collector is capturing significant plume intensity, i.e., plume "hits". In the second period, from ~14:10 to 14:12:30, the sampler collector inlet is out of the flare plume as evidenced by the rapid decrease in CO_2 concentration and the slower decrease in sample collector inlet temperature. This is likely due to the fact that the flange around the sample collector inlet has a large thermal mass while the volumetric flow rate through the sample collector is very high, ~ 2,000 scfm, and is rapidly ventilated with ambient air. Note that ambient air has a CO_2 concentration of ~ 380 ppmv, but the probe tip diluent (N_2) is causing a 17 fold dilution at the inlet to the probe. In the final section, from ~14:12:30 to 14:16, the sample is characterized by plume hits with increasing frequency. Dilution of the sample with dry nitrogen was required to prevent condensation of moisture in the sample transfer line.

The second analysis that will be considered prior to looking at the steps used to compute DRE for this event is the physical location of the sample collector inlet. The differential GPS system digitized the physical location of the sample collector. A top-down view of the event with the measured CO_2 concentration and flare location has been combined with wind data to look at the sample collector inlet location and wind during test point S4.1R1.

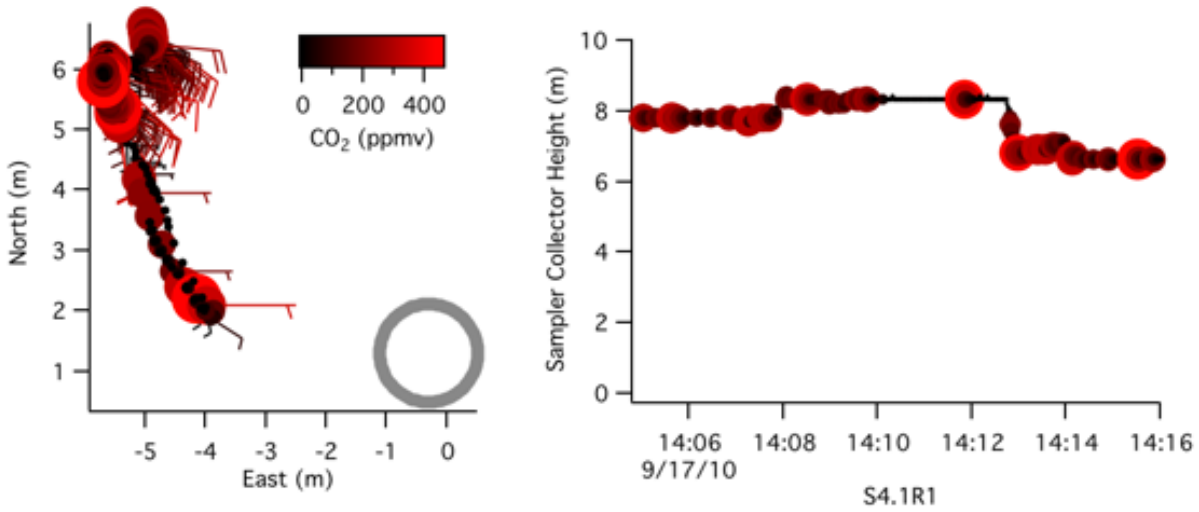

Figure 4-11. Sampler Collector Location and Wind Data. The left hand frame depicts the location of the center of the sample collector physically as meters (m) north and east of the flare (shown conceptually as a gray circle in the lower right hand corner); wind directions are shown as wind barbs ending at the point indicating the sample collector position; and the right hand frame shows the vertical position of the sample collector inlet. The shading of the data points in both panels are based on CO_2 concentration according to the color scale. The size of the point has been adjusted based on the large CO_2 'plume hits'.

The wind barbs that have been added to the top-down depiction of the sampler location (left hand frame of Figure 4-11) all roughly point back to the flare, shown as the grey circle in the bottom right of the frame. The wind for this event was from the southeast and varied during the test point from ~ 100 to 170 degrees. The ground crew maneuvered the sample collector inlet to intercept the plume to adjust for the intra-test wind changes. This is seen in the photograph depicted in Figure 4-7.

The time series for several species measured by the dilution probe (along with the CO_2 concentration discussed above) are plotted in Figure 4-12.

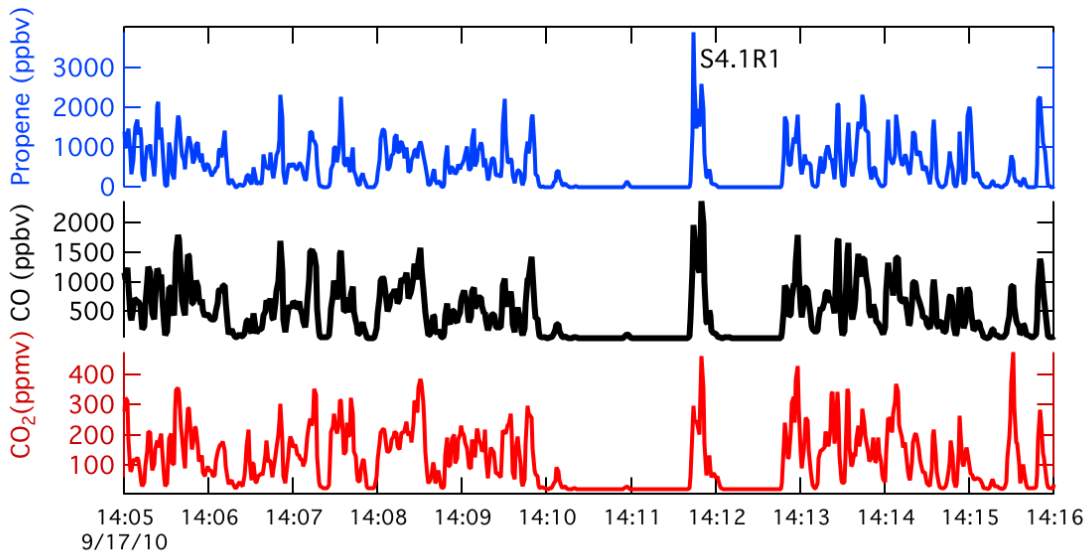

Figure 4-12. Time Series of S4.1R1 of CO_2, CO and Propylene Concentrations of the Dilution Probe. Each panel is the 1 Hz data for the dilution probe in mixing ratio by volume.

The characteristic pattern of the time series for the event, discussed in light of CO_2 concentration and sample collector inlet temperature is qualitatively mirrored in CO as well as unburned propylene. A simplistic approach to the evaluation of Equation 4.4 would be to insert the absolute mixing ratios depicted in the time series. This approach however would require that additional knowledge about the ambient dilution and ambient mixing ratios be accounted for. What is really of interest is the combustion-associated fraction. If the numerator and denominator of Equation 4.4 are divided by the CO concentration the following formula results.

$$CF^{propylene}(out) = \frac{propylene\ (ppmC)/CO}{propylene\ (ppmC)/CO + CO_2/CO + 1 + \sum other\ carbon\ (ppmC)/CO}$$

Eq. 4.5

The terms in Equation 4.5 are all intended to be *flare combustion associated* ratios. As a result, if the time-series data is plotted against CO rather than time, the following representations of the event result.

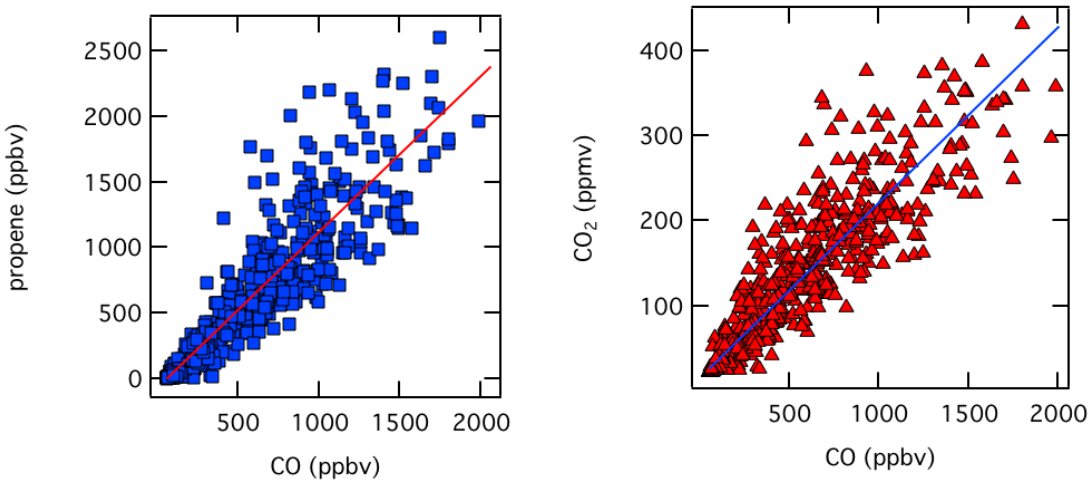

Figure 4-13. Propylene and CO_2 Concentrations Relative to CO Concentration in the Combustion-Associated Plume Intercept.

The relationship between the propylene and CO concentrations (left hand side of Figure 4-13) for the totality of event S4.1R1 is characterized by a linear slope of 1.19 ± 0.04 moles per mole, where the uncertainty is the 2 <sigma> precision determined from the fit assuming a normal distribution of error in the propylene measurement. The Pearson's R^2 statistic for this fit is 0.84. When the value is used in Equation 4.5, it must be converted to a ratio of ppmC, which in the case of propylene means multiplying by 3 to account for the three carbon atoms in propylene (e.g., 3.57 ± 0.12). The relationship between the CO_2 and CO concentrations (right hand side of Figure 4-13) is evaluated using a linear fit with slope 206 ± 4 ppmC per ppmC. The Pearsons R^2 for this fit is 0.89.

As a first step in the pursuit of evaluating Equation 4.5 and eventually DRE for this test point, these combustion-associated slopes will be used to evaluate Equation 4.5 using only three chemical forms for carbon (propylene, CO, CO_2).

$$CF^{propylene}\ (out) = \frac{(3.57\ \pm\ 0.12)}{(3.57\ \pm\ 0.12) + (206\ \pm 4) + 1} = (1.69\ \pm\ 0.06)\% \qquad \text{Eq. 4.5a}$$

Assuming there is no other form of carbon, the evaluation of Equation 4.5a, suggests that propylene in the *flare plume* is 1.69% of the total carbon considered in this example.

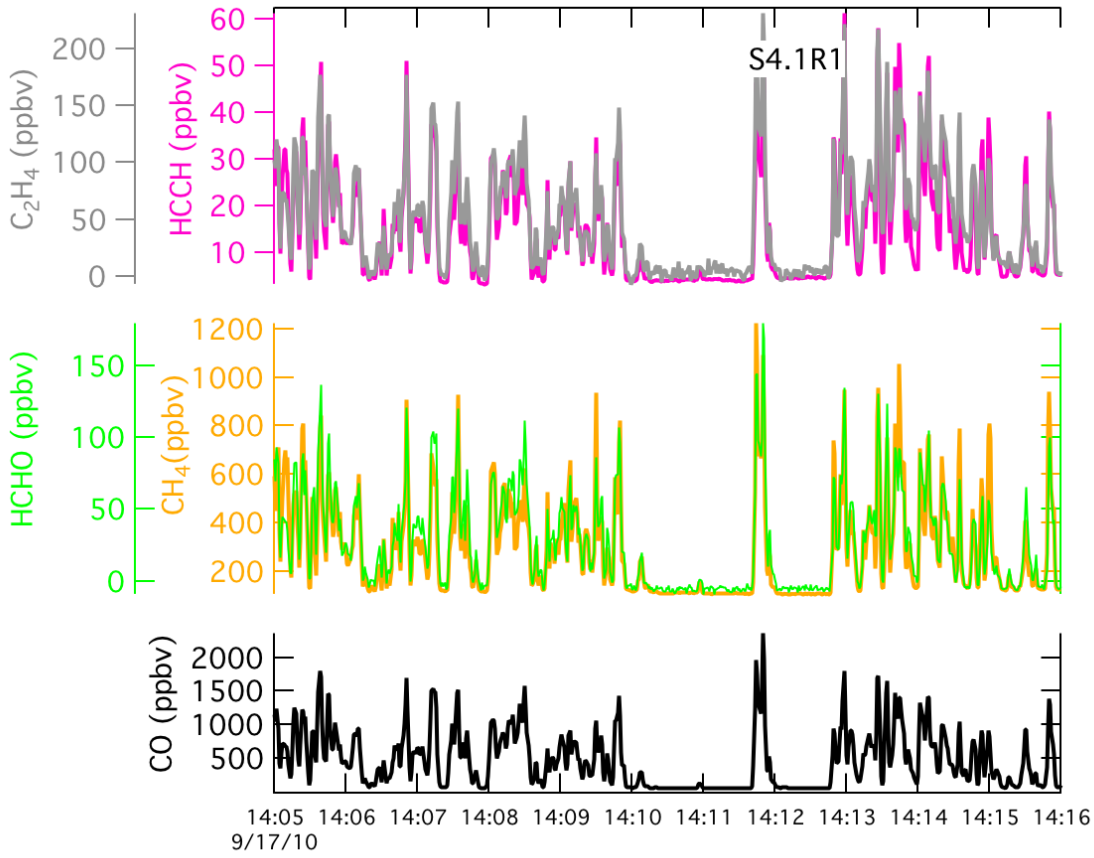

Figure 4-14. Time Series for CO Concentration and Other Trace Selected Hydrocarbons Species. The measurements of the dilution probe for test point S4.1R1 for ethene (C_2H_4), ethyne (C_2H_2), formaldehyde (HCHO) and methane (CH_4).

Time series data for this event for other trace forms of carbon in the matrix are depicted in Figure 4-14. Note that CO concentration has been repeated for reference from the previous figures. The relationship of the trace hydrocarbon concentration relative to CO concentration is summarized in Figure 4-15.

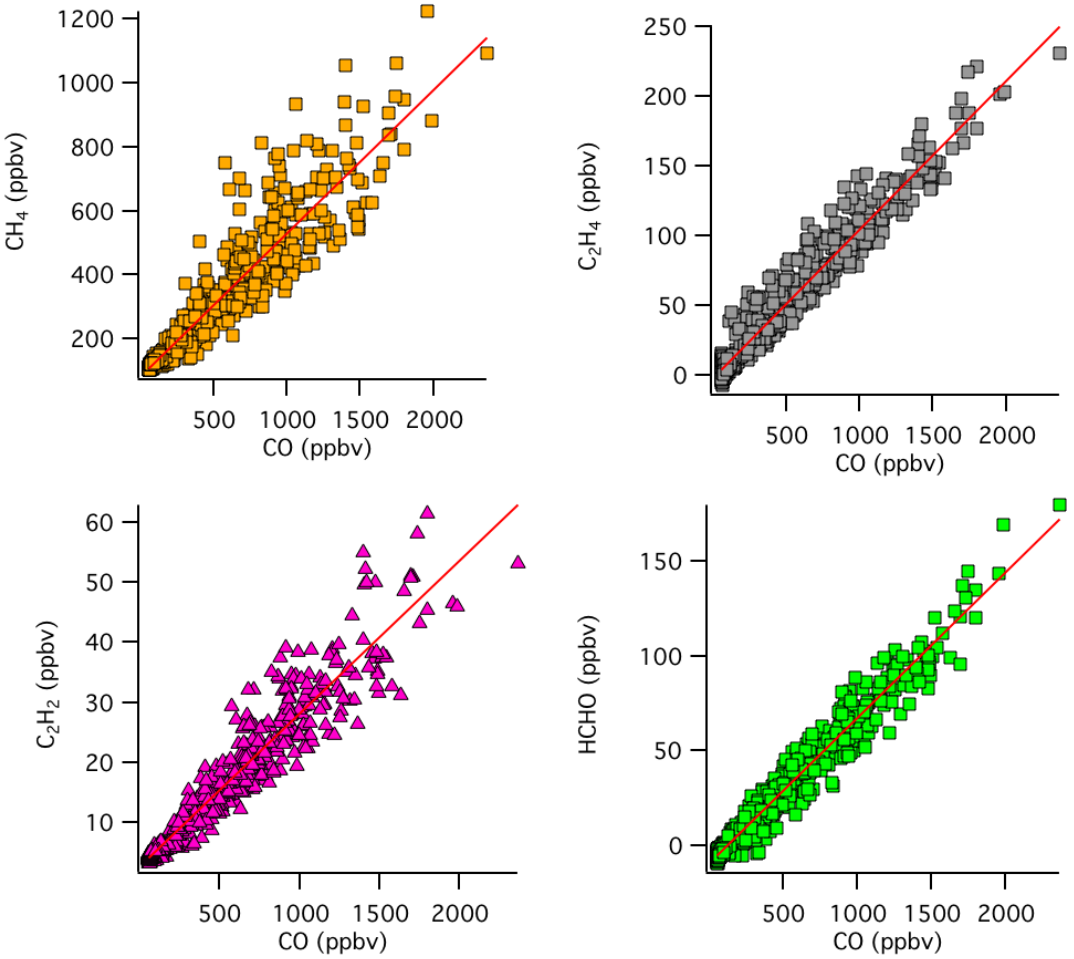

Figure 4-15. Correlation of Trace Hydrocarbon Concentration with CO Concentration for S4.1R1. The results of the fit parameters depicted by the red lines in each panel are tabulated in ppmC below.

Table 4-1. Fit Parameters for Selected Trace Hydrocarbons for S4.1R1

Species	ppmC/ppmC CO	2 <sigma>	R^2	Influence on CF for S4.1R1
CH_4	0.45	0.01	0.87	0.2%
C_2H_4	0.212	0.004	0.95	0.1%
HCHO	0.0767	0.0001	0.96	0.03%
C_2H_2	0.050	0.002	0.92	0.02%

The carbon fraction that results from including these trace species in the denominator of Equation 4.5 (the sum of 'other' carbon) is unchanged within the precision based error band, $CF^{propylene}$ (*out)* = 1.69%. Using the nominal 80/20 propylene/TNG mixture, it is estimated that

$CF^{propylene}$ (*in*) = 92.3%. This implies the DRE for this test point, based on the definition in Equation 4.1 is 1 – 1.69/92.3 or 98.17% (98.10 - 98.23%). An analogous form of the combustion efficiency equation can be derived.

Additional discussion of the sources of systematic error in this approach will be discussed in Section 7. The reader is also referred to Appendix I for additional information.

Remote Sensing Technologies

Remote sensing technologies were also included in this study to measure CE (IMACC and Telops) and/or flare emissions (Telops). The measurements made by the remote sensing technologies will be compared to the measurements made by ARI to assess and evaluate the performance of the remote sensing technologies (see Section 8.0).

5.0 Results of Flare Tests

The field tests were performed during the month of September 2010 at the Zink flare test facility in Tulsa, Oklahoma. The test plan (Appendix A) identified 56 test points, including replicates, to be performed on each of the air- and steam-assisted flares. Because of favorable weather conditions and more rapid than anticipated completion of test conditions, a larger number of test points than originally planned were completed. The actual number of test points and replicates that were performed were almost twice the number of steam test points and 27% more air test points than originally planned. These additional test points included tests using propane in place of propylene. Propane was not included in the original test plan. Summaries of the test results follow.

Summaries of all test data for the steam and air flare tests are included in Appendices D and E, respectively. The values for DRE and CE are presented in this report using three significant figures based on the probable uncertainty in these measurements as explained in Section 7 of this report. The standard deviation, δ, for the ARI DRE & CE values and for the CE values reported by the remote sensing contractors are also included in Tables D-1 and E-1 in Appendices D and E, respectively.

In these summaries, the terms steam-to-vent gas ratio (S/VG) and momentum flux ratio (MFR) are included to help characterize the flare operating parameters and are defined as follows.

$$S/VG = \frac{Total\ (center\ plus\ upper)\ steam\ assist\ flow\ rate\ (lb/hr)}{Vent\ gas\ flow\ rate\ (lb/hr)} \qquad \text{Eq. 5.1}$$

$$MFR = \frac{\rho_{czg} \cdot {v_{czg}}^2}{\rho_{air} \cdot {v_{wind}}^2} \qquad \text{Eq. 5.2}$$

where:
ρ_{czg} $= combustion\ zone\ gas\ density, lb/ft^3$
v_{czg} $= combustion\ zone\ gas\ velocity, ft/hr$
ρ_{air} $= ambient\ air\ density, lb/ft^3$
v_{wind} $= wind\ velocity, ft/hr$

The S/VG and the MFR are dimensionless quantities as the units in the numerator and denominator cancel out in both terms.

Also, in the graphs that follow where test series are shown on a graph, i.e., multiple test points and run, the values on the axes and in the legend are typical or nominal values for the test series. In the following narrative where data is discussed for a specific test point and run, the actual values obtained for the test point and run are cited.

Steam-Assisted Flare: DRE (propylene) and CE

Please refer to Figures 5-10a and 5-10b.
At a total steam assist flow rate of 970 lb/hr (S/VG = 1.04 and center steam = 540 lb/hr) for a vent gas LHV of 349 Btu/scf and constant flow rate of 930 lb/hr, the DRE (propylene) was 38.1% (S3.1 R1). No higher steam assist levels were performed at this combination of flare operating parameters since the DRE was already below 50%. The CE for this test point/run was 34.3%. The average wind speed during this test point/run was 2.6 mph. The MFR for this test point/run was 0.005.

At a total steam assist flow rate of 666 lb/hr (S/VG = 0.29, center steam = 555 lb/hr) for a vent gas LHV of 349 Btu/scf and constant flow rate of 2,335 lb/hr, the DRE (propylene) was 99.2% (S4.2 R3). Total steam assist levels greater than 666 lb/hr produced DREs below 99.2%. The CE for this test point/run was 98.9%. The average wind speed during this test point/run was 4.8 mph. The MFR for this test point/run was 0.092.

Please refer to Figures 5-11a and 5-11b.
At a total steam assist flow rate of 228 lb/hr (S/VG = 0.25, center steam = 0 lb/hr) for a vent gas LHV of 346 Btu/scf and constant flow rate of 926 lb/hr, the DRE (propylene) was 99.5% (S3.7 R1). Total steam assist levels greater than 228 lb/hr produced DREs below 99.5%. The CE for this test point/run was 99.3%. The average wind speed during this test point/run was 7.1 mph. When the total steam assist was reduced to zero (S3.6 R1), the DRE (propylene) was 99.9% and the CE was 99.8% for this test point/run. The average wind speed during this test point/run was 7.3 mph. The MFR for this test point/run was 0.003.

At a total steam assist flow rate of 327 lb/hr (S/VG = 0.14, center steam = 0 lb/hr) for a vent gas LHV of 363 Btu/scf and constant flow rate of 2,372 lb/hr, the DRE (propylene) was 98.3% (S4.4 R1). The CE for this test point/run was 97.6%. The average wind speed during this test point/run was 5.9 mph. The MFR for this test point/run was 0.032.

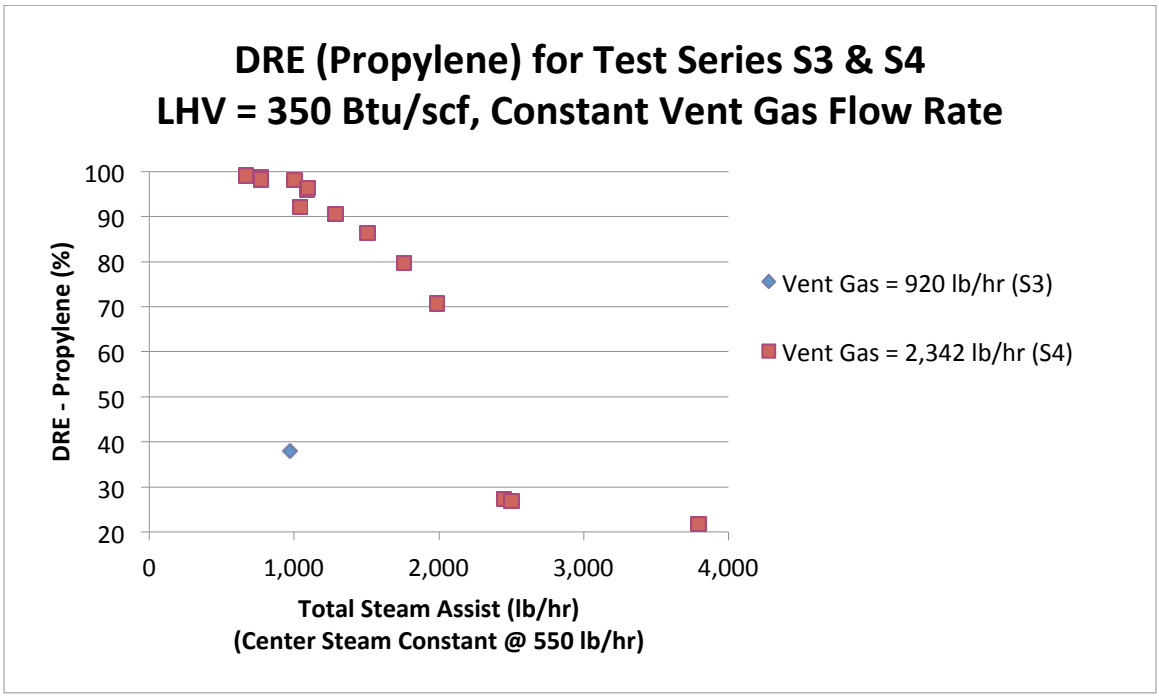

Figure 5-10a. DRE vs Steam Assist for Test Series S3 and S4

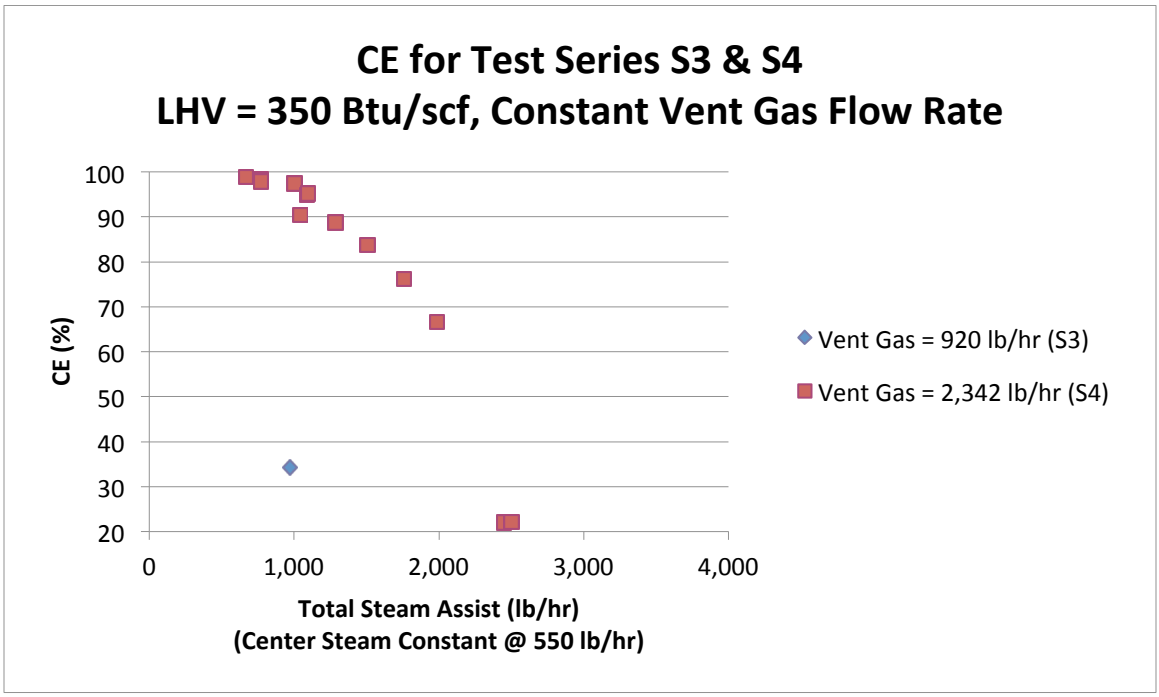

Figure 5-10b. CE vs Steam Assist for Test Series S3 and S4

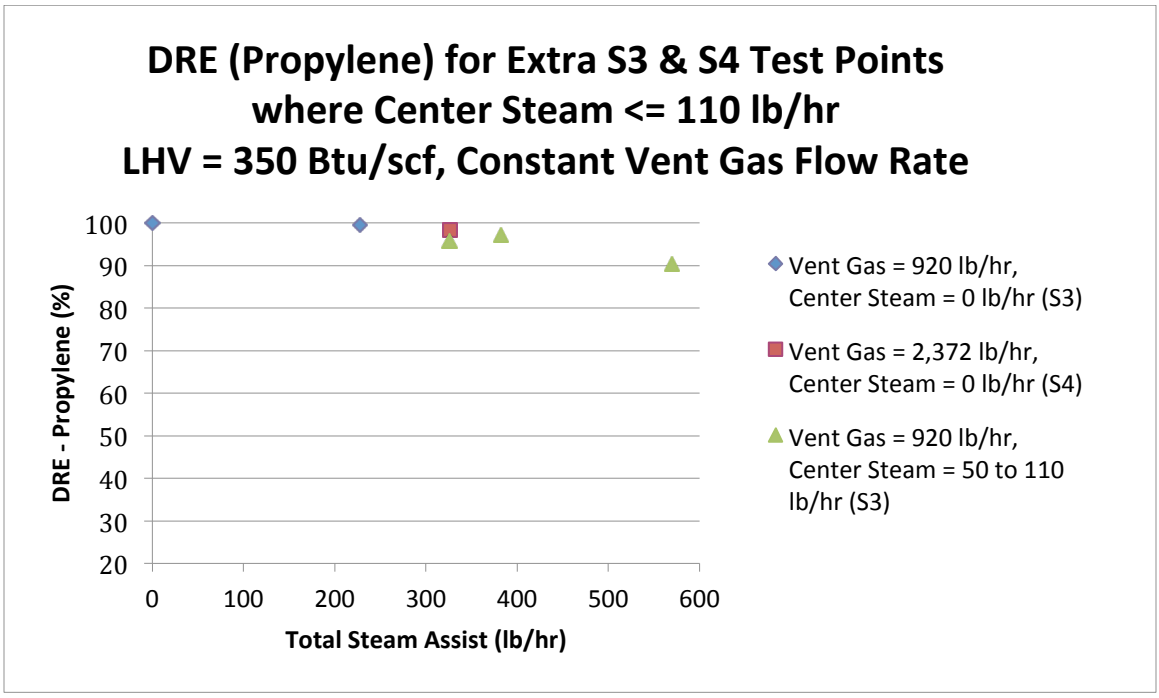

Figure 5-11a. DRE vs Steam Assist for Test Series S3 and S4 (Special - No Center Steam)

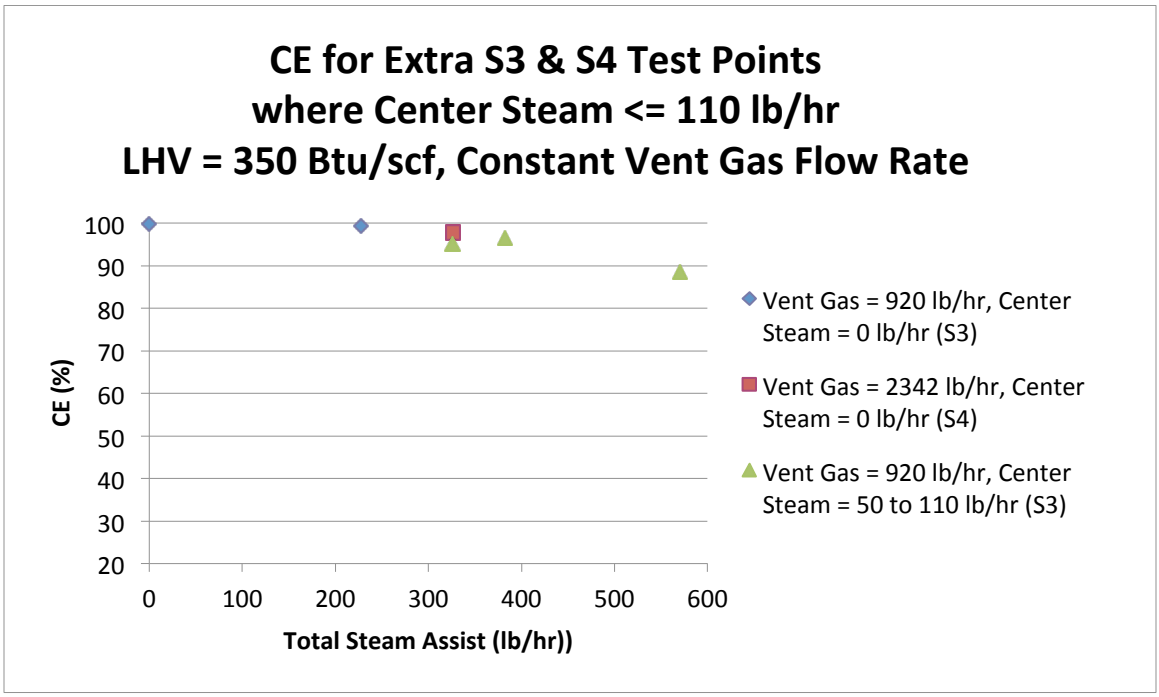

Figure 5-11b. CE vs Steam Assist for Test Series S3 and S4 (Special - No Center Steam)

Please refer to Figures 5-12a and 5-12b.
These two figures are composites of the data for all test points from Test Series S3 and S4 shown in the previous four figures. These graphs illustrate and compare the effect increasing steam rate has on DRE and CE at a LHV of approximately 350 Btu/scf for these two vent gas flow rates. Note that for the lower vent gas flow rate, the DRE and CE begin to decrease at a lower steam assist value, i.e., approximately 1,000 lb/hr vs 300 lb/hr total steam assist.

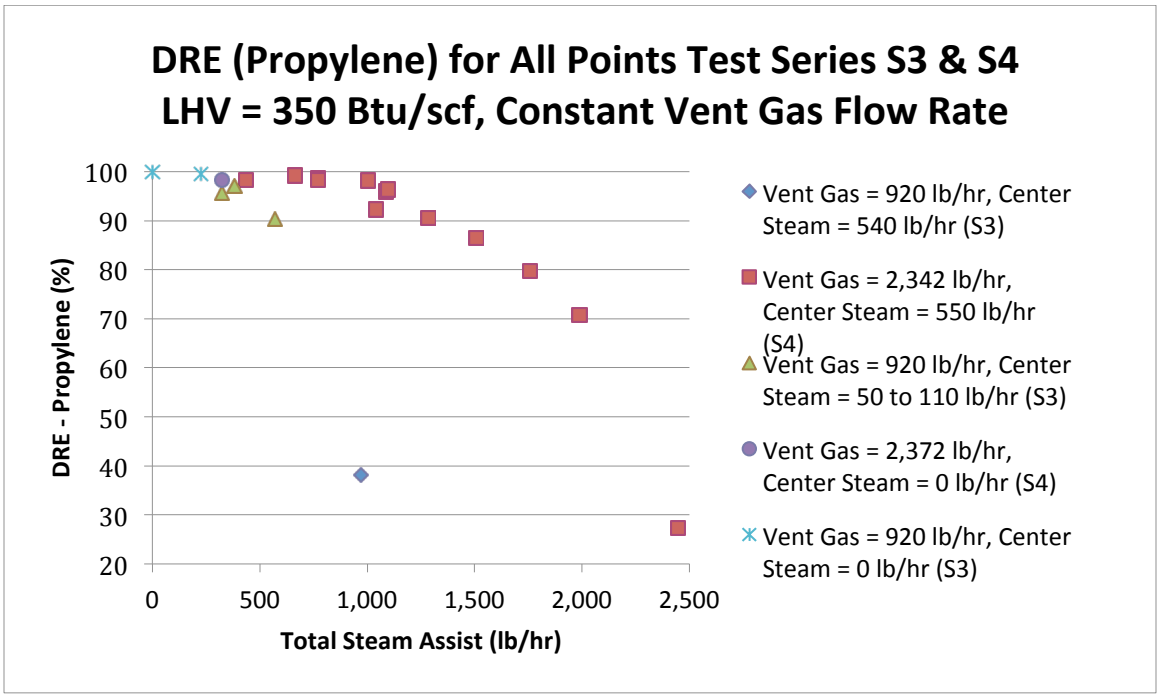

Figure 5-12a. DRE vs Steam Assist for All Test Series S3 and S4

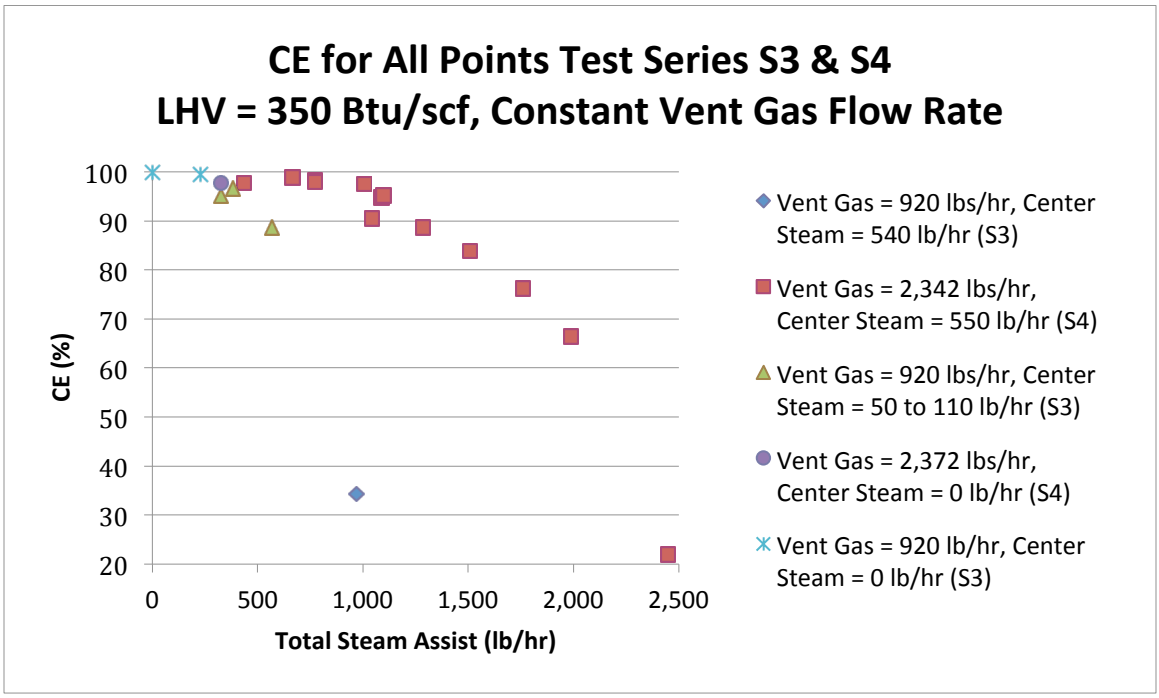

Figure 5-12b. CE vs Steam Assist for All Test Series S3 and S4

Please refer to Figure 5-13a and 5-13b.
At a total steam assist flow rate of 768 lb/hr (S/VG = 0.82, center steam = 488 lb/hr) for a vent gas LHV of 594 Btu/scf and constant flow rate of 940 lb/hr, the DRE (propylene) was 98.3% (S5.1 R1) or less. Total steam assist levels greater than about 768 lb/hr produced DREs below 98.3%. The CE for this test point/run was 98.0%. The average wind speed during this test point/run was 8.0 mph. The MFR for this test point/run was 0.008.

At a total steam assist flow rate of 1,529 lb/hr (S/VG = 0.63, center steam = 510 lb/hr) for a vent gas LHV of 625 Btu/scf and constant flow rate of 2,423 lb/hr, the DRE (propylene) was 99.3% (S6.1 Run 3). Total steam assist levels greater than about 1,529 lb/hr produced DREs below 99.3%. The CE for this test point/run is 98.9%. The average wind speed during this test point/run was 7.5 mph. The MFR for this test point/run was 0.032.

DRE (Propylene) and CE vs Steam-to-Vent Gas Ratio (S/VG)

Please refer to Figure 5-14a, 5-14b, 5-15a and 5-15b.
DRE (Propylene) vs S/VG for all test points in Test Series S3 and S4 is shown in Figures 5-14a and 5-15a. Figures 5-14b and 5-15b show CE vs S/VG for the same test points. Figures 5-15a and 5-15b are provided to focus on a smaller DRE range to provide greater resolution between data points for easier analysis.

Please refer to Figure 5-16a, 5-16b, 5-17a and 5-17b.
DRE (Propylene) vs S/VG for all test points in Test Series S5 and S6 is shown in Figures 5-16a and 5-17a. Figures 5-16b and 5-17b show CE vs S/VG for the same test points. Figures 5-17a and 5-17b are provided to focus on a smaller DRE range to provide greater resolution between data points for easier analysis.

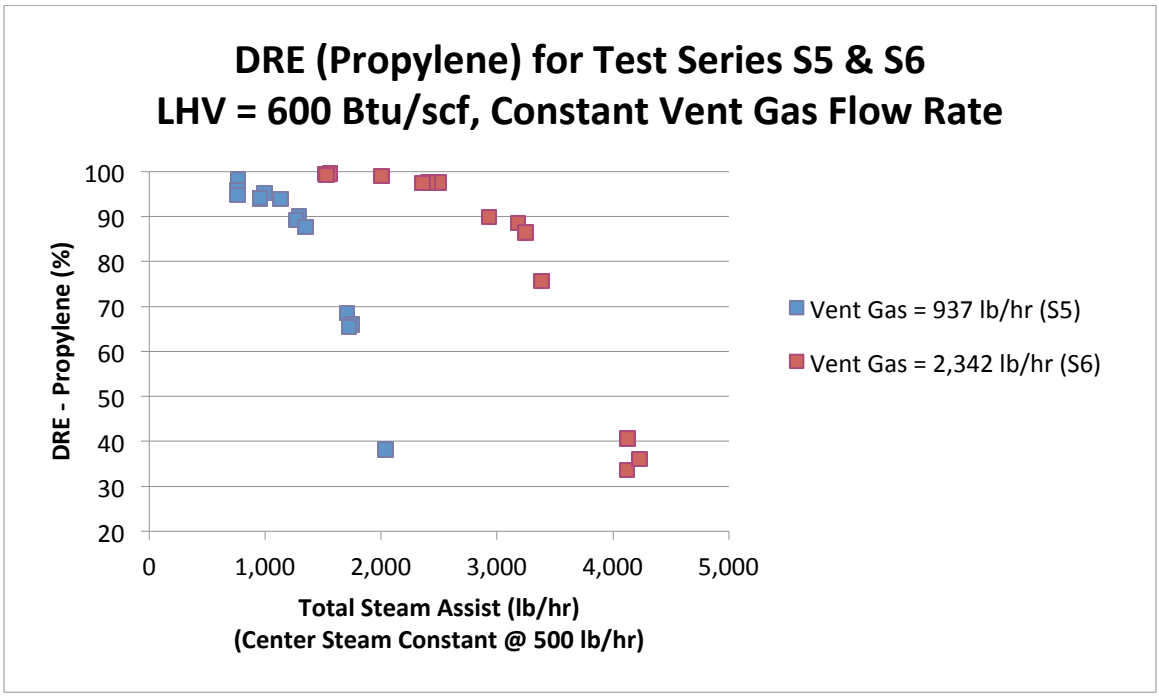

Figure 5-13a. DRE vs Steam Assist for Test Series S5 and S6

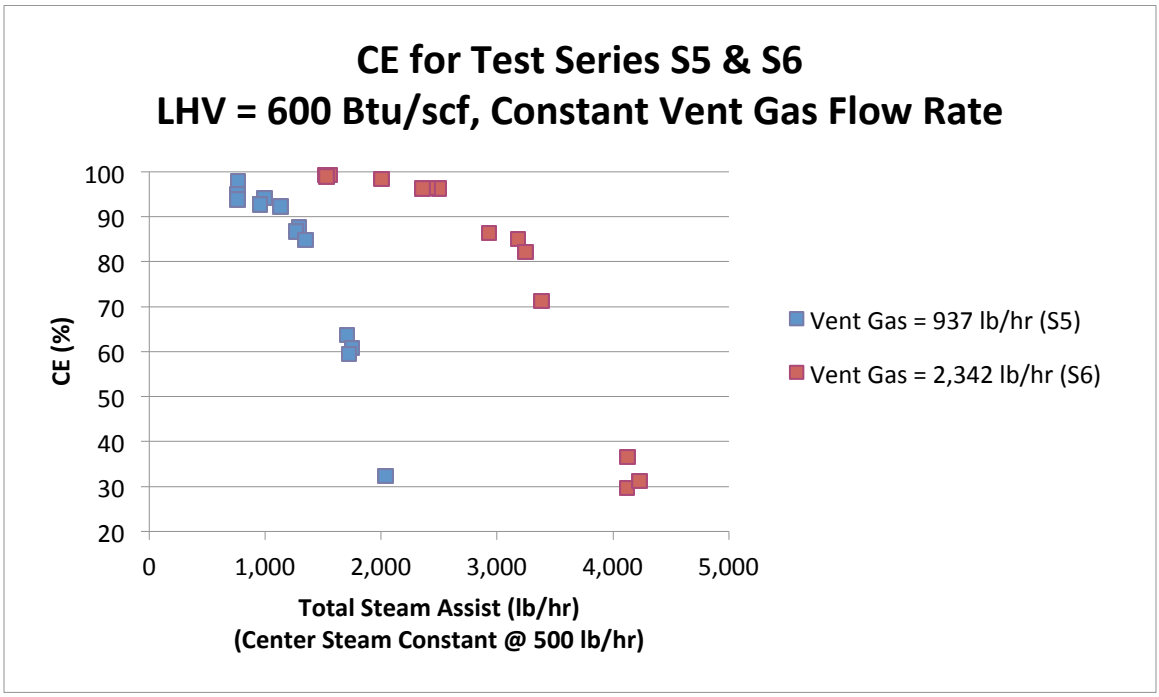

Figure 5-13b. DRE vs Steam Assist for Test Series S5 and S6

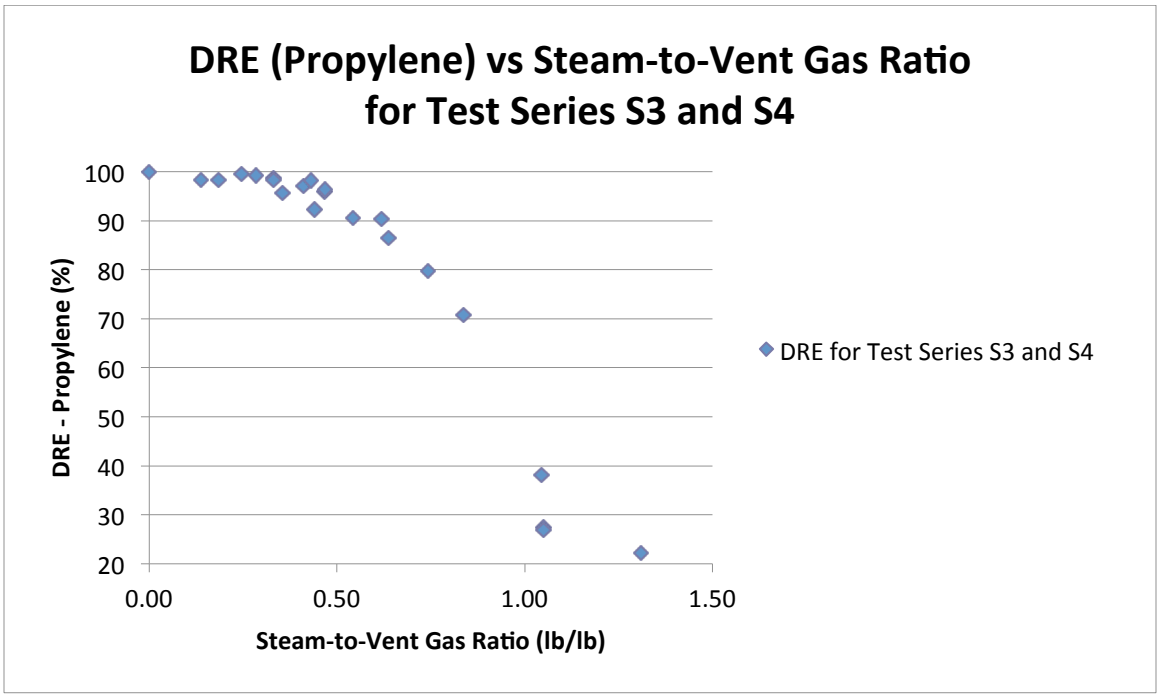

Figure 5-14a. DRE vs Steam-to-Vent Gas Ratio for All Test Series S3 and S4

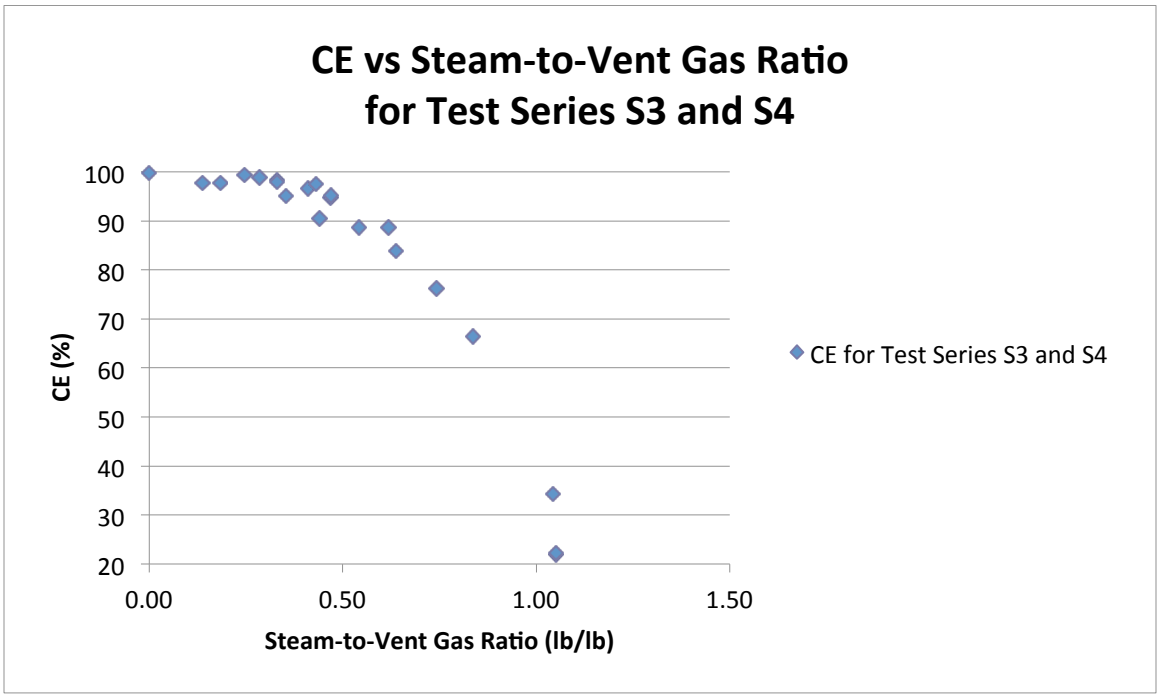

Figure 5-14b. CE vs Steam-to-Vent Gas Ratio for All Test Series S3 and S4

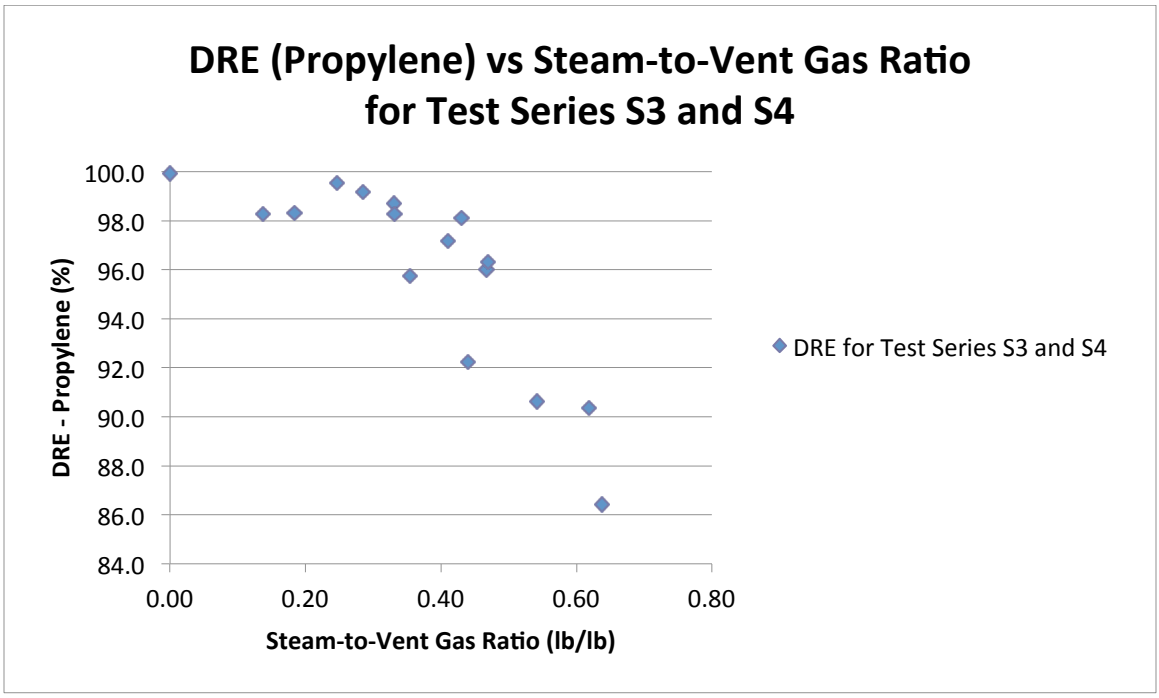

Figure 5-15a. DRE vs Steam-to-Vent Gas Ratio for All Test Series S3 and S4
(Note DRE (Propylene) range = 84 to 100%)

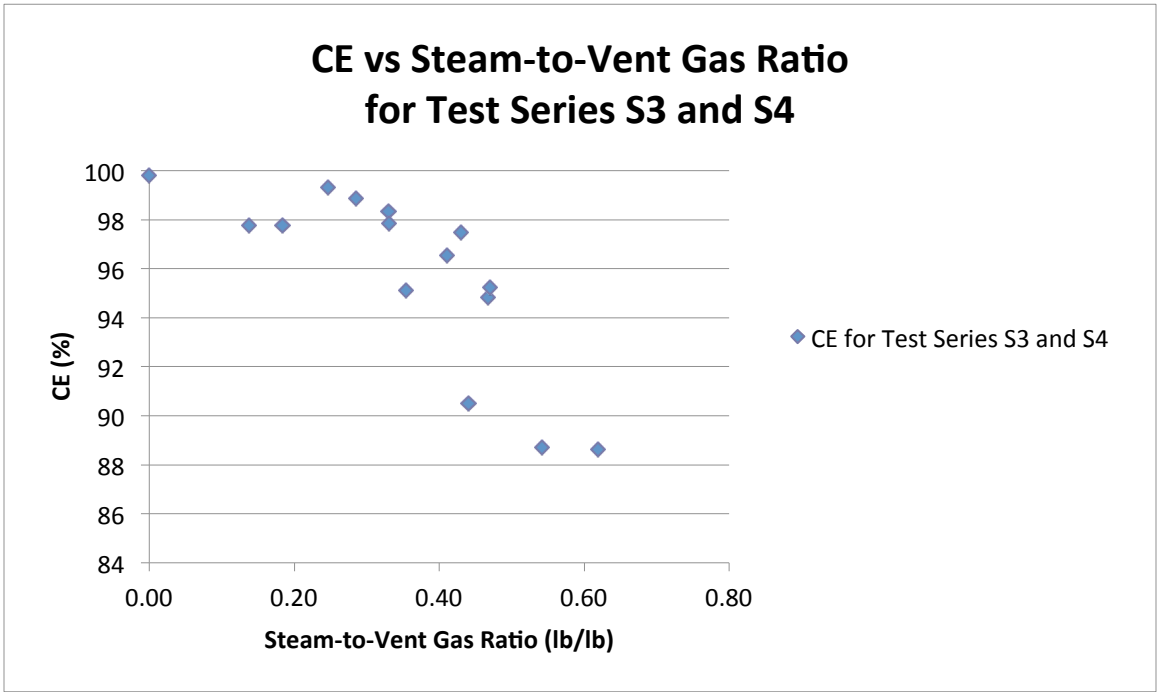

Figure 5-15b. CE vs Steam-to-Vent Gas Ratio for All Test Series S3 and S4
(Note CE range = 84 to 100%)

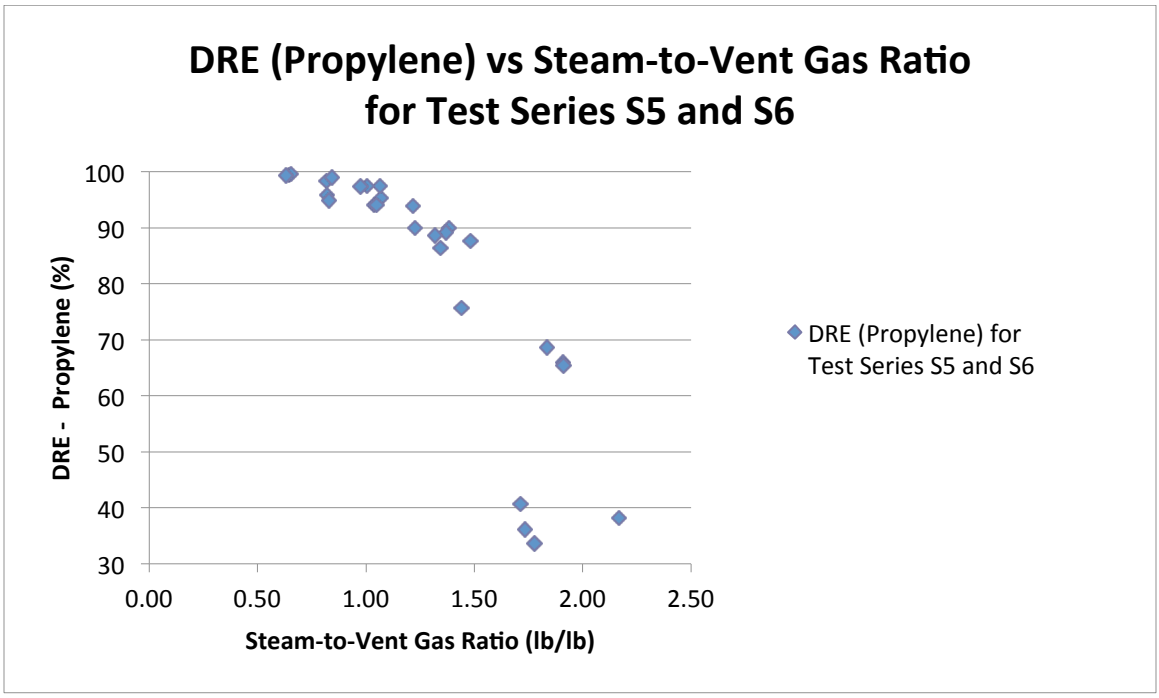

Figure 5-16a. DRE vs Steam-to-Vent Gas Ratio for All Test Series S5 and S6

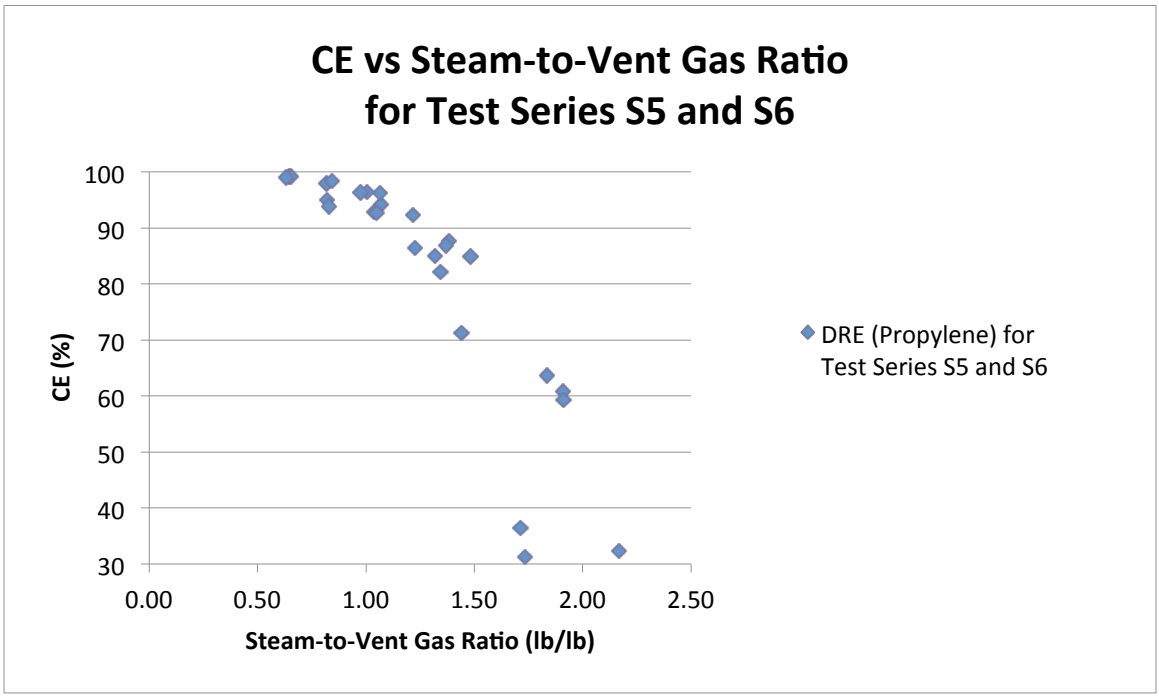

Figure 5-16b. CE vs Steam-to-Vent Gas Ratio for All Test Series S5 and S6

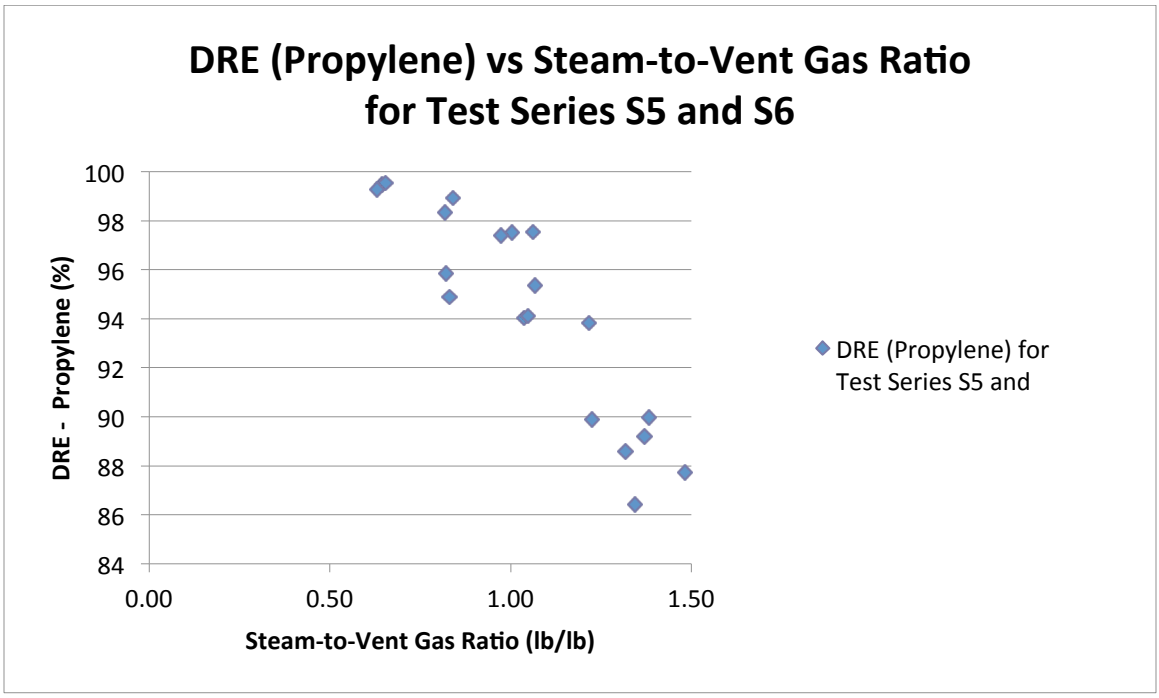

Figure 5-17a. DRE vs Steam-to-Vent Gas Ratio for All Test Series S5 and S6
(Note DRE (Propylene) range = 84 to 100%)

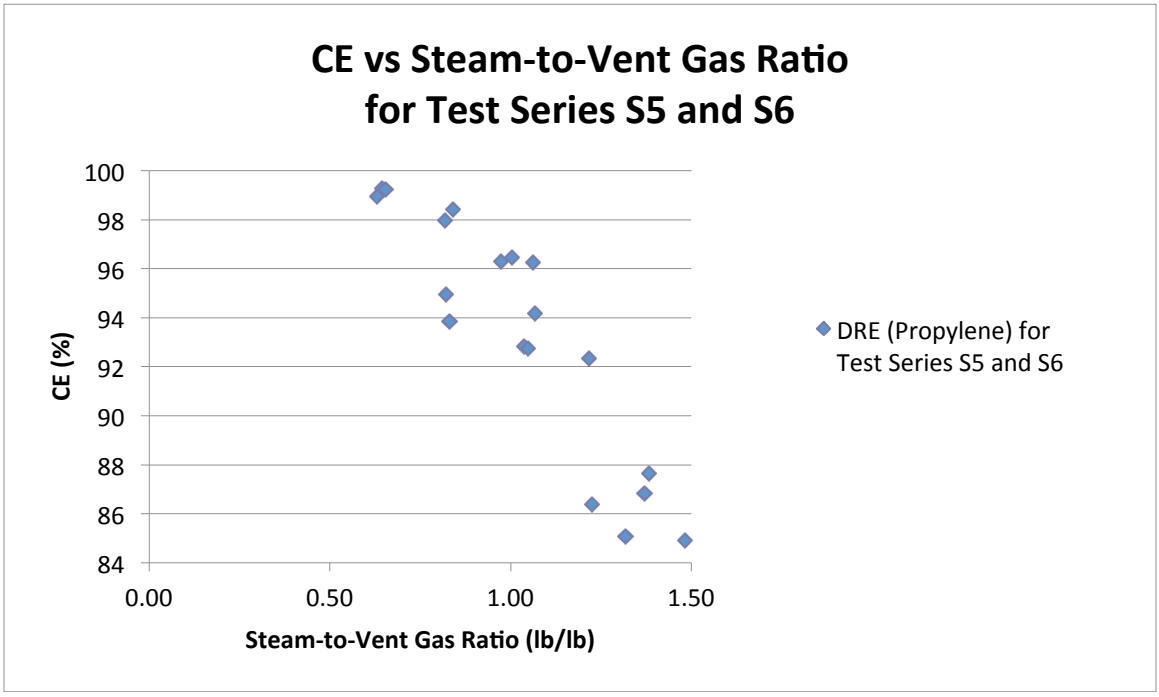

Figure 5-17b. CE vs Steam-to-Vent Gas Ratio for All Test Series S5 and S6
(Note CE range = 84 to 100%)

The next five test series illustrate the impact of center steam on DRE. Please refer to Figures 5-18a, 5-18b, 5-19a and 5-19b for these cases.

Using a center steam flow rate of 501 lb/hr and 536 lb/hr upper steam (S/VG = 0.34), at a vent gas LHV of 354 Btu/scf and a flow rate 3,028 lb/hr, the highest DRE achieved was 96.0% (S7.6 R1). The CE for this test point/run was 95.3%. The average wind speed during this test point/run was 10.8 mph. The MFR for this test point/run was 0.024.

Using no center steam and 534 lb/hr upper steam (S/VG = 0.22) and a vent gas LHV of 356 Btu/scf and a flow rate of 2,399 lb/hr, the highest DRE achieved was 98.0% (S8.1 R1). The CE for this test point/run was 97.6%. The average wind speed during this test point/run was 12.6 mph. The MFR for this test point/run was 0.007.

Using no center steam but twice as much upper steam (1,007 lb/hr, S/VG = 0.43) and a vent gas LHV of 347 Btu/scf and a flow rate of 2,364 lb/hr, the highest DRE achieved 94.4% (S9.1 R1). The CE for this test point/run was 93.3%. The average wind speed during this test point/run was 12.2 mph. The MFR for this test point/run was 0.007.

Using no center steam, an upper steam rate of 542 lb/hr (S/VG = 0.36) and a vent gas LHV of 353 Btu/scf and a flow rate of 2,348 lb/hr, the highest DRE achieved was 95.8% (S10.1 R1). The CE for this test point/run was 95.0%. The average wind speed during this test point/run was 10.9 mph. The MFR for this test point/run was 0.009.

Lastly, with 286 lb/hr of center steam and 830 lb/hr upper steam (S/VG = 0.35), a vent gas LHV of 355 Btu/scf and a flow rate of 2,354 lb/hr, the highest DRE achieved was 96.0% (S11.1 R1). The CE for this test point/run was 95.4%. The average wind speed during this test point/run was 10.5 mph. The MFR for this test point/run was 0.014.

Figures 5-19a and 5-19b are the same data as Figures 5-18a and 5-18b except the horizontal axis has been reversed to show a decline in DRE and CE as the values on the horizontal axis decrease from left to right.

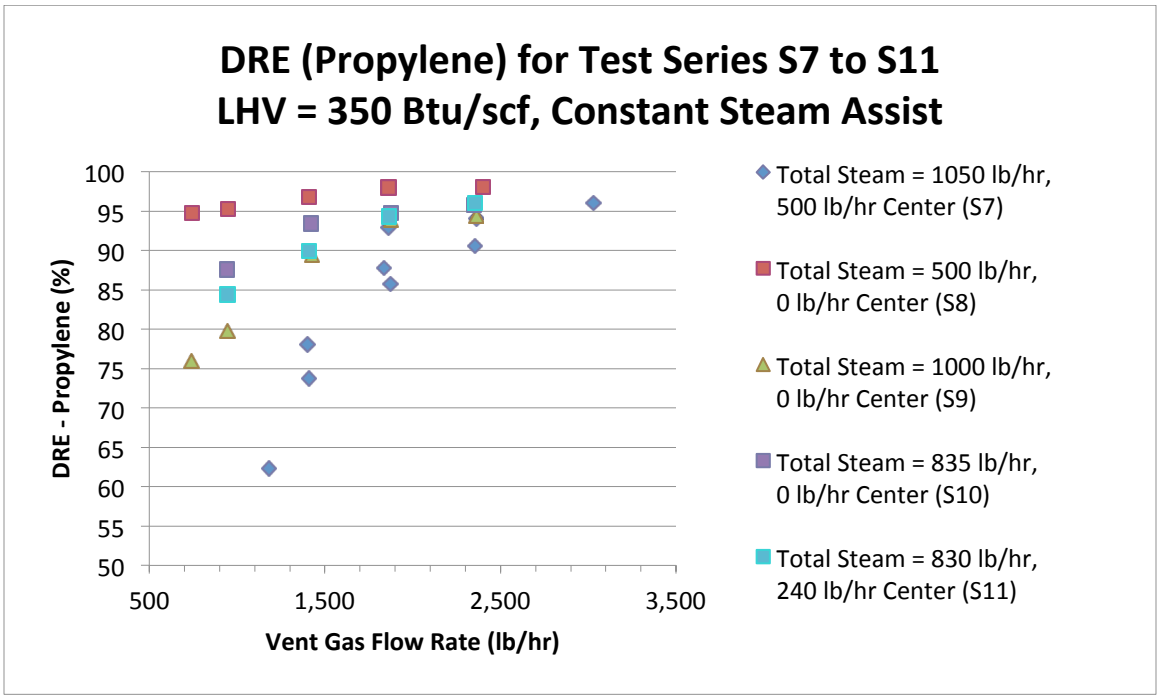

Figure 5-18a. DRE vs Vent Gas Flow Rate for Test Series S7, S8, S9, S10 and S11

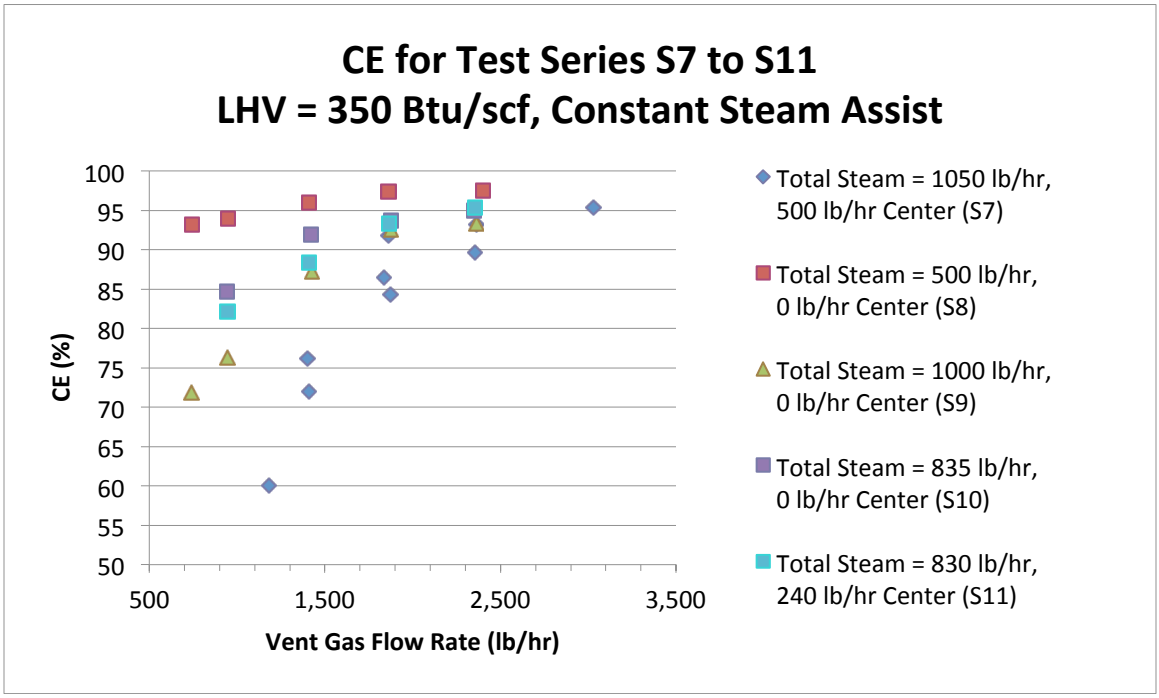

Figure 5-18b. CE vs Vent Gas Flow Rate for Test Series S7, S8, S9, S10 and S11

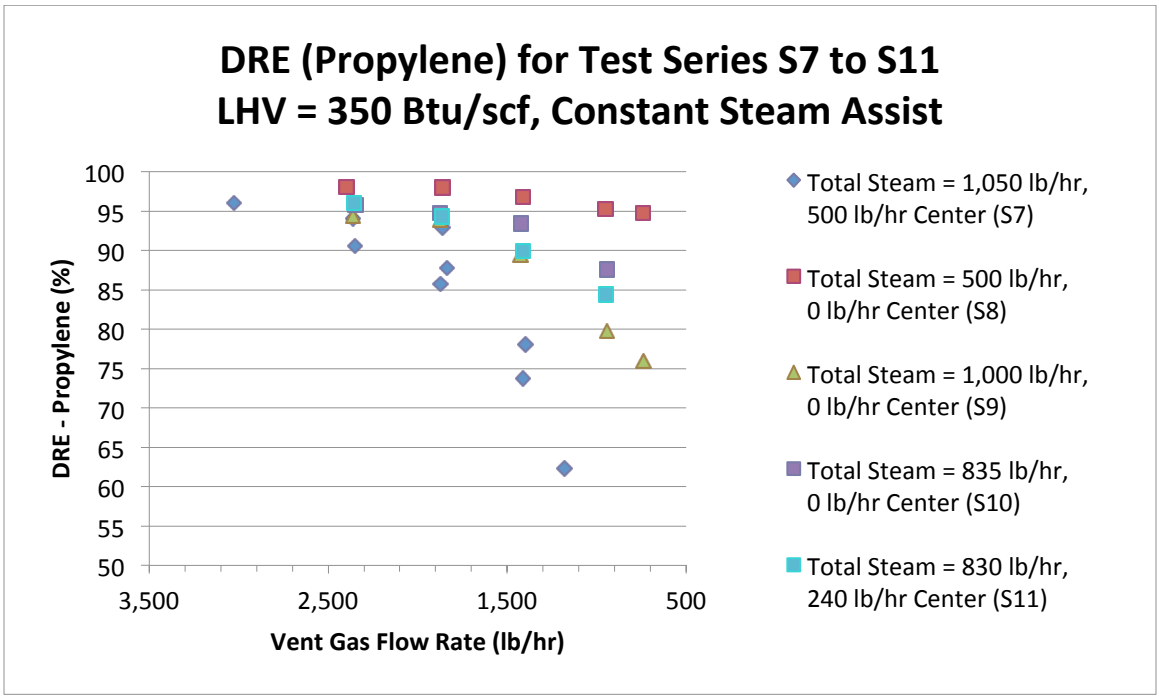

Figure 5-19a. DRE vs Vent Gas Flow Rate for Test Series S7, S8, S9, S10 and S11
(Note values on horizontal axis decrease from left to right)

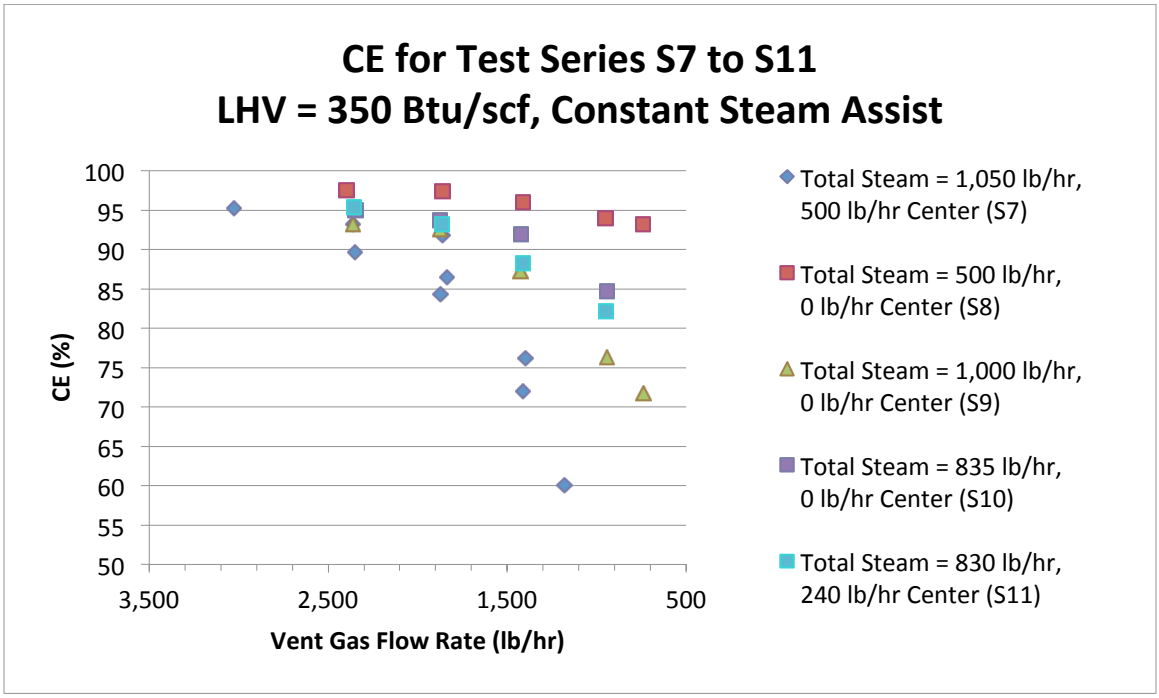

Figure 5-19b. CE vs Vent Gas Flow Rate for Test Series S7, S8, S9, S10 and S11
(Note values on horizontal axis decrease from left to right)

The Combustion Zone Gas Net Heat Value (CZG NHV), Btu/scf, is defined in this study as the ratio of the sum of the combustion heating value (LHV) of the vent gas going through the flare plus the combustion heating value of the flare pilots to the total volume of gases going to the flare, including steam, i.e., vent gas plus pilot gas plus total steam assist. It is expressed numerically as

$$CZG\ NHV = \frac{\left[(\mathrm{VG})(\mathrm{LHV_{VG}})(386.3/\mathrm{MW_{VG}})\right] + \left[(PG)(LHV_{PG})(386.3/MW_{PG})\right]}{\left[(\mathrm{VG})(386.3/\mathrm{MW_{VG}}) + (\mathrm{PG})(386.3/\mathrm{MW_{PG}}) + (\mathrm{S})(386.3/18.02)\right]} \qquad \text{Eq. 5.3}$$

where

CZG NHV =	combustion zone gas net heating value, Btu/scf
VG =	Vent gas mass flow rate, lb/hr
LHV_{VG} =	Vent gas lower heating value, Btu/scf
MW_{VG} =	Vent gas molecular weight, lb/lb-mol
PG =	Pilot gas mass flow rate, lb/hr
LHV_{PG} =	Pilot gas lower heating value, Btu/scf
MW_{PG} =	Pilot gas molecular weight, lb/lb-mol
S =	Total steam mass flow rate, lb/hr
386.3 =	Ideal gas volume (scf) per lb-mol at 68°F and 1 atmosphere
18.02 =	Steam molecular weight, lb/lb-mol

Please refer to Figures 5-20a, 5-20b, 5-21a, and 5-21b

Figure 5-20a plots the DRE (Propylene) vs CZG NHV for all test points in Test Series S3 through S6. Figure 21a plots the DRE (Propylene) vs CZG NHV for Test Series S7 through S11. Figures 5-20b and 5-21b have the horizontal axis reversed, i.e., the values on the axis decrease from left to right, and focus only on DRE and CE values above 84%, which is the more important section of these graphs for the study. It appears that until the CZG NHV gets above 300 Btu/scf for Test Series S3 through S6, does the DRE (Propylene) appear to have a single value of DRE above 98%. There is insufficient data to estimate a similar value for Test Series S7 through S11.

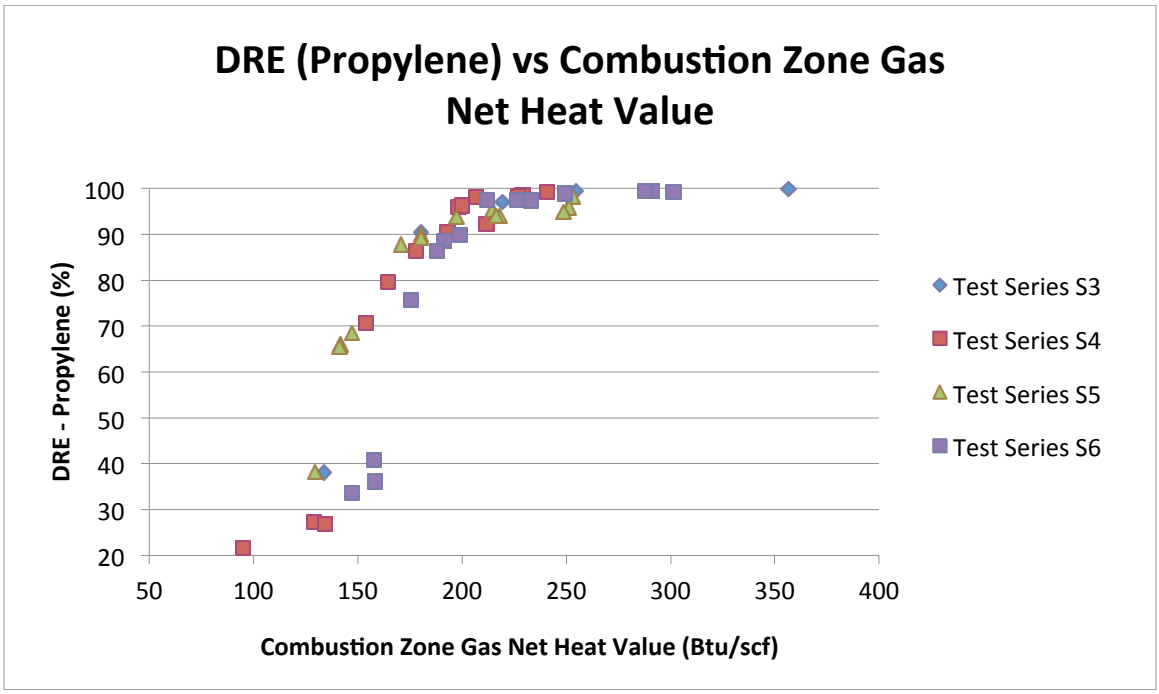

Figure 5-20a. DRE vs CZG NHV for Test Series S3, S4, S5 and S6

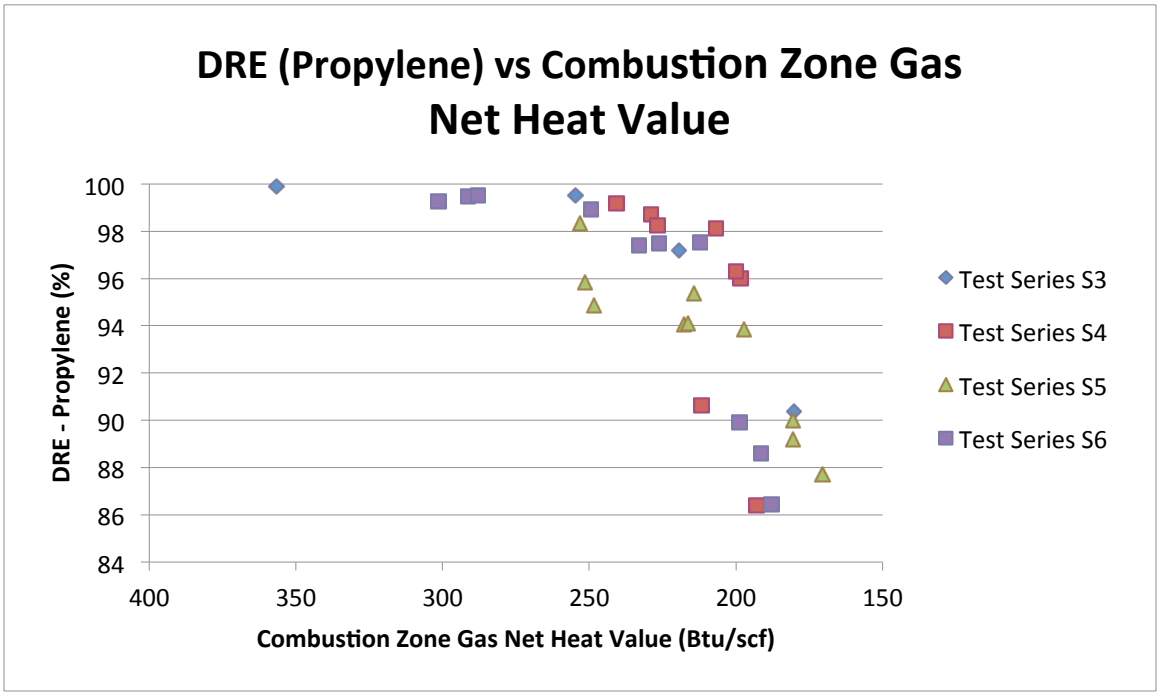

Figure 5-20b. DRE vs CZG NHV for Test Series S3, S4, S5 and S6
(Note vertical axis DRE range = 84 to 100% and
values on horizontal axis decrease from left to right)

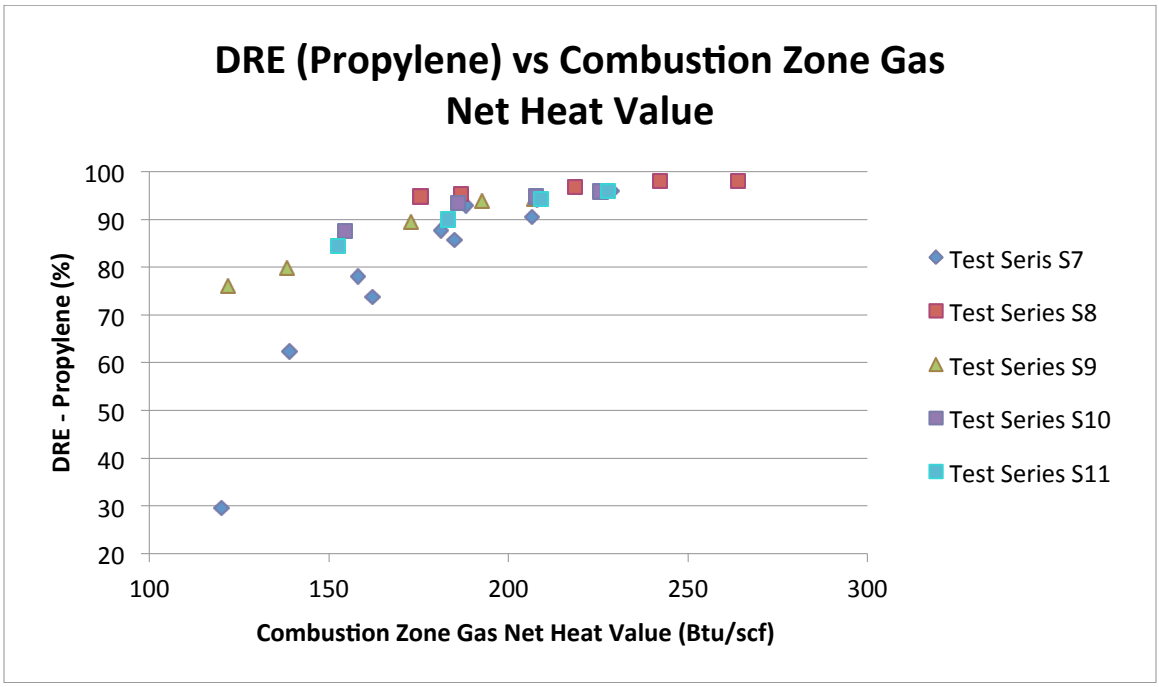

Figure 5-21a. DRE vs CZG NHV for Test Series S7, S8, S9, S10 and S11

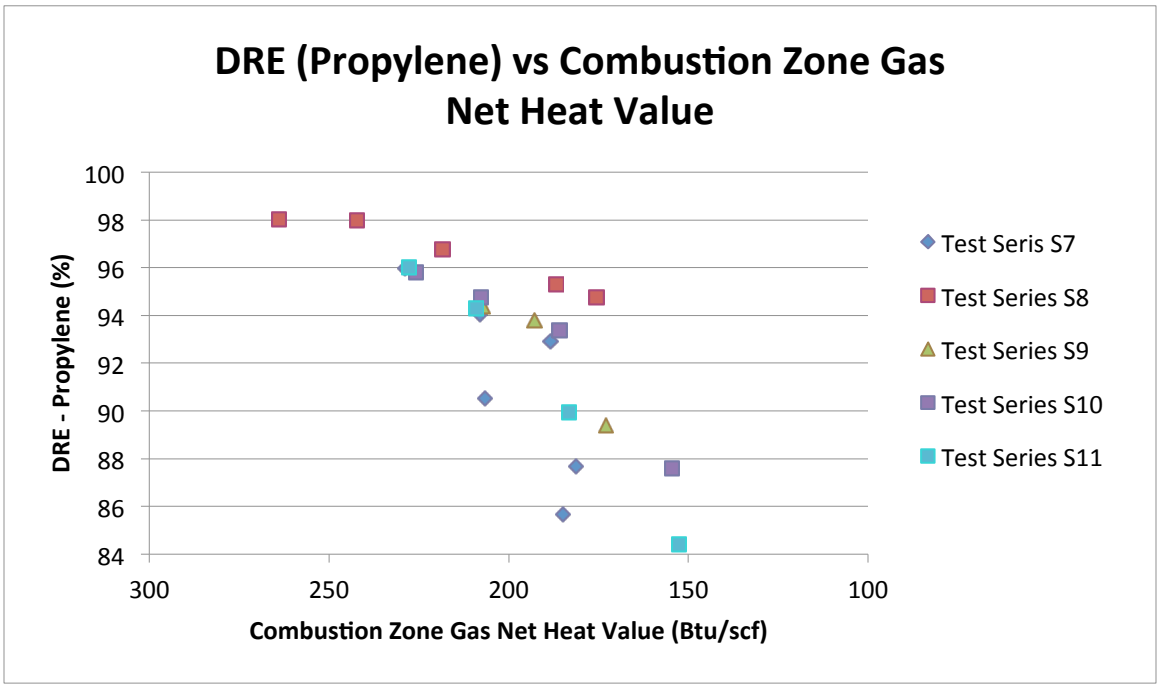

Figure 5-21b. DRE vs CZG NHV for Test Series S7, S8, S9, S10 and S11
(Note vertical axis DRE range = 84 to 100% and
values on horizontal axis decrease from left to right)

Air-Assisted Flare: DRE (Propylene) and CE

In the following summaries the term stoichiometric ratio (SR) will be used to represent the ratio of the actual air assist (lb/hr) used during a test point/run to the amount of theoretical air (lb/hr) required to provide the exact amount of oxygen for stoichiometric combustion of the fuel, i.e., amount of theoretical stoichiometric air (SA) to fuel ratio on a mass basis. The following theoretical SA to fuel ratios were used: propylene -14.807 lb/lb, propane – 15.246 lb/lb, and TNG – 15.737 lb/lb. All values for theoretical SA/fuel ratios are from *The John Zink Combustion Handbook* (Baukal, 2001). The value for TNG is based on the average composition shown in Table H-1. As an example, if 100,000 lb/hr of assist air were used during a test point/run and the amount of SA required was 20,000 lb/hr for the amount of fuel in the vent gas flow, the SR would be 5.0 (100,000 lb/hr ÷ 20,000 lb/hr). As can be seen from this example the SR is a dimensionless quantity as the units in the numerator and the denominator cancel each other out.

Please refer to Figures 5-22a and 5-22b.
At an air assist flow rate of 21,300 lb/hr (SR = 7.2), for a vent gas LHV of 339 Btu/scf and a constant flow rate of 902 lb/hr, the DRE (propylene) was 99.0% (A3.1 R3). Higher air assist levels produced lower DREs. The CE for this test point/run was 98.5%. The average wind speed during this test point/run was 10.4 mph. The MFR for this test point/run was 0.25.

At an air assist flow rate of 7,930 lb/hr (SR = 6.5), for a vent gas LHV of 351 Btu/scf and a constant flow rate of 355 lb/hr, the maximum DRE (propylene) was 97.0% (A5.1 R2). Higher air assist levels produced lower DREs. The CE for this test point/run was 96.6%. The average wind speed during this test was 9.0 mph. The average wind speed during this test point/run was 3.8 mph. The MFR for this test point/run was 0.53.

Please refer to Figures 5-23a and 5-23b.
At an air assist flow rate of 12,600 lb/hr (SR = 6.5), for a vent gas LHV of 584 Btu/scf and a constant flow rate of 352 lb/hr, the DRE (propylene) was 99.4% (A6.1 Run 3). Higher air assist levels produced lower DREs. The CE for this test point /run was 99.1%. The average wind speed during this test point/run was 13.8 mph. The MFR for this test point/run was 0.11.

At an air assist flow rate of 30,200 lb/hr (SR = 6.2), for a vent gas LHV of 559 Btu/scf and a constant flow rate 594 lb/hr, the DRE (propylene) was 99.4% (A4.6 Run 1). Higher air assist levels produced lower DREs. The CE for this test point/run was 98.9%. The average wind speed during this test point/run was 16.3 mph. The MFR for this test point/run was 0.43.

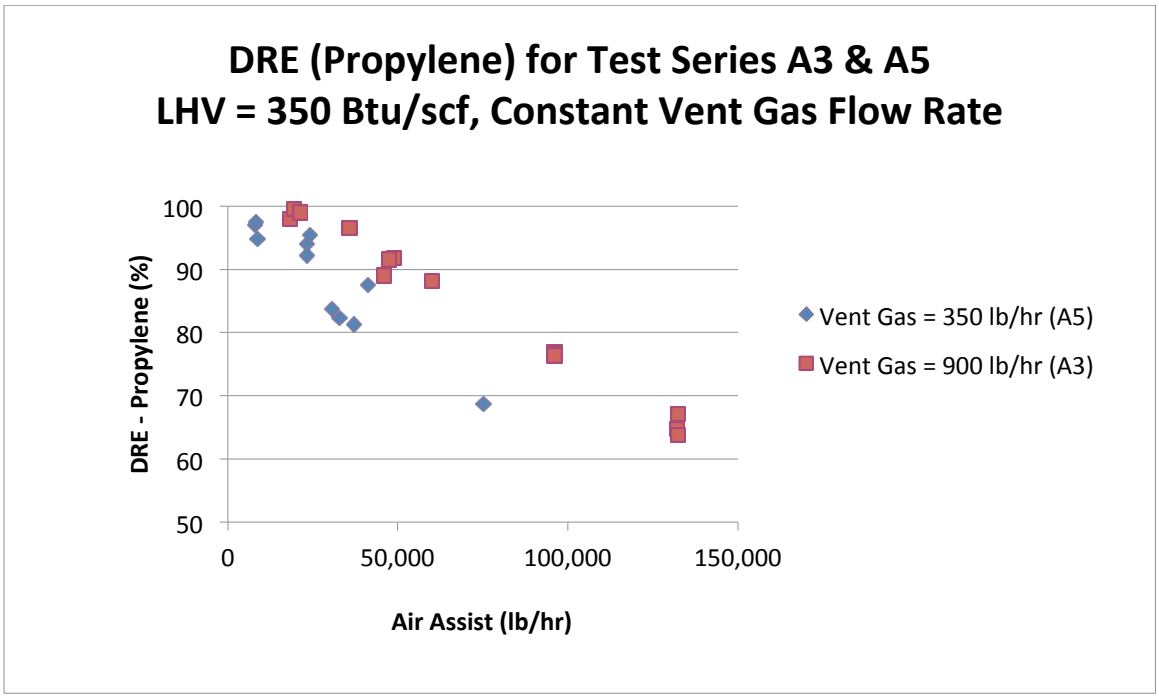

Figure 5-22a. DRE vs Air Assist for Test Series A3 and A5

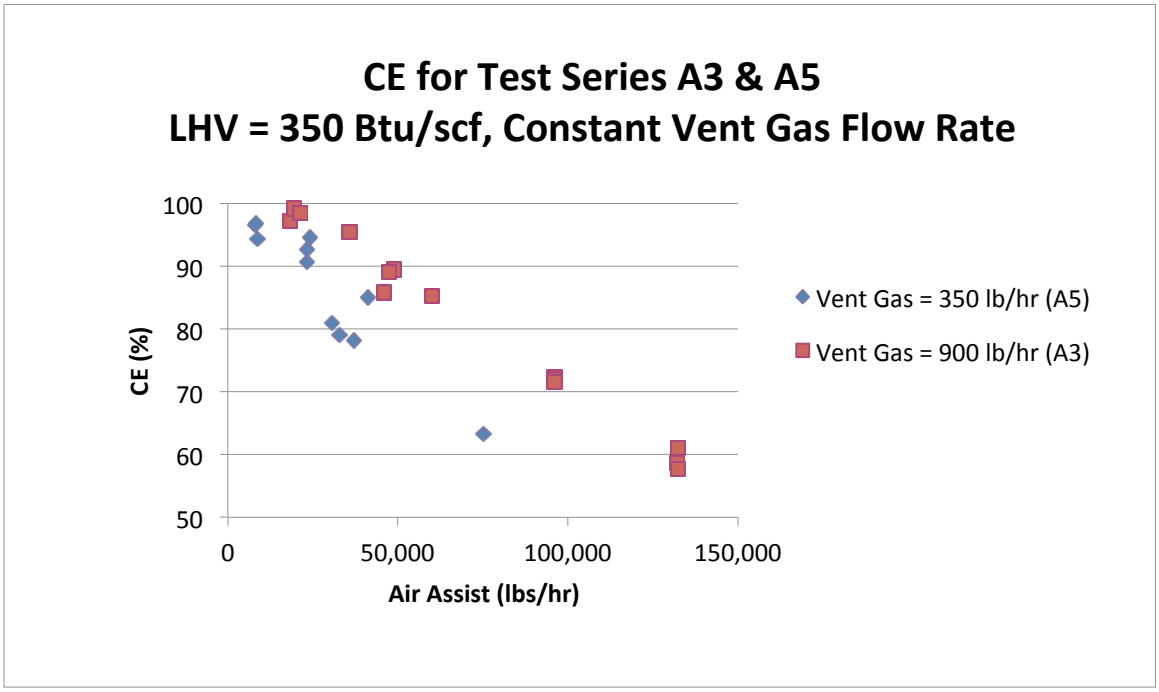

Figure 5-22b. CE vs Air Assist for Test Series A3 and A5

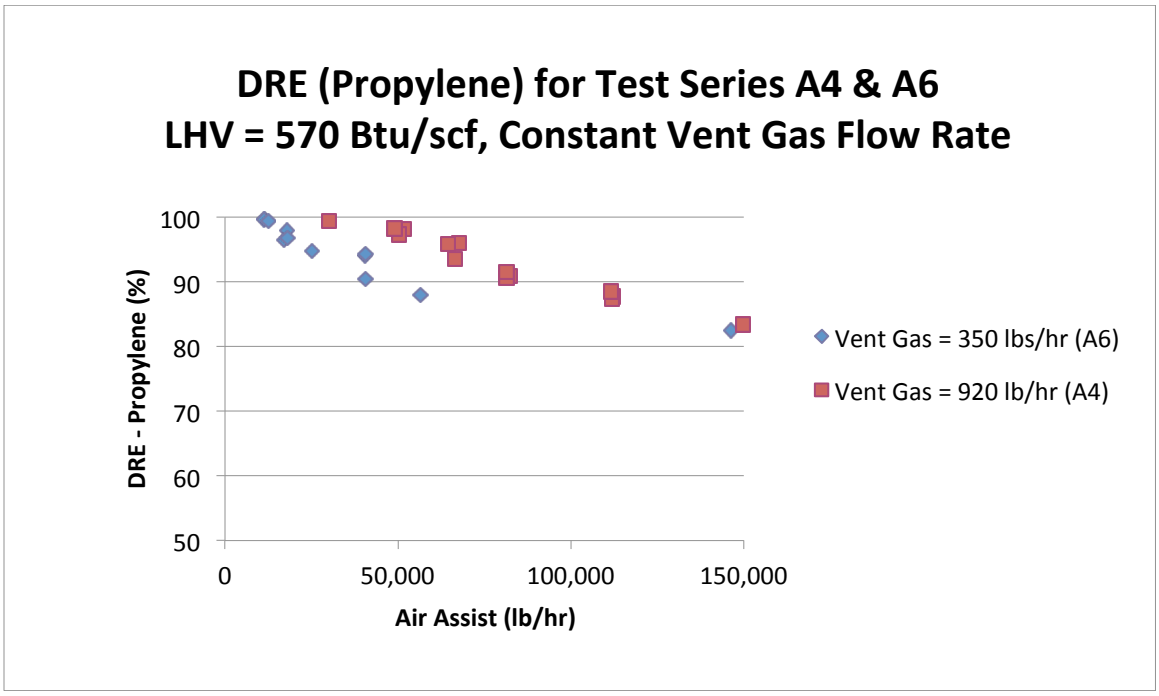

Figure 5-23a. DRE vs Air Assist for Test Series A4 and A6

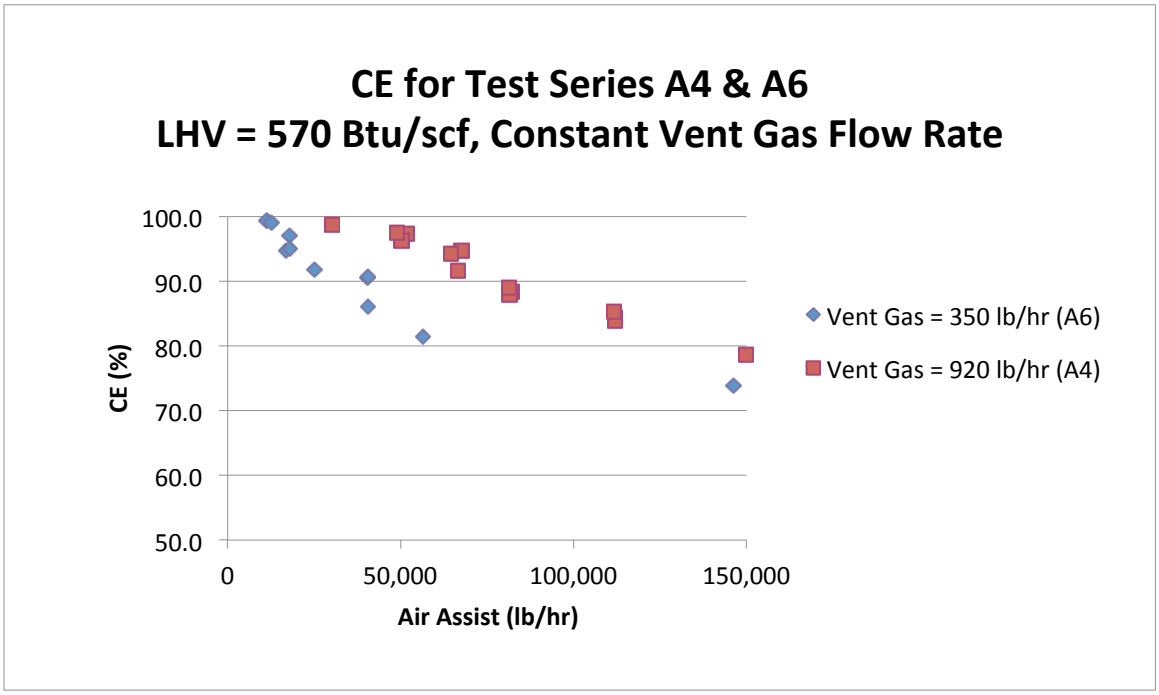

Figure 5-23b. CE vs Air Assist for Test Series A4 and A6

Steam-Assisted Flare: DRE (Propane) and CE

Please refer to Figures 5-24a and 5-24b.

For the combination of operating parameters shown in Figures 5-24a and 524b, with a vent gas flow rate of 2,363 lb/hr (S/VG = 0.44), the maximum DRE was 97.7% (S12.1 R1). The CE for this test point/run was 97.4%. The average wind speed during this test point/run was 2.9 mph. The MFR for this test point/run was 0.209.

For the combination of operating parameters shown in Figures 5-24a and 5-24b, with a vent gas flow rate 2,394 lb/hr (S/VG = 0.35), the maximum DRE was 98.3% (S13.1 R1). The CE for this test point/run was 98.0%. The average wind speed during this test point/run was 5.2 mph. The MFR for this test point/run was 0.059.

For the combination of operating parameters shown in Figures 5-24a and 5-24b, with a vent gas flow rate 2,370 lb/hr (S/VG = 0.23), the DRE was 99.1% (S14.1 R1). The CE for this test point/run was 98.9%. The average wind speed during this test point/run was 4.7 mph. The MFR for this test point/run was 0.051.

Air-Assisted Flare: DRE (Propane) and CE

Please refer to Figures 5-25a and 5-25b.

At an air assist flow rate of 7,120 lb/hr (SR = 5.5), for a vent gas LHV of 356 Btu/scf and a constant flow rate of 365 lb/hr, the DRE (propane) was 99.8% (A7.1 R2). Higher air assist levels produced lower DREs. The CE for this test point/run was 99.8%. The average wind speed during this test point/run was 3.8 mph. The MFR for this test point/run was 0.45.

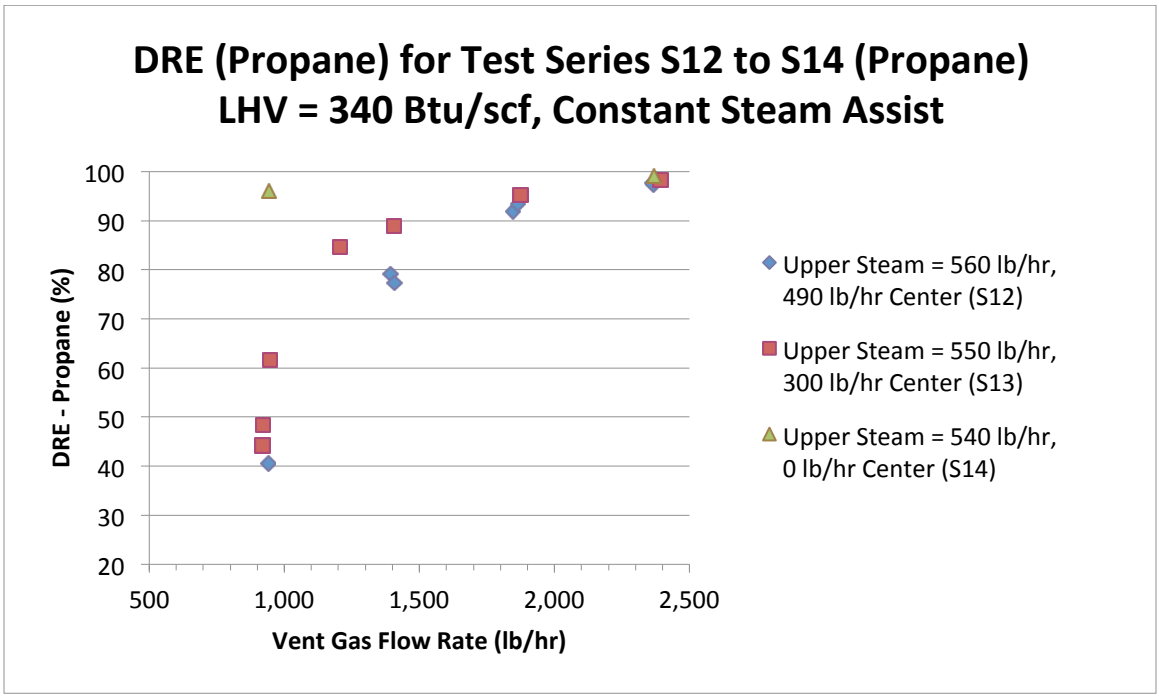

Figure 5-24a. DRE vs Vent Gas Flow Rate for Test Series S12, S13 and S14

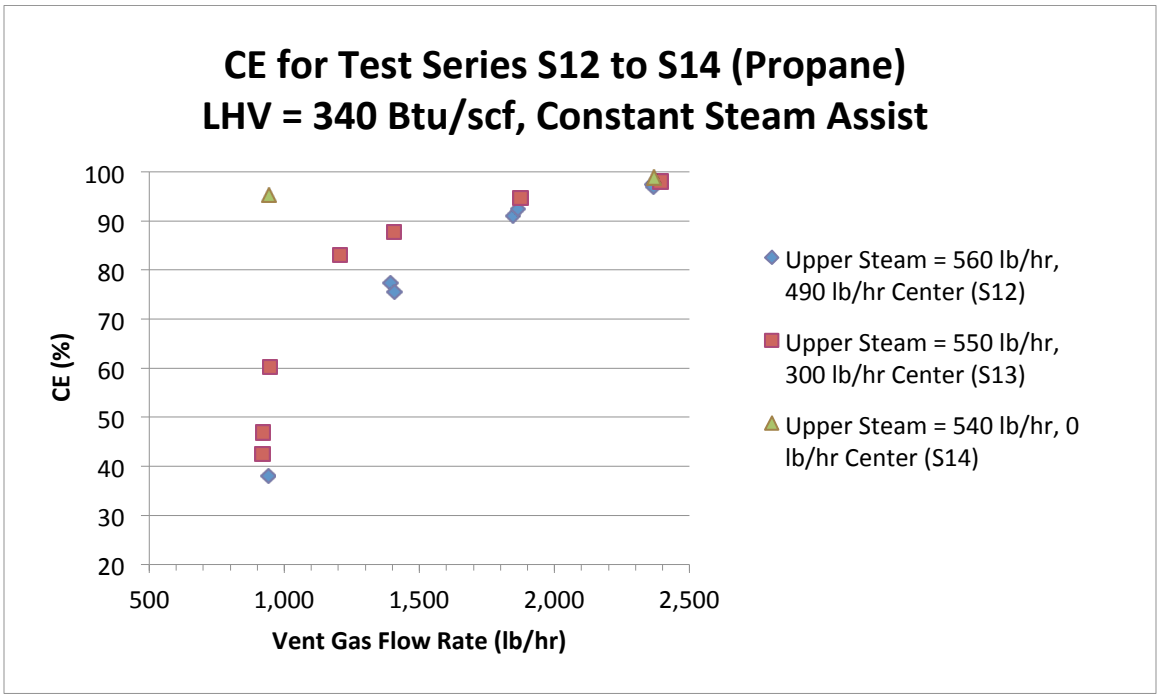

Figure 5-24b. CE vs Vent Gas Flow Rate for Test Series S12, S13 and S14

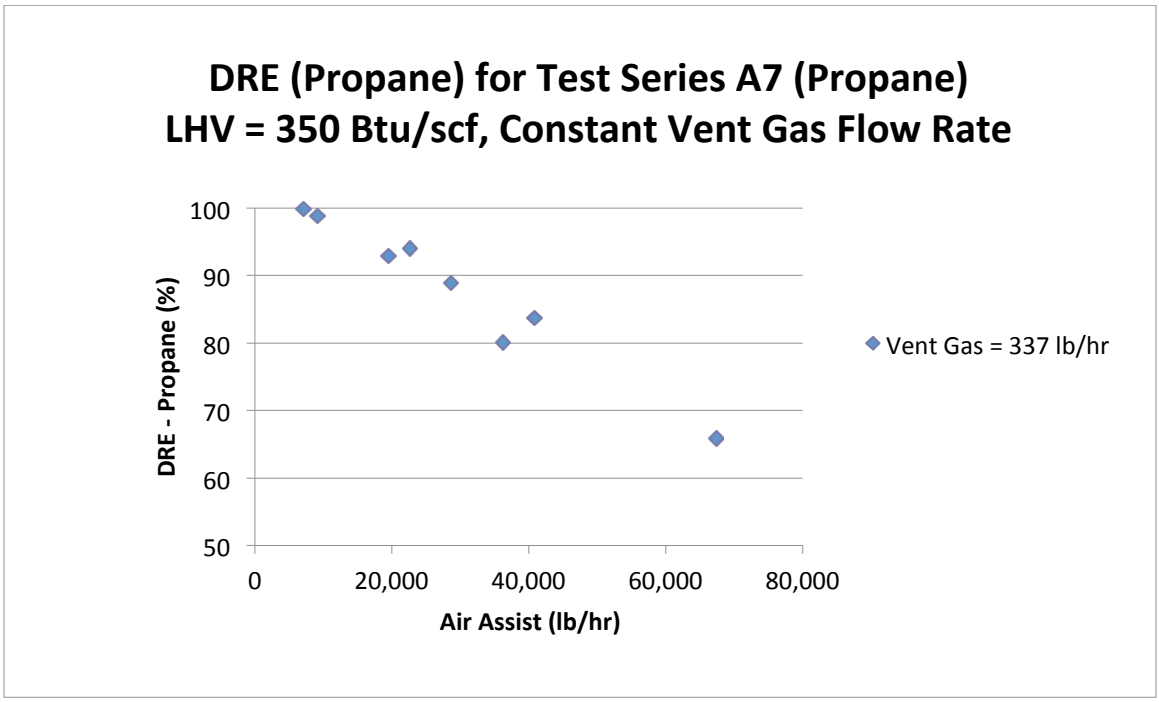

Figure 5-25a. DRE vs Air Assist for Test Series A7

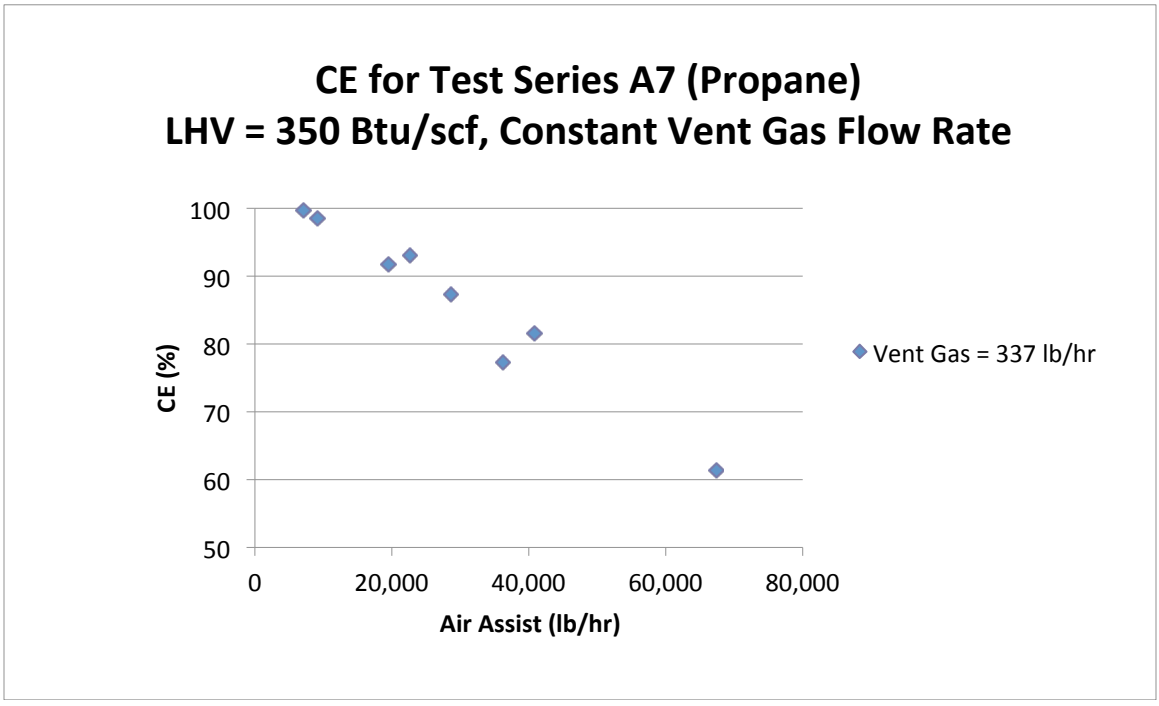

Figure 25b. CE vs Air Assist for Test Series A7

6.0 Discussion of Test Results

The study objectives for this project included assessing the performance of industrial flares operating with low vent gas flow rates (high turn down ratios) and low LHV vent gas properties and assessing the impact of air and steam assist on DRE and CE for these low flow, low LHV vent gas streams. The analyses of the test results will focus on answering the TCEQ Study Objectives even though many more questions could be addressed with these data. In this discussion, the flare performance will always be evaluated in terms of DRE and CE. When the term DRE is used in the propylene tests, it will always refer to DRE (propylene). When the term DRE is used in the propane tests, it will always refer to DRE (propane). The DRE was not computed for any other hydrocarbons during this test series.

Steam Flare Tests with Propylene (please refer to Table D-1 in Appendix D)
For the lowest nominal LHV (350 Btu/scf) and lowest nominal vent gas flow rate (920 lb/hr) used in the study for the steam flare tests, Figures 5-12a and 5-12b illustrate the sensitivity of the flare's performance to steam assist with this vent gas stream (S3), particularly the addition of center steam. The average wind speed for the S3 test series ranged between 2.6 mph and 7.5 mph. When the center steam was zero (Test Points S3.6 and S3.7) and total steam did not exceed about 230 lb/hr, the DRE and CE were the highest, in excess of 99%, even with the highest wind speed of the S3 test series (7.5 mph) during S3.5R2. However, as soon as the steam assist was progressively increased (Test Points S3.5 and S3.2) with average wind speeds ranging from 7.2 mph to 7.5 mph, comparable to or less than the Test Points S3.6 and S3.7, which had the highest DRE and CE, the DRE and CE progressively decreased. The DRE and CE were lowest, 36.1% and 34.3%, respectively, for S3.1R1, which had the lowest wind speed and nominal steam assist (center = 540 lb/hr, upper = 430 lb/hr) equating to a steam-to-vent gas ratio (S/VG) of 1.04. Industry reported to the TCEQ (email message from R. Nettles, TCEQ, to V. Torres, UT Austin, on September 8, 2010) prior to the study that this level of steam assist, is slightly lower than that recommended (center = 500 lb/hr, upper = 750 lb/hr) by flare manufacturers to industry for this size and model of steam flare.

This one test series showed three characteristics of this flare at these operating conditions:

1. Average wind speeds up to 7.5 mph do not prevent this flare from achieving 99% DRE and 99% CE but only at operating conditions that are not recommended by flare manufacturers.
2. This flare's performance curve as measured by DRE and CE versus steam assist, has a very short, almost nonexistent, DRE "shelf" that is adversely affected by the addition of center steam.
3. Steam assist levels (center steam = 500 lb/hr, minimum, and upper steam = 750 lb/hr , minimum) currently used by industry would be too high to achieve a DRE of 99%.

Using the same LHV (350 Btu/scf) and a vent gas flow rate of nominally 2,342 lb/hr (S4.2R3), the DRE is sustained at 99% for a slightly greater amount of steam assist (S/VG = 0.29), approximately 666 lb/hr total (center = 555 lb/hr) before the DRE and CE start to fall below 99%. Once again, steam assist levels currently used by industry would be too high to achieve a DRE of 99% and these levels of steam assist would not comply with Zink's recommended steam

levels for this flare tip, i.e., minimum continuous center steam = 300 lb/hr and 525 lb/hr upper steam.

For the highest nominal LHV (600 Btu/scf) used in this study for the steam flare tests and a nominal vent gas flow rate of 937 lb/hr (Test Series S5), as shown in Figures 5-13a and 5-13b, the flare's best performance in response to steam assist is similar to the S3 test series but more robust in its response to center steam. In Test Point S5.1, with center steam = 480 lb/hr and upper steam = 283 lb/hr (S/VG = 0.82), the average DRE was 96.4% and CE was 95.6%. The average wind speed was 8.0 mph during this test. Whereas, test point/run S3.2R2, with only 570 lb/hr total steam (52 lb/hr center, 518 lb/hr upper), resulted in a DRE of 90.4% and a CE of 88.6% with a very comparable average wind speed of 7.5 mph. No operating condition in the Test Series S5 would have achieved a DRE ≥ 99% with levels of steam assist of 500 lb/hr center steam and 750 lb/hr upper steam.

In Test Series S6 with the same nominal LHV (600 Btu/scf) and the higher vent gas flow rate of nominally 2,342 lb/hr, the DRE and CE exceed 99% (S6.1) and the DRE was sustained at almost 99% (S6.5) with additions of steam of up to approximately 2,000 lb/hr total (S/VG = 0.84). Average wind speeds in these two test series ranged from 7.5 mph to 8.0 mph. This combination of LHV and vent gas flow rate would achieve DRE ≥ 99% with levels of steam assist of 500 lb/hr center steam and 750 lb/hr upper steam.

While it appears from Figure 5-14a that a S/VG value of approximately 0.4 or less ensures that the DRE is above 98%, expanding the graph for the region greater that 84% (Figure 5-15a and Figure 5-15b) reveals something different. Examining Figure 5-15a and the data summary in Appendix D, there are multiple values for DRE for a given S/VG until the S/VG gets much closer to 0.15 or less for this LHV (= 350 Btu/scf) and vent gas flow rates. A similar trend is noted for the CE (Figure 5-15b) with the critical S/VG value to obtain CE = 98% being much less than 0.1, perhaps even close to zero, since in general, the CE values are less than the DRE values for a given S/VG.

As was seen at a LHV = 350 Btu/scf, it appears in Figure 16a that a S/VG = 0.9 or less would ensure a DRE of 98% or more. However, upon closer inspection of Figure 5-17a, in which the region DRE > 84% is expanded, and the summary data in Appendix D, once again due to multiple DRE values for a given S/VG, the S/VG must be less than about 0.70 to ensure a DRE above 98% for a LHV of 600 Btu/scf and these vent gas flow rates. As above, the S/VG must be less than 0.65 for the CE to be above 98%.

Air Flare Tests with Propylene (please refer to Table E-1 in Appendix E)
For the lowest nominal LHV (350 Btu/scf) and lowest nominal vent gas flow rate (350 lb/hr) used in this study for the air flare tests, Figures 5-22a and 5-22b illustrate the sensitivity of the flare's performance to air assist with this vent gas stream (A5). When the air assist was 8,330 lb/hr (SR = 7.0), the DRE for this test point/run (A5.1R3) was 97.4% and the CE was 96.9%. This was the lowest air assist rate that satisfied the study's definition of incipient smoke point so no lower air assist conditions were tested. As the air assist increased, the DRE and CE decreased almost linearly. The average wind speed for the A5 test series ranged from 2.1 mph to 5.6 mph.

For the same nominal LHV (350 Btu/scf) and a nominal vent gas flow rate of 900 lb/hr, when the air assist rate was at or very near the incipient smoke point, the air assist rate was 19,400 lb/hr (SR = 6.5), the DRE for this test point/run (A3.1R2) was 99.6% and the CE was 99.2%. As the air assist increased, the DRE and CE decreased almost linearly. The average wind speed for the A3 test series varied from 10.3 mph to 13.4 mph.

Equation 6.1 defines the air assist tip exit velocity.

$$air\ assist\ tip\ exit\ velocity\ (mph) = \frac{air\ assist\ (scfm)}{7.5\ ft^2} \times \frac{P_{STP}}{P} \times \frac{T}{T_{STP}} \times \frac{60\ min/hr}{5{,}280\ ft/mile} \qquad \text{Eq. 6.1}$$

where

air assist tip exit velocity (mph) = speed of the air assist in mph as it exits the flare tip
air assist (scfm) = volumetric flow rate of the air assist, scfm, from Table E-1
7.5 ft^2 = free flow area of the air assist only
P_{STP} = standard pressure, 14.696 psia
P = ambient air pressure, psia, from Table E-1
T (ºR) = ambient air temperature, ºF, from Table E-1, plus 459.7 ºR
T_{STP} (ºR) = standard temperature, ºR, 527.7 ºR (= 459.7 + 68)

For the flare tests conducted, the range of molecular weights of the vent gas were 29.6 lb/lb-mol to 30.8 lb/lb-mol, similar to or slightly greater than that of air, 28.96 lb/lb-mol. Exit velocities for the vent gas from Table 1 for Test Series A3 and A4 were 1.9 fps, for A5 and A7 were 0.8 fps and for A6 were 0.7 fps. Converting these vent gas exit velocities to mph we get Test Series A3 and 4 were 1.3 mph, A5 and A7 were 0.6 mph and A6 were 0.5 mph.

The volumetric flow rate for the air assist during this test series ranged from about 4,000 scfm to 29,400 scfm. Calculating the air assist tip exit velocity using Equation 6.1, these two volumetric flow rates equate to 6.4 mph and 47.1 mph, respectively. Comparing the air assist exit velocities with the vent gas exit velocities and their very comparable molecular weights, the velocity of the air assist will be the dominant driver in characterizing the momentum of the vent gas/air assist mixture exiting the tip of the flare, which is proportional to the square of the velocity.

At every test point in this A3 test series, the velocity of the air assist exiting the flare was equal to or greater than the wind speed except for A3.1. So the momentum of the vent gas/air assist mixture exiting the flare tip was greater than the momentum of the crosswind, i.e., MFR ≥ 1.0. Therefore, particularly at the higher air assist rates (> 9,000 scfm), any adverse effect from the wind speed during these test series was difficult to distinguish from the adverse air assist impact.

When the nominal LHV of 600 Btu/scf and the highest vent gas flow rate were used for the air flare tests (A4), for the test point/run A4.6R1, the DRE was 99.4% and the CE was 98.9% using an air assist rate of 30,200 lb/hr (SR = 6.2). The average wind speed for this test point was 16.3 mph. Using Equation 6.1, an air assist volumetric flow rate of 6,700 scfm equates to an air assist

exit velocity of 10.5 mph. Even when the average wind speed was 55% greater than the air assist exit velocity, the DRE was > 99%.

As with all of the other air flare tests, as the air assist increases, there appears to be a linear decrease in the DRE. In this test series, the decrease in DRE and CE has a slope that is less than in the previous tests.

Steam Flare Tests with Propane (please refer to Table D-1)
This test series (please see Figures 5-24a and 5-24b), conducted with the substitution of propane for propylene, was conducted at only one LHV, 350 Btu/scf.

With the knowledge of the propylene test series, and the greater challenges the test system had with variation of steam assist at low steam levels, the propane test series were conducted at three nominal steam assist conditions, each held constant when employed: center = 0 lb/hr, upper = 550 lb/hr; center = 300 lb/hr, upper = 550 lb/hr; and center = 500 lb/hr, upper = 550 lb/hr.

At a nominal LHV of 350 Btu/scf and a nominal vent gas flow rate of 2,342 lb/hr, with no center steam and 540 lb/hr upper steam (S/VG = 0.23) in test point/run S14.1R1, the DRE was 99.1% and the CE was 98.9%. The average wind speed for this test point/run was 4.7 mph (MFR = 0.051). When steam was added to the center, center = 300 lb/hr (S/VG = 0.35), the DRE decreased (S13.1R1) to 98.3% and the CE to 98.0%. The average wind speed for this test point/run was 5.2 mph (MFR = 0.059). As center steam was increased to 500 lb/hr (S12.1R1), S/VG = 0.44, the DRE decreased to 97.7% and the CE to 97.4%. The average wind speed for this test point/run was 2.3 mph (MFR = 0.209).

The remainder of the propane test series were conducted at combinations of lower vent gas flow rates and lower steam assist than Test Series 12.1 that did not achieve higher levels of DRE or CE than test point/run S14.1R1. No operating condition in the propane tests conducted would have achieved a DRE ≥ 99% with levels of steam assist of 500 lb/hr center steam and 750 lb/hr upper steam. The average wind speed during the propane test series varied from 0.5 mph to 7.2 mph.

Air Flare Tests with Propane (please refer to Table E-1)
This test series (please see Figures 5-25a and 5-25b), conducted with the substitution of propane for propylene, was conducted at only one LHV, 350 Btu/scf.

At a nominal LHV of 350 Btu/scf and a nominal vent gas flow rate of 350 lb/hr, with an air assist rate of 7,120 lb/hr (SR = 5.5) in test point/run A7.1R2, the DRE was 99.8% and the CE was 99.8%. The average wind speed for this test point/run was 3.8 mph (MFR = 0.45).

The remainder of the air flare propane test series was conducted at higher air assist rates, which produced progressively lower DREs and CEs. The average wind speed, during the air flare propane test series, varied from 3.6 mph to 5.8 mph.

Applicability of CZG NHV

Some (Marathon, November 2010; Marathon, May 2010) have used the CZG NHV (Equation 5-3) as a way to adjust the LHV of the vent gas to reflect other components that are added at and in the flare tip. What has been learned in this study is that the manner in which these components, i.e., center and upper steam, etc., are introduced affects the impact these contributors have on the combustion process just as importantly as does the amount of these components that are added. Center steam certainly acts as a diluent. But how much so and is the degree the same for all possible vent gas components? Upper steam adds oxygen and turbulence. Is this impact the same in all cases, i.e., how does crosswind and vent gas exit velocity affect the contributions of the upper steam? Do these contributions impact positively or negatively under all circumstances? The CZG NHV as presently defined is a volume term. Should it be a rate term reflecting the heating value flux through the tip?

More full-scale data and some computational fluid dynamics modeling are needed to address these questions. It was out of the scope of this effort to address the applicability of the CZG NHV in this study.

Effects of Wind on DRE and CE

As was stated in the scope, only one major parameter was not to be controlled during the testing: ambient conditions, including wind. Additionally the test plan in Section 3.0 did not include tests or instrumentation designed to quantify and characterize the effects of the wind on the flare's performance. Therefore no quantification of the winds effect will be presented. In response to comments received during the public comment period of the draft final report for this study, the TCEQ (email message from D. Nesvacil, TCEQ, to V. Torres, UT Austin, July 22, 2011) has submitted a bibliography of publicly available papers that include observation on wind effects on flare performance and results from flare testing under windy conditions. This bibliography is shown in Table 6.1.

Center and Upper Steam Effects on DRE

Center steam is used to provide added momentum to the vent gas flow so as to help prevent combustion from occurring inside the tip. The upper steam nozzles draw air into the steam and help to increase the mixing of the steam and air mixture with the vent gas exiting the flare tip. The air provides additional oxygen for combustion when the ambient air is unable to reach all parts of the combustion zone thereby helping to prevent smoking of the flare. A minimum continuous flow of steam is needed to prevent condensation from occurring in the steam lines and thermal shock in the upper steam ring and nozzles. It can also act as a windshield to reduce adverse wind effects on the flare flame (ANSI/API Standard 537, 2008).

But both forms of steam assist, as was seen in the data from this study, provide adverse effects on DRE and CE in different ways and in different amounts. Center steam acts as diluent of the vent gas because it adds no combustible heat content to the vent gas stream. A decrease in LHV reduces the hydrocarbon content (fuel) in the vent gas on a volume basis resulting in a lower DRE for the same steam-to-vent gas ratio. The exact magnitude of the decrease will depend on the LHV and combustion characteristics of the hydrocarbon fuels in the vent gas and the point of operation on the DRE curve.

In addition to the effects of upper steam described above, upper steam can also provide adverse effects on the flare performance. Upper steam can dilute the LHV of the vent gas prior to combustion and quench the combustion zone, both tending to decrease the DRE. In this study, the data suggest that when operating the steam flare used in this study at a DRE near 98%, if comparable flow rates of steam are introduced at the center and upper nozzles, the center steam will have a greater adverse effect on DRE than will the upper steam on the low flow, low LHV vent gas flows used in this study.

Comparison of Selected Data with US EPA 1983 Flare Study

After the public comment period for the draft final report, the TCEQ requested that a comparison of selected steam data from the US EPA 1983 Flare Efficiency Study (McDaniel 1983) be included in the final report. As these two studies had quite different objectives, were conducted using significantly different flare tips (8-inch diameter vs. 36-inch diameter; flare design with upper steam and no center steam vs. flare design with upper and center steam), different pilot designs and steam nozzle designs (personal conversation between R. Schwartz, John Zink Company, and V. Torres, UT Austin, September 27, 2010), EPA study was conducted primarily during winds speeds of less than 5 mph and vent gas exit velocities were significantly different (EPA 1983 Study: 1,035 fpm to 3,749 fpm vs. TCEQ 2010 Study: 30 fpm to 120 fpm), any comparison must be done with great caution and thoughtfulness.

In Figure 6-1, the CE (proplene) vs. S/VG ratio is shown for the 100% propylene flows (EPA 1983 Study: 2,183 Btu/scf and TCEQ 2010 Study: 2,149 Btu/scf) and for the low LHV flows EPA 1983 Study: 300 to 600 Btu/scf and TCEQ 2010 Study: 350 to 600 Btu/scf) for the steam flare tests whose flare operating conditions fall within these values. Please note that for all but one of the low LHV tests conducted during the EPA 1983 Study, no steam assist was used, i.e., S/VG = 0 lb/hr.

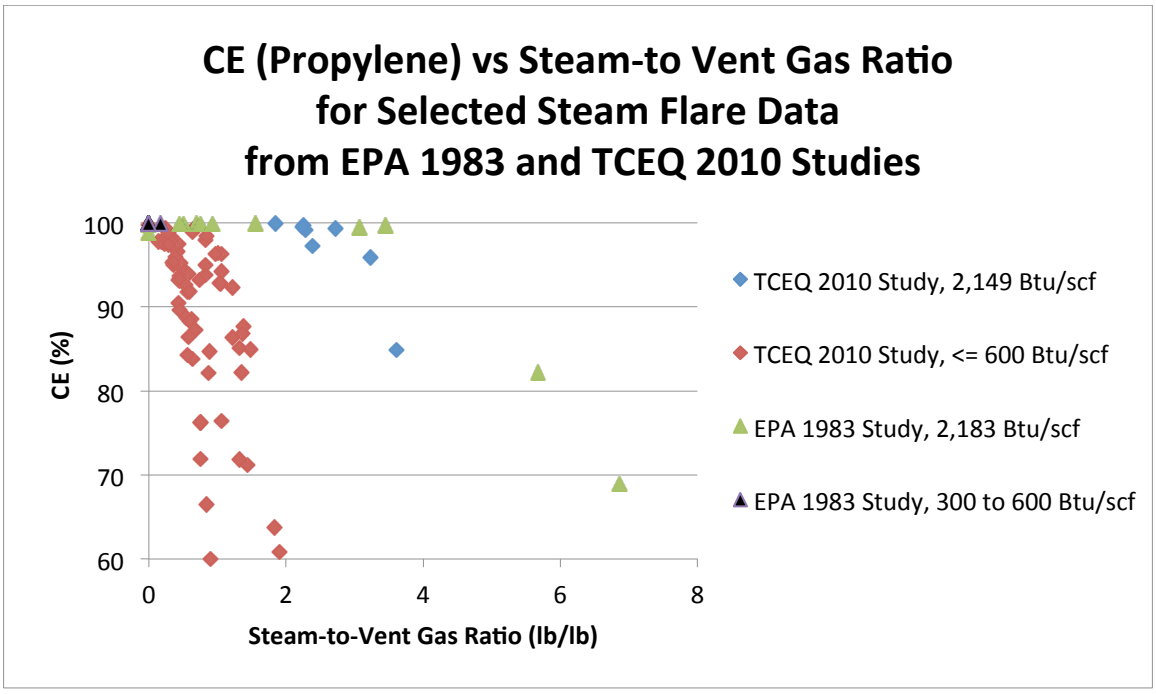

Figure 6-1. CE (Propylene) vs Steam-to-Vent Gas Ratio for Selected Data
from EPA 1983 and TCEQ 2010 Studies
(EPA 1983 study data taken from Table 4 in report)

For the 100% propylene (high LHV) vent gas tests, up to approximately an S/VG = 3, there is good agreement in the data between the two studies. Beyond that S/VG, the trends in the data are similar but the values begin to differ. For the low LHV vent gas tests (300 to 600 Btu/scf), the two study's results are significantly different for all data points except those in the TCEQ 2010 Study conducted with little or no steam assist. This is due to the fact that during the EPA 1983 Study, steam assist was not used for the low LHV vent gas tests except for one of the test points shown and that test was conducted with an S/VG = 0.168.

Links to Other Recent Full-Scale Flare Studies

There have been other studies conducted recently on full-scale flares. The TCEQ is providing access to some of these studies at the following website.

http://www.tceq.texas.gov/airquality/stationary-rules/flare_stakeholder.html

Table 6-1. Selected Papers and Reports on Wind Effects on Flare Performance

1	*Becker, R. [1974] "Ausbrandmessungen an Fackelflamen" (Measurement of residuals of flare stacks – in German), Messen + Steuern, 32, pp. 23-25.*
2	*Bourguignon, E., Johnson, M.R., and Kostiuk, L.W. [1999] "The use of a closed-loop wind tunnel for measuring the combustion efficiency of flames in a cross flow." Combustion and Flame, 119, pp.319-334.*
3	*Gogolek, P., Hayden, A.C.S., and Madrali, S. [2001] "Performance and Speciation of Solution Gas Flares Tested in the CANMET Flare Test Facility - Final Report." CETC report to PTAC.*
4	*Gogolek, P.E.G., and Hayden, A.C.S. [2002] "Efficiency of Flare Flames in Turbulent Crosswind." Advanced Combustion Technologies, Natural Resources Canada, American Flame Research Committee Spring Meeting, May.*
5	*Gogolek, P.E.G., and Hayden, A.C.S. [2004] "Performance of flare flames in a crosswind with nitrogen dilution." Journal of Canadian Petroleum Technology, 43, pp. 43-47.*
6	*Gogolek, P.E.G., Caverly, A., Pohl, J., Schwarz, R., and Seebold, J. [2010] Emissions from Elevated Flares – A Survey of the Literature. CANMET Energy, Natural Resources Canada, prepared for the International Flaring Consortium.*
7	Gollahalli and Parthasaronthy, R.P., "Turbulent Smoke Points in a Cross-Wind," Research Testing Services Agreement No. RTSA 3-1-98, University of Oklahoma, Norman, OK, August (1999).
8	*Haus, Rainer, Wilkinson, Rob, Heland, Jorg, and Schafer, K. [1998] "Remote sensing of gas emissions on natural gas flares." Pure and Applied Optics, 7, pp.853-862.*
9	*Howell, L.W., Poudenx, P.D., Johnson, M.R., Wilson, D.J. and Kostiuk, L.W. [2003]. "Flare Stack Diameter Scaling." Combustion Canada Conference 2003, Calgary, AB.*
10	*Johnson, Matthew R., Majeski, Adrian J., Wilson, David J., and Kostiuk, Larry W. [1998] "The Combustion Efficiency of a Propane Jet Diffusion Flame in Cross Flow." Fall Meeting of the Western States Section of the Combustion Institute, Seattle, Washington, 98F-38.*
11	*Johnson, M.R., and Kostiuk, L.W. [1999] "Effects of a Fuel Diluent on the Efficiencies of Jet Diffusion Flames in a Crosswind." The Combustion Institute, Canadian Section, 1999 Spring Technical Meeting, Edmonton, AB.*
12	*Johnson, M.R., Zastavniuk, O., Wilson, D.J., and Kostiuk, L.W. [1999] "Efficiency Measurements of Flares in a Cross Flow." Combustion Canada 1999, Calgary, AB.*
13	*Johnson, M.R., Zastavniuk, O., Dale, J.D., and Kostiuk, L.W. [1999] "The Combustion Efficiency of Jet Diffusion Flames in Cross-flow." Joint Meeting of the United States Sections - The Combustion Institute.*
14	*Johnson, M.R., and Kostiuk, L.W. [2000] "Efficiencies of Low-Momentum Jet Diffusion Flames in Crosswinds." Combustion and Flame, 123, pp. 189-200.*
15	*Johnson, M.R., Wilson, D.J., Kostiuk, L.W. [2000] "A Fuel Stripping Mechanism for Low-momentum Jet Diffusion Flames in a Crossflow."Combustion Science and Technology, 169, pp. 155-174.*
16	*Kalghatgi, G.T. [1981] "Blow-Out Stability of Gaseous Jet Diffusion Flames. Part II: Effect of Cross Wind", Combustion Science and Technology, 26, pp. 241-244.*

Table 6.1 Selected Papers and Reports on Wind Effects on Flare Performance (Continued)

17	*Kostiuk, L.W., Johnson, M.R., and Prybysh, R.A. [2000] "Recent Research on the Emission from Continuous Flares." Combustion and Environment Group, Department of Mechanical Engineering, University of Alberta.*
18	*Kostiuk, L.W., Majeski, A.J., Poudenx, P., Johnson, M.R., Wilson, D.J. [2000] "Scaling of Wake-Stabilized Jet Diffusion Flames in a Transverse Air Stream", Proceedings of the Combustion Institute, 28, pp. 553-559.*
19	*Kostiuk, L.W., Johnson, M.R., and Thomas, G. [2004] "University of Alberta Flare Research Project Final Report November 1996 – September 2004" Combustion and Environment Group, Department of Mechanical Engineering, University of Alberta.*
20	Mellqvist, J. [2001] "Flare testing using the SOF method at Borealis Polyethylene in the summer of 2000." Chalmers University of Technology.
21	Pohl, J., Gogolek, P., Schwartz, R., and Seebold, J., "The Effect of Waste Gas Flow & Composition Steam Assist & Waste Gas Mass Ratio Wind & Waste Gas Momentum Flux Ratio Wind Turbulence Structure on the Combustion Efficiency of Flare Flames" accessed July 22, 2011, at: http://www.tceq.state.tx.us/assets/public/implementation/air/am/workshop/20040127-28/Flare_Effects_on_Combustion_Efficiency-JohnPohl.pdf
22	*Shore, D [2007] "Improving Flare Design – From Art to Science." AFRC-JFRC 2007 Joint Meeting, Waikoloa, Hawaii.*
23	*Siegel, K.D. [1980] "Degree of Conversion of Flare Gas in Refinery Elevated Flares." Ph.D. Thesis in Engineering Science, University of Karlsruhe, February. (in German and translated into English by The Language Center, Inc.)*
24	*Strosher, M. [1996] "Investigations of Flare Gas Emissions in Alberta (Final Report 1996)." Alberta Research Council.*

7.0 Accuracy and Precision of Plume Sampling System Measurements

The sources of 'error' in the extractive plume sampling methodology employed during the flare tests are addressed in this section. The known sources of bias, variability and noise present in this methodology are defined and addressed in this discussion. Before outlining the section, however, as an introduction we first consider a qualitative discussion looking at two chronological test points with different assist rates. The sampling measurement dataset has been described in Section 5. This introduction is a review of the method for determining the carbon fraction carried by propylene in the flare plume. It also depicts the time series data for two consecutive tests with different DRE on the same scale to illustrate the qualitative differences in the measurements.

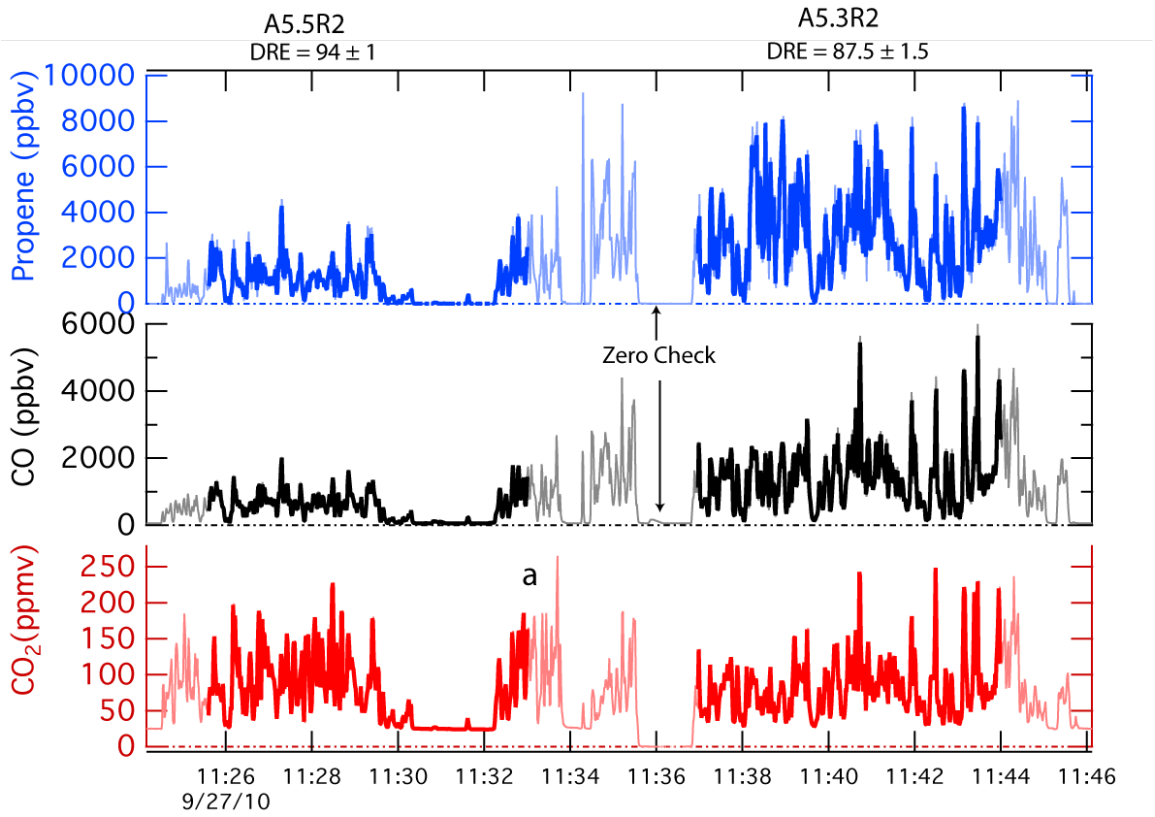

Figure 7-1. Time Series During Air Flare Tests A5.5R2 and A5.3R2. The time series for the sample collector data is plotted for CO_2, CO and propylene. The official stable test periods are denoted by the heavier line style. The point marked "a" is where the flare operational parameters were changed as described in the text. The "zero check" refers to overblowing the sample probe tip with dilution air to verify instrument zero drift performance. The assist air for Tests A5.5R2 and A5.3R2 was 23,100 lb/hr and 41,300 lb/hr, respectively.

Figure 7-1 depicts a time series for propylene, carbon monoxide and carbon dioxide. The light coloring is the complete data time series and the two heavier line sections are the test conditions A5.5R2 and A5.3R2. The tests depicted here were run on the air flare using 80% propylene/20%

TNG for the vent gas composition. The wind direction during the pair of events was consistently from the north (bearing 339° and 340° respectively). The median wind speed for the events depicted here were 3.1 and 5.0 mph respectively. The most significant change was the increase in air assist rate (made in the control room at or near the point marked "a") which increased the air assist from 23,100 lb/hr to 41,300 lb/hr. The change in air assist was the only planned difference between A5.5R2 and A5.3R2.

Inspection of Figure 7-1 reveals that the relative magnitude of high frequency plume intercepts by the sample collector for CO_2 is qualitatively similar for the two test conditions. The CO and propylene however are significantly increased (A5.3R2 relative to A5.5R2). Although it is not depicted in the figure, the identical increases appear for methane, acetylene, ethylene, formaldehyde, and acetaldehyde. The carbon balance methodology, described briefly in Section 4 and more thoroughly in Appendix I, uses the following expression for determining DRE.

$$DRE/100 = 1 - \frac{\left[\frac{propylene_{out}\ (molesC)}{C_{out}\ (molesC)}\right]}{\left[\frac{propylene_{in}\ (molesC)}{C_{in}\ (molesC)}\right]} = 1 - \frac{CF^{propylene}\ (out)}{CF^{propylene}\ (in)} \qquad \text{Eq. 7.1}$$

In Equation 7.1, CF refers to the carbon fraction for the superscripted species and the DRE would be for propylene. The (*in*) term refers to the vent gas mixture, where the carbon fraction carried by propylene has been set according to the relative flow rates of propylene and TNG, but verified with gas chromatographic measurements (typically twice per test point). The (*out)* term refers to the flare plume emission to the atmosphere. Due to complete and partial combustion, there are several potential forms the vent gas carbon can take. "Complete combustion" will produce CO_2 and a minor amount of CO and some trace hydrocarbons. The computation of CF must account for all forms of carbon in the flare plume. The expression for CF in the flare plume, derived in Appendix I, is repeated here as Equation 7.2.

$$CF^{propylene}(out) = \frac{propylene\ (ppmC)/CO}{propylene\ (ppmC)/CO + CO_2/CO + 1 + \sum other\ carbon\ (ppmC)/CO} \qquad \text{Eq. 7.2}$$

In Equation 7.2, each of the terms divided by CO are intended to be the 'flare plume associated' ratios. Figure (7-1) suggests that a time series analysis can extract the flare-associated ratios without any need to artificially subtract ambient levels or even know the extent of dilution if the time response for each of the instruments has been matched and any time offsets between the vectors accounted for.

Although Figure 7-1 depicts two different test conditions, where the difference in the air assist rate is driving an obvious difference in DRE, the purpose of this section is to discuss the accuracy and precision in the DRE and CE reported by the sampling method. This section focuses on the topics below and will conclude with some overall assessment of the uncertainty in this approach.

- 7.1 Instrumentation Error
  - a. Measurement accuracy (e.g., "span errors")
  - b. Measurement precision (e.g., Instrument noise)
- 7.2 Intra-test variability
  - a. Vent gas composition variability
  - b. Flare assist and operational control variability
  - c. Sample intercept variability
    - i. Height of sample probe
    - ii. Wind/transverse location of sample probe
- 7.3 Test Condition Reproducibility

7.1.a Measurement Accuracy

The majority of the analytical instruments used for the *in-situ* sampling were chosen for their speed, sensitivity, accuracy and whenever possible their selectivity. Appendix I contains a description of the calibration procedures and results for each instrument. As was discussed in Section 4, the major constituents that determine DRE in the 80% propylene/20% TNG vent gas composition tests are CO_2, CO, propylene and methane. The other trace hydrocarbon species constitute a smaller portion of the carbon in the exhaust. The accuracy of the specific trace hydrocarbon measurements does not affect the overall uncertainty in carbon fraction to the same extent as CO_2, CO, propylene and methane. The accuracy of these species is more germane to the efforts to close the carbon balance which is discussed elsewhere. The CO_2 concentration was measured using three different Licor brand non-dispersive infrared gas analyzers. The CO and methane concentrations were measured using different ARI quantum cascade laser (QCL) instruments based on tunable infrared laser differential absorption spectroscopy (TILDAS). The propylene was measured using proton transfer reaction mass spectrometry (PTRMS) and was verified using gas chromatography using a flame ionization detector (GC-FID).

Table 7-1. Measurement Accuracy and Calibration Checks for Selected Species

Compound	Analytical Accuracy[1]	Calibration Check[2]
CO_2	1%	1%
CO	3%	1%
Methane	6%	2%
Propylene via PTRMS	15%	4%

Table Notes

[1]The tabulated analytical accuracy is the overall systematic uncertainty present in the specific method as deployed in general. It is either a manufacturer's specification or is based on a propagation of systematic error present in the technique.

[2]The tabulated calibration check is an assessment of how well the specific instrument used for the test and data post-processing returned the input value when checked via some independent standard. The PTRMS calibration check tabulated here is explained in the text.

The overall theoretical analytical accuracy for selected measurements is tabulated in Table 7-1 along with the *in-field* calibration evaluation. The instrument calibrations are described in Appendix-I. In the case of propylene quantification via PTRMS, the calibration check is the raw level of agreement between the returned mixing ratios (concentrations) measured during the test at 1 Hz averaged and compared to the periods where the GC-FID was also sampling from the diluted flare plume sample.

The combined implication of instrument span error on the measured DRE should not be random. Based on the calibration checks that were performed over the course of the measurement period, for these species no obvious abrupt change in calibration or instrument sensitivity occurred. As a

result, the instrument span source of error should be regarded as a uniform potential bias, thus consistent throughout the entire dataset. An estimate of the magnitude of this source of error is depicted in Figure 7-2. The variability in the uncertainty versus DRE expressed in Figure 7-2 reflects the associated accuracy of the different instruments. At high DRE where most of the carbon is CO_2 the uncertainty approaches the accuracy limit (± 1%) that measurement. At low DRE the uncertainty increases towards the accuracy limit imposed by the measurement of propylene by the PTRMS technique.

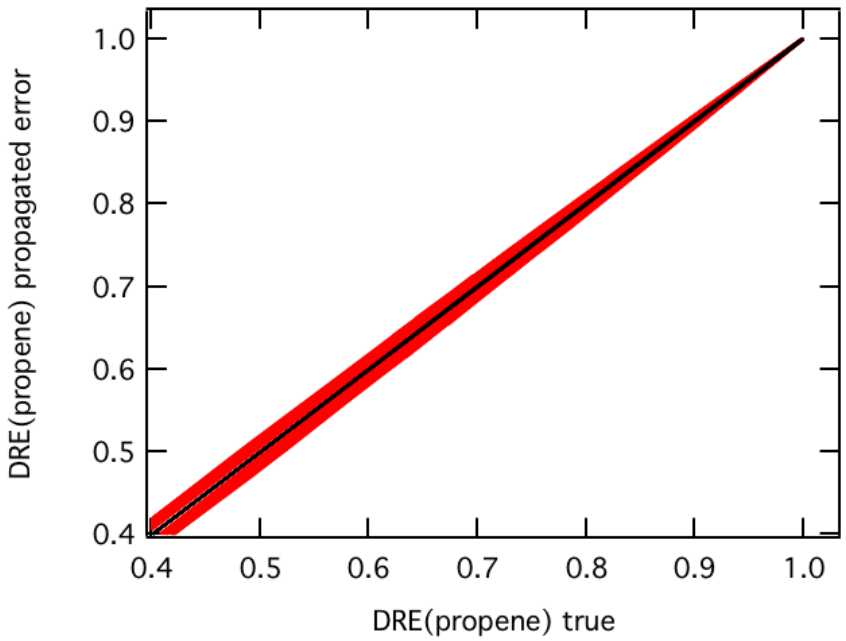

Figure 7-2. DRE Instrument Span Error for the 80/20 Propylene/TNG Vent Gas Conditions. The red band reflects the propagated error sources in Table 7-1 expressed as DRE.

7.1b Measurement Precision

The majority of the results discussed in this report were derived from test conditions that exceeded 8 minutes in duration. As a result, the random noise associated with each specific instrument does not appreciably influence the computed carbon fraction when the whole test period is used as an ensemble.

Table 7-2. Instrument Precision Specifications

	Low Scale Noise (1σ)	High Scale Noise (1σ/average)
Propylene	1.6 ppbv	6%
CO_2	38 ppbv	< 1%
CO	800 pptv	< 1%
Methane	3 ppbv	< 1%

In Table 7-2 some precision related benchmarks are tabulated for the instrument as operated during the study. The low scale noise refers to the baseline instrument noise when the sample was at the lower ranges of signal detected in this study. The high-scale noise is more related to the proportional noise and has been quantified by expressing the ratio of 1 standard deviation of the sample to the mean value for the mid point of the calibration range for the instrument. The random noise performance of the instrument is not expected to appreciably influence the carbon fraction or DRE for the test point.

7.2.Intra-test variability

Several parameters might vary during the test period where the flare has been called *stable*. The vent gas composition could be drifting during the event or not what was specified for the nominal composition for the test point. Operational characteristics (e.g., assist rate, total vent gas flow) might be drifting or variable. The sample collector flare plume intercept events (see Figure 7-1 for the nature of plume intercept events) will be influenced during the test by factors such as the height of the sample collector and the gusting nature of a variable wind.

7.2.a Vent gas composition variability

The method for measuring the vent gas composition is described in detail in Appendix G. The TRC mobile laboratory collected a sample of the vent gas and analyzed the hydrocarbon concentration using GC every 5 minutes. The calibrated response for each of the peaks in the chromatogram was used to quantify the mixing ratio of the species in the vent gas exhaust. The carbon fraction of propylene in the vent gas, for the test conditions which nominally used 80%/20% propylene/TNG is computed from the measurement data using the following formula.

$$CF^{propylene}\ (in) = \frac{3 \times [propylene]}{3 \times [propylene] + 1 \times [methane] + 2 \times [ethane] + \sum n[other\ VOC]}$$

Eq. 7.3

In Equation 7.3, the bracketed species are the molar mixing ratios by volume and *n* is the carbon number for the specific compound.

The vent gas composition was nominally set by separately controlling the flow of propylene and TNG. An estimate of the carbon fraction of propylene in the vent gas can be computed using only the measured flow rates of the constituents.

$$CF^{propylene}(in)^{flow} = \frac{3/42 \times F^{propene}\ (lb\ hr^{-1})}{3/42 \times F^{propylene}\ (lb\ hr^{-1}) + 1/16 \times F^{methane}\ (lb\ hr^{-1})} \qquad \text{Eq. 7.4}$$

In Equation 7.4, the contribution of ethane (present in TNG) has been ignored.

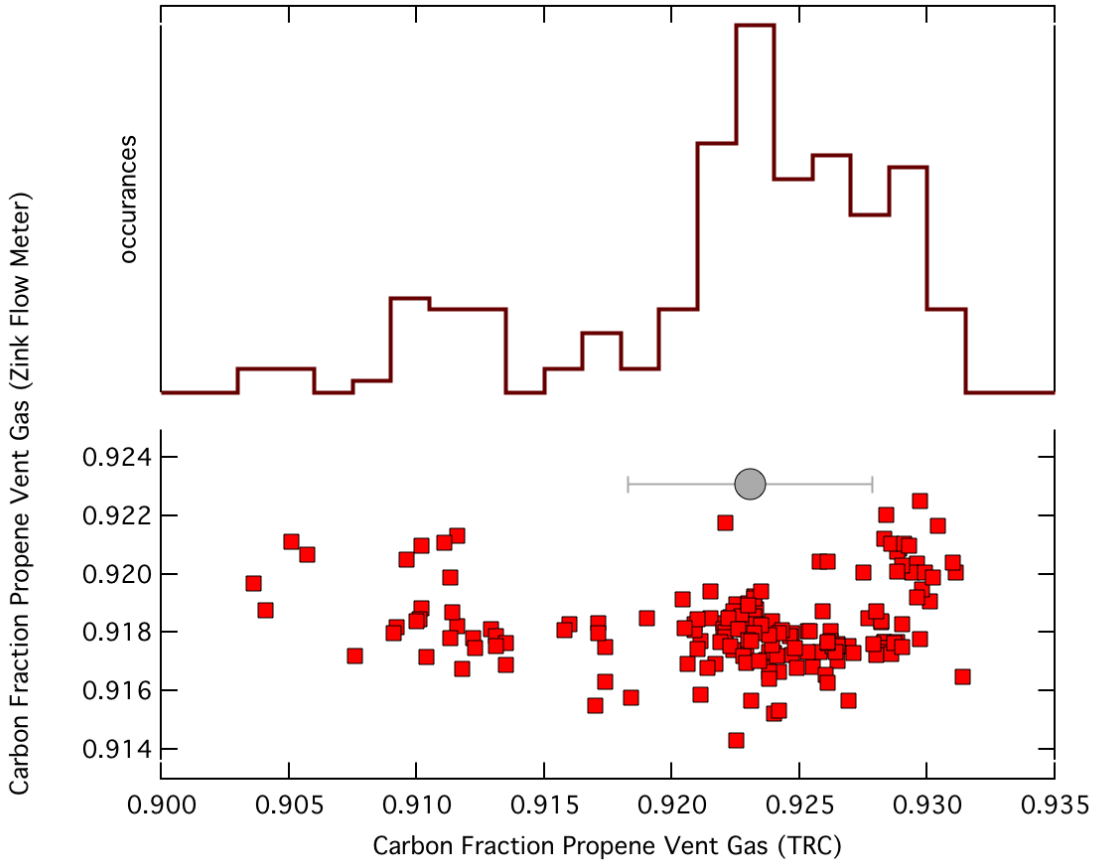

Figure 7-3. Carbon Fraction of Propylene in the Vent Gas for the 80/20 Propylene/TNG Composition. In the lower panel, for each test point (red squares) the estimate based on relative flow rates is compared to the composition measurements. In the lower panel the grey circle is the nominal propylene carbon fraction. In the upper panel, a histogram of the TRC measurement results is depicted.

Figure 7-3 compares the carbon fraction of propylene in the vent gas computed using the flow rate data to the actual measurement using GC. Equation 7.1 uses the carbon fraction of propylene in the vent gas to compute DRE. The apparent variability based on the TRC measurements is 0.5%, 1σ of a Gaussian fit of the histogram of measurements. Based on the level of agreement observed between the flow rate and direct measurement methods, and the magnitude of variability in the resulting vent gas propylene carbon fraction, this source of error is not considered to be significant.

7.2.b Flare assist and operational control variability

Zink personnel controlled the operation of the flare burners (air- and steam-assisted) and the vent gas composition nominally by separately controlling the flow of propylene (or propane), TNG and nitrogen. The process control instrumentation monitors were digitized and recorded. Prior to the establishment of a particular test point, the flare controls were set. Typically, three minutes elapsed while the flare control system was adjusted and monitored for stability. During the stable test periods, no modifications were made to the flare control parameters. Examination of the time series of the digitized parameters for flow assist rate (total steam and center steam for the steam flare and air flow for the air flare) does not suggest the control system had significant drift during the test point. At two points during the test, the near-real time diagnostics of flare control parameters alerted the control room when something was not following the test design and the data for the test point was set aside. The digital data record does not reveal any significant changes or variability in the operational flare control parameters.

7.2.c Sample collection variability

The purpose of the TCEQ Comprehensive Flare Study was to determine the representative DRE as a function of flare operational parameters. It was not part of the project to quantify inhomogeneity in the combustion at varying flare radii. The study design deliberately attempted to sample a large volume of air and force mixing before characterizing the sampled constituents. Furthermore, during the project design phase, the sample collector was assumed to be at least two flame lengths away from the flare center to sample the plume at a location where combustion had ceased.

Using estimates of stoichiometric combustion and the measured volumetric flow rate of the sample collector, it was estimated that the sample collector extracted approximately 15 - 20% of the total flare plume volume. At the distances the sample collector was deployed (away from the flare center), the flare combustion products were unavoidably diluted by an unknown, uncontrolled amount of non-combustion ambient air prior to entering the sample collector. It is clear that the sampler rapidly pulled in air that was highly influenced by the flare plume. Based on measurements of the inlet probe temperature, the portion the flare plume that entered the sampler was between 50° and 140° Fahrenheit above the measured ambient temperature. The air mass sampled during plume encounters had increases in CO_2 concentration that were a factor of 2 to 50 times greater than the concentration of CO_2 in the ambient air (e.g., the *diluted* flare plume had CO_2 mixing ratios of 800 ppmv to 2%).

The time series analysis approach used to generate the terms in Equation 7.2 that have the form of carbon-containing-compound per CO is not sensitive to the dilution by ambient air. In effect,

this method is based on the variability in the dilution extent so that the concomitant increases in carbon-containing-compound and CO clearly reveal the flare plume associated ratio when compared to the mixing ratios in ambient air.

The most important data quality indicator for DRE determined in the sampling methodology is its insensitivity to the extracted ratio with the chosen test time periods. To the extent that the 'plume hits' converge, this methodology asserts that the deduced DRE is the representative DRE needed to assess the emissions to the atmosphere.

To test the intra test point variability that this analysis produces, test condition S4.6R1 has been partitioned into different intervals. The entire test point (approximately 10.5 min) has been partitioned into bins whose time intervals are ten seconds, twenty seconds, forty seconds and one minute and processed using the same methodology as used for the total ensemble analysis. The results of this analysis are depicted in Figure 7-4. The red diamond is the result from the whole event taken as an ensemble and reduced to a single DRE using Equation 7.2. The dark blue histogram in Figure 7-4 reflects the DRE for each of the shorter duration time periods. The central value of this histogram (fit to a Gaussian function) agrees well with the tabulated value 98.1% vs. 98.3%.

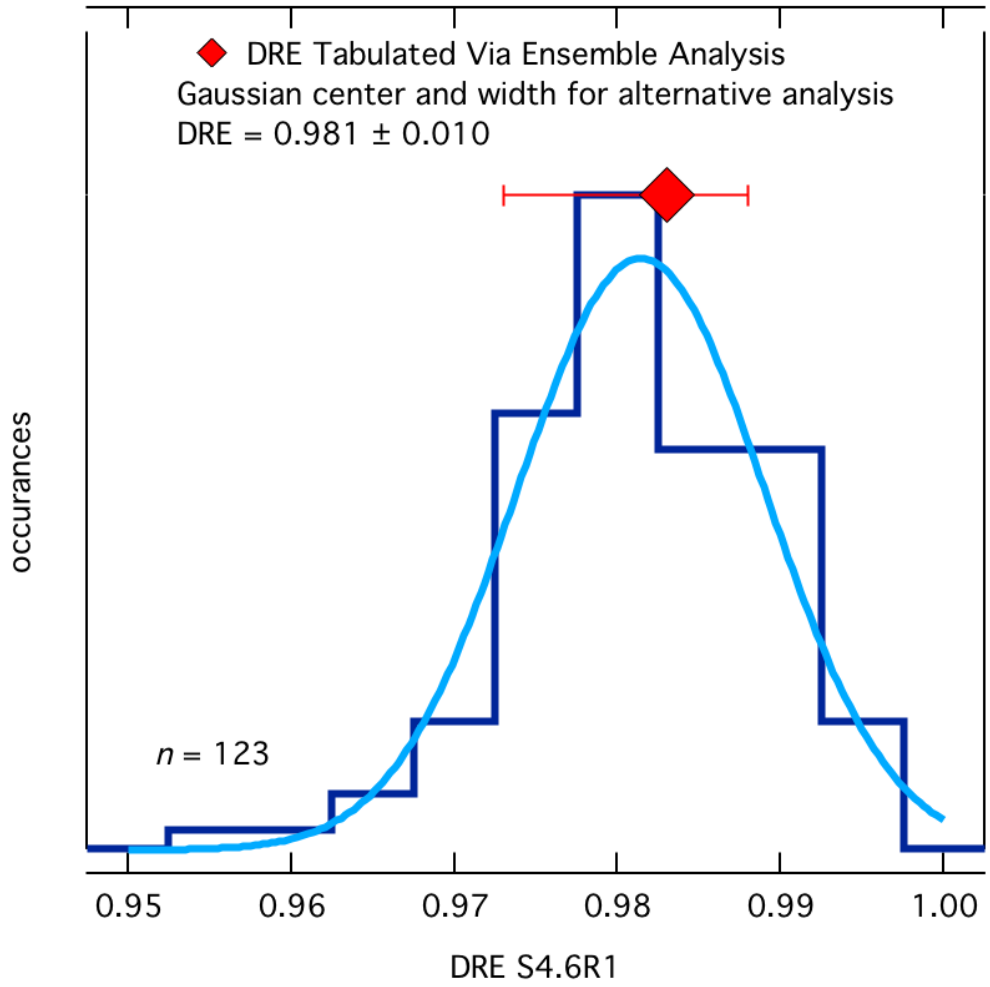

Figure 7-4. DRE Variability Analysis for S4.6R1. The graph depicts the tabulated "ensemble" DRE and error bars (red diamond) along with the results of finer scale analysis described in text (histogram results and Gaussian fit).

7.2.c.i Height of sample probe

The height of the sample probe was varied during many of the tests. Some additional tests were conducted for vertical profiling. Test point/run S4.1R1, described earlier in Section 4, was one of the test points where the sample collector was moved in the vertical direction to test whether or not a difference in the sampled DRE would be observed. There were tests, with DRE less than 70%, that exhibited some vertical variability and these results are a part of ongoing analyses. For the cases where the DRE was greater than 85%, no detectable dependence on DRE with sample collector height was observed.

An alternative analysis of S4.1R1 results has been performed to evaluate the effect on DRE of sample collector height as well as to evaluate the extractive sampling method. Figure 7-5 plots the sample collector height time series along with observed total carbon (C) concentration. This analysis was conducted independently from ARI. Figure 7-5 is color coded into three segments, where DRE is calculated for each segment using the 1-second data and an independently derived

formula for DRE. The time series analysis here does not use either the 'ensemble' slope or the time segment analysis.

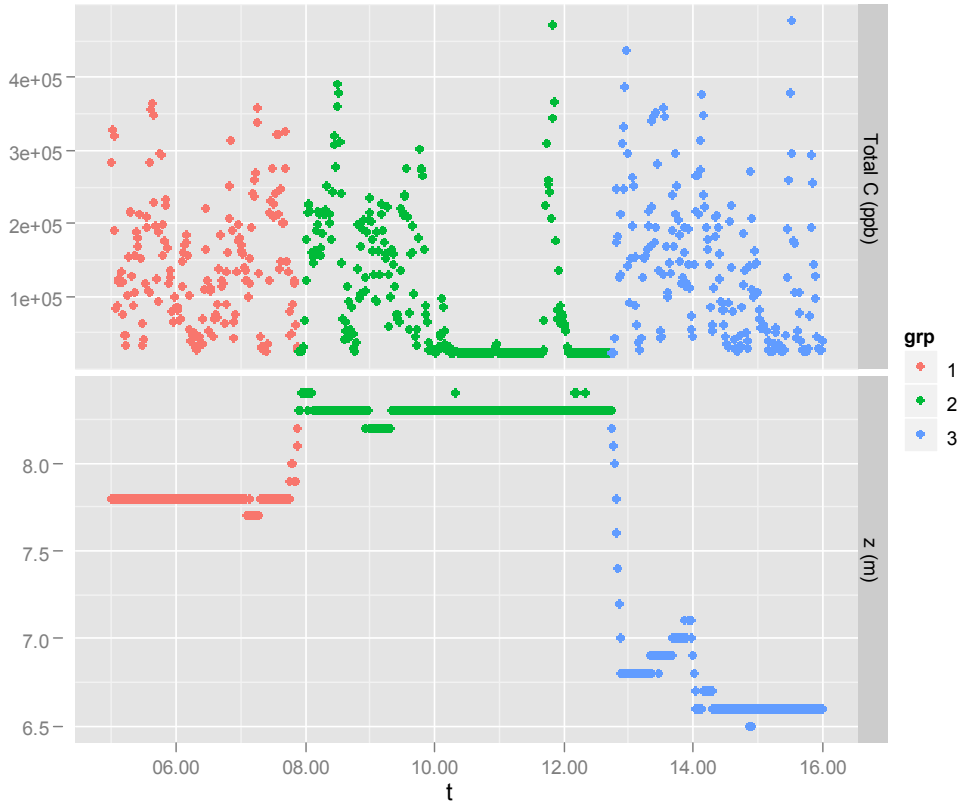

Figure 7-5. Grouping by Sample Collector Height (z). See text for description of the color banding

Figure 7-6 depicts the results for the alternative methodology to compare DRE with sample collector height This analysis which is based on the second-by-second calculations, from instrumentation that had time responses between 0.9 and 1.2 seconds). The results of a statistical analysis are tabulated in Table 7-3. For this analysis, which had a relatively high DRE, the DRE does not vary with sample collector height.

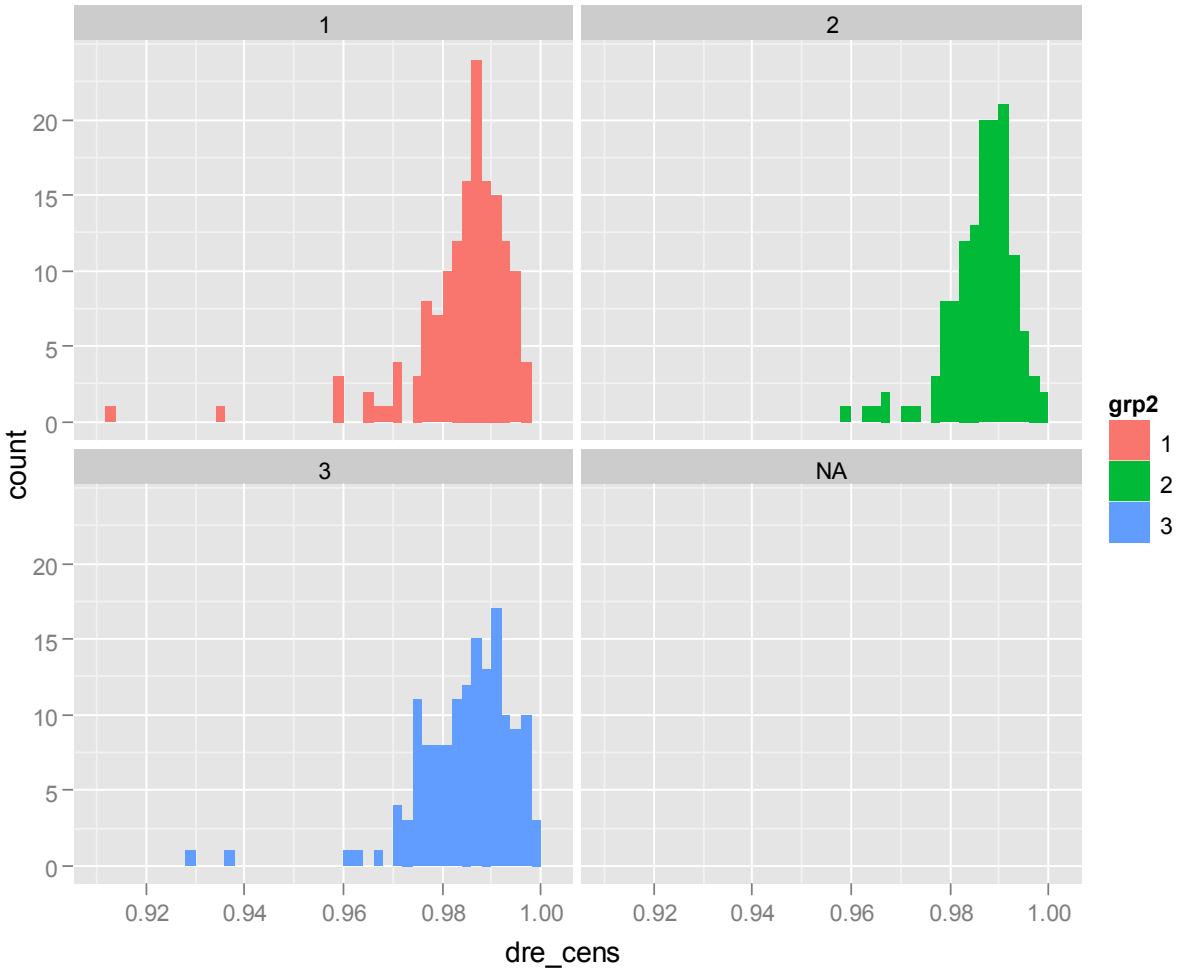

Figure 7-6. Histogram of Second-by-Second DRE Grouped by Sample Collector Height

Table 7-3. Summary of Second-by-Second DRE by Sample Collector Height Groups

Group No.	Accepted Records	Dropped Records	Mean (%)	Std. Dev. (%)	Min (%)	1Q (%)	Median (%)	3Q (%)	Max (%)
1	150	24	98.45	1.05	91.33	98.17	**98.64**	99.03	99.69
2	134	157	98.66	0.68	95.94	98.34	**98.77**	99.08	99.96
3	147	49	98.49	1.00	92.97	97.97	**98.65**	99.14	99.91
All Data	431	230	98.53	0.93	91.33	98.17	**98.69**	99.08	99.96

For the same grouping used above, DRE was verified using the slope methodology. These values are shown in Table 7-4. The net ensemble DRE calculated with this procedure agrees with the value reported in the ARI analysis. Table 7-4 shows relevant statistics from the analysis and subsequent calculations used to derive DRE. Also, the slope methodology did not indicate the

sample collector height as a significant variable in explaining the variation in DRE. The estimated range in DRE using the slope methodology was far smaller than the estimated range determined with the second-by-second method. This result is expected, as the nature of the estimates determined by each method is different. If the 1-second analysis method is used, the standard deviation captures the spread of the observation. If the slope method is used, the standard error is for the slope and it uses all of the observations to derive the slope. This method does not include a measure of spread of each data point. The slope method should also be less sensitive to the estimate of total carbon in the ambient air.

Table 7-4. Estimated DRE Based on Slope Approach for Each of the Sample Collector Height Groups. Mid values are calculating using best estimates of slopes. Low/high value of CF and DRE are estimated using best estimate ± 2σ, assuming that CO_2 and C_3H_6 do not correlate.

Group No.	CO^2/CO slope		C_3H_6/CO slope		CF (C_3H_6)			DRE		
	best estimate	std. err.	best estimate	std. err.	Low (%)	mid (%)	High (%)	Low (%)	**mid** (%)	High (%)
1	182.69	6.99	3.28	0.13	1.503	1.754	2.045	97.78	**98.10**	98.37
2	205.66	4.05	3.60	0.08	1.577	1.714	1.861	97.98	**98.14**	98.29
3	205.97	8.81	3.86	0.13	1.576	1.829	2.128	97.69	**98.02**	98.29
All Data	199.38	3.52	3.57	0.06	1.637	1.752	1.875	97.97	**98.10**	98.23

7.2.c.ii Wind influence probe

Between the real time diagnostics of temperature, CO_2 concentration and the video record, it was straightforward to reposition the sample collector whenever there was a significant wind shift. During each test, the near real time analysis of the data stream suggested that the extracted DRE was not strongly influenced by changes in the wind.

The measurements of DRE using the bulk sample collector (which rapidly collected a large volume of air that contained a mixture of the flare plume and ambient air) *did not* exhibit a strong sensitivity to gusting and changes in the winds. This is not an assertion that the degree of flare plume was not dependent on wind speed and direction. When the wind direction changed, the sample collector had to be repositioned to the new location 'downwind'of the flare. However, the data suggest that at the typical distance downwind from the flare, the DRE from the sample that was collected depended more on the flare operational parameters than on the wind parameters.

In general, the test conditions were favorable for obtaining data to address the study objectives. As the study objectives were not to develop a correlation between DRE and wind speed, additional analysis would be required to attempt to determine a relationship between DRE and crosswind speed for the two flare models used in this study.

7.3 Test Condition Reproducibility

The test conditions were typically repeated three times for the core test series. The measurements were not done chronologically; they were mixed throughout the test interval or in some cases conducted on completely different days. The repeatability between test runs is analyzed in Section 10. When the DRE was greater than 80%, the apparent variation in DRE determined for separate test times was low (generally less than 4%). When the DRE was less than 70%, the values for the DRE sometimes varied as much as 30% of the average DRE. There is little reason to believe that this variation is caused by an instrumental or a systematic artifact. Determining the reasons for this difference in reproducibility is part of the ongoing analysis. It should be noted that the degree of reproducibility at DRE greater than 80% is a strong indicator of quality test data. This particularly relates to determining the effect of flare operating parameters on the DRE compared to the effect of air and steam assist when there is a rapid decrease in DRE.

8.0 Measurements Made by Remote Sensing Technology Instruments

There were three remote sensing technologies participating in the study: IMACC PFTIR and AFTIR spectrometers, Telops Hyper-Cam passive imaging radiometric spectrometer, and LSI FLIR GasFindIR and thermal IR cameras. The LSI cameras provide visual images of hydrocarbons in the gas phase and are useful in detection of these gases but cannot be used for quantitative assessment of flare combustion. The discussion in this section will focus on the IMACC and Telops instruments, which can measure parameters that can be used to calculate the combustion efficiency of the flare. Telops can also make mass flow rate measurements of hydrocarbons in the plume. However, the final quality assured Telops data were provided in February 2011 so comparison of the Telops mass flow rate results will be provided as an addendum to this report in September.

As summarized in Section 3, the measurement of emissions in samples extracted from the plume and analyzed by ARI provided the baseline or reference DRE and CE values against which the remote sensing technologies would be compared. The results of the analyses of the extractive samples and determination of DRE and CE by ARI were not provided to IMACC or Telops. Subsequent to the field tests, IMACC and Telops submitted their CE measurements for each test run, including their standard deviation (σ) for their measurements.

Three statistical criteria were selected to compare the measurements of IMACC and Telops with the ARI values. The first two are the mean difference and the standard deviation of the difference. These terms are defined numerically as follows.

$$mean\ difference = \frac{\sum_{i=1}^{N} ABS\ (CE_{RS} - CE_{ARI})_i}{N} \qquad \text{Eq. 8.1}$$

$$standard\ deviation = \sqrt{\frac{\sum_{i=1}^{N} [(CE_{RS} - CE_{ARI})_i]^2}{N-1}} \qquad \text{Eq. 8.2}$$

where

mean difference =	average of the absolute values of the difference between the CE determined by the remote sensing contractor and the CE determined by ARI for test point *i*
standard deviation =	standard deviation of the differences between the CE determined by the remote sensing contractor and the CE determined by ARI for the test point *i*
CE_{RS} =	combustion efficiency determined by the remote sensing contractor for the test point *i*
CE_{ARI} =	combustion efficiency determined by ARI for the test point *i*
N =	total number of test points in the subset

The third criterion is data return. Data return is the percentage of the total number of possible test points for which data were reported. It is defined numerically as follows.

$$data\ return = \frac{Number\ of\ test\ points\ for\ which\ data\ were\ reported}{Total\ number\ of\ test\ points} \times 100 \qquad \text{Eq. 8.3}$$

Tables D-1 and E-1 summarize data for all flare test results, including the IMACC and Telops CE and standard deviation, σ, by test series and run number. The CE values of ARI, IMACC and Telops for all steam flare tests have been graphed in Figure 8-1. These same data for all air flare tests are shown in Figure 8-2. As can be seen from these graphs, the scatter between values tends to increase significantly after about CE = 80%. Since the focus of this study is about DRE and CE above 90%, there is less importance in examining the performance of these remote sensing technologies much below CE = 90%. Therefore, the remainder of the comparison of these remote sensing technologies will focus on their performance in the range 100% ≥ CE ≤ 80%.

To more easily compare IMACC's and Telops' data with ARI's, the CE data have been extracted from Tables D-1 and E-1 and sorted by ARI CE (CE_{ARI}) value in descending order for the range 100% ≥ CE ≤ 80% in Tables D-2 and E-2. On the assumption that the accuracy of the CE values may not be constant across this entire range, the data have been further divided as follows: $CE_{ARI} \geq 95\%$; $90 \geq CE_{ARI} < 95\%$; $85\% \geq CE_{ARI} < 90\%$; and $80\% \geq CE_{ARI} < 85\%$. The difference between the IMACC's and Telops's CE values and the CE_{ARI} values are shown in each table. At the bottom of the column of the CE differences are the mean difference and the standard deviation of the CE differences are calculated as described in Equations 8-1 and 8-2. These two criteria are summarized in Table 8-1, where data return has also been calculated from the data in Tables D-2 and E-2.

Steam Flare Tests

The CE data for the four ranges are graphed in Figures 8-3 to 8-6 in descending CE order. As shown in Table 8-1, the mean difference and the standard deviation of the CE differences for the IMACC AFTIR and PFTIR increase as the CE_{ARI} decreases. The mean difference and the standard deviation of the CE differences for the Telops CE values do not have a clear trend. In examining the differences in CE values in Table D-2, the IMACC AFTIR and Telops values tend to be biased (sum of the differences) lower than the CE_{ARI} values. The PFTIR values do not appear to have a bias relative to CE_{ARI}.

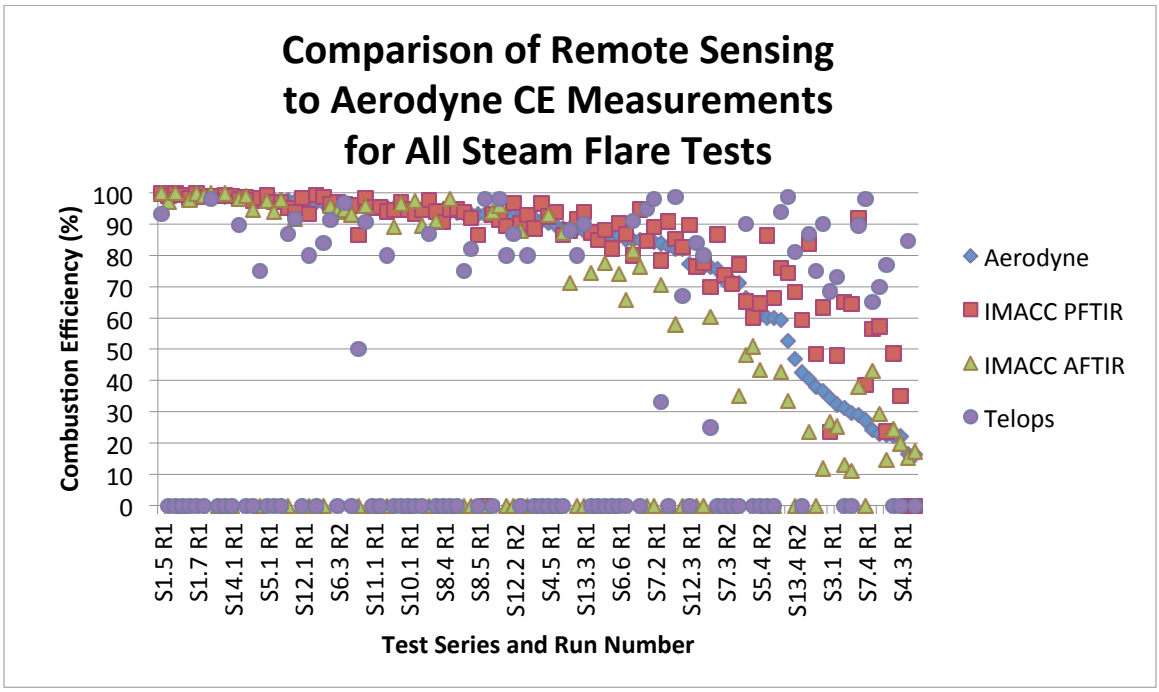

Figure 8-1. Comparison of All Remote Sensing Measurements Made to ARI Steam Flare CE Measurements

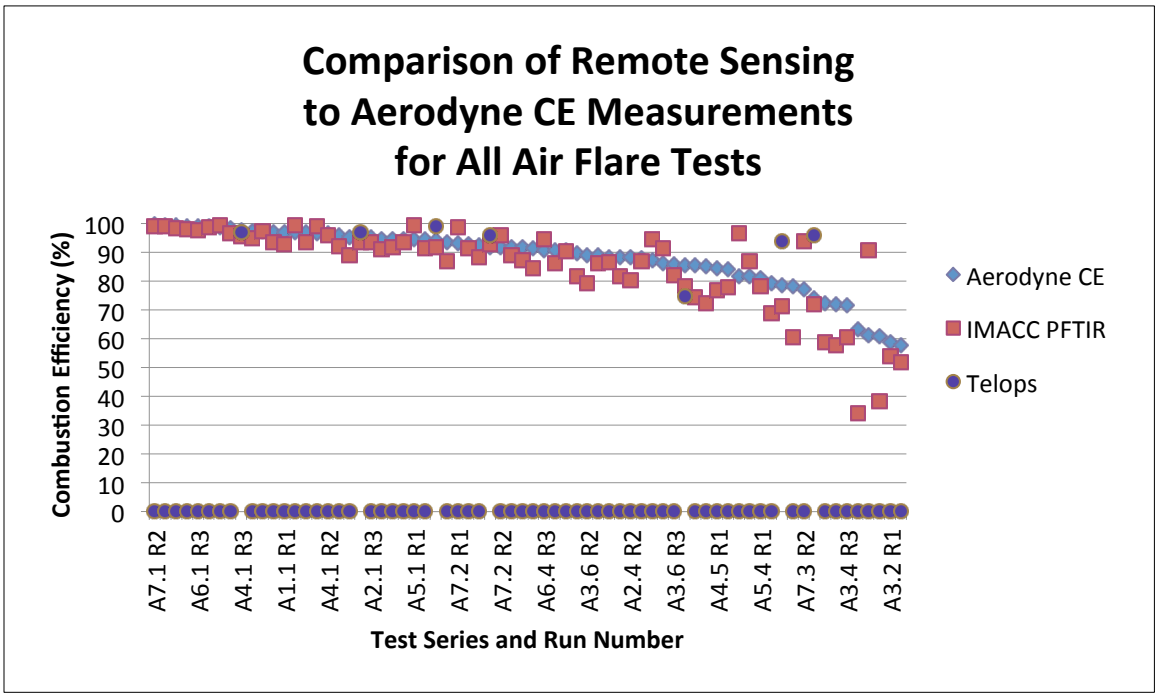

Figure 8-2. Comparison of All Remote Sensing Measurements Made to ARI Air Flare CE Measurements

Table 8-1. Summary of Comparison Criteria for Remote Sensing CE Values for CE_{ARI} > 80%

Steam					
Range	Criterion	Telops	AFTIR	PFTIR	ARI
$CE_{ARI} \geq 95\%$	Mean Difference (% pts)	20.2	1.7	1.1	
	Standard Deviation (% pts)	32.2	2.5	2.1	
	Data Return (%)	39	100	100	
	Number of Test points	14	22*	36	36
$90\% \leq CE_{ARI} < 95\%$	Mean Difference (% pts)	9.6	3.2	2.2	
	Standard Deviation (% pts)	11.3	3.7	2.9	
	Data Return (%)	40	100*	95	
	Number of Test points	8	8	19	20
$85\% \leq CE_{ARI} < 90\%$	Mean Difference (% pts)	3.8	12.2	2.8	
	Standard Deviation (% pts)	6.1	14.8	3.4	
	Data Return (%)	27	100*	100	
	Number of Test points	3	6	11	11
$80\% \leq CE_{ARI} < 85\%$	Mean Difference (% pts)	18.8	12.2	4.6	
	Standard Deviation (% pts)	26.1	16.7	5.9	
	Data Return (%)	75	100*	100	
	Number of Test points	6	4	8	8
Air					
Range	Criterion	Telops	AFTIR	PFTIR	ARI
$CE_{ARI} \geq 95\%$	Mean Difference (% pts)	1.2		1.9	
	Standard Deviation (% pts)	2.0		2.5	
	Data Return (%)	10		100	
	Number of Test points	2		21	21
$90\% \leq CE_{ARI} < 95\%$	Mean Difference (% pts)	4.4		3.5	
	Standard Deviation (% pts)	6.3		4.1	
	Data Return (%)	11		100	
	Number of Test points	2		18	18
$85\% \leq CE_{ARI} < 90\%$	Mean Difference (% pts)	NMR		5.5	
	Standard Deviation (% pts)	NMR		6.5	
	Data Return (%)	0		100	
	Number of Test points	0		10	10
$80\% \leq CE_{ARI} < 85\%$	Mean Difference (% pts)	10.2		8.5	
	Standard Deviation (% pts)	10.2		9.9	
	Data Return (%)	13		100	
	Number of Test points	1		8	8

NMR = No CE vales were reported for these tests.

*Instrument not on site to obtain measurements during some of these test points.

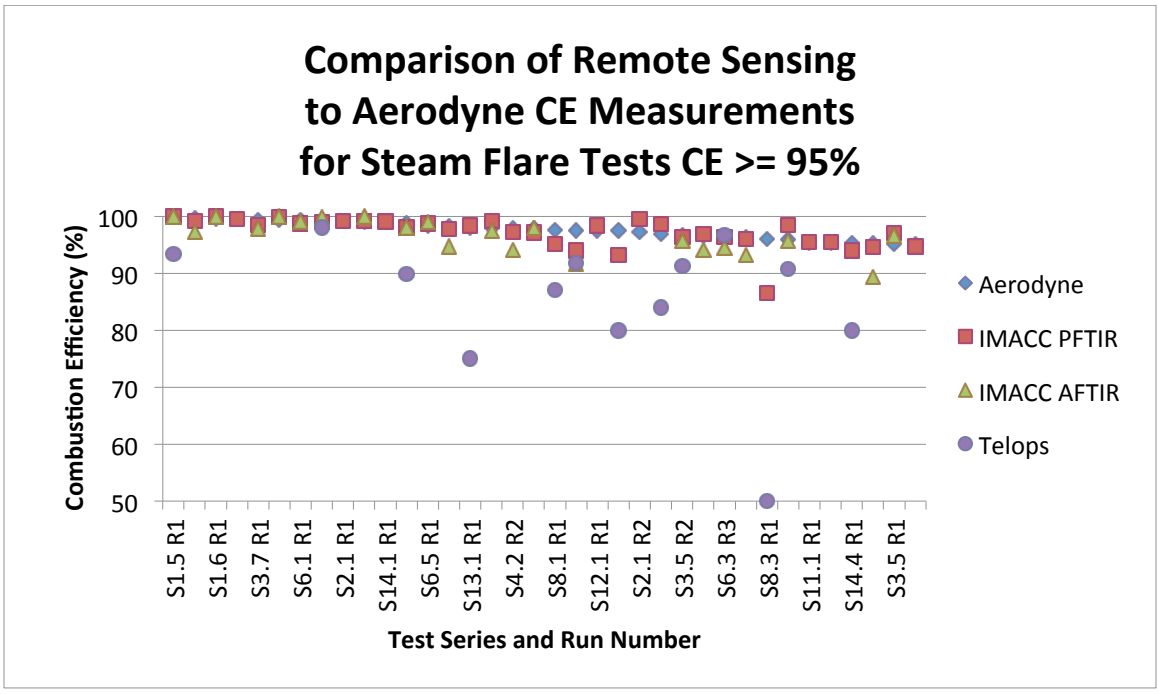

Figure 8-3. Comparison of All Remote Sensing Measurements Made to ARI Steam Flare CE Measurements ≥ 95%

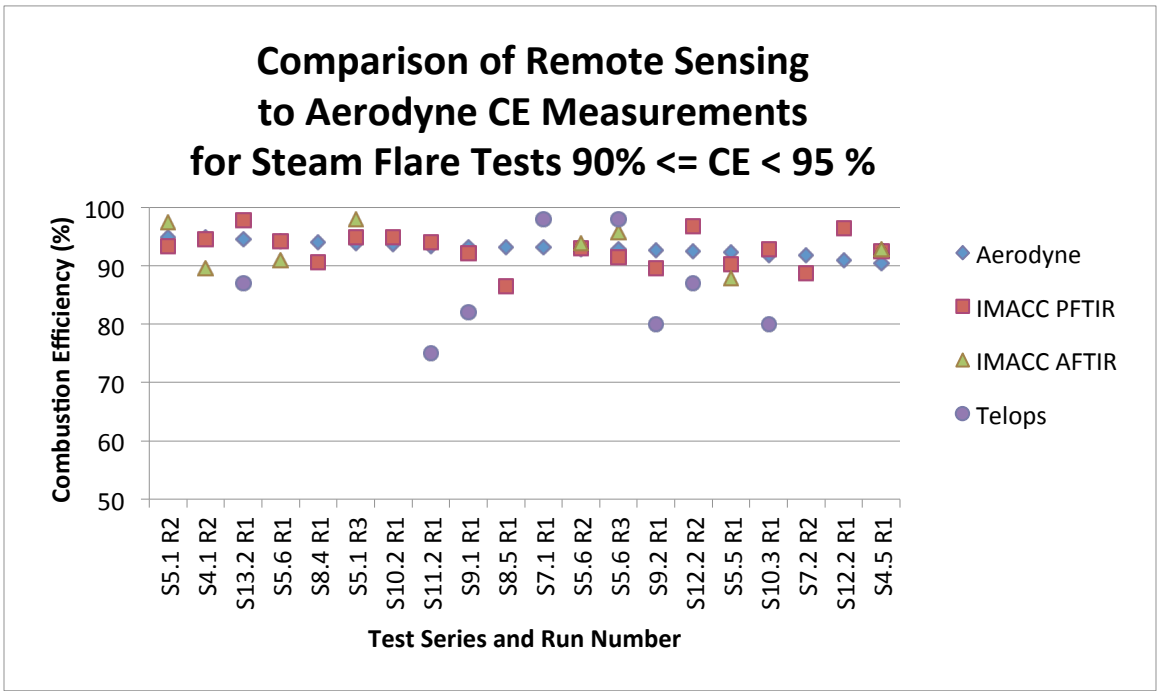

Figure 8-4. Comparison of All Remote Sensing Measurements Made to ARI Steam Flare CE Measurements 90% ≤ CE_{ARI} <95%

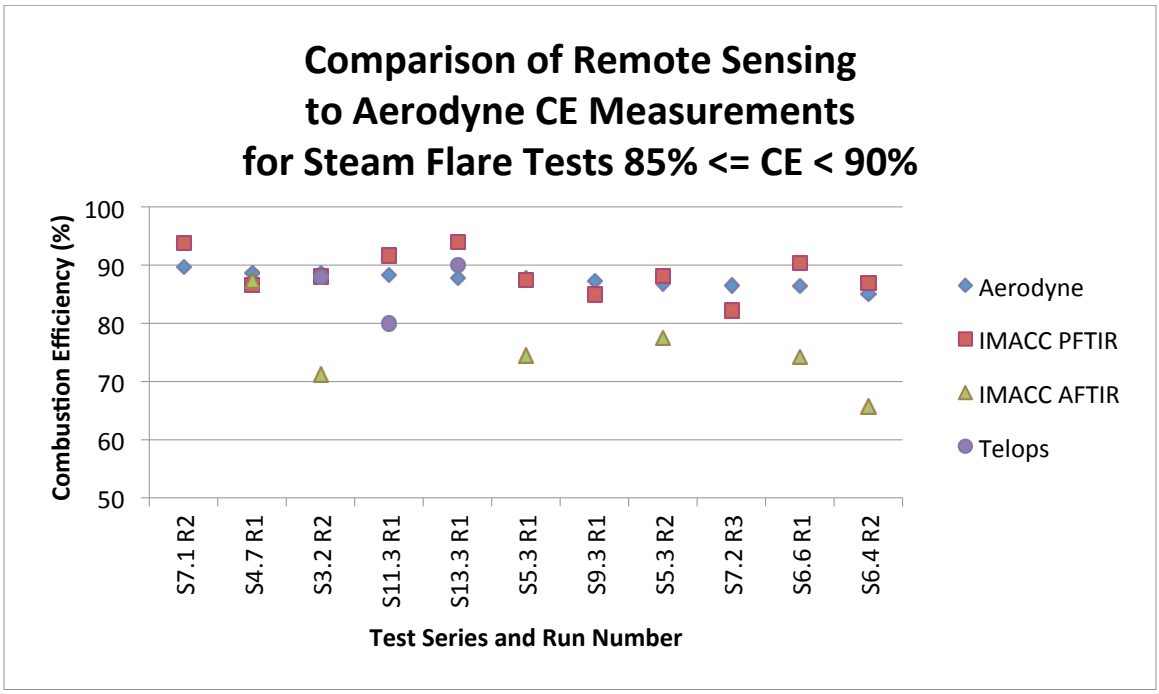

Figure 8-5. Comparison of All Remote Sensing Measurements Made to ARI Steam Flare CE Measurements 85% ≤ CE_{ARI} <90%

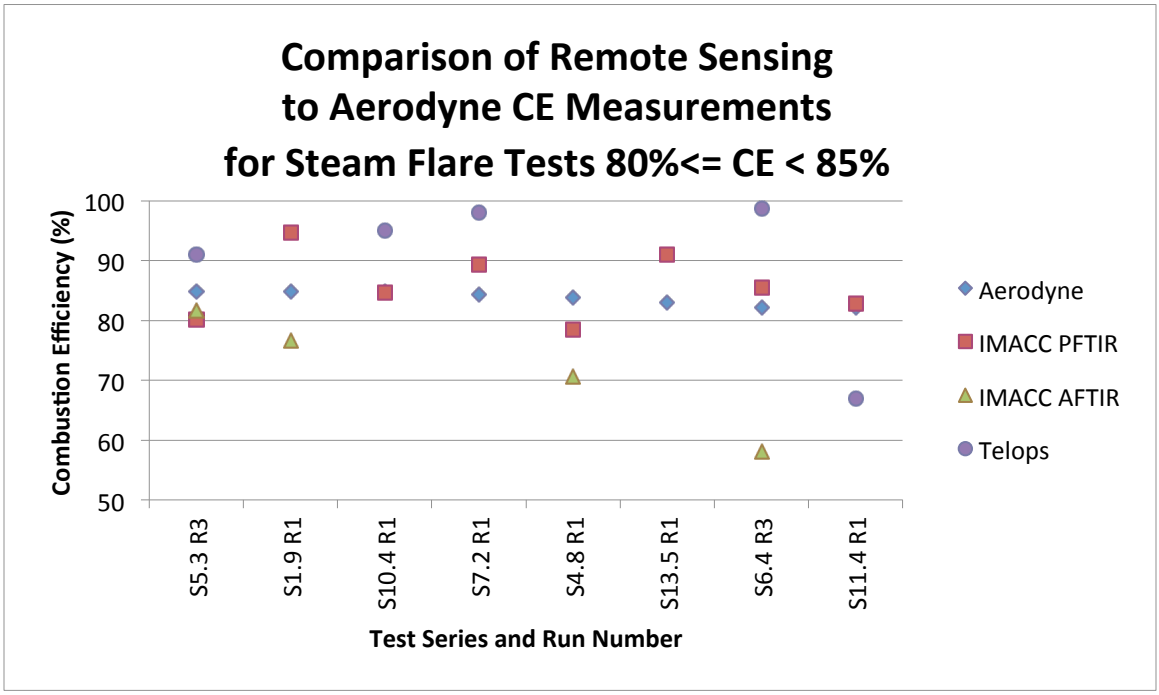

Figure 8-6. Comparison of All Remote Sensing Measurements Made to ARI Steam Flare CE Measurements 80% ≤ CE_{ARI} <85%

In examining the data return in Table 10-1, the IMACC AFTIR was 100% in all four ranges, while the PFTIR was 100% in all ranges except $90\% \leq CE_{ARI} < 95\%$, where it was 95%. Data return for the Telops CE values was 40% or less for all ranges except $80\% \leq CE_{ARI} < 85\%$, where it was 75%.

Air Flare Tests

The CE data for the four ranges are graphed in Figures 10-7 to 10-10. As shown in Table 10-1, the mean difference and the standard deviation of the CE differences for the IMACC PFTIR increase as the CE_{ARI} decreases. The IMACC AFTIR was not deployed for any of the air flare tests. In examining the CE differences in Table E-2, the data tend to be biased low relative to the CE_{ARI} values.

The number of Telops data points, five, for all four ranges of the air flare tests are too few to statistically develop trend data. Additionally, the data return for these four CE_{ARI} ranges did not exceed 13%. Therefore, no additional analyses will be performed on the Telops air flare data.

In summary, the IMACC PFTIR mean differences for the range $CE_{ARI} \geq 90\%$ for both the air and steam flare tests averaged 2.2 percentage points, with an average standard deviation of the CE differences of 2.9 percentage points and average data return of 99%.

The IMACC AFTIR mean difference for the range $CE_{ARI} \geq 90\%$ for the steam flare tests averaged 2.5 percentage points, with an average standard deviation of the CE differences of 3.1 percentage points and an average data return of 100%.

The Telops mean difference for the range $CE_{ARI} \geq 90\%$ for the steam flare tests averaged 14.9 percentage points, with an average standard deviation of the CE differences of 22.8 percentage points and an average data return of 39%.

Data Processing

All participants were required to submit their preliminary data within six weeks of completion of the field campaign. Telops was unable to do so. Their report explains some of the challenges they had in making measurements and processing the large volume of data generated by their sensor and the number of test points conducted in this study.

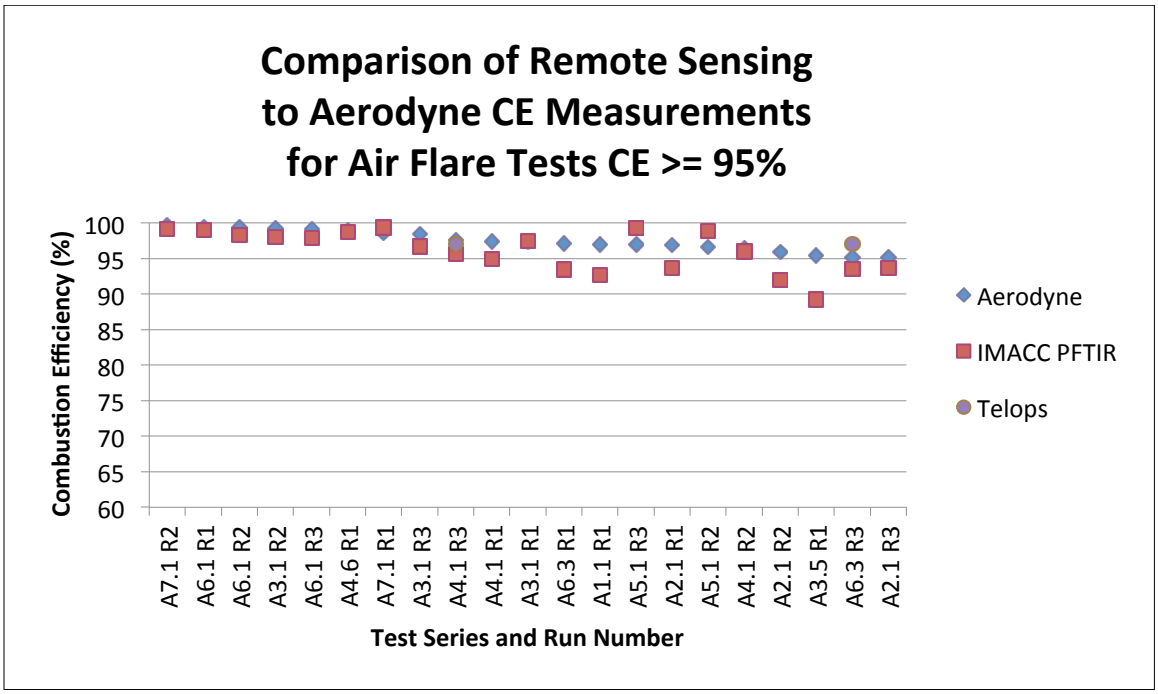

Figure 8-7. Comparison of All Remote Sensing Measurements Made to ARI Air Flare CE Measurements ≥ 95%

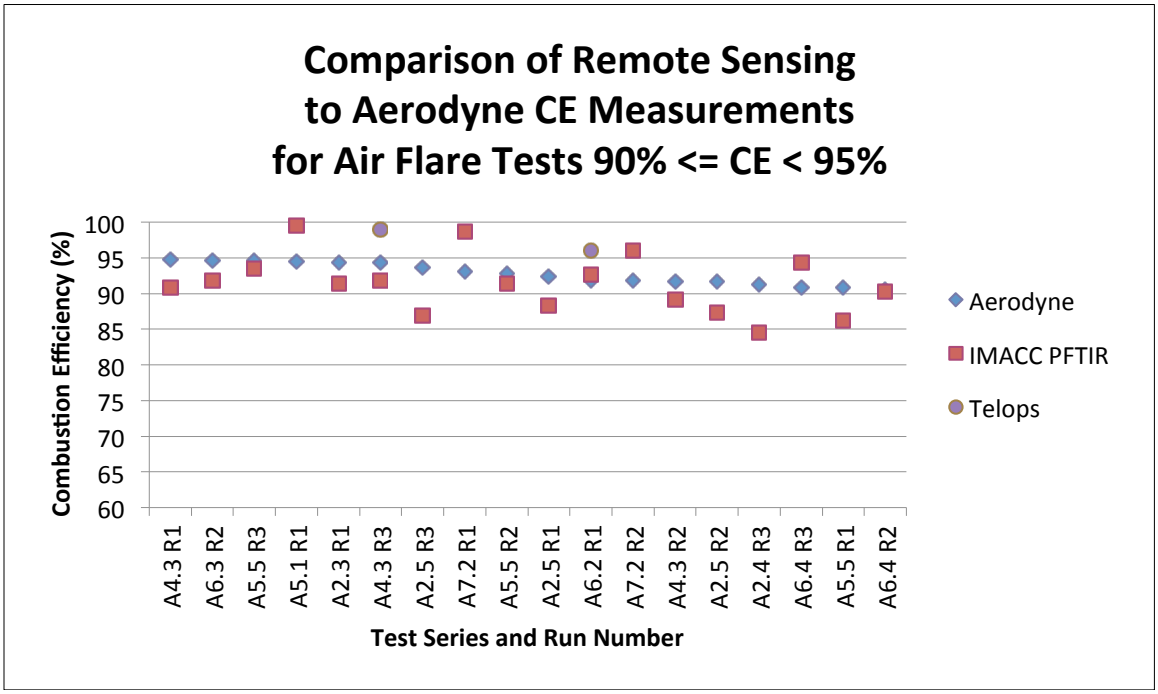

Figure 8-8. Comparison of All Remote Sensing Measurements Made to ARI Air Flare CE Measurements 90% ≤ CE_{ARI} <95%

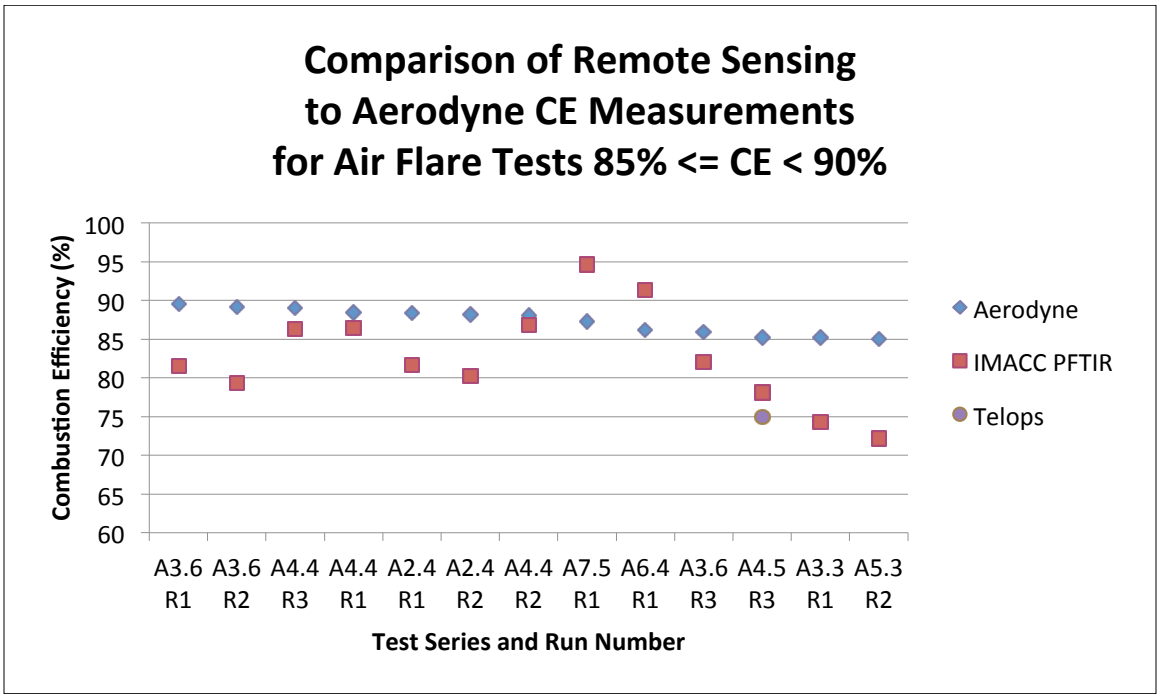

Figure 8-9. Comparison of All Remote Sensing Measurements Made to ARI Air Flare CE Measurements 85% ≤ CE_{ARI} <90%

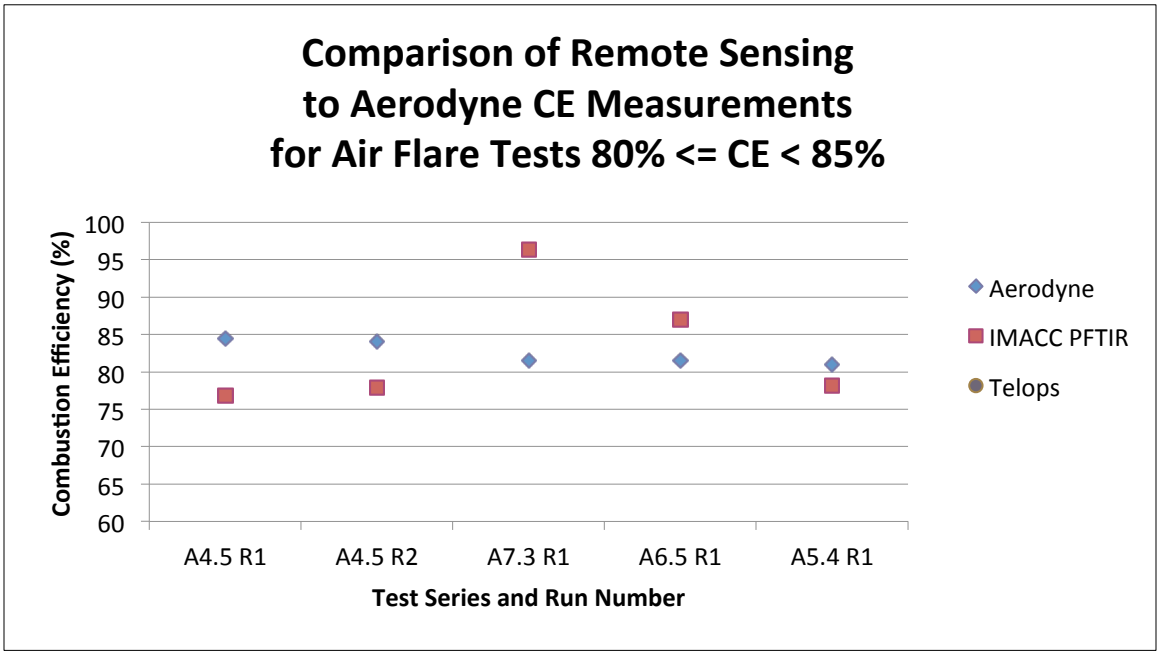

Figure 8-10. Comparison of All Remote Sensing Measurements Made to ARI Air Flare CE Measurements 80% ≤ CE_{ARI} <85%

Summary of the Development of Passive FTIR (PFTIR) Flare Monitoring

The following information is provided in response to a comment received by the TCEQ during the public comment period for the draft flare study report. It was provide by Bob Spellicy, IMACC (email message from R. Spellicy, IMACC, to V. Torres, UT Austin, July 8, 2011).

> The PFTIR methodology used in this study was developed over many years. It was initially constructed for a flare test at John Zink in 1984, which was funded by the US EPA Office of Research and Development in Research Triangle Park, NC. After that test, there was little interest in passive monitoring until the 2003 TCEQ test at John Zink. This was the first test that afforded an opportunity to challenge the methodologies. It also provided controlled data of a high quality so the algorithms and procedures could be tested and upgraded. Again, little was done until September of 2009 when the Marathon, Texas City test was conducted. IMACC and Clean Air Engineering approached this test believing more development would be required to perfect the passive technology. In reality, only minor alterations were needed in the algorithms and the calibration procedures. Between the Texas City test and the TCEQ 2010 Flare Study, several major flare programs were undertaken. These included**:** INEOS – Addyston, Ohio November 2009, Shell - Deer Park, Texas February 2010, and Marathon – Detroit, Michigan July 2010. All of these programs added to the knowledge of the passive techniques and allowed for further refinement of the procedures. The instrumentation, procedures, and algorithms used in the TCEQ 2010 Flare Study were extensively modified and upgraded from that used in the 2003 TCEQ test. The improvements in data quality since that test reflect the developments.

9.0 Summary of Speciation of Emissions Measured During Propylene Tests

Excluding CO and CO^2, Table 6-1 lists the hydrocarbon species typically found during the flare tests conducted with propylene/TNG flare tests and their weight ratios to propylene. An explanation of the determination of these weight ratios follows.

The sum of all carbon containing species was compared to a measurement of CO^2 following passage over an oxidation catalyst. The carbon budget balance was estimated by comparing the sum of the specific compounds to the total carbon proxy measurement. The specific compounds, named or quantified as sums, together with CO and CO^2 account for 98% of the ppmC carbon measured using the oxidation catalyst method. The error in the overall ppmC measurement technique is 4% (Appendix I). The combined error in the sum of all carbon containing compounds (weighted by the estimated contribution to ppmC) is 7%. Additional discussion of the carbon balance in the extractive sampling method will be discussed in future publications focused on this issue. The forms of carbon containing species that would elude detection in the analytical suite are either not transmitted through the sample line or believed to be highly unlikely given knowledge of the vent gas composition. Thus, it is believed that we have achieved carbon balance was achieved within the systematic capability of the instruments as operated during the test. The 13 species tabulated below, in addition to CO and CO^2 constitute 97.3% of the total carbon. These VOCs are the by-products of propene/methane partial and incomplete combustion.

NOx was also measured during the flare tests, but it is not included because NOx was measured using a commercial chemiluminescence analyzer. This instrument did not meet the data quality objectives over all the ranges of DRE observed.

Using the data from Table 9-1, the measured emissions tabulated for each of the propylene/TNG flare tests in Appendix F, Tables F-4 and F-5 in descending ARI DRE order.

In Table 9-2, the measured emissions (lb/hr) for propylene, methane, total VOCs and THCs are listed for five steam and five air tests with DREs approximately 90% and above. As points of reference, the Test Point, Run Number and propylene flow rate (lb/hr) in the vent gas along with the DRE for the test point/run number are also included with the estimates.

As an example, S3.6R1 with DRE (propylene) = 99.9%, the measured emissions were 0.13 lb/hr propylene and 0.15 lb/hr total VOCs. At a DRE (propylene) = 96.0% (S4.1R2), the measured emissions were 19.21 lb/hr propylene and 21.78 lb/hr total VOCs. And finally, at DRE (propylene) = 89.9% (S11.3R1), the measured emissions were 29.61 lb/hr propylene and 32.46 lb/hr total VOCs.

Table 9-1. List of Hydrocarbons Emissions Found in Plume During Propylene Flare Tests and Their Weight Ratio to Propylene

Air Flare				
DRE Range	>98	>95-98	>80-95	≤80
Species	lb species per lb propylene			
Acetylene	0.06253619	0.045724095	0.043341381	0.021789857
Ethylene	0.030726667	0.020664	0.017978	0.009274
Propylene	1	1	1	1
Butene isomers	0.000207107	0.000167293	0.001650667	0.004800533
Formaldehyde	0.046316429	0.030311429	0.024688571	0.012678571
Acetaldehyde	0.030758095	0.019197619	0.014572381	0.006882857
Propanal	0.000966611	0.000695296	0.00066758	0.000404082
Acrolein	0.0186396	0.014219933	0.009904	0.003840427
Methanol	0.002015086	0.00140419	0.00156259	0.001172952
Acetone	0.001159934	0.000834355	0.000801096	0.000484898
Propylene-Oxide	0.001449917	0.001042944	0.000556317	0.000202041
Methane	0.131809524	0.131809524	0.131809524	0.131809524
Ethane	0.010281143	0.010281143	0.010281143	0.010281143

Steam Flare				
DRE Range	>98	>95-98	>80-95	≤80
Species	lb species per lb propylene			
Acetylene	0.022798286	0.016445	0.01615219	0.010398143
Ethylene	0.038847333	0.027816	0.019898	0.009073333
Propylene	1	1	1	1
Butene isomers	0.000320947	0.00027444	0.002077067	0.007318667
Formaldehyde	0.058759286	0.038423571	0.026517857	0.010231429
Acetaldehyde	0.037277429	0.022619143	0.015254381	0.005405295
Propanal	0.001090317	0.001003566	0.00085347	0.000531901
Acrolein	0.0288852	0.0233274	0.0124624	0.005854933
Methanol	0.00131581	0.001346133	0.001088305	0.000779581
Acetone	0.001308381	0.001204279	0.001024164	0.000638282
Propylene-Oxide	0.001635476	0.001505349	0.000711225	0.000265951
Methane	0.131809524	0.131809524	0.131809524	0.131809524
Ethane	0.010281143	0.010281143	0.010281143	0.010281143

Table 9-2. Summary of Selected Emissions Measured During Flare Tests

Test Point	Run Number	Vent Gas	Measured				ARI
		Propylene	Propylene	Methane	TVOC	THC	DRE
		lb/hr	lb/hr	lb/hr	lb/hr	lb/hr	(%)
S3.6	1	189	0.13	0.02	0.16	0.17	99.9
S8.1	1	510	9.95	1.31	11.3	12.7	98.0
S4.1	2	484	19.3	2.55	21.9	24.7	96.0
S5.6	2	312	18.6	2.46	20.4	23.1	94.0
S11.3	1	297	30.0	3.95	32.8	37.1	89.9
A6.1	1	118	0.35	0.05	0.41	0.46	99.7
A6.3	1	118	2.38	0.31	2.70	3.04	98.0
A4.3	3	298	12.4	1.64	14.1	15.8	95.8
A5.5	2	71.5	4.32	0.57	4.82	5.43	94.0
A6.4	1	118	11.4	1.50	12.7	14.3	90.4

10.0 Quality Assurance

Quality assurance for this study began with the development and approval of a Category 2 Quality Assurance Project Plan. This plan was followed during all phases of the testing from maintenance of certificates of conformance for gas standards and factory calibration of instruments, where appropriate, to initial calibration of instruments pre-test through daily calibration checks, most performed at least twice per day on critical measurement systems like the TRC and ARI instruments. An overview of the calibration activities and copies of the supporting documentation for field calibrations are included Appendix K by company.

Data Quality Indicators

During a flare test, there were four parameters that provided indications of the quality of the data being collected during the testing. These four parameters were: the sample collector inlet gas temperature as measured by the three thermocouples at the inlet; the live video feed of the LSI visible, IR and two FLIR cameras used to position the collector and view the flare plume as it traveled to the sample collector; ratios of key combustion emission concentrations; and repeatability of results. Additionally, post testing a fifth parameter also provided an indication of the the quality of the data. This fifth indicator was the degree of agreement in CE ≥ 85% between one of the remote sensing technology measurements and the extractive measurements made by ARI has provided further independent corroboration of the level of quality of the data from this study. Each will now be discussed.

Average Sample Collector Inlet Temperature

One of the most important criteria in obtaining a DRE and CE that reflects the all combustion that has occurred in the flare, is to ensure that emission measurements are made far enough downwind of the plume to ensure no further combustion is occurring in the plume. Since one product of combustion is heat, then an elevation of the plume temperature above the steam assist temperature would indicate some degree of combustion. Conversely, no or little combustion would result in a plume temperature at or below the steam assist temperature. So the anticipated steam temperature, approximately 250°F, was selected as an upper temperature limit for the collector inlet temperature. Indeed the steam temperatures ran in the range of 220°F to 300°F during the test series. On the lower end, the ambient temperature would be an indicator that the collector inlet could be outside the plume, i.e., any increase in temperature above ambient temperature would certainly indicate thermal effects of the plume and therefore being in some portion of the plume exhaust.

But what if there was little or no steam assist as in the case of the air flare. Because the gauge used in the definition of the incipient smoke point involves distances two flame lengths from the flare tip, it was critical to always locate the sample collector inlet no closer in distance than this point in the plume. The first test point run was on the steam flare with the vent gas all propylene. This was a “practice” test to allow all participants to acquaint their systems with the protocol to be used. It allowed us to fine tune positioning of the collector. This test showed that just past two flame lengths away, the average collector inlet temperature was in the range of 150°F to 170°F. If the collector were backed away to an average collector inlet temperature of about 105°F, the signal required by ARI to adequately measure emissions had not degraded sufficiently, i.e.,

greater dilution with ambient air, to adversely affect the accuracy of their measurement. So the temperature range of 105°F to 150°F was used for the steam-assisted flare tests as the average sample collector inlet temperature range where ARI measurements could be made that complied with the data quality objectives for their measurements of plume emissions needed to calculate DRE and CE. This assumed of course that that the collector was in a plume with a high level of combustion, i.e., strong thermal signal.

Four Way Video Camera Images

In practice, it was learned that with the test parameters and equipment that the flame could never be extinguished, i.e., snuff the flame, with the maximum flow of steam or air assist designed for this project. So the case of no combustion for the composition of the vent gas used never occurred in this test series. For the case of poor combustion or significant incomplete combustion, the UT Austin team depended on the two GasFind IR cameras, whose image of the plume actually improved with greater signal, i.e., when there were more unburned hydrocarbons in the plume.

Figure 10-1 is video image produced by LSI using the four cameras used during the field tests. The Sony visible light camera, aimed approximately perpendicular to the travel of the plume, produced the top left image. The GasFind IR-stationary camera, aimed looking approximately perpendicular to the travel of the plume, produced the bottom left image. The GasFind IR-mobile camera, aimed approximately coincident with the travel of the plume, produced the bottom right image. The thermal IR camera, aimed at approximately the same angle as the GasFind IR-stationary camera, produced the top right image. These four cameras were used to help find the plume when there was minimal flame or a plume that was invisible to the naked eye and to verify that the unburned products of combustion were traveling in the same path as the thermal products of combustion. The sample collector can be seen in each of the images near the flare plume. The sample collector inlet would be positioned to intersect the largest portion of the plume. It was easy to line up the collector to intersect the plume if the wind direction was not changing rapidly. Fortunately for the study team, as can be seen in Appendix J, during the 7 to 10 minutes period of a test run, the wind direction did not change significantly during most of the test series. For those few runs where the wind direction was changing significantly, the collector would be repositioned frequently during the test to stay in the plume using the average collector inlet temperature, the real-time images of the four video cameras, and the ratios of concentrations of flare emissions in the plume measured by ARI. For these tests, longer run times were employed to obtain sufficient data to provide repeatable results.

Figure 10-1. LSI Four-Way Video Images. LSI four-way video images were used to help position the sample collector. Top left, Sony visible light camera looking approximately perpendicular to plume travel; bottom left, GasFind IR-Stationary looking approximately perpendicular to plume travel; bottom right, GasFind IR-Mobile looking approximately coincident with plume travel; and thermal IR viewing at approximately the same angle as GasFind IR-Stationary.

Wind Speed and Direction Levels and Variation and Key Emission Concentration Ratios
The duration of most test runs was in the range of 7 to 10 minutes, except as noted above when the wind was changing direction frequently during this period or if there was a request by TRC or ARI for additional time to make their measurements. The spatial impact of a change in wind direction is best examined with an example. If the collector were in line with the center of the plume and the wind direction changed 5°, at a distance of 20 ft from the flare, the centerline of the collector inlet would then be 1.8 ft from the line of travel of the plume in this new wind direction. With an effective draw of 2 ft in diameter, the centerline of the plume would be 0.8 ft from the edge of the effective draw of the collector. The collector would now be drawing from a section of the plume that was 0.8 ft from the center of the plume. As ARI was able to make measurements at a frequency of 1 Hz, they were able to monitor the change in emission measurements and key ratios as the direction of the wind changed. Key emission concentration ratios, e.g., propylene to carbon monoxide, methane to carbon monoxide, carbon dioxide to carbon monoxide, were an excellent indicator of the impact of the change in the relative position of the collector on the measurement of flare emissions. For a given test run and ambient wind conditions, these ratios should be a constant value representing the net result of the combustion reactions taking place in the flare combustion zone. If these ratios remained relatively constant as the wind direction changed, then representative measurements of the plume emissions were still

occurring. If all the ratios began to change and there had been no change in the flare operating parameters, i.e., lower carbon dioxide to carbon monoxide ratio, and the ratios approach atmospheric ratios of these values, then the collector was not sufficiently in the plume and repositioning was needed. This approach was also employed if the wind direction were changing in a cyclic manner where repositioning of the collector would have been impractical. In this latter situation, the time period of the test run for collection of data would be extended until sufficient periods of data collection in the plume established repeatable emission concentration ratios representative of the combustion occurring for the test being conducted.

Similar to the case of the cyclic change in wind direction, small changes in wind speed were addressed in the same manner, i.e., the time period of the test run for collection of data would be extended until sufficient periods of data collection in the plume established repeatable emission concentration ratios representative of the combustion occurring for the test being conducted.

Repeatability of DRE and CE Results

Another indicator to aid in evaluating the quality of the data is the repeatability of the data. Table 10-1 presents a summary the percent standard deviation of the DRE and CE for each test point where there were 3 repetitions of the flare test conditions and the average DRE for the three runs was greater than 60%. The percent (%) standard deviation (DRE) is defined as follows:

$$\%\ Standard\ Deviation\ (DRE) = \left(\frac{Standard\ Deviation\ (DRE)_{runs}}{Average\ \ DRE_{runs}}\right) \times 100 \qquad \text{Eq. 10.1}$$

Equation 10.1 can also be used to calculate % Standard Deviation (CE). When calculating the % Standard Deviation (CE), then all terms on the right refer to CE values rather than DRE values.

It can be seen from these data in Table 10.1, that the maximum % standard deviation (DRE) was 8.3%, with all remainder Test Series less than 4.2%. In more than 79% of the cases, % standard deviation (DRE) was less than 2%. This typically low % standard deviation indicates a high degree of repeatability in the test system and in the measurements providing greater confidence that the data are not random results.

Comparison with Independent Measurement of Remote Sensing Technology – IMACC PFTIR

Not known during the field tests but upon analysis of measurements made by IMACC using their PFTIR spectrometer, in this study's range of greatest interest, i.e., CE ≥ 85%, these two independent measurement methods show very good agreement. As these measurements were made employing a single blind approach, this level of agreement provides additional independent confirmation of the study's data quality for the CE measurements.

Each of these five factors taken separately would not necessarily ensure a high degree of data quality. But taken together, they provide strong evidence to support the conclusion that the DRE and CE measurements made by the flare plume extractive sampling system are reliable data of high quality

Table 10-1. Repeatability of Test Results

Test Series	ARI Extractive Sample Results			
	Average DRE	% Standard Deviation (DRE)	Average CE	% Standard Deviation (CE)
S2.1	99.2	0.8	98.7	1.3
S4.1	96.8	1.2	95.8	1.5
S4.2	98.7	0.5	98.3	0.5
S5.1	96.4	1.8	95.6	2.2
S5.3	89.0	1.3	86.5	1.6
S5.4	66.6	2.5	61.3	3.6
S5.6	94.5	0.8	93.2	0.9
S6.1	99.4	0.1	99.1	0.2
S6.3	97.5	0.1	96.3	0.1
S6.4	83.6	8.3	79.5	9.2
S7.2	88.8	4.2	87.5	4.4
A2.1	97.2	0.6	95.9	0.9
A2.4	93.0	1.7	89.3	2.0
A2.5	95.1	0.8	92.6	1.1
A3.1	98.8	0.8	98.3	1.0
A3.2	65.2	2.6	59.1	2.9
A3.4	76.6	0.4	72.0	0.4
A3.6	90.8	1.7	88.2	2.3
A4.1	97.9	0.5	97.1	0.7
A4.3	95.2	1.4	93.6	1.8
A4.4	91.0	0.5	88.5	0.6
A4.5	87.9	0.7	84.6	0.8
A5.1	96.4	1.5	96.0	1.4
A5.3	83.7	4.0	80.8	4.6
A5.5	93.9	1.7	92.7	2.1
A6.1	99.6	0.2	99.3	0.2
A6.3	97.1	0.8	95.6	1.4
A6.4	92.9	2.4	89.2	2.9

11.0 Conclusions

1. At a vent gas LHV = 350 Btu/scf and flow rates of 0.1% and 0.25% of rated design capacity (propylene) for the John Zink Model EE-QSC-36" steam flare this flare design was able to achieve DREs (propylene) of > 99% and CE > 99%. At a nominal vent gas flow rate 937 lb/hr (0.1%), an S/VG = 0.25 or less was required to achieve a DRE (propylene) > 99%. This S/VG would equate to a total steam assist of approximately 234 lb/hr, which would be less than the minimum recommended (as reported by industry) steam-assist rates of center = 500 lb/hr and upper = 750 lb/hr for this flare. The John Zink Company LLC recommends continuous minimum center steam of 300 lb/hr and 525 lb/hr upper steam for this flare design. This study does not recommend that steam assist rates less than that recommended by the flare manufacturer be used.

2. At a vent gas LHV = 350 Btu/scf and flow rates of 0.25% and 0.65% of rated design capacity (propylene) for the John Zink Model LHTS-24/60 air flare, this flare model was able to achieve DREs (propylene) of > 99% and CE > 99%.

3. The most efficient flare operation, as measured by the DRE and CE, for the flare operating conditions tested, was achieved at or near the incipient smoke point (ISP). Higher efficiencies could have been achieved with steam or air assist slightly less than the ISP assist value but this condition, i.e., a smoking flare, would not have been in compliance with 40 CFR § 60.18. Therefore, the minimum levels of steam or air assist that comply with the flare manufacturer's recommendations should be used when possible.

4. At these low vent gas flow rates (nominally 937 lb/hr and 2,342 lb/hr) and low LHVs (nominally 350 Btu/scf and 600 Btu/scf), the flare performance curve of DRE vs steam assist has a very short to non-existent "shelf" before the DRE falls off to less than 98%. Beyond this point, the DRE and CE decrease almost linearly as steam assist increases.

5. For nominal LHVs of 350 Btu/scf and 600 Btu/scf and vent gas flow rates of 359 lb/hr and 937lb/hr, air flare test data showed that an air-to-fuel ratio (lb/lb) of approximately 6.0 or less produced a DRE > 99%. Higher levels of air assist produced lower DREs in an almost linearly decreasing manner.

6. The IMACC PFTIR and AFTIR mean differences between their values of CE and the ARI values of CE averaged 2.2 and 2.5 percentage points, respectively, and had average standard deviations of the CE differences of 2.9 and 3.1 percentage points in the range $CE_{ARI} \geq 90\%$ for the air and steam flare tests. The PFTIR and AFTIR had average data returns of 99% and 100% in this range.

7. The Telops Hyper-Cam mean differences between their values of CE and the ARI values of CE averaged 14.9 percentage points, with an average standard deviation of the CE differences of 22.8 percentage points in the range $CE_{ARI} \geq 90\%$. The Telops Hyper-Cam had average data return of 39% in this range.

References

Baukal, Jr., Charles E. (2001). *The John Zink Combustion Handbook*, CRC Press, New York.

Environ International Corporation, (2009). *Control of HRVOC Emissions in Flares at Low Flow Conditions, Project 2009-53 (DRAFT Interim Report)*.

Flare Details for General Refinery and Petrochemical Service, American Petroleum Institute ANSI/API Standard 537, Washington, DC, 2008.

Green, Don W. and R. Perry, (2008). Perry's Chemical Engineer's Handbook, 8th Edition, McGraw-Hill, New York, 2008.

Hashmonay, Ram A.,Ravi M. Varma, Mark Modrak, and Robert H. Kagman, Simultaneous Measurement of Vaporous and Aerosolized Threats by Active Open Path FTIR. http://www.dtic.mil/cgi-bin/GetTRDoc?AD=ADA449529&Location=U2&doc=GetTRDoc.pdf (accessed May 18, 2010).

Marathon Petroleum Company, LP, Detroit Refinery. Performance Test of a Steam-Assisted Elevated Flare with Passive FTIR – Detroit, Final Report. Detroit, Michigan, November 2010.

Marathon Petroleum Company, LLC, Texas Refining Division. Performance Test of a Steam-Assisted Elevated Flare with Passive FTIR, Final Report. Texas City, Texas, May, 2010.

McDaniel, Marc, *Flare Efficiency Study*, United States Environmental Protection Agency, Report No. 600/2-83-052, July 1983.

National Physical Laboratory, *Measurement of VOC Emissions from Petrochemical Industry Sites in the Houston Area Using Differential Absorption Lidar (DIAL) During Summer 2007, Draft for Comment*. Texas Commission on Environmental Quality, February 2008.

Texas Commission on Environmental Quality, (2009). *Proposal for Grant Activities No. 582-8-86245-FY09-04, Comprehensive Flare Study, Tracking Number 2008-01, Amendments 1 & 3 (2010)*.

The University of Texas at Austin, (2010). *Quality Assurance Project Plan for Texas Commission on Environmental Quality Comprehensive Flare Study Project, PGA No. 582-8-862-45-FY09-04, Tracking No. 2008-81, Rev. 1*. The University of Texas at Austin, August 2010.

United States Government. *Code of Federal Regulations - Standards of Performance for New Stationary Sources, General Control Device and Work Practice Requirements, 40CFR § 60.18*. http://edocket.access.gpo.gov/cfr_2009/julqtr/pdf/40cfr60.18.

URS Corporation. *Passive FTIR Phase I Testing of Simulated and Controlled Flare Systems: Final Report*. Texas Commission on Environmental Quality, June 2004.

CEEPR **Center for Energy and Environmental Policy Research**

The effect of variability in industrial emissions on ozone formation in Houston, Texas

by

Mort Webster, Junsang Nam, Yosuke Kimura, Harvey Jeffries, William Vizuete, David T. Allen

07-008 **August 2007**

A Joint Center of the Department of Economics, Laboratory for Energy and the Environment, and Sloan School of Management

The effect of variability in industrial emissions on ozone formation in Houston, Texas

Mort Webster[1,*] Junsang Nam[2], Yosuke Kimura[2], Harvey Jeffries[3], William Vizuete[3], David T. Allen[2]

[1]Massachusetts Institute of Technology, Department of Earth, Atmosphere, and Planetary Sciences, E40-408, 77 Massachusetts Avenue, Cambridge, MA 02139

[2] University of Texas, Center for Energy and Environmental Resources, 10100 Burnet Road, M/S R7100, Austin, TX 78758

[3]University of North Carolina, Department of Environmental Sciences and Engineering, School of Public Health, Chapel Hill, NC 27599

*author to whom correspondence should be addressed, fax 617-253-9845 mort@mit.edu

Abstract

Ambient observations have indicated that high concentrations of ozone observed in the Houston/Galveston area are associated with plumes of highly reactive hydrocarbons, mixed with NO_x, from industrial facilities. Ambient observations and industrial process data, such as mass flow rates for industrial flares, indicate that the VOCs associated with these industrial emissions can have significant temporal variability. To characterize the effect of this variability in emissions on ozone formation in Houston, data were collected on the temporal variability of industrial emissions or emission surrogates (e.g., mass flow rates to flares). The observed emissions variability was then used to construct region-wide emission inventories with variable industrial emissions, and the impacts of the variability on ozone formation were examined for two types of meteorological conditions, both of which lead to high ozone concentrations in Houston. The air quality simulations indicate that variability in industrial emissions has the

potential to cause increases and decreases of 10-52 ppb (13-316%), or more, in ozone concentration. The largest of these differences are restricted to regions of 10-20 km^2, but the variability also has the potential to increase region wide maxima in ozone concentrations by up to 12 ppb.

Keywords: Photochemical Grid Model, highly reactive volatile organic compounds (HRVOC), ozone, uncertainty analysis, Monte Carlo simulation.

Introduction

Ambient observations have indicated that ozone formation in the Houston/Galveston (HG) area is faster and more efficient, with respect to NO_x consumed, than other urban areas in the United States. This results in highly localized but extreme ozone events, frequently in excess of the National Ambient Air Quality Standards (NAAQSs) for ozone. It is believed that these unique characteristics of ozone formation in the Houston metropolitan area are associated with plumes of highly reactive hydrocarbons, which have been observed in airborne measurements (Kleinman et al., 2003; Ryerson et al., 2003) over or near the industrial Houston Ship Channel area. Thus, accurate quantification of industrial emissions, particularly of reactive hydrocarbons, is critical to effectively address the rapid ozone formation and the consequent high ozone events in the Houston metropolitan area.

Industrial emissions of hydrocarbons, from non-electricity generating units (NEGUs), have traditionally been assumed to be continuous at constant levels for the State Implementation Plan (SIP) development and photochemical modeling purposes. However, observational data collected during the Texas Air Quality Study in 2000 showed that industrial emissions of hydrocarbons from NEGUs have significant temporal variability (Murphy and Allen, 2005; Vizuete, 2005).

Variability in industrial emissions of hydrocarbons can be ascribed to the occurrence of both episodic emission events and variable continuous emissions. Murphy and Allen (2005) have investigated characteristics of emission events in the HG area with a focus on highly reactive volatile organic compounds (HRVOCs; defined in Texas air quality regulation as ethylene, propylene, isomers of butene and 1,3-butadiene); characteristics of emission events examined included event magnitude, event duration and source types. These emissions events

are discrete non-routine emissions events, of more than permitted amounts, with reporting required under Texas law. Since 2003, reporting is required of emissions events of over 100 lbs. of a specific compound, or over 5000 lbs of VOCs if composed of less than 2% of individual highly reactive species. Murphy and Allen (2005) showed that depending on the time, location, and magnitude of the emission event, ozone concentrations can be increased by as much as 100 ppb. Nam et al (2006) performed additional analysis using a subdomain model, and showed that 1.5% of emission events would produce an additional 10 ppb of ozone, and 0.5% of events would produce more than 70 ppb of additional ozone.

Vizuete (2005) investigated the physical and chemical processes of ozone formation and accumulation in the HG area during a small number of large magnitude emission events. Nam et al. (2006) developed computationally efficient photochemical models and examined the impact, on ozone formation in the HG area, of emission events using a stochastic characterization of the emission events described by Murphy and Allen (2005). While the previous studies provided important information on impacts of emission variability on ozone formation in the HG area, they are limited in the sense that the episodic emission events account for just a part of emission variability and contribute to just 10% of the mass of annual HRVOC emissions. As described in later sections of this paper, data from emissions monitors for several industrial sources show that there is considerable variability in routine emissions that is not high enough to require reporting as an event, but may significantly impact ozone formation. If so, representing this variability may be critical in developing ozone control strategies, since different strategies will target different parts of the probability distribution of emissions.

The overall goal of this work is to estimate potential changes in ozone formation and accumulation in the HG area due to variability in continuous hydrocarbon emissions. Because

the variability may be an important consideration in developing control strategies, this study focuses on establishing the methodology and the importance of emissions variability on ozone formation. The impact on control strategies is explored in a subsequent study. Variability in VOC emissions will be simulated based on observations of emission variability from a group of industrial sources in the HG area, and a stochastic emission inventory generator, described in the Methods section. The characterization of VOC emissions variability and the impacts of the variability on ozone formation in the Houston area are described in the Results.

Methods

The stochastic emissions inventory generator

Observations from various emission sources and ambient measurements indicate that industrial emissions of VOC have significant temporal variability. For example, Figure 1 shows the hourly measurements of the mass flow rate to a typical flare at an industrial facility in the Houston area over the course of a year. Variability in mass flow to a flare represents the variability in emissions if combustion efficiency is constant and likely represents a lower bound on emission variability if combustion efficiency decreases at high or low flows. Although the annual average mass flow rate (blue horizontal line at 2.93 kilo-lb/hr) is below the permitted annual average mass flow rate (purple line at 3.43 kilo-lb/hr), the significant temporal variability in mass flow leads to frequent exceedances of the annual average emission rate. While temporal variability is large compared to the mean, this variability does not necessarily result in a reportable emission event. The maximum allowable flow to the flare of Figure 1, when averaged on a daily basis, is 34,700 lb/hr. Only a few of the instances of high flow rates exceed this

amount and are reportable as emission events. Data from other emission sources also exhibit high variability, with different temporal patterns.

The motivating question for this study is: does the variability in VOC emissions from point sources contribute to ozone exceedences in Houston-Galveston? If, for example, the occasional spikes of extremely high VOC emissions as seen in Figure 1 are a major cause for ozone exceedences, then this has a strong implication for control strategies. Rather than lower the annual average of VOC emissions, it may be much more effective to eliminate the high emissions spikes. Before this can be explored, however, a method for representing the stochastic emissions process must be developed.

A probabilistic model of the stochastic emissions generating process was constructed. To simulate the observed temporal patterns, sampling from a simple probability density function (PDF) is not sufficient; samples from a single PDF cannot characterize the flare flow. Standard time series methods are similarly unable to capture the characteristic patterns in the VOC emissions. For example, in Figure 2, the cumulative distribution function (CDF) is shown for the observations from Flare 1 and for a simulation of an auto-regressive moving-average (ARMA) with all significant terms. While the ARMA fit approximates the mean, it does not reproduce the standard deviation or the tails of the observations. Another application area where standard time series approaches have proven insufficient is in forecasting electricity prices in deregulated markets. Time series of electricity prices show similar volatility and extreme jumps with low frequency. Recent work in that area (Johnson & Barz, 1999; Knittel and Roberts, 2001) has shown jump-diffusion and markov process models to be superior, and a similar approach is used here.

Mass flows to the flare in Figure 1 are composed of various components in magnitude, including nearly constant, routinely variable, and allowable episodic mass flow rates (Figure 3). Therefore a more appropriate model for this process is a mixture of multiple PDFs (Cornell, 2002), each accounting for one of the components of the mass flow variability. To determine the form of the PDF (normal or log-normal) that should be used for the nearly constant, routinely variable and allowable episodic mass flows, normal probability plots are used (Figure 4). A normal probability plot (Hogg and Ledolter, 1992, p. 137) graphs the quantiles of the observations against the standardized normal scores, defined as $\left(z = \frac{Y - \overline{Y}}{s} \right)$. $\overline{Y}$ is the mean emission rate and *s* is the standard deviation of the normal function that best fits the emission rate. If the observations are normally distributed, the plot will form a straight line with a slope of 1/s and will intersect the point ($\overline{Y}$, 0). In addition, the log of the sorted observations are plotted against the standardized normal scores; if the relationship is linear between the inverse normal and the logarithm of the mass flow rate, it is reasonable to assume that the mass flows are lognormal. An alternative would be to graph the sorted observations against the quantiles of an assumed distribution, known as a ”q-q plot”. The advantage of the normal probability plot used here is in identifying breaks between different components, each with different means and variances. The q-q plot, by contrast, is best suited to assessing whether the data is drawn from a single theoretical distribution.

By looking for regions of the observations that are linear with constant slope and intercept, the different components of the distribution can be identified. Continuing with the example emissions from Figure 1, a total of three components of variable mass flows were identified: one normal distribution and two lognormal distributions, as indicated with the colored lines in Figure 4. In addition, the mean and standard deviation of the distribution were obtained

from the midpoint and slope of the fitted line, respectively. Figure 5 shows resultant PDFs for each component identified (Figure 5a) and the normalized PDFs based on the proportion of mass flow associated with each component (Figure 5b) for the mass flow rates shown in Figure 1. When these distributions of mass flows are used for other flares in the HG area, the distributions are scaled such that the mean of the distribution exactly equals the deterministic value for hourly emissions, and that the coefficient of variation, defined as the standard deviation normalized by the mean, is preserved.

Once PDFs for each emission mode are calculated, the duration of emissions in one mode, before transition to another mode, is simulated using an exponential distribution function. Exponential distributions are probability distributions widely used to model the time between events. Each hour's emissions is identified as belonging to one of the three component PDFs determined as above. Thus the time series is converted into a series of the number of hours in a given state before a jump to the next state (a Poisson model). The mean time for an exponential distribution for each component is then calculated. For the flare flow in Figure 1, mean time was calculated as 7.41, 4.41 and 1.15 hour for the nearly constant, routinely variable, and allowable episodic emission components, respectively, and the distribution of the duration in each component is shown in Figure 6.

Overall, the algorithm for generating emission samples is to (1) randomly sample the mode of emissions using the proportions of each emission mode, (2) randomly sample the number of hours to remain in the current mode using the exponential distributions for the selected emission mode, and (3) randomly sample the emission rate for each hour based on the PDF of emission rates for the current mode. In sampling emissions in step (3), an autocorrelation of 0.99 with the emission rate of the previous hour is imposed. Hourly emissions

from a source are sampled as a random draw from a standard normal distribution, and then transformed to a sample from the current component normal or lognormal distribution. The emissions from each source for each hour is sampled by imposing correlation with the previous hour's emissions from that source, using a standard algorithm for sampling correlated normal variates (Press et al, 1992). The autocorrelation of 0.99 was estimated from the observations, and is a reasonable model of a continuous industrial process, since the best predictor of one hour's activity level and operating conditions is the previous hour's. Based on the number of hours selected in step (2), step (3) is repeated. For example, if the first component, nearly constant, was selected in step (1) and two-hour duration was selected in step (2), then emission rates would be randomly sampled from the PDF of the first component for two hours before randomly selecting the next component. This method produces samples of emissions that closely match the cumulative distribution properties of the observations. Note that this model of emissions includes only permit allowable emission rates. Emission events above permitted levels are not included. The nature and impacts of these emission events have been described by Murphy and Allen (2005) and Nam, et al. (2006).

Application of stochastic emission inventory to the HG area

A set of observations similar to that shown in Figure 1 were obtained from various flares and cooling towers in the HG area. The models to simulate emission variability were developed using the process described in the previous section. Table 1 summarizes these observations and parameters for the models developed. Emissions from different sources exhibit different patterns of variability, but only limited data on that variability is available. For this study, therefore, individual flares, cooling towers and other point sources in the HG area were assigned one of the

unit operation models developed and overall time-varying emissions from the point sources were simulated with the model. Because of the limited data available, we randomly assign a variability pattern to each source in the emissions inventory. Cooling towers were randomly assigned one of the cooling tower models. Flares were randomly assigned one of the flare models. Stack and fugitive emissions were assumed to be lognormally distributed, as shown in Table 1. The mean of the selected model for simulating emissions is scaled to be equal to the average emission rates in the inventory for each emission source. In addition, the standard deviation of the models was scaled to preserve the coefficient of variation (the ratio of the standard deviation to the mean) shown in Table 1. For emission sources other than flares, all emissions except VOCs were kept intact throughout the simulation. For flares, both VOC and NO_x emissions were assumed to scale with flow rate, so for flares, the same pattern of variability was assumed for both VOC and NO_x emissions. The composition of the emissions from all sources was assumed to be constant, with only the temporal variability in the magnitude of emissions changing.

Because so few emissions sources had hourly emissions monitoring data available, it is not clear whether the variability of emissions in the region as a whole is over- or underestimated. As a first study of the importance of this variability, the available data and random assignment have been used as a type of bootstrapping. However, there are reasons to believe that this may be a reasonable first-order estimate: the sample emissions data come from among the largest sources in the HG area, and it has been shown (UNC, 2004) that the largest few sources dominate the VOC emissions. For example, the top 20 flares are responsible for 45% of all flare VOC emissions. Nevertheless, data from more point sources are needed to better characterize the variability, and this is one area that future analysis could focus.

Table 2 compares the mean, standard deviation, and several fractiles of the observations with simulations of 10,000 hours of the corresponding stochastic emission model. Figure 7 compares the cumulative distribution function (CDF) of the observations with the CDF of emissions for four of the flares.

Air quality modeling

The impact of industrial point source variability on ozone formation was assessed using the Comprehensive Air Quality Model with extensions (CAMx) (Environ, 2004). In this work, a computationally efficient version of CAMx, referred to as a sub-domain model and described by Nam, et al (2006), was used. The overall strategy in developing the sub-domain model was to (1) identify a geographical region (sub-domain), from a full, 3-D photochemical model, (2) create a computationally efficient photochemical model of the sub-domain, and (3) analyze many scenarios or snapshots of variable emissions using the sub-domain model. Steps 1 and 2 in the development of the model are analogous to the methods used by Nam, et al (2006) and are only summarized here. Step 3 is described in the results section.

The geographical region (sub-domain) to be modeled is the HG 1 km domain, shown as the region in red in Figure 8. CAMx simulations using the full domain, shown in Figure 8, were used to develop boundary and initial conditions for the sub-domain. Details of the meteorological modeling and the VOC and NOx emission inventory development for simulation of the full domain are available from the TCEQ (2006) and from Nam, et al (2006). Briefly, meteorological inputs were based on results from the NCAR/Penn State Mesoscale Meteorological Model version 5 (MM5). Emission inventories were prepared by the Texas Commission on Environmental Quality (TCEQ). The TCEQ data includes a MOBILE6-based

inventory developed for on-road mobile source emissions, and emissions for non-road mobile and area sources developed using the U.S. EPA's NONROAD model, using local activity data when available. Biogenic emission inventories were estimated using the GLOBEIS emission model with locally developed land cover data. Point source emissions data were developed with TCEQ's point source database and special inventory. Approximately 150 tons/day of reactive olefin species were added to approximately 100 point sources in the domain, based on ambient measurements made by aircraft (Ryerson et al., 2003). These point source inventory additions are commonly referred to as the imputed inventory, since the added emissions were estimated based on ambient measurements rather than reported inventories. The imputed point source inventory and the other components of the emission inventory, described above, were used as the base case in this work and will be collectively referred to as the imputed inventory. In short, TCEQ's standard emissions inventory was used for all sources without change except for selected VOC emissions (and VOC and NOx emissions from flares) from point sources. The mean of emissions from these sources in the stochastic runs are equal to the TCEQ emissions in its inventory, as described above. Both the sub-domain modeling and the full domain modeling in the region with industrial emissions were performed at a 1 km spatial resolution.

The full domain model was used to establish initial conditions and time varying boundary conditions for the sub-domain model. Calculations reported by Nam, et al (2006) indicate that the sub-domain model responds to temporal variability in industrial emissions in a manner that correlates (r^2>0.96) with the response of the full domain model.

The sub-domain model was run for two episode days: 25 August and 30 August, 2000. These two days were selected because there was rapid ozone formation on both days and distinctly different meteorological conditions on the two days had the potential to lead to

different processes for ozone formation and accumulation. Details of the meteorological conditions on these two days have been reported by Nam, et al (2006).

Results and Discussion

The Results and Discussion will be presented in two parts. The first part summarizes the stochastic emission inventories; the second part describes the air quality modeling based on those inventories.

Stochastic emission inventories

Figure 9 shows probability distributions for 500 random realizations of one day's emissions (12,000 samples of hourly emissions), and numerical values of the mean, standard deviation, and selected percentiles are given in Table 3. Note that the total of all VOC emissions from the industrial point sources show relatively little variation in any given hour. This is a consequence of the Law of Large Numbers: the variance of a sum is significantly smaller than the variance of any individual component. Similarly, the sum of all hydrocarbon flares in Houston Galveston shows a relatively small variance. The mean of these distributions is virtually equal to the values from the deterministic emissions inventory.

As the area and the time period over which emissions are reported decrease, however, emission variability becomes more evident. The VOC emissions from two 1-km by 1-km grid cells near the Ship Channel, where significant VOC sources are concentrated, have 95% probability bounds that span more than a factor of two (Figure 9c; Table 3). A third grid cell near downtown Houston has 95% bounds that span a factor of 1.6. The three largest flares in the Houston Galveston region have 95% probability bounds that span factors of 9, 4, and 16, respectively (Table 3).

In addition to variability of any individual source, which can be quite large, it is important to explore other statistical properties of the combination of point sources. Figure 10 shows the probability, in any given hour, that at least N sources have emissions greater than or equal to a factor of 2, 5, and 10 times its annual average emissions, examining N over the range from 1 to 9. Only the 50 largest point sources, in terms of annual average emission rates, are considered. These sources comprise 20% of the total VOC emissions. For example, there is a 40% chance in any one hour that 8 or more of these large sources are emitting at greater than twice their average value. There is an 8.6% chance that at least 2 sources will emit more than five times their average in the same hour, and there is a 12% chance that in any hour, one of these sources will be emitting 10 times their average rate.

Impacts of VOC emission variability on ozone formation

A total of 50 sets of stochastic emission inventories were randomly generated with the models described in the Methods section and simulations representing 25 August and 30 August, 2000 were performed using these inventories, for a total of 100 simulations. Figure 11 shows the differences in ozone concentration on 25 August between using the 45th stochastic inventory and the deterministic imputed inventory. The 45th stochastic inventory showed the largest increase in ozone concentration for the August 25 meteorology, as shown in Figure 12. Since the stochastic inventory has both higher and lower VOC emissions across the HG area over the course of the day, ozone concentrations using the stochastic inventory are both higher and lower than using the imputed inventory without VOC emission variability depending on time of day and location. At conditions that lead to maximum difference in ozone concentration, ozone concentrations predicted using the stochastic inventory are approximately 82 ppb higher than using the imputed

inventory without variable VOC emissions. Ozone concentrations are also up to 6 ppb lower using the stochastic inventory than using the imputed inventory with constant industrial emissions.

Figure 12 summarizes the maximum changes in ozone concentrations that were observed, both positive and negative, when all 50 stochastic emission inventories were used for simulations on 25 August and 30 August, 2000. Specifically, the quantity presented is the maximum difference in ozone concentration between using the stochastic inventory and the deterministic inventory. On the top and bottom of each column, the ozone concentration for the stochastic inventory, at the time when the maximum difference occurred, is indicated in ppb. In the simulations of 25 August, the maximum difference in ozone concentration is largest when the 45^{th} stochastic emission inventory was used; the ozone concentrations are 24 ppb and 106 ppb when the deterministic and the stochastic inventory were used, respectively, at conditions that lead to the maximum increase in ozone concentration. In the simulations of 30 August, the largest maximum difference in ozone concentration occurred when the 48^{th} stochastic inventory was used; a 43 ppb decrease in ozone concentration was predicted, relative to the deterministic imputed inventory. The probability distributions of maximum difference in ozone concentration for both days are shown in Figure 13. The maximum increase in ozone concentration at any hour and location from including the variability in VOC point-source emissions has 90% bounds of 11-52 ppb for the August 25 meteorology and 10-23 ppb for the August 30 meteorology. In percentage terms, the maximum difference in ozone concentration between the stochastic and deterministic version had a 90% probability of being between 13% and 316% for August 25, and between 10% and 85% on August 30. In order to give a sense of the range of uncertainty, Figure 14 shows the hourly spread of ozone concentrations for two grid cells discussed above, (39,55)

and (40, 43). Note that for (39, 55), the uncertainty is large enough to affect whether or not ozone exceeds the one-hour standard of 120 ppb. The early morning peak in Figure 14b is a result of the meteorology for August 25, when there was a period of stagnation from 6am to 11am, and a low mixing height. Then winds increased and advected the high ozone to the west. This is a typical meteorology pattern for Houston, and is the most common pattern for extreme ozone exceedence days.

Simulations of the two episode days exhibit different responses of ozone formation due to variable point source emissions. For example, the 45th stochastic inventory led to a maximum difference in ozone concentration of 82 ppb in a grid cell which is the 40th to the east and the 54th to the north from the southwest corner of the region in red, shown in Figure 11, at 7am 25 August. At the same time of day and location on 30 August, the ozone concentration was not affected by variable point source emissions. Distinctly different meteorological conditions on the two days led to these different behaviors of ozone formation for the same stochastic emission inventory.

This change in ozone concentration did not always increase the peak ozone concentration in the 1-km domain over the course of the day. For example, on 25 August the daily maximum ozone concentration using the stochastic inventory is up to 11.9 ppb higher and up to 6 ppb lower than when the non-stochastic imputed inventory was used, depending on the stochastic inventory used. The average and standard deviations for the increases and decreases in the sub-domain wide daily maximum ozone concentrations were 3.3±2.9 and 2.4±1.7, respectively. These results can be contrasted with a maximum increase of 82 ppb and a maximum decrease of 56 ppb, shown in Figure 12, and average increases and decreases of 24±15 and 17±14, respectively. A total of 31 out of the 50 sets of stochastic inventories led to increases in daily maximum ozone

concentration in the sub-domain. For 30 August, the daily maximum ozone concentration increased for 37 sets of stochastic inventories. The maximum increase in the peak ozone concentration in the 1-km domain was approximately 10.7 ppb and maximum decrease was approximately 4.5 ppb.

In summary, variability in continuous industrial emissions has the potential to have a significant impact on ozone formation in the Houston-Galveston area. Increases and decreases of 10-52 ppb or more in ozone concentration are possible as a result of emission variability. The largest of these differences are restricted to regions of 10-20 km^2 (see Figure 11), but the variability also has the potential to increase region wide maxima in ozone concentrations by to 12 ppb.

These results raise important questions about effective ozone control strategies for ozone in the Houston Galveston region, and perhaps other regions with significant petrochemical industrial facilities such as Baton Rouge or New Jersey. If some of the high ozone episodes are the result of less frequent higher than average emission rates, rather than the mean emissions, control strategies that lower the annual average may prove ineffective at reducing ozone exceedances. Further, strategies that target the upper tails of the distribution may have very different, perhaps lower, compliance costs than traditional approaches. This is an important area for future inquiry.

References

Cornell, J., 2002. *Experiments with mixtures: designs, models, and the analysis of mixture data*. Wiley, New York.

Environ International Corporation (Environ), 2004. User's Guide: Comprehensive Air Quality Model with Extensions (CAMx), Version 4.03, Document and model are available online at http://www.camx.com

Environ International Corporation (Environ), 2006. Comprehensive Air Quality Model with Extensions (CAMx) Pre-processors, Accessed January 2006 at http://www.camx.com/down/support.php

Hogg, R. V., Ledolter, J., 1992. *Applied Statistics for Engineers and Scientists*. Macmillan Publishing Company, New York.

Johnson, B. Barz, G., 1999. "Selecting Stochastic Process for Modelling Electricity Prices." *Energy Modelling and the Management of Uncertainty*, Risk Publications.

Kleinman, L.I., Daum, P.H., Imre, D., Lee, Y.N., Nunnermacker, L.J., Springston, S.R., Weinstein-Lloyd, J., Rudolph, J., 2002. Correction to "Ozone production rate and hydrocarbon reactivity in 5 urban areas: A cause of high ozone concentration in Houston". Geophys. Res. Lett. 30 (12), 1639.

Knittel, C. R., Roberts, M., 2001. "An Empirical Examination of Deregulated Electricity Prices," POWER WP-087, University of California Energy Institute.

Murphy, C.F., Allen, D.T., 2005. Hydrocarbon emissions from industrial release events in the Houston- Galveston area and their impact on ozone formation. Atmospheric Environment 39 (21), 3785-3798.

Nam, J., Kimura, Y., Vizuete, W., Murphy, C.F., Allen, D.T., 2006. Modeling the impacts of emission events on ozone formation in Houston, Texas. Atmospheric Environment 40 (28), 5329-5341.

Press, W. H., Teukolsky, S. A., Vetterling, W. V., Flannery, B. P., 1992. *Numerical recipes in C.* Cambridge University Press, Cambridge, England; New York, N.Y.

Ryerson, T.B., Trainer, M., Angevine, W.M., Brock, C.A., Dissly, R.W., Fehsenfeld, F.C., Frost, G.J., Goldan, P.D., Holloway, J.S., Hubler, G., Jakoubek, R.O., Kuster, W.C., Neuman, J.A., Nicks, D.K., Parrish, D.D., Roberts, J.M., Sueper, D.T., Atlas, E.L., Donnelly, S.G., Flocke, F., Fried, A., Potter, W.T., Schauffler, S., Stroud, V., Weinheimer, A.J., Wert, B.P., Wiedinmyer, C., Alvarez, R.J., Banta, R.M., Darby, L.S., Senff, C.J., 2003. Effect of petrochemical industrial emissions of reactive alkenes and NOx on tropospheric ozone formation in Houston, Texas. J. Geophys. Res. 108 (D8), 4249.

Texas Commission on Environmental Quality (TCEQ), 2006. Houston-Galveston-Brazoria Ozone SIP Mid-Course Review Modeling, Accessed January 2006 at http://www.tceq.state.tx.us/implementation/air/airmod/data/hgb1.html

University of North Carolina, 2004. Stochastic Emission Inventories of Continuous Emissions. Houston Advanced Research Center, H13.2003 Final Report Appendix B, available at http://files.harc.edu/Projects/AirQuality/Projects/H013.2003/H13AppendixB.pdf

Vizuete, W., 2005. Implementation of Process Analysis in a three dimensional air quality model, PhD thesis, University of Texas.

Source name (number of observations)	Type	Component	Number of observations	Normalized proportion	Mean time	Normal or Lognormal	Standard deviation	Mean or Mean (LN Value)
Flare 1	Flare	1	4913	0.599	7.41	N	0.34	2.43
(8208)		2	3223	0.393	4.41	LN	0.36	1.23
		3	68	0.008	1.15	LN	0.8	2.19
Flare 2	Flare	1	360	0.501	3.34	N	0.8	1.89
(720)		2	331	0.460	3.5	N	2.5	4.99
		3	28	0.039	2.63	LN	0.33	2.45
Flare 5	Flare	1	1757	0.486	3.09	N	225.52	758.83
(3624)		2	1706	0.472	5.36	N	1197.5	1721.7
		3	147	0.041	1.04	LN	0.71	8.08
HC Flare	Flare	1	128	0.071	0.52	LN	1.12	0.07
(1800)		2	1625	0.903	15.28	LN	0.26	0.9
		3	46	0.026	1.35	LN	0.3	1.58
Olefins Flare	Flare	1	1078	0.599	14.18	N	0.53	1.6
(1800)		2	700	0.389	10.58	N	3.1	4.91
		3	21	0.012	6.5	LN	0.42	2.95
FCCU	Flare	1	12383	0.743	195.31	N	3	20
(17533)		2	4270	0.256	17.85	N	11.93	29.38
		3	12	0.001	12.6	LN	1.2	3.97
Merox Flare	Flare	1	307	0.056	10.65	N	874.78	4.63
(17543)		2	15705	0.914	200.07	N	100.19	494.09
		3	1152	0.03	45.6	LN	0.001	6.63
Low Pressure	Flare	1	200	0.011	9.37	LN	0.48	3.04
Flare		2	16830	0.971	229.58	LN	0.05	3.23
(17543)		3	314	0.018	132.63	LN	0.52	3.46
General Service	Flare	1	16892	0.964	155.47	N	1.66	21.45
#1		2	405	0.023	2	LN	0.38	3.26
(17543)		3	233	0.013	5.78	LN	0.43	3.47
General Service	Flare	1	17322	0.67	508.65	N	1.31	17.8
#2		2	141	0.25	4	LN	0.08	3.05
(17543)		3	70	0.08	2.9	LN	0.7	3.26
Cooling Tower 1	Cooling	1	243	0.779	5.72	LN	0.2	-2.69
(314)	Tower	2	64	0.221	0.8	LN	0.3	-0.73
Cooling Tower 2	Cooling	1	98	0.291	4.26	N	6.3	0.23
(340)	Tower	2	148	0.439	2.61	N	0.39	0.67
		3	91	0.270	2.29	LN	0.68	0.28
Stacks/ Fugitives		1	NA	1	NA	LN	0.56	-0.15

Table 1. Observations from emission sources and fitted parameters

Flare Name		mean	stdev	0.05	0.1	0.25	0.5	0.75	0.9	0.95
Flare 1	Actual	2.92	1.65	2.09	2.21	2.40	2.66	3.10	3.81	4.43
	Simulation	2.90	0.95	2.07	2.17	2.38	2.70	3.10	3.63	4.29
Flare 2	Actual	3.71	2.64	1.09	1.34	1.97	2.81	4.78	7.42	9.64
	Simulation	3.73	3.02	1.09	1.32	1.84	2.91	4.33	7.36	11.07
Flare 5	Actual	1398.85	1278.19	614.25	682.75	819.50	1042.51	1703.33	2514.84	2696.56
	Simulation	1311.27	698.98	629.79	704.06	832.58	1024.56	1571.65	2469.56	2669.95
HC Flare	Actual	2.47	0.74	1.44	1.72	2.01	2.43	2.86	3.28	3.69
	Simulation	2.54	0.71	1.53	1.72	2.09	2.51	2.93	3.32	3.58
Olefins Flare	Actual	3.11	2.77	1.07	1.29	1.60	1.92	4.29	5.85	6.92
	Simulation	2.98	2.41	1.00	1.20	1.51	1.94	4.30	5.77	6.81
FCCU	Actual	21.87	7.90	14.10	17.42	19.02	20.63	23.98	29.58	34.76
	Simulation	22.23	5.41	16.10	16.92	18.85	21.17	23.71	31.25	34.51
Merox Flare	Actual	500.21	136.97	284.82	342.40	432.96	501.94	582.40	660.94	737.14
	Simulation	488.84	150.79	42.98	351.78	435.32	512.64	572.60	630.95	684.81
Low Pressure	Actual	25.54	1.89	23.67	24.10	24.54	25.05	26.41	27.59	28.20
	Simulation	25.56	1.87	23.17	23.49	24.39	25.20	26.62	27.70	28.59
General Service #1	Actual	21.70	2.11	18.96	19.50	20.44	21.67	22.85	23.49	24.05
	Simulation	21.86	3.07	18.40	18.96	19.85	20.89	22.17	23.90	24.68
General Service #2	Actual	17.85	1.45	15.86	16.17	16.79	17.65	19.09	19.42	19.61
	Simulation	17.68	1.37	15.59	15.97	16.62	17.41	19.07	19.34	19.54
Cooling Tower #1	Actual	0.18	0.24	0.02	0.03	0.06	0.09	0.20	0.50	0.59
	Simulation	0.19	0.23	0.02	0.03	0.06	0.09	0.20	0.53	0.66
Cooling Tower #2	Actual	0.75	0.57	0.16	0.21	0.30	0.68	0.94	1.33	1.72
	Simulation	0.79	0.72	0.18	0.22	0.32	0.68	0.95	1.49	1.89

Table 2. Comparison of mean, standard deviation, and selected fractiles of VOC emissions between actual emissions samples (see Table 1) and 10000 simulated hours from the stochastic emission generator.

Percentile	All Sources	All Flares	(40, 43)	(18, 51)	(39, 55)	3 Flares with Highest Avg Emi.		
0.01	6.77	1.21	0.015	0.023	0.023	0.043	0.049	0.005
0.025	6.83	1.24	0.016	0.024	0.024	0.052	0.061	0.010
0.05	6.87	1.27	0.016	0.026	0.026	0.062	0.077	0.023
0.25	7.02	1.35	0.018	0.031	0.031	0.107	0.096	0.056
0.5	7.14	1.41	0.019	0.035	0.035	0.156	0.101	0.069
0.75	7.27	1.48	0.021	0.041	0.041	0.229	0.106	0.083
0.95	7.48	1.61	0.024	0.051	0.051	0.391	0.216	0.131
0.975	7.57	1.66	0.026	0.055	0.055	0.469	0.249	0.157
0.99	7.69	1.73	0.028	0.061	0.060	0.558	0.283	0.202
mean	7.15	1.42	0.020	0.037	0.037	0.183	0.112	0.074
stdev	0.19	0.11	0.003	0.008	0.008	0.109	0.042	0.045

Table 3. Mean, standard deviation, and selected fractiles of point source VOC emissions (tons/hr) in Houston Galveston.

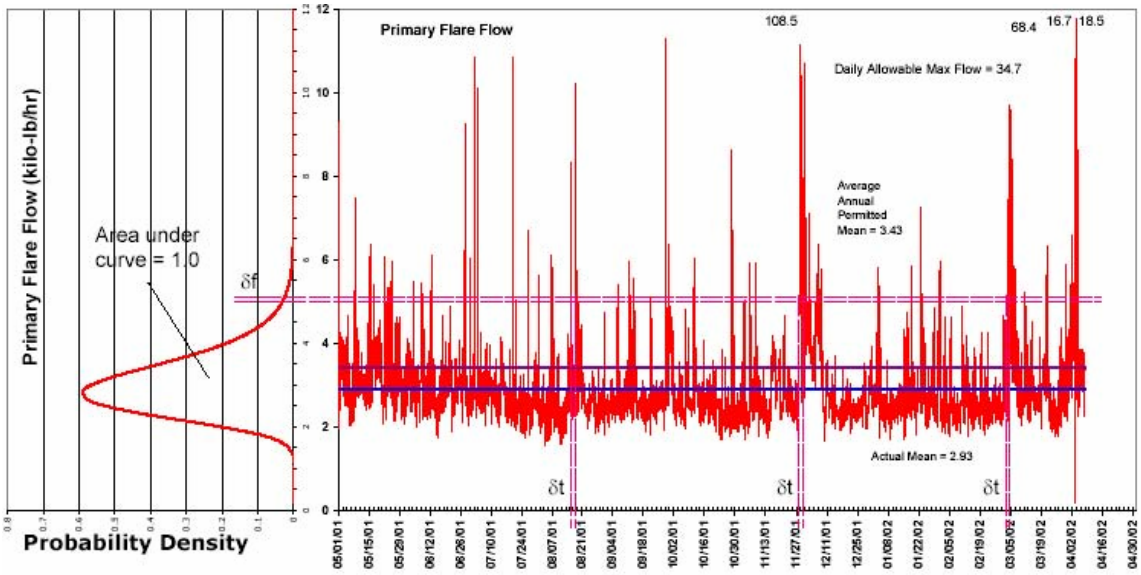

Figure 1. Probability distribution function (PDF) and time series of mass flow rate to a flare at an industrial facility in the HG area.

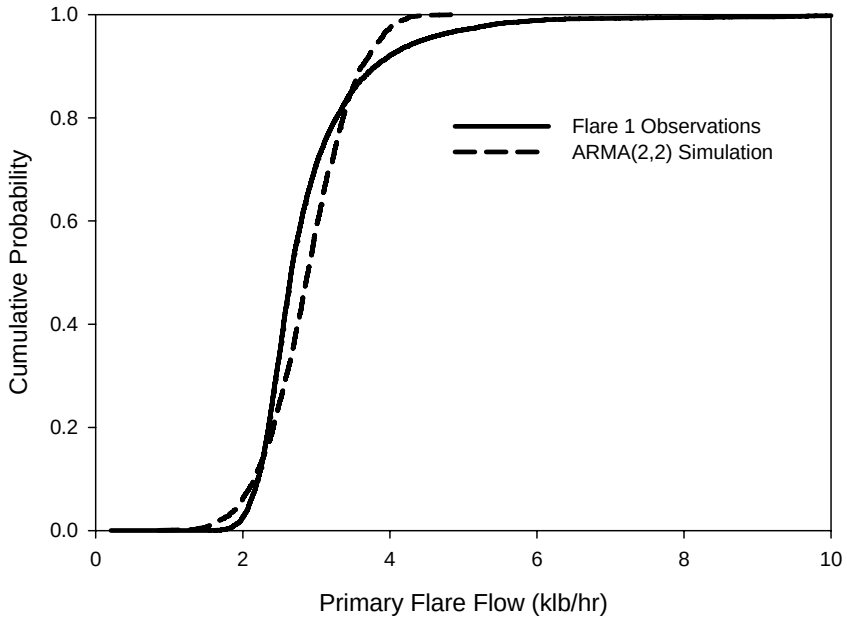

Figure 2. Cumulative Distribution Functions for observations from Flare 1 and from an auto-regressive moving-average (ARMA) model.

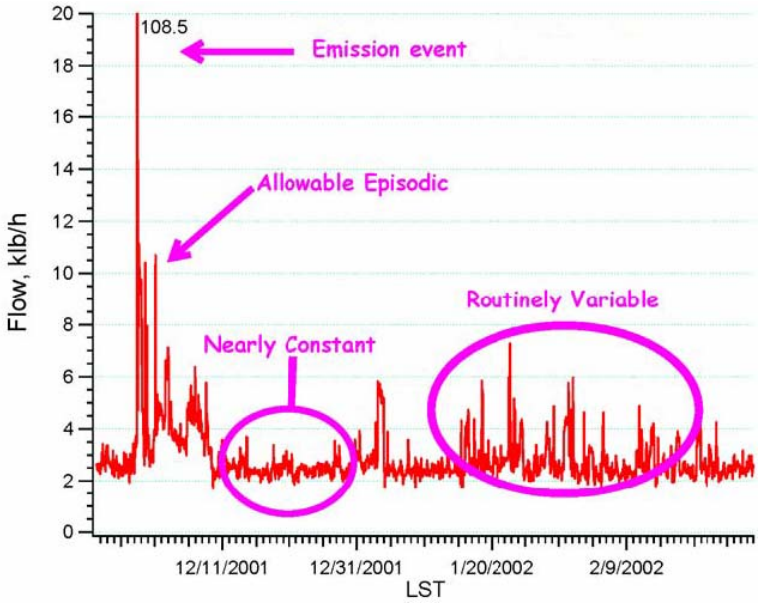

Figure 3. Components of mass flows: emission event, allowable episodic, routinely variable and nearly constant.

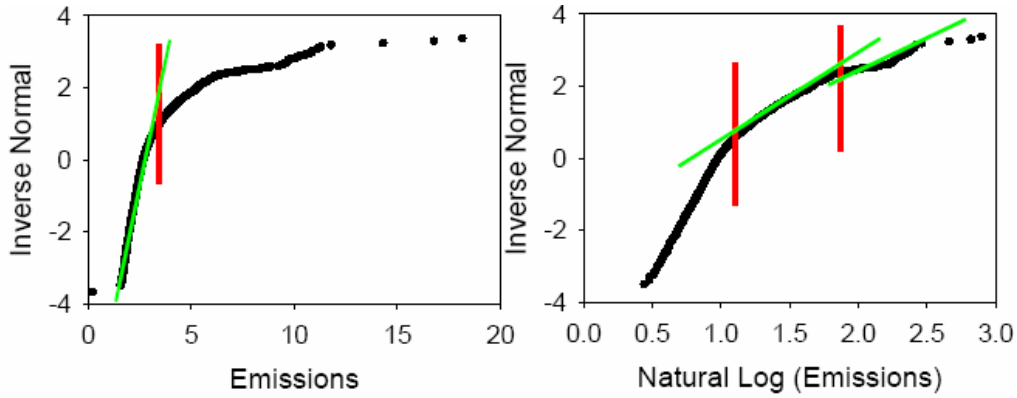

Figure 4. Decomposition into three PDFs of emissions from flare shown in Figure 1. Inverse normal is expressed in the standard form (z) in relation to the mean and standard deviation $\left(z = \frac{Y - \overline{Y}}{s} \right)$.

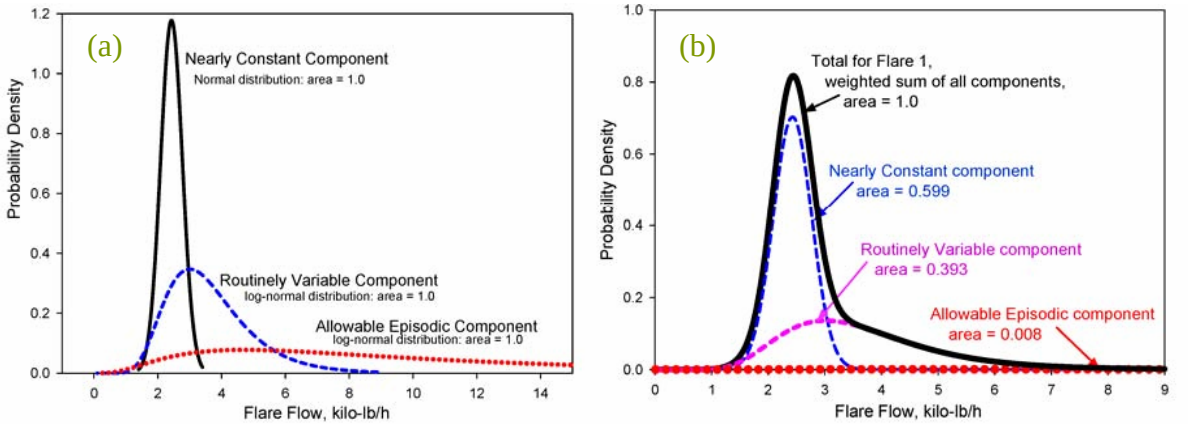

Figure 5. (a) PDFs for each component of emissions from the flare in Figure 1 (b) normalized PDFs of three components based on the proportion of each emission component

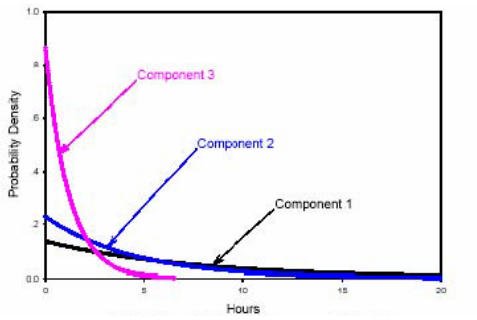

Figure 6. Time within each emission component before transition to next component

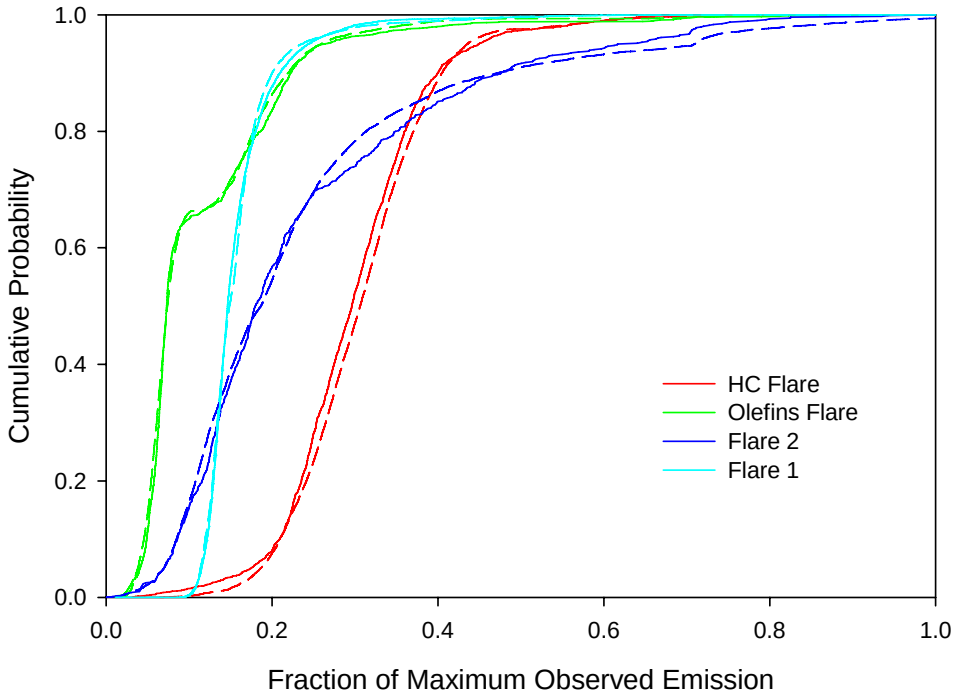

Figure 7. Comparison of cumulative probability distribution functions for observed (solid lines) and 10,000 simulated hours (dashed lines) for four flares. X-axis shows emissions as a fraction of the maximum observed emission.

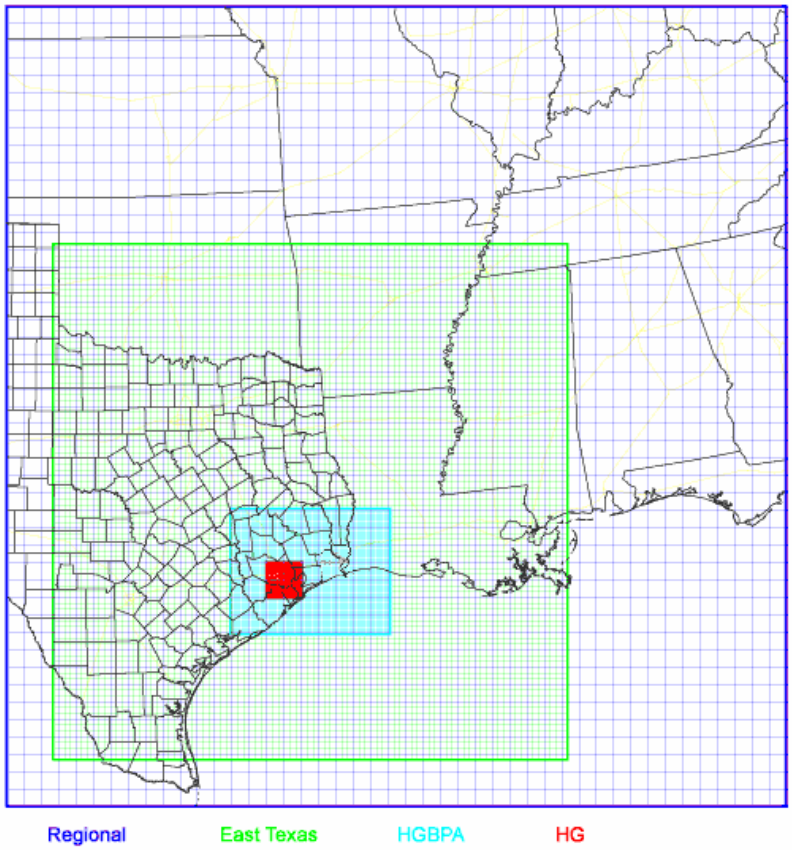

Figure 8. Modeling domain used in the study. The Regional, East Texas, Houston-Galveston-Beaumont-Port Arthur (HGBPA), and Houston Galveston (HG) nested domains had 36, 12, 4 and 1 km resolution, respectively.

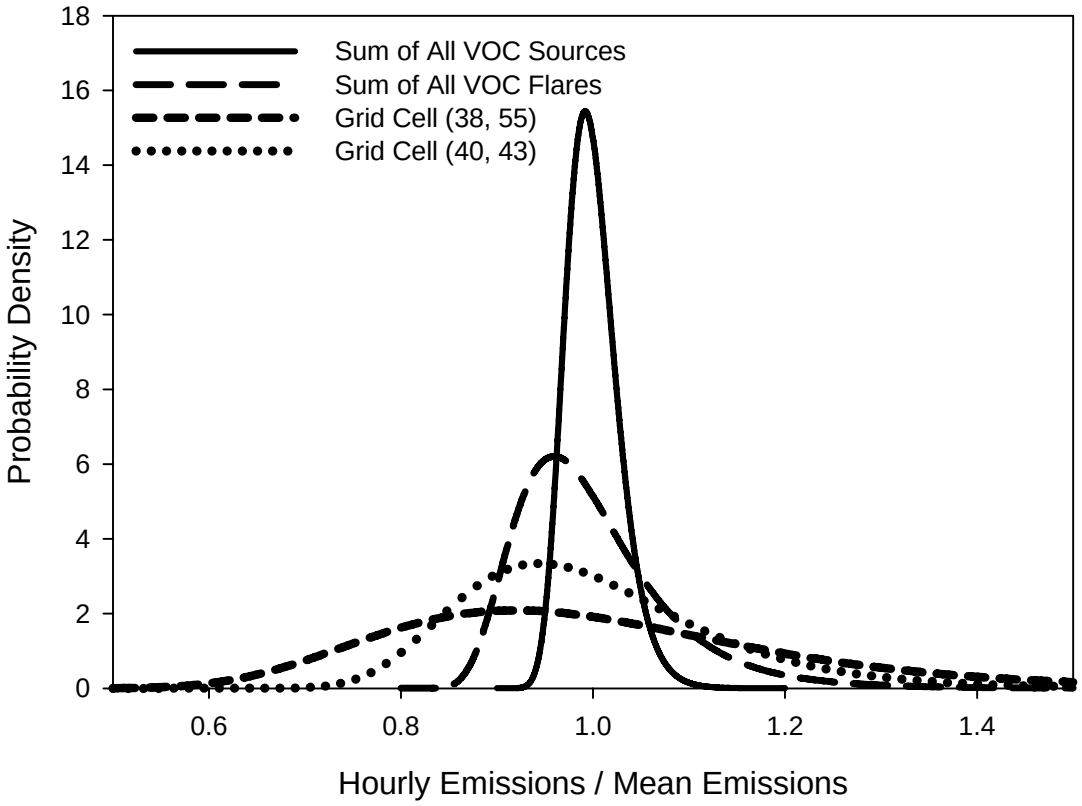

Figure 9. Variability of hourly VOC emission rates for all industrial point sources in the HG domain (solid line), all industrial flares in the HG domain (long dash), and for the industrial point sources within two representative 1 km^2 grid cells.

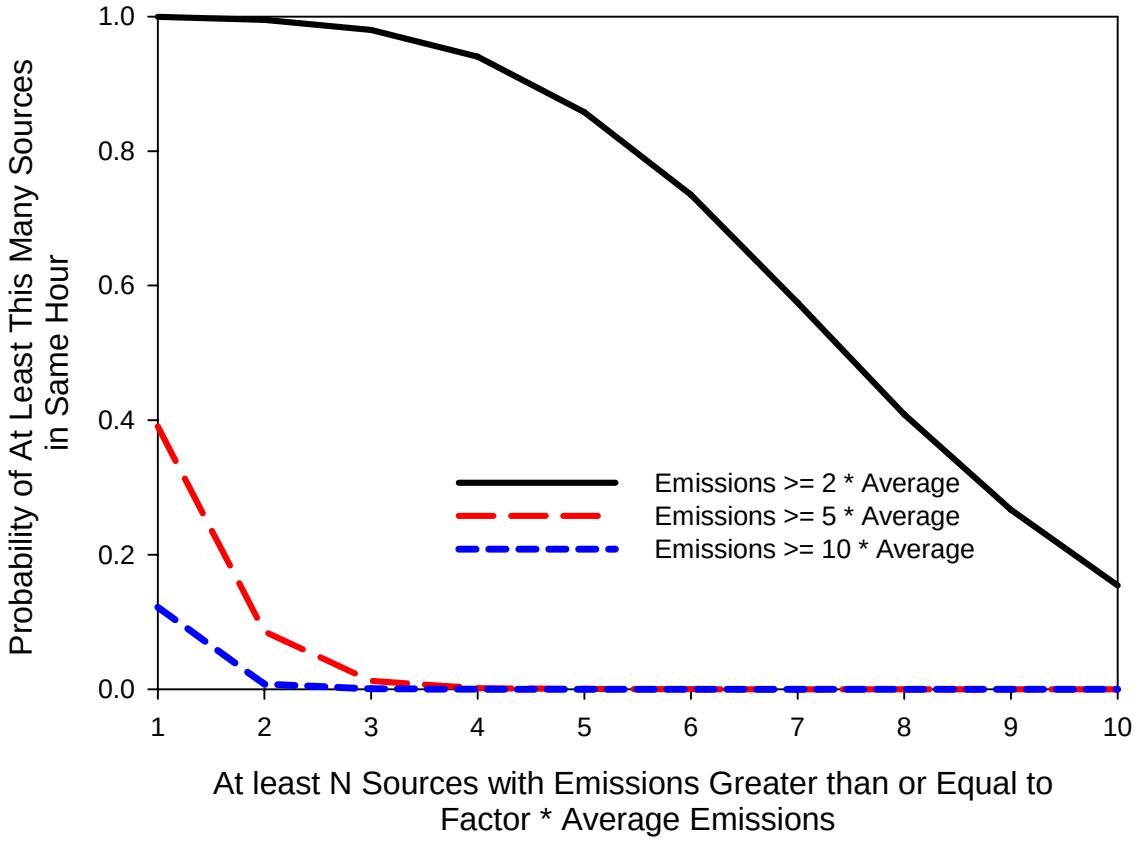

Figure 10. The probability that N or more point source emissions are a factor of 2, 5, and 10 times their annual average within the same hour.

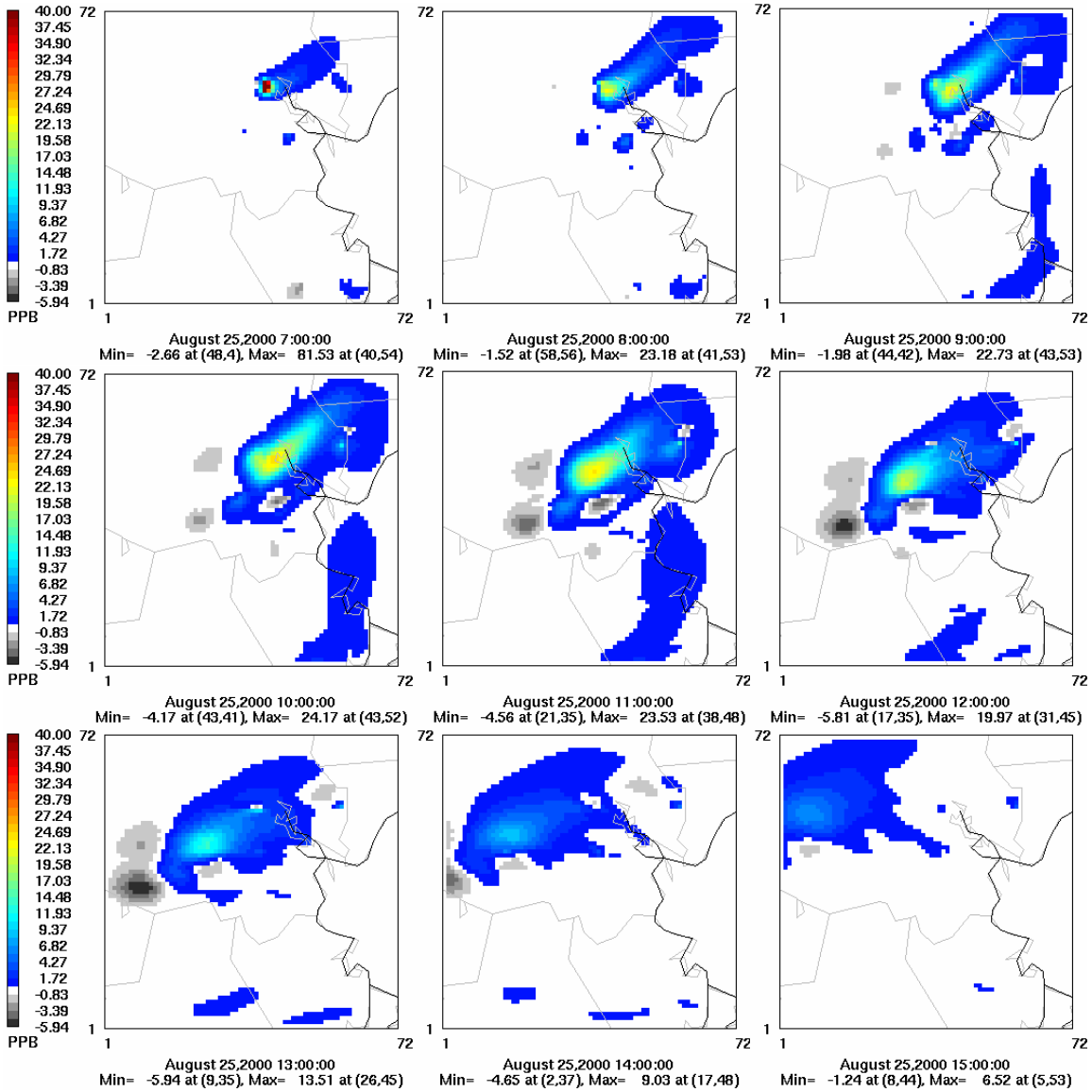

Figure 11. Difference in ozone concentration for 25 August from 700 hr to 1500 hr between using the 45th stochastic imputed emission inventory and using the deterministic imputed inventory.

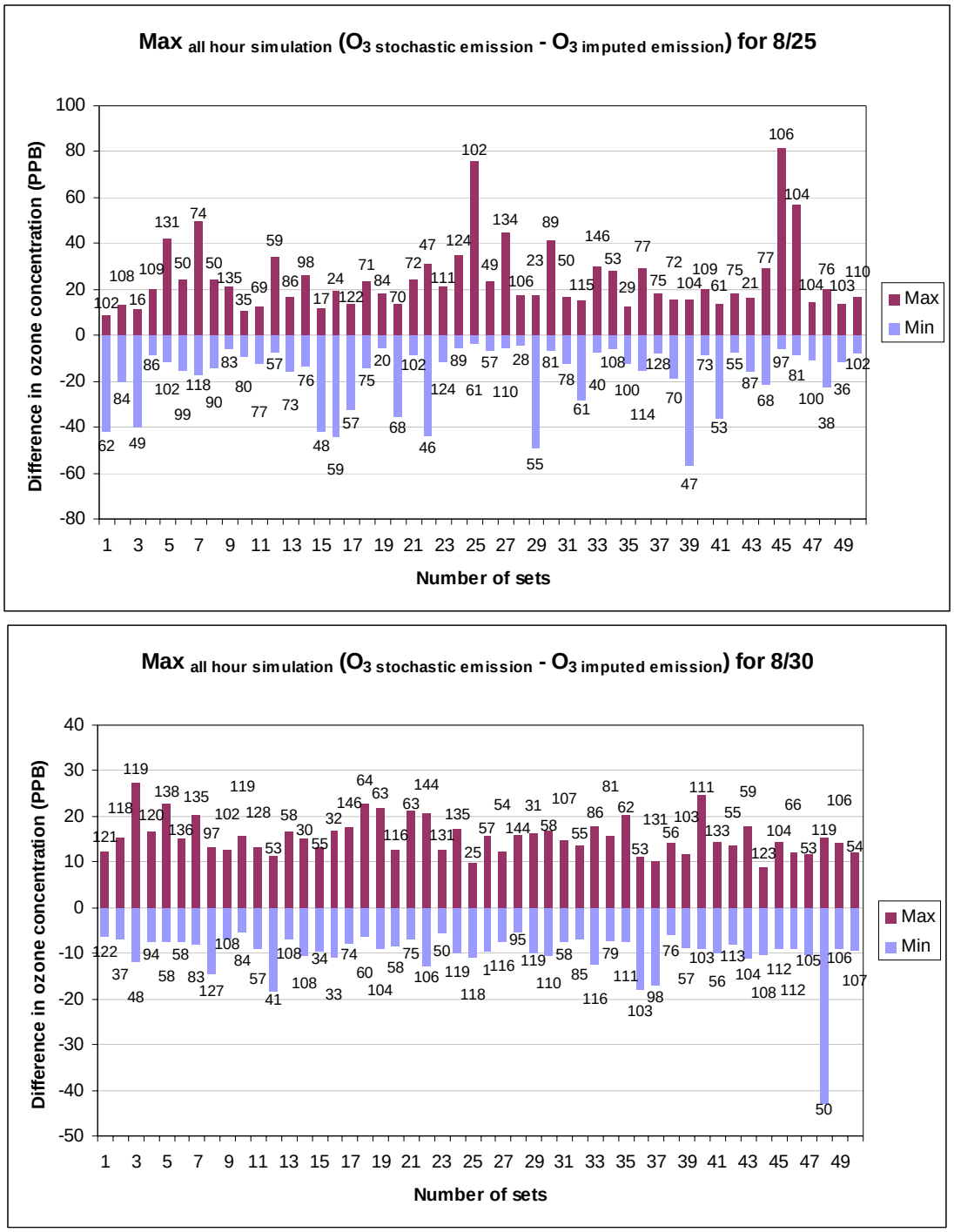

Figure 12. Maximum difference in ozone concentrations in one day simulations representing 25 August and 30 August, 2000. The difference is taken between the imputed inventory with constant industrial emissions and the stochastic inventory for 10 instances of the stochastic

inventory. Ozone concentrations (ppb), using the stochastic inventory, at the time the maximum difference was observed are indicated on the top and bottom of each column.

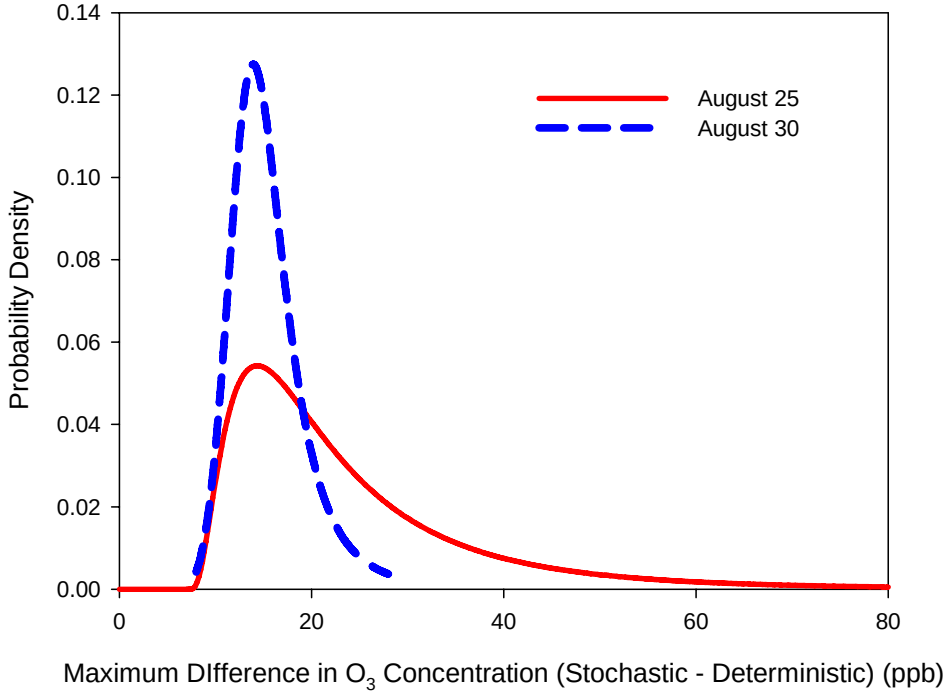

Figure 13. Probability distributions of maximum difference in ozone concentrations in one day simulations representing 25 August and 30 August, 2000.

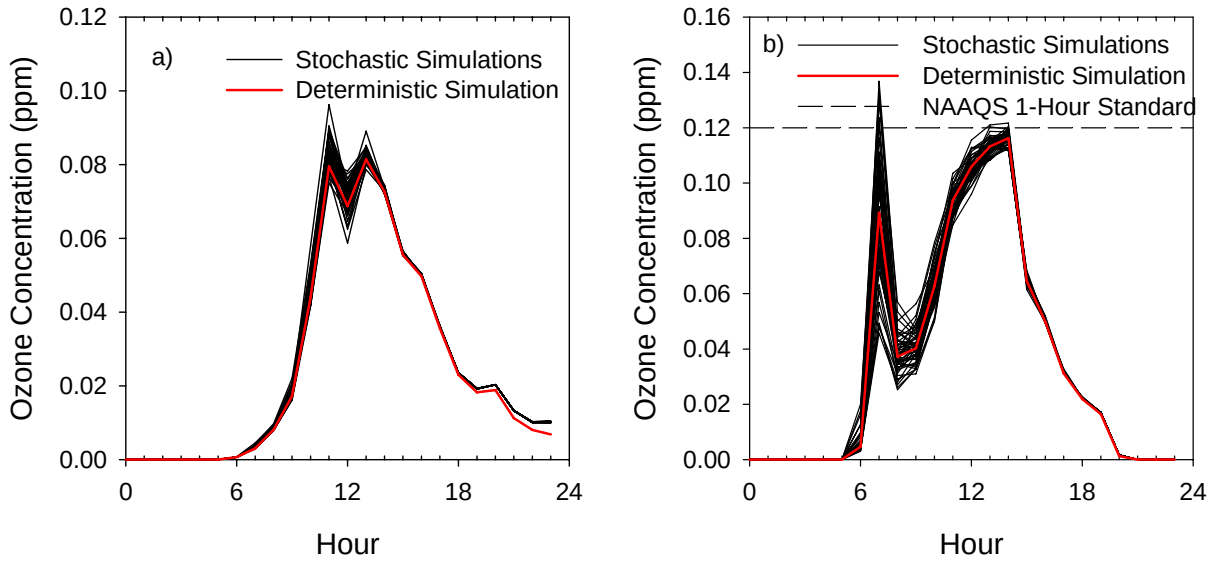

Figure 14. Hourly ozone concentrations from the 50 simulations for two grid cells on August 25: a) grid cell (40, 43), and b) grid cell (39, 55). Black lines show all 50 simulations with stochastic emissions inventory, and red line shows simulation with deterministic emissions inventory.